

FY20 NRL DOD HPCMP ANNUAL REPORTS



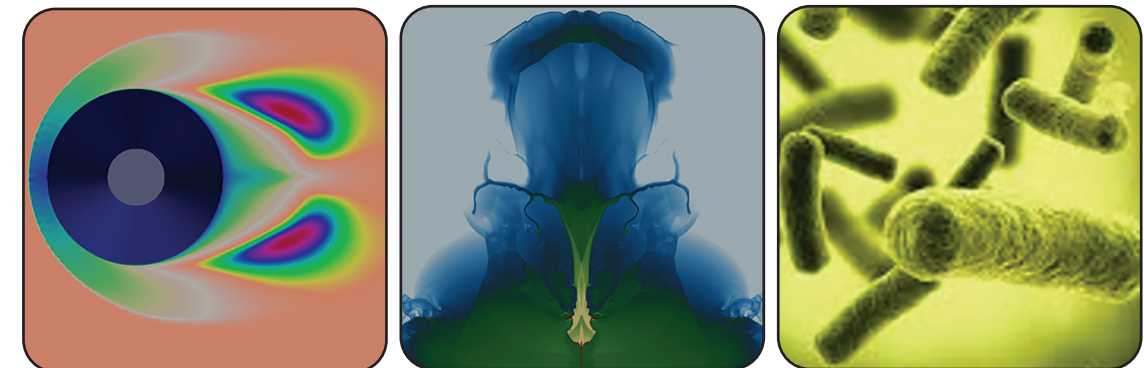
FY20 NRL DoD High Performance Computing Modernization Program Annual Reports

EDITED BY
BONNIE J. ASSAD

PREPARED BY
PORTIA A. SHINGLER AND BETH A. HOWELL

*Center for Computational Science
Information Technology Division*

December 22, 2021



Distribution A: Approved for public release; distribution is unlimited.

REVIEWED AND APPROVED
NRL/PU/5594--21-666
RN: 21-1231-2774
December 2021

Stanley Chincheck
Superintendent, Information Technology Division

REPORT DOCUMENTATION PAGE

*Form Approved
OMB No. 0704-0188*

The public reporting burden for this collection of information is estimated to average 1 hour per response, including the time for reviewing instructions, searching existing data sources, gathering and maintaining the data needed, and completing and reviewing the collection of information. Send comments regarding this burden estimate or any other aspect of this collection of information, including suggestions for reducing the burden, to the Department of Defense, Executive Service Directorate (0704-0188). Respondents should be aware that notwithstanding any other provision of law, no person shall be subject to any penalty for failing to comply with a collection of information if it does not display a currently valid OMB control number.

PLEASE DO NOT RETURN YOUR FORM TO THE ABOVE ORGANIZATION.

1. REPORT DATE (DD-MM-YYYY) 22-12-2021		2. REPORT TYPE Publication		3. DATES COVERED (From - To) 01 October 2019 - 30 September 2020	
4. TITLE AND SUBTITLE FY20 NRL DoD High Performance Computing Modernization Program Annual Reports				5a. CONTRACT NUMBER	
				5b. GRANT NUMBER	
				5c. PROGRAM ELEMENT NUMBER	
6. AUTHOR(S) Portia A. Shingler and Beth A. Howell				5d. PROJECT NUMBER	
				5e. TASK NUMBER	
				5f. WORK UNIT NUMBER	
7. PERFORMING ORGANIZATION NAME(S) AND ADDRESS(ES) Naval Research Laboratory 4555 Overlook Avenue SW, Washington, DC 20375-5320				8. PERFORMING ORGANIZATION REPORT NUMBER	
9. SPONSORING/MONITORING AGENCY NAME(S) AND ADDRESS(ES) Office of Naval Research 875 N. Randolph Street Arlington, VA 22217				10. SPONSOR/MONITOR'S ACRONYM(S) ONR	
				11. SPONSOR/MONITOR'S REPORT NUMBER(S)	
12. DISTRIBUTION/AVAILABILITY STATEMENT Approved for public release; distribution is unlimited.					
13. SUPPLEMENTARY NOTES					
14. ABSTRACT These reports summarize the accomplishments of the NRL Principal Investigators who received computer allocations on the DoD HighPerformance Computing Modernization Program Shared Resource Center.					
15. SUBJECT TERMS Biomechanics, network encryption device, constitutive modeling, hyperelastic, viscoelastic constrained optimization, parameter estimation, model calibration, computational modeling					
16. SECURITY CLASSIFICATION OF:			17. LIMITATION OF ABSTRACT	18. NUMBER OF PAGES	19a. NAME OF RESPONSIBLE PERSON
a. REPORT	b. ABSTRACT	c. THIS PAGE			Bonnie Assad
U/U	U/U	U/U	Unlimited	179	19b. TELEPHONE NUMBER (Include area code) 202-767-2046

Introduction

This book is a compilation of reports on all of the work accomplished by NRL scientists and engineers and their collaborators using the DoD High Performance Computing Modernization Program's (HPCMP) resources for fiscal year 2019. The reports encompass work performed by researchers at all three NRL sites: Washington, DC, Stennis Space Center, Mississippi, and Monterey, California.

These reports are categorized according to the primary Computational Technology Area (CTA) as specified by the HPCMP, and include resources at the DOD Supercomputing Resource Centers (DSRC) as well as the Affiliated Resource Centers (ARC). This volume includes three indices for ease of reference. These are an author index, a site index, and an NRL hierarchical index of reports from the branches and divisions at NRL.

THIS PAGE INTENTIONALLY LEFT BLANK

Table of Contents

Computational Structural Mechanics (CSM)

Atomistic Modeling of Structural Materials2

E. Antillon, N. Bernstein, and M. Johannes
Naval Research Laboratory, Washington, DC

Computational Analysis of Warfighter Brain Injury and Protective Equipment.....4

X.G. Tan and R.N. Saunders
Naval Research Laboratory, Washington, DC

Stochastic Methods for Uncertainty Quantification in Computational Mechanics.....6

K. Teferra and R.N. Saunders
Naval Research Laboratory, Washington, DC

Geometric, Constitutive and Loading Complexities in Structural Materials8

S.A. Wimmer¹, R.N. Saunders¹, A. Arcari², P. Brewick¹, H. Ryou¹, and J.G. Michopoulos¹
¹*Naval Research Laboratory, Washington, DC*
²*Excet, Inc., Springfield, VA*

Computational Fluid Dynamics (CFD)

The Impact of Foam and Aerosol Dynamics on Fire, Explosion Safety, and Suppression (Mechanisms of Water Mist Suppression of a Burning Solid Surface)12

X. Zhuang¹ and R. Ananth²
¹*ASEE Postdoctoral Fellow, Naval Research Laboratory, Washington, DC*
²*Naval Research Laboratory, Washington DC*

Simulations of Laser-plasma Interactions and the Radiation Hydrodynamics of High-velocity Laser-accelerated Matter14

J.W. Bates, A.J. Schmitt, and K. Obenschain
Naval Research Laboratory, Washington, DC

Flame Acceleration and Deflagration-to-Detonation Transition in Obstructed Channels.....16

V.N. Gamezo¹ and A.Y. Poludnenko²
¹*Naval Research Laboratory, Washington, DC*
²*University of Connecticut, Storrs, CT*

Hypersonic Reactive Flow Modeling.....18

G.B. Goodwin and C.L. Bachman
Naval Research Laboratory, Washington, DC

Advanced Two Phase CFD Model.....	20
T.D. Holman	
<i>Naval Research Laboratory, Washington, DC</i>	
High-Fidelity CFD Simulations of High-Speed Flows in Realistic Atmospheric Conditions.....	22
D.A. Kessler, R.F. Johnson, and A. Hess	
<i>Naval Research Laboratory, Washington, DC</i>	
Jet Noise Reduction Studies	24
Y. Khine	
<i>Naval Research Laboratory, Washington, DC</i>	
Simulations of the Ionosphere/Plasmasphere/Thermosphere System	26
J. Krall ¹ and J.D. Huba ²	
¹ <i>Naval Research Laboratory, Washington, DC</i>	
² <i>Syntek Technologies, Fairfax, VA</i>	
Numerical Investigation of Advanced Military Aircraft Noise Reduction Concepts.....	28
J. Liu and Y. Khine	
<i>Naval Research Laboratory, Washington, DC</i>	
Numerical Simulations of Turbulence Impact on Optical Signal Transmission and Near-Surface Turbulence.....	30
S. Matt	
<i>Naval Research Laboratory, Stennis Space Center, MS</i>	
Predicting Fluid-Structure Interaction for Military Applications.....	32
D.R. Mott, Y. Khine, and A.D. Kercher	
<i>Naval Research Laboratory, Washington, DC</i>	
Advanced Computational Models that Exploit Emerging Computer Architectures	34
K. Obenschain and A. Moses	
<i>Naval Research Laboratory, Washington, DC</i>	
Direct Numerical Simulation of Fluid-Sediment Wave Bottom Boundary Layer	36
A.M. Penko ¹ , W.S. Kearney ² , S.P. Bateman ¹ , J.A. Simeonov ¹ , J. Calantoni ¹ , J. Veeramony ¹ , and W. Lee ³	
¹ <i>Naval Research Laboratory, Stennis Space Center, MS</i>	
² <i>ASEE Postdoctoral Fellow, Naval Research Laboratory, Stennis Space Center, MS</i>	
³ <i>NRC Postdoctoral Fellow, Naval Research Laboratory, Stennis Space Center, MS</i>	

Applications of FEFLO Incompressible Flow Solver	38
R. Ramamurti	
<i>Naval Research Laboratory, Washington, DC</i>	
Detonations with Multi-Phase Flows for Propulsion.....	40
D.A. Schwer	
<i>Naval Research Laboratory, Washington, DC</i>	
Numerical Simulations of Noise Generated by Non-Circular Advanced Military Aircraft Nozzles.....	42
K. Viswanath and R. Ramamurti	
<i>Naval Research Laboratory, Washington, DC</i>	
High-Temperature and Rarefied Gas Dynamics in Hypersonic Flows	44
E.W. Hyde, G.B. Goodwin, J.R. Maxwell, and R.E. Rogers	
<i>Naval Research Laboratory, Washington, DC</i>	
Integrated Radiation Shield Design for 3D Printing	46
M. McDonald, L. Enloe, and M. Georjin	
<i>Naval Research Laboratory, Washington, DC</i>	
Multidimensional Chemically Reacting Fluid Dynamics with Application to Flameless Combustors	48
R.F. Johnson	
<i>Naval Research Laboratory, Washington, DC</i>	
<u>Computational Biology, Chemistry, and Materials Science (CCM)</u>	
Development of Advanced Pulsed-Power Applications.....	52
P.E. Adamson	
<i>Naval Research Laboratory, Washington, DC</i>	
Quantum-Chemical Simulation of Surface-Science Experiments.....	54
V.M. Bermudez	
<i>Naval Research Laboratory, Washington, DC</i>	
Multiple Length and Time Scale Simulations of Material Properties	56
N. Bernstein	
<i>Naval Research Laboratory, Washington, DC</i>	
Improved Calculation of Solid-Phase Heats of Formation Using Intermolecular Interactions Observed in Crystal Structures	58
I.D. Giles and G.H. Imler	
<i>Naval Research Laboratory, Washington, DC</i>	

Surfaces and Interfaces in Oxides and Semiconductors	60
C.S. Hellberg	
<i>Naval Research Laboratory, Washington, DC</i>	
Marine Biofilm Metaproteomics	62
W.J. Hervey, J. Schultzhause, G. Ellis, and G.J. Vora	
<i>Naval Research Laboratory, Washington, DC</i>	
Synthetic Biology for Military Environments	64
W.J. Hervey, J.R. Compton, D.H. Leary, and G.J. Vora	
<i>Naval Research Laboratory, Washington, DC</i>	
Materials for Energy Storage and Generation.....	66
M. Johannes	
<i>Naval Research Laboratory, Washington, DC</i>	
Calculation of Fundamental Physical Parameters for Lower Dimensional Materials	68
C.M. Krowne ¹ and X. Sha ²	
¹ <i>Naval Research Laboratory, Washington, DC</i>	
² <i>General Dynamics IT Corporation, Falls Church, VA</i>	
Dielectric Functions for Cesium Lead Halide Perovskites.....	70
A. Shabaev, K. Jensen, and S. Lambrakos	
<i>Naval Research Laboratory, Washington, DC</i>	
Calculation of Materials Properties via Density Functional Theory and Its Extensions	72
J.L. Lyons	
<i>Naval Research Laboratory, Washington, DC</i>	
DFT Studies of Small Molecule Adsorption on Monolayer Transition Metal Dichalcogenide Films	74
F.K. Perkins ¹ and C.H. Sharp ²	
¹ <i>Naval Research Laboratory, Washington, DC</i>	
² <i>National Research Council Postdoctoral Research Associate, Naval Research Laboratory, Washington DC</i>	
Numerical Studies of Semiconductor Nanostructures.....	76
T.L. Reinecke ¹ and S. Mukhopadhyay ²	
¹ <i>Naval Research Laboratory, Washington, DC</i>	
² <i>National Research Council Postdoctoral Program, Washington, DC</i>	
First-Principles Simulations of Condensed-phase Decomposition of Energetic Materials	78
I.V. Schweigert	
<i>Naval Research Laboratory, Washington, DC</i>	

Point Defects and Interfaces in Two-Dimensional Materials	80
D. Wickramaratne	
<i>Naval Research Laboratory, Washington, DC</i>	
Atomistic Simulations of Navy-relevant Materials	82
D. Fragiadakis	
<i>Naval Research Laboratory, Washington, DC</i>	
<u>Computational Electromagnetics and Acoustics (CEA)</u>	
Structural-Acoustic Response of Stiffened Elastic Cylindrical Shell.....	86
S. Dey, M. Villa, E.L. Mestreau, R.M. Aubry, M. Williamschen, W.G. Szymczak, and D. Williams	
<i>Naval Research Laboratory, Washington, DC</i>	
Acoustic Parameter Variability over an Ocean Reanalysis (AVORA).....	88
J.P. Fabre	
<i>Naval Research Laboratory, Stennis Space Center, MS</i>	
Intense Laser Physics and Advanced Radiation Sources.....	90
D.F. Gordon ¹ , J. Penano ¹ , L. Johnson ¹ , J. Issacs ¹ , D. Kaganovich ¹ , B. Hafizi ¹ , and A. Davidson ²	
¹ <i>Naval Research Laboratory, Washington, DC</i>	
² <i>National Research Council Postdoctoral Program, Washington, DC</i>	
Multidimensional Particle-in-Cell Modeling of Ultrashort Pulse Laser with Solid Targets	92
G.M. Petrov	
<i>Naval Research Laboratory, Washington, DC</i>	
Computer-Aided Design of Vacuum Electronic Devices.....	94
G. Stantchev ¹ , S. Cooke ¹ , J. Petillo ² , A. Jensen ² , and S. Ovtchinnikov ²	
¹ <i>Naval Research Laboratory, Washington, DC</i>	
² <i>Leidos, Billerica, MA</i>	
Flowfield and Transport Models for Navy Applications.....	96
W.G. Szymczak and A.J. Romano	
<i>Naval Research Laboratory, Washington, DC</i>	
Low Grazing Angle Radar Backscatter.....	98
J.V. Toporkov, J.D. Ouellette, and M.A. Sletten	
<i>Naval Research Laboratory, Washington, DC</i>	

Climate Weather Ocean Modeling (CWO)

Coupled Ocean-Wave-Air-Ice Prediction System.....102

R. Allard¹, T. Campbell¹, E. Douglass¹, D. Hebert¹, T. Jensen¹, T.A. Smith¹, and M. Phelps²

¹*Naval Research Laboratory, Stennis Space Center, MS*

²*Perspecta, Stennis Space Center, MS*

Atmospheric Process Studies104

N. Barton, T. Whitcomb, J. Ridout, K. Viner, J. McLay, W. Crawford, M. Liu, T. Hogan, and C. Reynolds

Naval Research Laboratory, Monterey CA

Data Assimilation Studies Project106

W.F. Campbell and B. Ruston

Naval Research Laboratory, Monterey, CA

Coastal Mesoscale Modeling – COAMPS-TC Intensity Prediction108

J.D. Doyle

Naval Research Laboratory, Monterey, CA

The Effect of Langmuir Turbulence in Upper Ocean Mixing.....110

Y. Fan

Naval Research Laboratory, Stennis Space Center, MS

Bio-Optical Modeling and Forecasting112

J.K. Joliff, S. Ladner, T.A. Smith, and C. Wood

Naval Research Laboratory, Stennis Space Center, MS

Investigation and Implementation of GPU Capability to Next Generation

Weather Prediction Code NEPTUNE114

Y. Khine

Naval Research Laboratory, Washington, DC

Coastal Mesoscale Modeling116

W.A. Komaromi and P.A. Reinecke

Naval Research Laboratory, Monterey, CA

Coastal Mesoscale Modeling – COAMPS-TC118

W.A. Komaromi

Naval Research Laboratory, Monterey, CA

Multi-scale Characterization and Prediction of the Global Atmosphere from the Ground to the Edge of Space using Next-Generation Navy Modeling Systems.....	120
J.P. McCormack ¹ , S.D. Eckermann ¹ , C.A. Barton ¹ , F. Sassi ¹ , J. Kelly ¹ , M.A. Herrera ¹ , K.W. Hoppel ¹ , D.D. Kuhl ¹ , D.R. Allen ¹ , J. Ma ² , and J.L. Tate ²	
¹ Naval Research Laboratory, Washington DC	
² Computational Physics Inc., Springfield VA	
Eddy-Resolving Global/Basin-Scale Ocean Modeling.....	122
E.J. Metzger and J.F. Shriver	
Naval Research Laboratory, Stennis Space Center, MS	
High Resolution Global Ocean Reanalysis	124
E.J. Metzger	
Naval Research Laboratory, Stennis Space Center, MS	
Rogue Wave Probability Estimator for WAVEWATCH III.....	126
M. Orzech and J. Dykes	
Naval Research Laboratory, Stennis Space Center, MS	
Probabilistic Prediction to Support Ocean Modeling Projects.....	128
C.D. Rowley ¹ , L.F. Smedstad ¹ , C.N. Barron ¹ , R.S. Linzell ² , P.L. Spence ² , T.L. Townsend ¹ , M. Yaremchuk ¹ , J.C. May ¹ , T.A. Smith ¹ , J.J. Osborne ¹ , G.G. Panteleev ¹ , B.P. Bartels ² , C.J. DeHaan ² , B.R. Maloy ¹ , Z.W. Lamb ³	
¹ Naval Research Laboratory, Stennis Space Center, MS	
² Perspecta, Stennis Space Center, MS	
³ General Dynamics Information Technology, Falls Church, VA	
Guidance for Heterogeneous Observation System (GHOST)	130
L.F. Smedstad ¹ , C.N. Barron ¹ , P.L. Spence ² , C.D. Rowley ¹	
¹ Naval Research Laboratory, Stennis Space Center, MS	
² Perspecta, Stennis Space Center, MS	
Dynamics of Coupled Models	132
I. Shulman, B. Penta, S. Cayula, and C.D. Rowley	
Naval Research Laboratory, Stennis Space Center, MS	
Variational Data Assimilation	134
S. Smith ¹ , L.F. Smedstad ¹ , C.N. Barron ¹ , B.P. Bartels ² , M. Carrier ¹ , J. Crout ³ , J. D’Addezio ¹ , C.J. DeHaan ² , S. deRada ¹ , R. Helber ¹ , Z.W. Lamb ² , R.S. Linzell ² , B.R. Maloy ¹ , J.C. May ¹ , H. Ngodock ¹ , J.J. Osborne ¹ , G.G. Panteleev ¹ , I. Pasmans ⁴ , M. Phelps ² , C.D. Rowley ¹ , T.A. Smith ¹ , I. Souopgui ⁴ , P.L. Spence ² , T.L. Townsend ¹ , K. Weber ¹	
¹ Naval Research Laboratory, Stennis Space Center, MS	
² QinetiQ North America, Stennis Space Center, MS	
³ American Society for Engineering Education, Stennis Space Center, MS	
⁴ University of New Orleans, Stennis Space Center, MS	

Signal Image Processing (SIP)

Reducing the Burden of Massive Training Data for Deep Learning138
L.N. Smith, E.A. Gilmour, S.N. Blisard, and K.M. Sullivan
Naval Research Laboratory, Washington, DC

Space and Astrophysical Science (SAS)

Electromagnetic Pulses from Hypervelocity Impacts on Spacecraft142
A. Fletcher
Naval Research Laboratory, Washington, DC

Global Kinetic Simulations of Space Plasma Waves and Turbulence144
A. Fletcher
Naval Research Laboratory, Washington, DC

Modeling Propagation of Ionospheric Disturbances Initiated by Magnetospheric Substorms146
J. Haiducek¹ and J. Helmboldt²
¹*National Research Council Postdoctoral Fellow, Naval Research Laboratory, Washington, DC*
²*Naval Research Laboratory, Washington, DC*

Dynamic Phenomena in the Solar Atmosphere.....148
K.J. Knizhnik
Naval Research Laboratory, Washington, DC

Development of a Weather Model of the Ionosphere150
S.E. McDonald¹, F. Sassi¹, C.A. Metzler¹, J.L. Tate², and M.S. Dhadly¹
¹*Naval Research Laboratory, Washington, DC*
²*Computational Physics, Inc., Springfield, VA*

Navy Ionosphere Model for Operations152
S.E. McDonald¹, C.A. Metzler¹, J.L. Tate², R.K. Schaefer³, P.B. Dandenault³,
A.T. Chartier³, G. Romeo³, G.S. Bust³, and R. Calfas⁴
¹*Naval Research Laboratory, Washington, DC*
²*Computational Physics, Inc., Springfield, VA*
³*The Johns Hopkins Applied Physics Laboratory, Laurel, MD*
⁴*The University of Texas at Austin Applied Research Laboratories, Austin, TX*

Radio and Gamma-ray Searches for Millisecond Pulsars and Radio Transients ...154
P.S. Ray¹ and J. Deneva²
¹*Naval Research Laboratory, Washington, DC*
²*George Mason University, Fairfax, VA*

Thermosphere & Ionosphere Numerical Models and Ensemble Methods.....156
D.P. Drob, M. Jones, and M.S. Dhadly
Naval Research Laboratory, Washington, DC

Other (OTH)

Simulation of High Energy-Radiation Environments160
J. Finke and A. Hutcheson
Naval Research Laboratory, Washington, DC

Author Index163

Division Index.....166

Site Index168



Computational Structural Mechanics

CSM covers the high-resolution multidimensional modeling of materials and structures subjected to a broad range of loading conditions including quasistatic, dynamic, electromagnetic, shock, penetration, and blast. It also includes the highly interdisciplinary research area of materials design, in which multiscale modeling from atomistic scale to macro scale is essential. CSM encompasses a wide range of engineering problems in solid mechanics, such as material or structural response to time- and history-dependent loading, large deformations, fracture propagation, shock wave propagation, isotropic and anisotropic plasticity, frequency response, and nonlinear and heterogeneous material behaviors. High-performance computing for CSM addresses the accurate numerical solution of conservation equations, equation of motion, equations of state, and constitutive relationships to model simple or complex geometries and material properties, subject to external boundary conditions and loads. CSM is used for basic studies in continuum mechanics, stress analysis for engineering design studies, predicting structural and material response to impulsive loads, and modeling response of heterogeneous embedded sensors/devices. DoD application areas include conventional underwater explosion and ship response, structural acoustics, coupled field problems, space debris, propulsion systems, structural analysis, total weapon simulation, weapon systems' lethality/survivability (e.g., aircraft, ships, submarines, and tanks), theater missile defense lethality analyses, optimization techniques, and real-time, large-scale soldier- and hardware-in-the-loop ground vehicle dynamic simulation.

Title: Atomistic Modeling of Structural Materials
Author(s): E. Antillon, N. Bernstein, and M. Johannes
Affiliation(s): Naval Research Laboratory, Washington, DC
CTA: CSM

Computer Resources: HPE SGI 8600 [AFRL, OH]; Cray XC40/50 [ERDC, MS]

Research Objectives: The basic objective is to understand fundamental deformation mechanisms responsible for mechanical strength and stability for superior alloys in naval applications. Of particular importance are austenitic steels, which can achieve a balance of strength, ductility, stability and corrosion resistance. Because of the large content of iron, spin-polarized calculations become necessary to capture a magneto-volume coupling that arises on this class of alloys. First-principles codes are used to measure critical inputs to an Integrated Computational Materials Engineering (ICME) framework that replaces the trial-and-error design approaches with a more predictive material design approach.

Methodology: The Vienna Ab-initio Simulation Package (VASP) is used to perform all density functional theory calculations. Austenitic steel alloys prove to be challenging because these materials are stable only in the paramagnetic state, which is an intrinsically high-temperature phenomenon involving dynamically disordered spins that break local symmetry but produce FCC structure on average. To emulate the paramagnetic state, we follow an averaging scheme that couples the lattice and magnetic degrees of freedom in a supercell via a statistical averaging method known as Magnetic Sampling Method. This approach is applied to measure point defect information in a model 316L steel alloy composition.

Results: We have investigated a model austenitic steel alloy $Fe_{0.70}Ni_{0.12}Cr_{0.18}$ using spin-polarized DFT. By sampling different disordered magnetic and chemical states, we have measured structural point defects energetics in vacancies, substitutional atoms, solute-vacancy migration paths, as well as other material properties such as elastic moduli and phonon dispersion. The results then are used to populate solute-solution strengthening and diffusion models to predict yield stress and diffusivities in this alloy system respectively, and these predictions are compared against experimental values found in the literature. The results obtained underline the importance of choosing the correct reference state to compute point defect information in 3d-transition metallic alloys.

DoD Impact/Significance: The objectives as given above have immediate relevance for military interests. The problems of designing superior steel alloys is relevant to designing surface and underwater Navy vessels. Our calculations provide a fundamental input into the ICME framework to connect accurate atomic-scale calculations of deformation modes to the overall mechanical properties of steel alloys. This framework opens the possibility to combine computational and experimental methods to achieve the desired balance of superior strength and stability relative to 316L stainless steel that is currently in use.

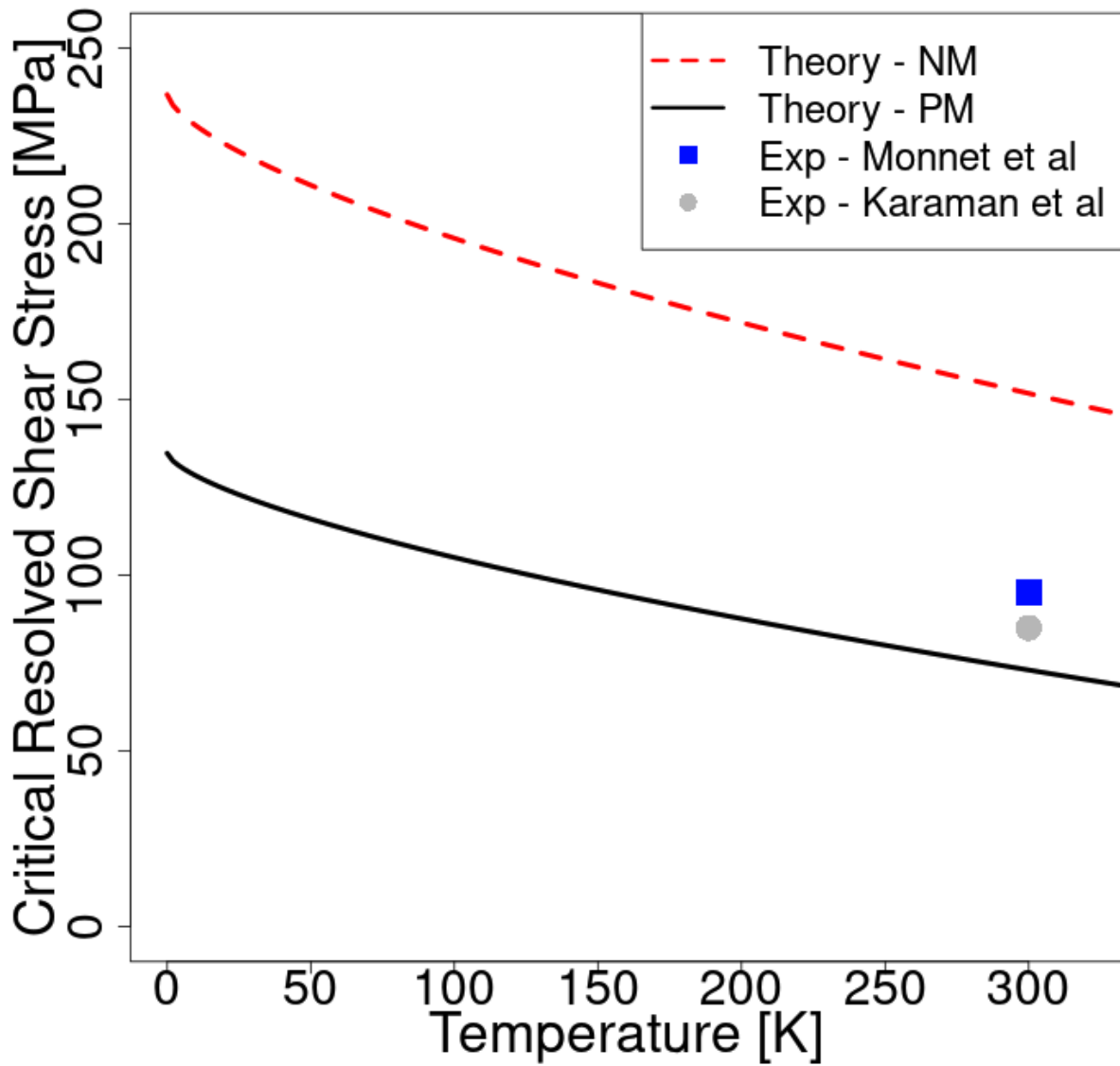


Figure 1. Component of CRSS due to solid-solution hardening vs temperature. The lines show the prediction due to VC model using non-magnetic (dashed) and paramagnetic (solid) inputs from first-principles calculations. The experimental values are obtained from single pillar experiments.

Title: Computational Analysis of Warfighter Brain Injury and Protective Equipment

Author(s): X.G. Tan and R.N. Saunders

Affiliation(s): Naval Research Laboratory, Washington, DC

CTA: CSM

Computer Resources: HPE SGI 8600 [NAVY, MS]; HPE SGI 8600, SGI ICE X [AFRL, OH]; Cray XC40 [ARL, MD]; Cray XC40/50 [ERDC, MS]

Research Objectives: The research objective of this project is to develop methods to prevent and mitigate injury to warfighters. This involves computational analysis of blasts, ballistics and blunt impacts on personal protective equipment (PPE) and induced traumatic brain injury (TBI). Computational methods, such as finite element analysis, are used to conduct the computational analysis. The use of HPC resources is vitally important to this project due to the high fidelity of the models of interest. A typical model to analyze traumatic brain injury requires approximately 24 hours on 216 CPUs. One of the primary outcomes of this research will be the accumulation of a significant number of simulations that will be used to construct correspondence relationships between humans and animals and to achieve optimal protection design.

Methodology: The project uses finite element methods extensively, but the work is not restricted to finite element methodologies. Nonlinear material mechanical constitutive response features are highlighted in much of the work performed. Implicit and explicit solution methods are used as appropriate. The primary finite element codes used are Abaqus, CoBi and CTH. User subroutines are used for specialized material constitutive response when applicable. Multiphysics analysis is used to couple the fluid and structure analysis. Typically, Abaqus/Viewer, ParaView, VisIt, IDL, and Matlab are used for visualization of results in formats such as VTU and HDF5, including animation. For model development, the project typically uses CUBIT, ABAQUS/CAE, Simpleware, IDL, and in-house software. Large run times and large model sizes are often required for the multiphysics/multistep nonlinear finite element/volume analysis jobs.

Results: This project involves work in several topical areas. Work has been performed in the analysis of combat helmet performance integrating blunt impact and blast loadings, optimization of helmet pad placement to reduce mild TBI, and simulation of ballistic impact events of armor systems against various threats. Representative results for the analysis of the TBI and combat helmet protection against both blast loads and blunt impacts are presented. The high-fidelity CFD and FE modeling approach was used to analyze the helmet performance. The parametric studies were conducted to assess the energy absorption for different suspension geometry and material morphology for different loadings by, e.g., the free field explosion, as shown in Fig. 1. Biomechanical metrics were utilized to relate the helmet protection performance with the mild TBI assessment. It was found that the helmet system provides the protection in the blast condition and the blunt impact. Moreover, the helmet with 5-pad suspension performs closely to the helmet with 7-pad suspension, while the helmet with 5-pad suspension provides the better thermal comfort in hot and humid environments.

DoD Impact/Significance: Insights gained from this project are necessary for the advancement from concept to application. Navy/DoD expected results are an improved understanding of traumatic brain injuries for Navy/DoD applications. New insights will be gained through quantifying the effects of anatomical and material property differences on the mechanical response of quantities correlated with traumatic brain injury, which will affect warfighter health in terms of improved protective gear and improved understanding of the correlation between mechanical response thresholds and traumatic brain injuries. The development of techniques to model population-wide anatomical variability will provide insight into the importance of the fit of protective gear.

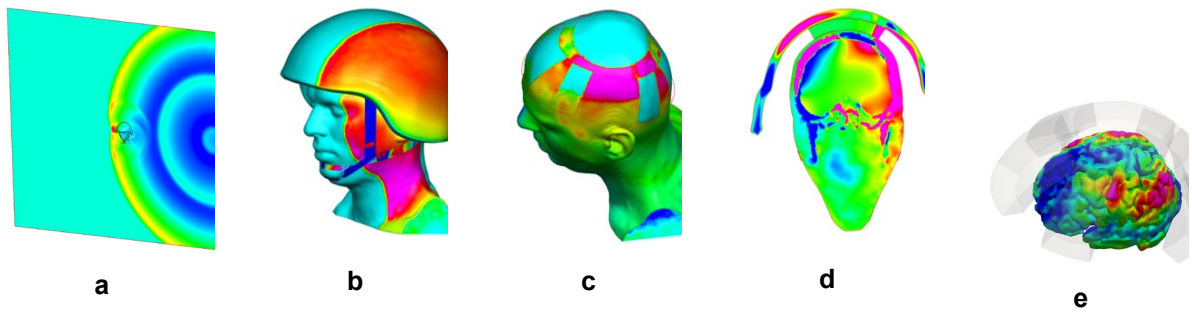


Figure 1. Selected snapshots of side blast on head and helmet system: a) blast reflection and diffraction around head and helmet, b) blast overpressure on head and helmet, c) blast overpressure beneath helmet and between pads, d) pressure in head and helmet system at coronal plane, e) maximum pressure on brain (7-pad suspension in transparent view).

Title: Stochastic Methods for Uncertainty Quantification in Computational Mechanics

Author(s): K. Teferra and R. Saunders

Affiliation(s): Naval Research Laboratory, Washington, DC

CTA: CSM

Computer Resources: HPE SGI 8600 [AFRL, OH], [NAVY, MS]; Cray XC40/50 [ERDC, MS]

Research Objectives: The research objective for the work in FY20 is to predict the microstructure evolution of additively manufactured (AM) 316L stainless steel. Additive manufacturing is a promising materials-processing technique because of its ability to tailor part geometry. However, being a new processing technique that has a significantly different thermal history than traditional, wrought-processing techniques, the effect on material microstructure and properties is not established at the level of reliability required for design standards. Understanding the effect of heat source-processing parameters on the temperature field and microstructure evolution falls within microstructure characterization, which is a necessary and essential component of material accreditation. Our goal is to be able to model and simulate this process in order to establish validated, predictive modeling capability such that rapid assessment of build strategies can be made.

Methodology: This work focuses on implementing modifications to the cellular automata finite element (CAFE) model necessary to make it optimal for simulating solidification of AM metals in order to simulate large enough (on the order of $0.5\text{--}1\text{ cm}^3$) polycrystalline microstructures such that crystallographic texture can be analyzed sufficiently. A separation of temporal scales is proposed such that solidification analysis is treated independently as subcycles within each discrete time step associated with the temperature field. It is observed that a very small portion of the simulation domain is active during a given time step. This region is identified in each time step and the CAFE analysis is distributed among all the system processors. Through these improved efficiencies, large polycrystalline microstructures are simulated for stainless steel by achieving the parallel scalability not achievable without the modifications.

Results: Large polycrystalline microstructures are simulating for AM 316L processed through laser powder bed fusion. Material properties are derived from its composition as well as microstructural configuration, which depends on the processing technique used in fabrication. Common laser scan patterns and laser parameters, including scan speed and laser power, were analyzed. Simulations using 144 processors take on the order of 35 hours to simulate domains with voxel size of [300, 300, 500]. Figure 1 shows results demonstrating the parallel scalability as well as representational microstructure morphology and crystallographic statistics via pole figures.

DoD Impact/Significance: Enhanced structural material performance in terms of durability and strength-to-weight ratio, as well as manufacturability are essential ingredients toward transforming fleet capabilities. Additive manufacturing (AM) may eventually become a commonplace manufacturing technique for both military and civilian applications. Understanding the relationship between AM processing parameters and microstructure morphology can provide guidance to material designers to achieve manufacturing of materials with desired properties.

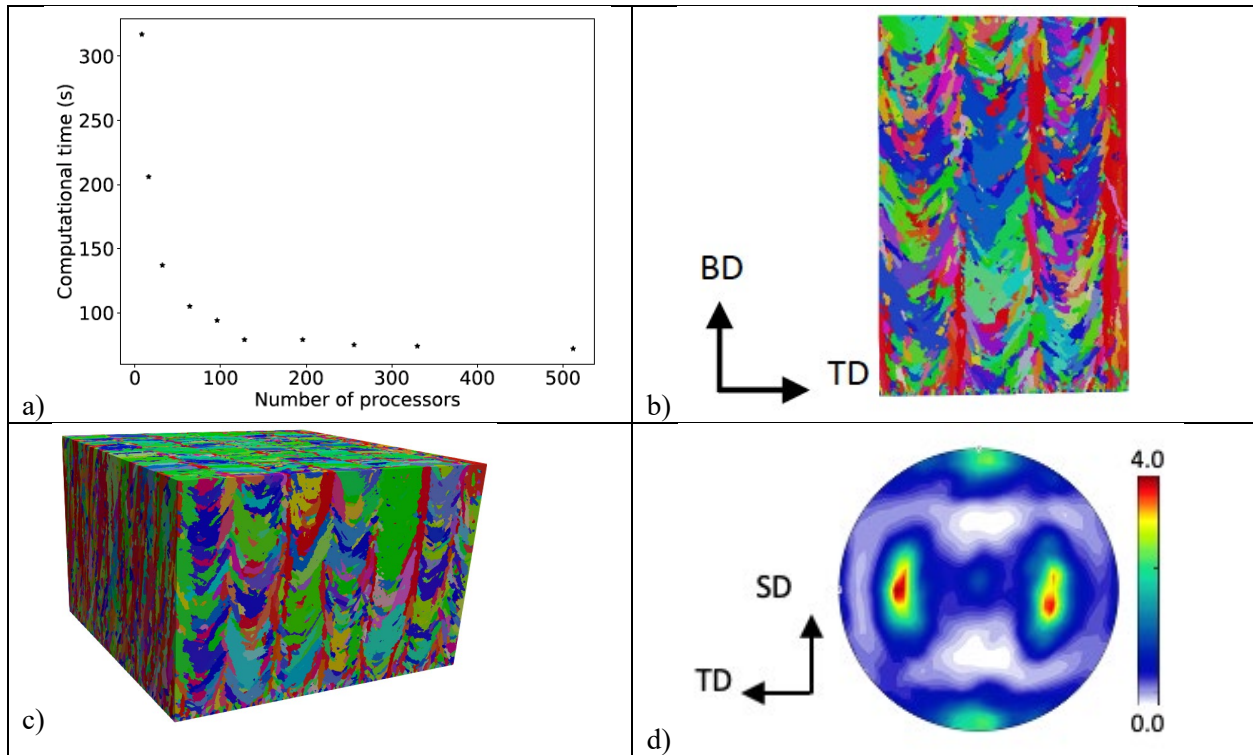


Figure 1. Results of a cellular automata finite element simulation. a) Plot of number of processors versus time to simulate one time step, demonstrating parallel scalability, b) Scan direction cross section of back-and-forth laser pattern, c) Isometric view of simulation, d) $\langle 0 0 1 \rangle$ pole figure of sample.

Title: Geometric, Constitutive and Loading Complexities in Structural Materials

Author(s): S.A. Wimmer¹, R.N. Saunders¹, A. Arcari², P. Brewick¹, H. Ryou¹, and J.G. Michopoulos¹

Affiliation(s): ¹Naval Research Laboratory, Washington, DC; ²Excet, Inc., Springfield, VA

CTA: CSM

Computer Resources: HPE SGI 8600 [AFRL, OH], [NAVY, MS]; SGI ICE X [AFRL, OH]

Research Objectives: The research strives to develop rational bases and mathematical descriptions of complex material responses for structural and novel evolving materials. Structural integrity and life cycle evaluations require an understanding of material responses. Analytical models and techniques cannot describe complex materials and often do not account for interactions, complex geometries, or multiphysics loading. Finite-element methods are used to develop models involving multifunctional materials, novel evolving materials, and multiphysics. In order to accurately model the nonlinear response of conventional structural materials, rate dependence, large deformation, and damage-accumulation mechanisms must be understood and represented accurately. The performance of the overall structure or system also is examined via parameters such as kinematics, geometric complexities, loading path dependencies, and interaction between loading types.

Methodology: The project uses finite-element methods extensively. Nonlinear material constitutive response features are highlighted in much of the work. Implicit and explicit solutions methods are used as appropriate. The primary finite-element code used is ABAQUS. Coupled material responses, such as electric-thermal or electrical-mechanical-thermal, are exercised for evaluation of these effects. Model development is done with CUBIT, ABAQUS/CAE, ScanIP, or in-house software. Large run times and large model sizes are often required for the multistep nonlinear finite-element analysis jobs.

Results: This project involves work in several topical areas. Work has been performed on creating image-based microstructural models, modeling multilayer ceramic structures, modeling stress corrosion cracking, modeling biofoulants, and modeling transparent armor delamination. Representative results for the topic of image-based microstructural modeling are discussed. Process-structure-property (PSP) linkages are one of the most sought-after goals in additive manufacturing (AM), especially at the microscale, where grain structures of AM components are vastly different from their conventionally manufactured counterparts. To represent the structure-property linkages, AM-like microstructural representative volume elements (RVEs) (Fig. 1a) are generated and simulated using crystal plasticity finite element (CPFE) modeling in ABAQUS. The result is a stress-strain response that can be homogenized over grains in the RVE or the whole RVE (Fig. 1b). In order to build a data-driven model, the former representation is selected to increase the amount of available data, and this is done for 50 different RVEs (Fig. 1c). From this data, 70% is selected for training a functional Gaussian process and the other 30% is withheld for model evaluation. The mean results of the trained model on the withheld data are shown in Fig. 2a along with a representative prediction of an individual grain response. The mean result is nearly indistinguishable from the mean of the crystal plasticity data. Figures 2b–2d show the application of the trained model on previously unseen RVEs and show high levels of accuracy. The CPFE responses took 60–80 hours of 48 CPUs on AFRL’s Mustang, while the fGP took less than a minute on a standard laptop.

DoD Impact/Significance: The prediction of full PSP linkages could enable online prediction of AM part properties while being built. This will allow certifiable parts to be printed and used as replacements outside of a laboratory or a traditional manufacturing environment, e.g., shipboard AM machines to print replacement parts quickly while at sea. Furthermore, a data-driven approach aids in the determination of the inverse property-process relationship to create parts with previously unattainable properties.

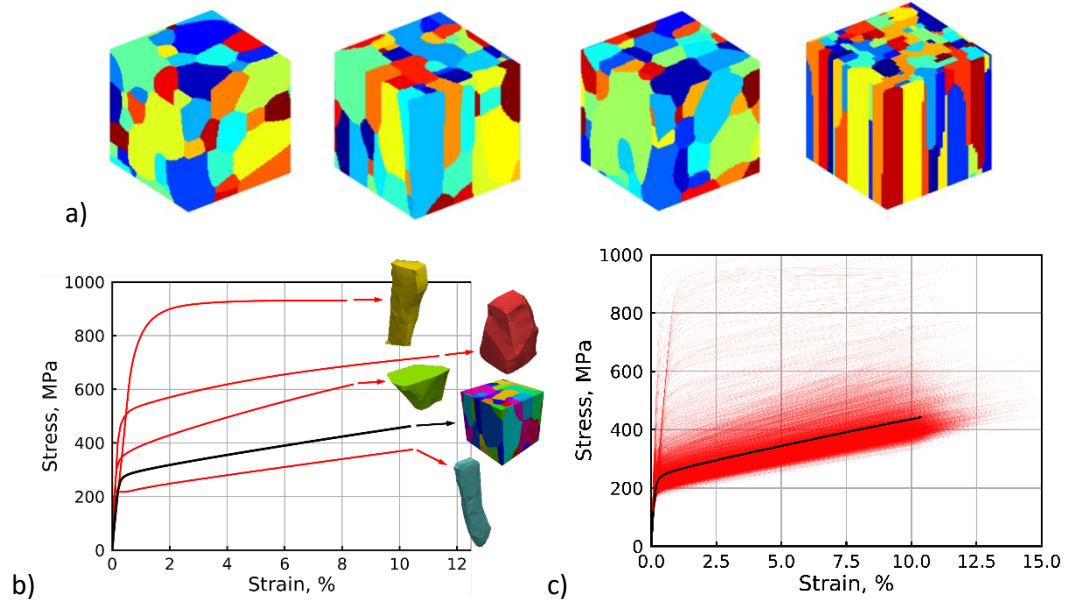


Figure 1. (a) Four sample RVEs representing features seen in AM microstructures, (b) stress-strain response homogenized over the whole RVE (black) and over grains in the RVE (red), and (c) the grain-homogenized stress-strain data used for model training

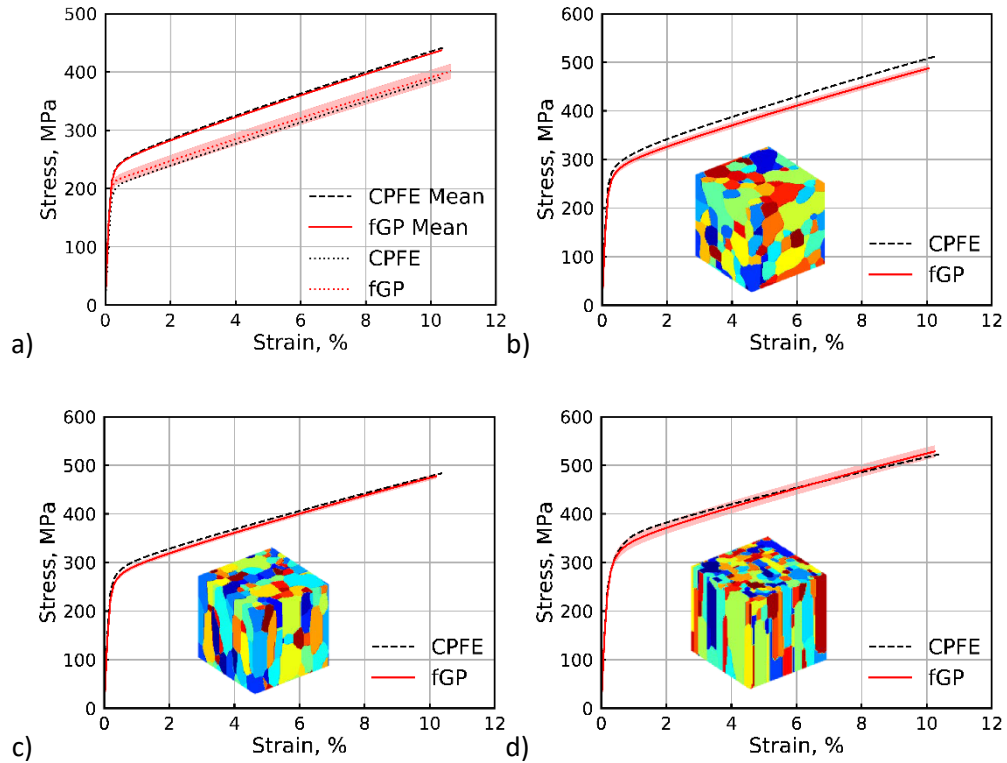


Figure 2. (a) Mean fGP prediction with 95% prediction interval for all withheld data along with a representative prediction of an individual grain response. Stress-strain results for three previously unseen RVEs with (b) equiaxial, (c) elongated, and (d) highly elongated microstructures.

THIS PAGE INTENTIONALY LEFT BLANK

CFD

Computational Fluid Dynamics

CFD covers high-performance computations whose goal is the accurate numerical solution of the equations describing fluid motion and the related use of digital computers in fluid dynamics research. CFD is used for basic studies of fluid dynamics for engineering design of complex flow configurations and for predicting the interactions of chemistry with fluid flow for combustion and propulsion. It is also used to interpret and analyze experimental data and to extrapolate into regimes that are inaccessible or too costly to study. Work in the CFD CTA encompasses all Reynolds number flow regimes and scales of interest to the DoD. Incompressible flows are generally slow (e.g., governing the dynamics of submarines, slow airplanes, pipe flows, and air circulation) while compressible flows are important at higher speeds (e.g., controlling the behavior of transonic and supersonic planes, missiles, and projectiles). Fluid dynamics, itself, involves complex physics, such as boundary layer flows, transition to turbulence, and turbulence dynamics that require continued scientific research. CFD also must incorporate complex additional physics to deal with many real-world problems. These effects include additional force fields, coupling to surface atomic physics and microphysics, changes of phase, changes of chemical composition, and interactions among multiple phases in heterogeneous flows. Examples of these physical complexities include Direct Simulation Monte Carlo and plasma simulation for atmospheric re-entry, microelectromechanical systems (MEMS), materials processing, and magnetohydrodynamics (MHD) for advanced power systems and weapons effects. CFD has no restrictions on the geometry and includes motion and deformation of solid boundaries defining the flow.

Title: Impact of Foam and Aerosol Dynamics on Fire, Explosion Safety, and Suppression (Mechanisms of Water Mist Suppression of a Burning Solid Surface)

Author(s): X. Zhuang¹ and R. Ananth²

Affiliation(s): ¹ASEE Postdoctoral Fellow, Naval Research Laboratory, Washington, DC; ²Naval Research Laboratory, Washington DC

CTA: CFD

Computer Resources: SGI ICE X [AFRL, OH]

Research Objectives: The objective of this work is to develop computational models to understand differences among perfluorocarbon, siloxane, and glycoside surfactants and their effects on heptane-water interfacial structure, packing density, and other properties.

Methodology: The molecular dynamics (MD) simulations were performed on surfactants to simulate heptane/surfactant-monolayer/water interface with constant number of molecules, pressure, and temperature (*NPT*) ensemble. NAMD is used to run the MD simulations, and VMD, CHARMM, and Python were used for the trajectory analyses and properties calculations. A large variety of siloxane surfactants were studied to investigate the effects of changes to surfactants' tail and head structures on the interfacial properties relating to lamella stability and fuel/surfactant packing at the interface. Besides pure surfactants, surfactant mixtures also were studied to investigate their effect on interfacial properties.

Results: MD simulations were performed to predict a variety of interfacial properties. Packing of surfactants at an interface are quantified by area per molecule, order parameter, the number of hydrogen bonds, and the heptane atomic number density, which may be related to heptane transport rate. We also calculated the ratio of number of heptane fuel molecules to surfactant molecules, which may be related to degradation rate. Figures 1a and 1b show the interfacial structures for pure surfactants and binary mixtures with an alkyl-glycoside surfactant, respectively. We found that the packing of pure capstone (fluorocarbon surfactant) is tightest and most ordered, and that the monoglycoside packed tighter and more ordered than diglycoside. Pure trisiloxane surfactant has the loosest packing and is relatively less ordered, which agrees with the surface area per molecule A . The smaller the A , the higher the packing density. Capstone has the smallest A , followed by mono- and diglycosides, and trisiloxane has the highest A . The pure capstone has the least penetration of heptane into the monolayer, followed by mono- and diglycosides, and pure trisiloxane has the most heptane penetration lengths. A mixture of capstone with monoglycoside (ratio 3:2) packs more tightly and also has less heptane penetration than either pure capstone or the monoglycoside. Even though pure trisiloxane has a large A , the area per molecule decreased significantly when the trisiloxane is mixed with monoglycoside, and a similar trend is found in heptane penetration lengths.

DoD Impact/Significance: Per- and polyfluoroalkyl substances (PFAS) in aqueous film forming foams (AFFF) for firefighting pose environmental and health problems. Therefore, PFAS must be replaced as required by the National Defense Authorization Act (NDAA passed by US Congress in 2020). The challenge is that while fluorine-free foams can be much more environmentally friendly, they do not currently match the high fire-suppression performance of PFAS for pool fires. Computational models of fluorine-free siloxane surfactants are developed to optimize their molecular structures for increased packing at an interface. Increased packing can create better barriers for fuel traveling through a foam layer and increased fire suppression. The MD simulations provide structural features of potential surfactants for synthesis and experimental investigations, and facilitate the development of environmentally safe and more effective firefighting foams.

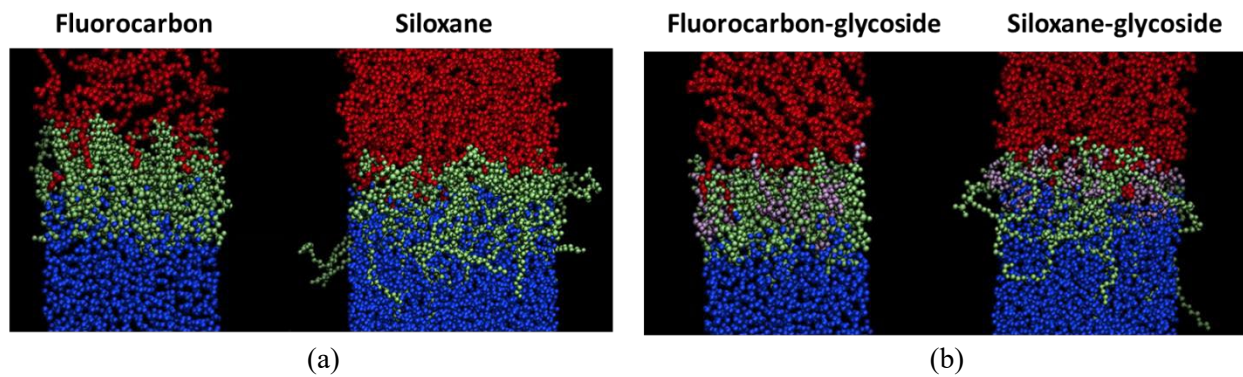


Figure 1. MD predictions of heptane-water interfacial structures with surfactants at 25 °C: (a) single component zwitterionic perfluorocarbon-sulfonamide alkylbetaine vs, OH-terminated polyoxyethylene-trisiloxane ($X=OH$, $n=10$), (b) two-component mixtures with nonyl-monoglycoside. Water, heptane, perfluorocarbon, trisiloxane, and glycoside surfactants are shown in blue, red, green, green, and pink spheres, respectively.

Title: Simulations of Laser-plasma Interactions and the Radiation Hydrodynamics of High-velocity Laser-accelerated Matter

Author(s): J.W. Bates, A.J. Schmitt, and K. Obenshain

Affiliation(s): Naval Research Laboratory, Washington, DC

CTA: CFD

Computer Resources: HPE SGI 8600 [AFRL, OH]; Cray XC40 [ARL, MD]; Cray XC40/50 [ERDC, MS]

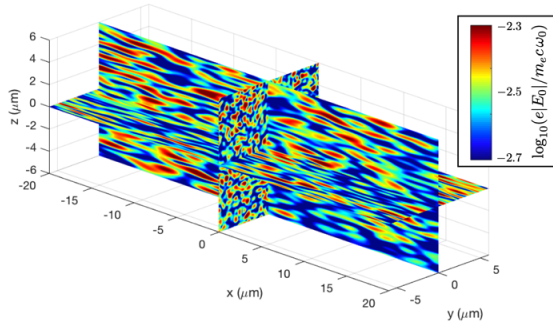
Research Objectives: The two principal obstacles to thermonuclear fusion with laser-driven implosions are hydrodynamic and laser-plasma instabilities. The objective of this research is to gain a better understanding of the physics underlying these phenomena and also to develop practical strategies for their mitigation using the numerical codes LPSE, FastRad3D and ASTER.

Methodology: LPSE is a wave-based, massively parallel computer code designed to model laser-plasma instabilities, which can scatter laser light away from inertial-confinement-fusion (ICF) targets before its energy gets absorbed and also can generate suprathermal electrons, which can preheat the thermonuclear fuel and can spoil high fusion gains. The most significant varieties of laser-plasma instabilities for ICF today are: two-plasmon decay (TPD), stimulated Raman scattering (SRS), stimulated Brillouin scattering (SBS) and cross-beam energy transfer (CBET) — all of which can be modeled with the LPSE code. The level of physical detail in LPSE is intended to lie between more fundamental particle-in-cell codes and full-scale radiation-hydrodynamic codes such as FastRad3D and ASTER, which are used to simulate full ICF implosions. Like LPSE, FastRad3D and ASTER are massively parallel codes, and while they do not account for laser-plasma instabilities, they do model a variety of other complex physical processes important for laser fusion such as laser absorption, radiation transport, thermonuclear burn and hydrodynamic instabilities. We are using all three of these codes in an effort to improve our understanding of the physics of ICF implosions and to develop target designs that are less susceptible to the deleterious effects of both hydrodynamic and laser-plasma instabilities.

Results: Our primary results for FY2020 were obtained using the LPSE code in three spatial dimensions to model beams on the OMEGA laser facility at the University of Rochester. These simulations predict that CBET can be quenched among overlapped, frequency-tripled, Nd:glass laser beams with both spatial smoothing and a Gaussian bandwidth of about 8 THz ($\Delta\omega/\omega_0 \sim 1\%$, where $\Delta\omega/2\pi$ and ω_0 are the laser bandwidth and angular frequency, respectively); see Fig. 1. As part of this study, we also demonstrated that “wavelength detuning” using three discrete “colors” of narrowband laser light — a technique that is currently available on large-scale laser facilities like the National Ignition Facility — can suppress CBET to an extent, but its efficacy plateaus once the frequency separation of the lasers greatly exceeds the resonance width of the CBET instability. Although the bandwidths of existing high-power lasers are too small to suppress CBET directly, experimental efforts are underway to develop broadband laser drivers for ICF applications. The results of our simulations of CBET have helped to justify the necessity for such laser development and also to quantify the bandwidth levels that are needed. It is expected that broadband lasers will be beneficial for mitigating other varieties of laser-plasma instabilities as well, which is a subject of ongoing research.

DoD Impact/Significance: Suppression of hydrodynamic and laser-plasma instabilities will expand the design space available for viable ICF target designs, which will benefit the National ICF program and auxiliary research efforts related to stockpile stewardship.

(a)



(b)

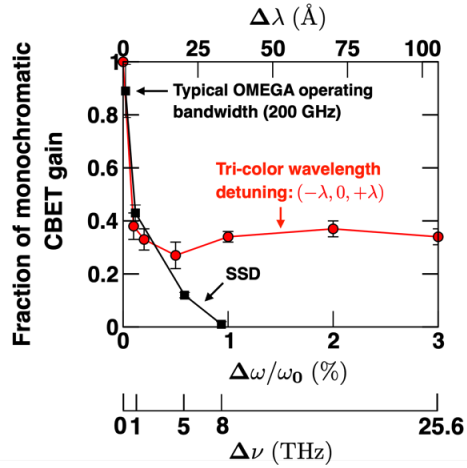


Figure 1. LPSE simulation results modeling cross-beam energy transfer (CBET) on the OMEGA laser. The plot in (a) shows the three-dimensional laser-speckle pattern created in a small volume of an ICF plasma by a “hex” of six, overlapped monochromatic beams from OMEGA emanating from the left side of the simulation box (with a total intensity of 7×10^{14} W/cm²) and directed along the positive x-axis. Because the plasma flows supersonically in the negative-x direction, energy can be transferred resonantly from these beams to a counterpropagating probe laser (not shown); the amplified intensity of the probe laser exiting the left boundary then determines the CBET gain, which is plotted in (b) for lasers with different categories and amounts of bandwidth. The black curve in (b) shows the results for beams smoothed by spectral dispersion (SSD), which is the form of bandwidth used on the OMEGA laser. To fully quench CBET, our simulations predict that an SSD bandwidth of at least 8 THz would be required, which is significantly larger than what is currently possible on OMEGA, but may be achievable in the future by exploiting certain nonlinear optical processes. Note that the data points shown in (b) are averages of five-run simulation ensembles to account for variations in random speckle patterns and polarization states of the lasers and error bars denote one standard deviation from the mean value.

Title: Flame Acceleration and Deflagration-to-Detonation Transition in Obstructed Channels

Author(s): V.N. Gamezo¹ and A.Y. Poludnenko²

Affiliation(s): ¹Naval Research Laboratory, Washington, DC; ²University of Connecticut, Storrs, CT
CTA: CFD

Computer Resources: HPE SGI 8600, SGI ICE X [AFRL, OH]; SGI ICE X [ARL, MD]; Cray XE6m, Cray XC40/50 [ERDC, MS]

Research Objectives: Model, understand, and predict complex reactive-flow phenomena leading to the detonation initiation, including the deflagration-to-detonation transition (DDT).

Methodology: We study properties of high-speed turbulent flames and transition to a detonation by computing the flame acceleration in obstructed channels. The computations are performed using the reactive CFD code ALLA, which solves compressible reactive Navier-Stokes equations on a dynamically adapting Cartesian structured mesh. The adaptive mesh refinement (AMR) is implemented on a cell-by-cell basis using the fully threaded tree data structure. The mesh refinement is dynamically controlled by gradients of density, pressure, velocity, and composition. The advective fluxes are computed in a directionally split manner using an explicit Godunov-type numerical method incorporating the Colella-Glaz Riemann solver. The method is second-order accurate in both space and time. Viscous, thermal, and diffusion fluxes are computed using second-order finite differences. The reactive terms are added using the operator-splitting technique. The mass fraction and corresponding energy increments for the one-step Arrhenius kinetics are computed using the analytical solution of the reaction rate equation at constant density and temperature. ALLA allows stationary solid bodies of an arbitrary shape to be embedded in the computational domain using the staircase solid boundaries that are refined to the level $L_{MAX}-1$, where L_{MAX} is the finest level of the adaptive mesh.

Results: We analyzed flame acceleration and DDT in stoichiometric methane-air mixtures in channels with obstacles for a range of scales and obstacle configurations. We varied the channel height d in the range of 0.17–3 m, the blockage ratio br in the range of 0.3–0.7, and the scaled distance between obstacles L/d in the range of 0.5–1.5 to study their effects on the distance to DDT, L_{DDT} , and the distance to the shock-flame complex, L_{SF} . The results show two main effects. The increase of br and the decrease of L/d promote the flame acceleration and reduce L_{SF} and L_{DDT} . Some configurations with higher br and smaller L/d prevent detonation development, even though local detonations may form in isolated pockets of unburned material between obstacles. These local detonations appear behind the leading edge of the flame and cannot spread downstream. As a result, the leading shock and the flame never merge, and continue to propagate as a quasi-steady-state shock-flame complex. This complex is characterized by a strong shock followed by a thick, compressed layer of unburned material and a turbulent flame. A collision of this complex with solid structures generates high pressures and strong reflected shocks that can ignite a detonation. This detonation propagates in a shock-compressed material and results in extremely high wall pressures exceeding pressures produced by a regular detonation by a factor of 5 to 10. Both L_{DDT} and L_{SF} are important measures of a destructive potential for a particular reactive mixture and channel geometry. The distance L_{SF} at which the shock-flame complex forms is particularly relevant for channels with high br where L_{SF} can be significantly shorter than L_{DDT} . For the maximum computed channel height 3 m, which is typical of a coal mine tunnel, the minimum $L_{DDT} = 28$ m was observed for $br = 0.3$, $L/d = 0.5$, and the minimum $L_{SF} = 18$ m was extrapolated for $br = 0.7$, $L/d = 0.5$.

DoD Impact/Significance: Understanding flame acceleration and DDT provides insights for further development of turbulent combustion models for large-eddy simulations of high-speed regimes. These models are critical for the design of the next generation of propulsion and energy conversion systems, such as scramjet engines, rotating-detonation engines, high-pressure turbines, etc. They also can be used to predict effects of accidental gas explosions in industrial environments and can help mitigate these effects.

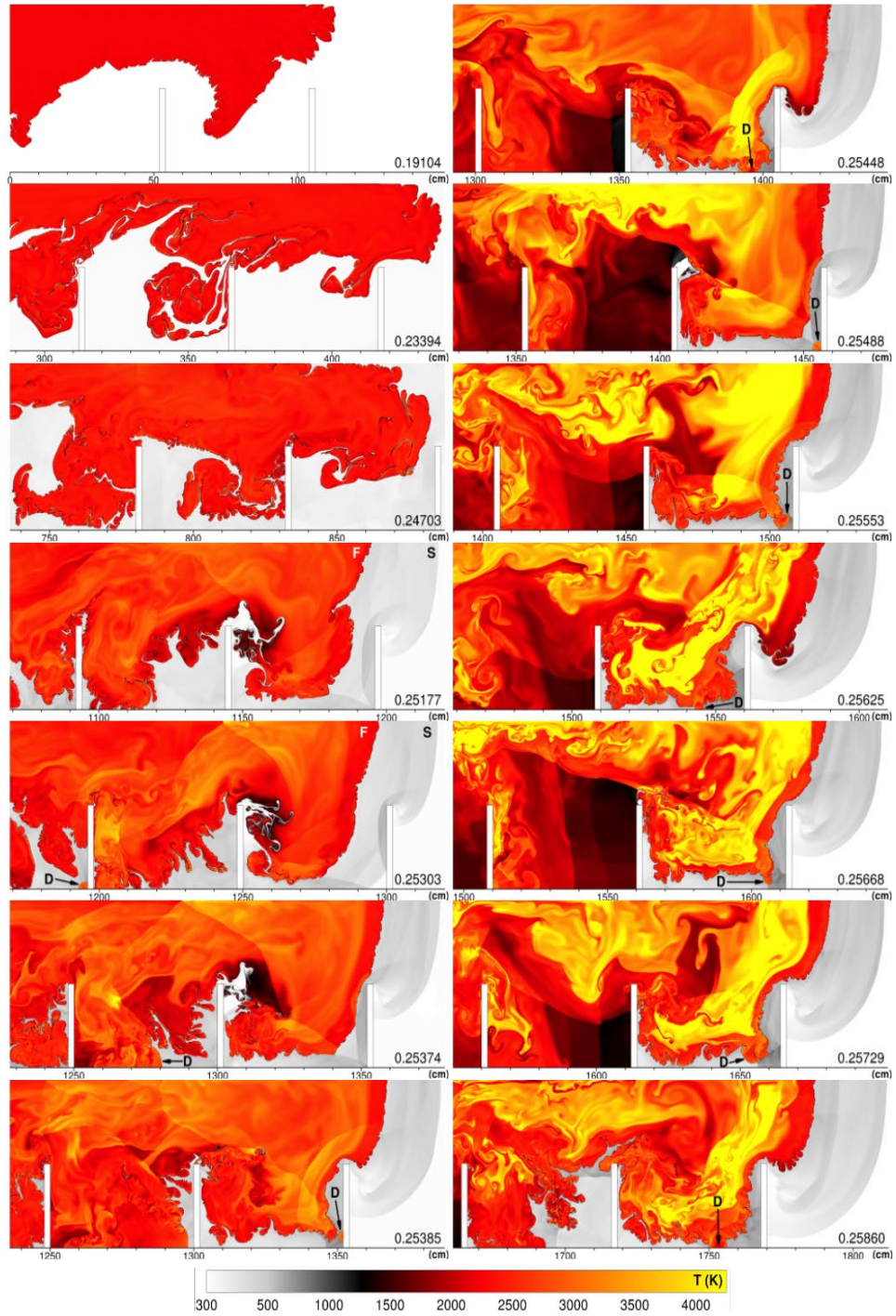


Figure 1. Time sequence of temperature fields showing the flame evolution in channel with obstacles, including the propagation of shock (S) - flame (F) complex, and the formation of isolated detonations (D).

Title: Hypersonic Reactive Flow Modeling
Author(s): G.B. Goodwin and C.L. Bachman
Affiliation(s): Naval Research Laboratory, Washington, DC
CTA: CFD

Computer Resources: SGI ICE X [ARL, MD]

Research Objectives: The objective of this research is to characterize the effect of a high-speed flowfield and unsteady/nonuniform boundary conditions on the ignition and combustion processes in hypersonic airbreathing engines. This research encompasses a broad range of system types, sizes, and scales, from smaller combustors used for analyzing the fine details of the underlying combustion physics to larger applied systems such as ramjets and supersonic combustion ramjets (scramjets), in which quantification of combustor efficiency and reliability is a primary goal.

Methodology: One of the predominant challenges in using air-breathing engines for hypersonic flight (typically greater than five times the speed of sound) is that the extremely fast flow speeds through the engine present a challenging environment for reliable ignition of the fuel and stable combustion. One method for combusting the fuel in the engine within the very short time scales is to use a supersonic combustion wave, a detonation, to rapidly burn the high-speed flow of fuel-air mixture. This hypersonic propulsion concept is called an oblique detonation wave engine (ODWE). The research conducted under this subproject uses high-fidelity computational fluid dynamics (CFD) to simulate the high-speed, chemically reacting flow in the combustors of an idealized ODWE. A large study was conducted in which the effect of fuel-air mixture conditions, engine geometry, and boundary conditions on the ignition and stability of oblique detonation waves was examined.

Results: In the simulation results shown in Fig. 1, the premixed fuel (ethylene, in this case) and air are flowing in from the left boundary at a temperature of 700 K, a pressure of 1 atm, and a speed of Mach 5. The flow impacts a wedge surface (white region in lower right) and ignites as the fuel-air mixture's temperature increases dramatically following impact with the wedge. The figure shows several combustion phenomena occurring after the ignition event. Near the leading edge of the wedge there is a detonation wave, shown by the significant jump in temperature. This is followed by an induction region where the fuel-air mixture has not ignited, but is heated as it passes through a shock wave. The preheated mixture then reacts as it passes through a deflagration front (subsonic combustion wave). Some of the preheated mixture does not pass through the deflagration front and instead passes through an underdriven detonation wave, or a detonation that is propagating at a speed less than its equilibrium speed. Finally, an oblique detonation wave forms (labeled ODW), which processes the fuel-air mixture that has not already chemically reacted nor passed through the induction region. Subsonic regions of the flow are marked in the numerical schlieren (density gradient) contours.

DoD Impact/Significance: The impact of this research is an increased fundamental understanding of the fine-scale ignition and combustion physics in hypersonic airbreathing engines. In particular, ODWE are difficult to study experimentally with the resolution that is achieved in high-fidelity CFD simulations. Simulating these environments to understand ignitability, combustion stability, and efficiency is a crucial step toward development of a flight-ready system.

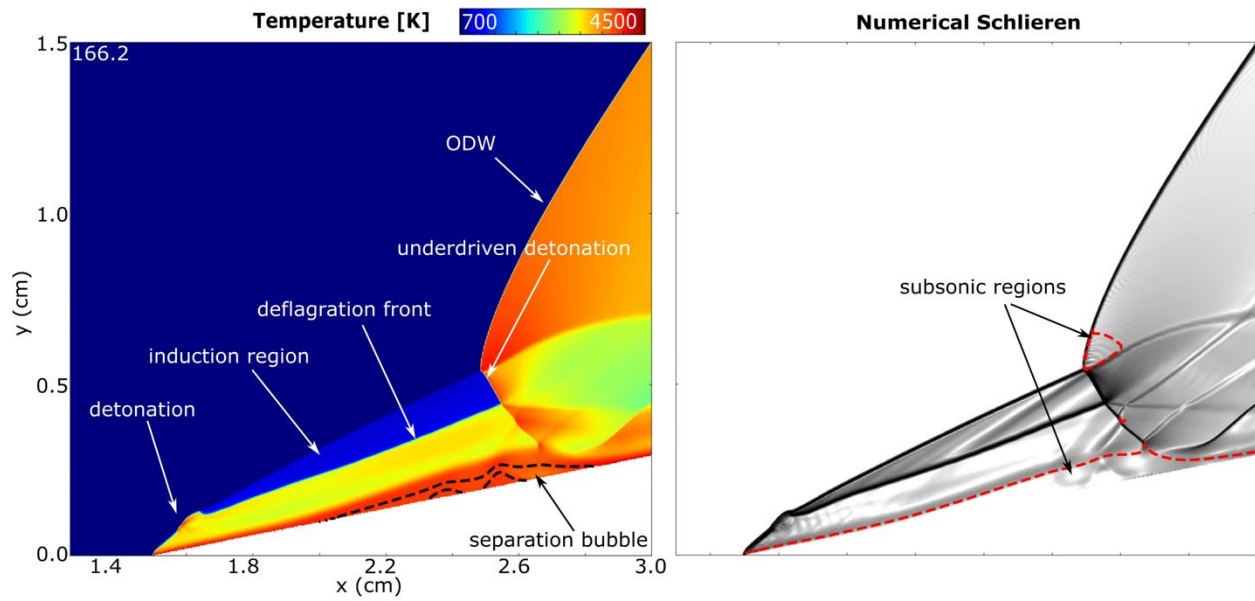


Figure 1. Results from a computational fluid-dynamics simulation of an oblique detonation wave combustor in a Mach 5 flow of premixed ethylene and air are shown. The left image shows temperature contours and the right shows numerical schlieren, or density gradient. Several different combustion waves were observed at this step in the simulation, as labeled in the figure.

Title: Advanced Two Phase CFD Model
Author(s): T.D. Holman
Affiliation(s): Naval Research Laboratory, Washington DC
CTA: CFD

Computer Resources: Cray XC40 [ARL, MD]

Research Objectives: Two-phase heat transfer devices are the state of the art in thermal system architecture, especially the Loop Heat Pipe (LHP) architecture. Because they have no moving parts, these devices are ideal for use in space environments. Numerically simulating the internal flow of two-phase heat-transfer devices will give a better understanding of their behavior in different environments in which they are tested and operate. The primary objectives are to verify physical oscillation mechanisms, designed to minimize instability regions, and to implement control methods to mitigate unavoidable instability regions through numerical modeling and experimental testing. These oscillations have been shown to precede/cause loop heat pipes to shut down inadvertently, a most undesirable occurrence that is not addressed by existing loop heat pipe theory. This inadvertent shutdown is often referred to as a loop heat pipe failure.

Methodology: Continued development of numerical and analytical models, a continued experimental program to confirm the accuracy of the analytic and numerical models, and use of these models to study and design loop heat pipes to mitigate the effects of oscillatory behavior. The end results are tools that will be utilized for design of LHPs for future space assets. The basic approach is: 1) Utilize analytical model predictions of oscillations in closed loop two-phase heat transfer systems and experience to narrow down parameter space of mechanisms that cause oscillations. 2) Mitigate unavoidable oscillations through closed-loop control. 3) Utilize the analytical and numerical models to design proof-of-concept robust LHP. 4) Test proof-of-concept robust LHP design. This is expected to be an iterative process.

Results: A third potential method for eliminating thermal fluid oscillations is to place a mechanical pump in line with the reservoir/evaporator subassembly (see Fig 1). The addition of a mechanical pump to a standard capillary-driven LHP gives the system enough pressure head that additional high-power auxiliary evaporators can be added, allowing the system to acquire and transport much more heat than a standard LHP with a single capillary evaporator. A numerical effort was started to determine the validity, stability, and pressure distribution of a pump-assisted loop heat pipe (PA-LHP). The high-power LHP was modified to include an ammonia bearingless pump in line with the LHP evaporator and three auxiliary high-power evaporators. The high-power LHP had four fans mounted to its condenser plate to reject heat from the LHP and the testing was conducted in ambient conditions. The test was conducted with and without the pump. The LHP worked solo at 300 W and 750 W with the liquid flow going through the non-operating mechanical pump without any noticeable penalty due to the pump existence. The testing confirmed the numerical predictions that the PA-LHP operates smoothly with varying heat loads on the LHP and auxiliary evaporators. Two papers have been published and all have been well received; one journal article has been written but is still under review. One patent has been submitted.

DoD Impact/Significance: A unique model has been created that can predict where oscillatory behavior in LHPs can occur and can predict the frequency/amplitude of the oscillations. The model is still being developed to add more features, but this unique tool allows NRL to design more robust loop heat pipes.

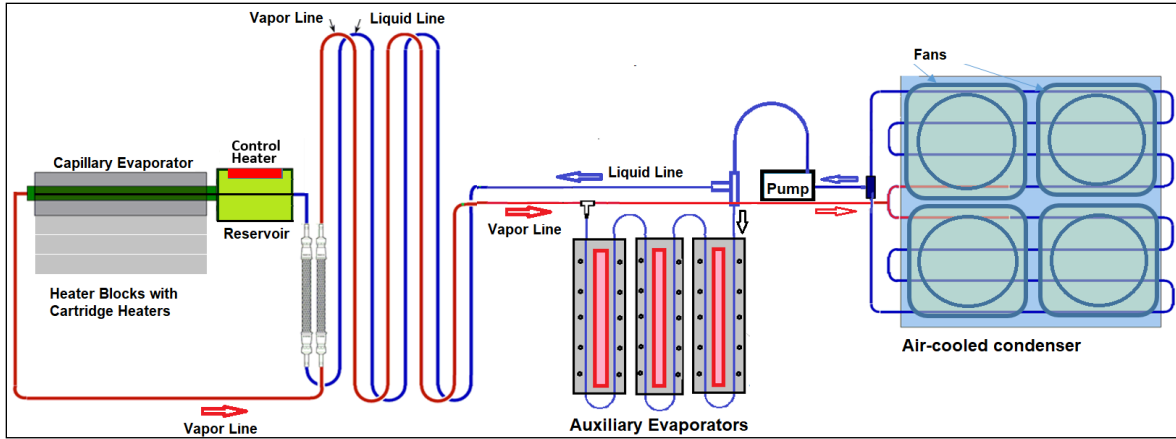


Figure 1. Top view of the numerically simulated PA-LHP under study.

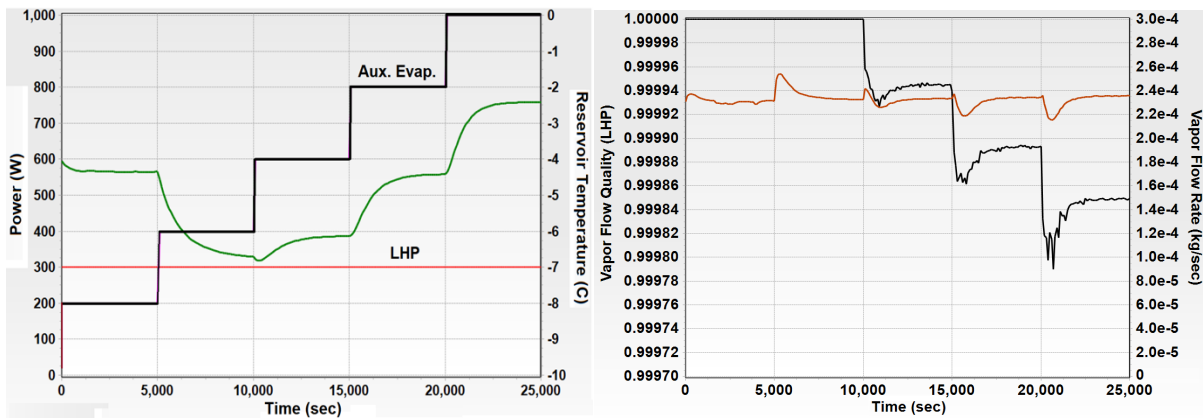


Figure 2. Reservoir temperature affected by power steps on the auxiliary evaporators (left) and variation of the LHP vapor flow quality and flow rate due to power steps on auxiliary evaporators.

Title: High-Fidelity CFD Simulations of High-Speed Flows in Realistic Atmospheric Conditions

Author(s): D.A. Kessler, R.F. Johnson, and A. Hess

Affiliation(s): Naval Research Laboratory, Washington, DC

CTA: CFD

Computer Resources: SGI ICE X [AFRL, OH], [ARL, MD]; Cray XC40/50 [ERDC, MS]; HPE SGI 8600 [NAVY, MS]

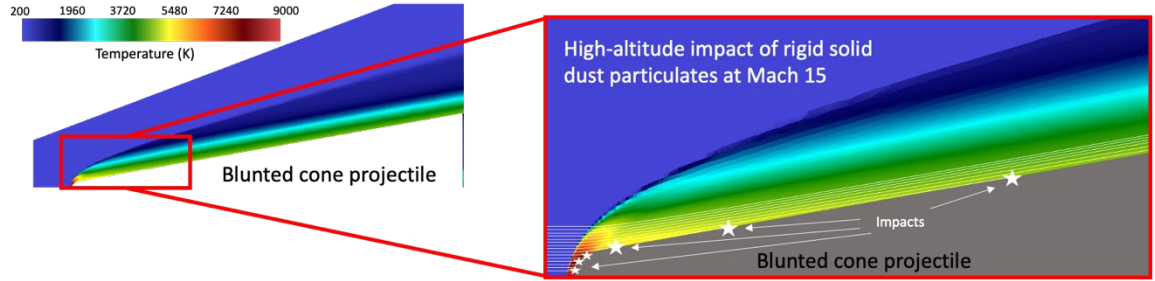
Research Objectives: Develop an improved physical understanding of how the aerodynamic performance of hypersonic vehicles changes when considering real-gas effects associated with high-altitude, high-speed flows and multiphase effects associated with interactions with atmospheric cloud formations or precipitation events.

Methodology: In this work, we are using NRL's JENRE^{®1} multiphysics tool to test the state-of-the-art physics models required for simulating two-phase hypersonic flows, including non-equilibrium energy transfer, surface ablation, non-equilibrium turbulence, high-temperature air chemistry, droplet and ice crystal breakup, and impact-mediated erosion. This requires performing high-fidelity and high-resolution simulations of the chemically reacting, two-phase flows associated with model vehicles and projectiles.

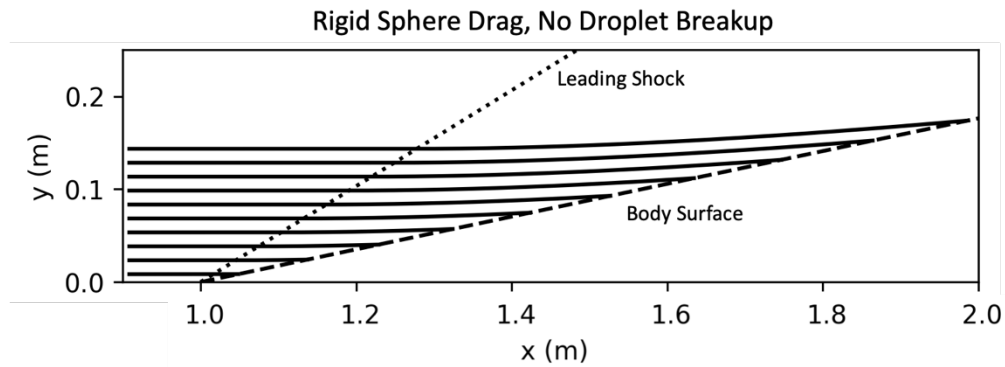
Results: Suspended particulates and droplets in the atmosphere present a significant erosion risk to vehicles traveling at high-supersonic and hypersonic speeds. During this past year, we have begun to lay the foundation for high-fidelity simulations of such phenomena by exploring and comparing common models for drag and droplet breakup. We have been considering two disparate scenarios: high-altitude, high-Mach number flows in dusty environments and low-altitude, moderate Mach-number flows in precipitating environments. In the former, the most critical physics submodel is the drag model used for the solid particles. The particle Mach number (based on the relative velocity between a particle and the background flow), particle Knudsen number (based on altitude and particle size), and the particle shape can play large roles on the computed drag and particle trajectories. Figure 1a shows the trajectories of several solid 10-micron-diameter particles in a Mach 15 flow around a blunted cone projectile as they approach and impact the body. For the latter scenario, the liquid droplets can deform and split into multiple smaller droplets, making the multiphase flow physics significantly more complex. Understanding and properly modeling the interplay between the drag and breakup models will be critical to characterizing potential impact events by the size, quantity, location, and incidence angle of the droplets. Figures 1b and 1c show the trajectories of droplets with initial diameters of 100 microns computed for a common Mach 3 flow over a sharp 10-degree wedge using two different sets of physical submodels. The resulting trajectories indicate the strong sensitivity of the likelihood of impact to these underlying models. A simplified rigid sphere model predicts 100% impact, whereas a model accounting for droplet distortion and wave-induced droplet breakup predicts droplet impact to be quite rare. Increased drag and continuous mass loss due to the fluid dynamic instabilities allow the droplets to adjust more rapidly to the changes in the background flow. While we find this to be physically-reasonable droplet behavior, it is clear that additional experimental data will be required to fully evaluate and tailor the models to give accurate impact predictions.

DoD Impact/Significance: Achieving a global prompt strike capability and countermeasures for similar technologies under development by our adversaries are critical for protecting our fleet and maintaining naval superiority. This work will provide an improved understanding of parameters critical to hypersonic vehicle performance and survivability in non-ideal operating environments.

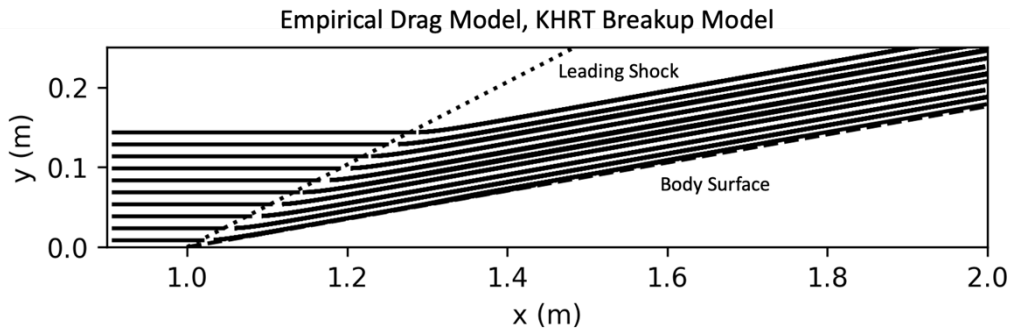
¹ JENRE[®] is a registered trademark of the Department of the Navy.



(a)



(b)



(c)

Figure 1. (a) Temperature field and rigid solid particle trajectories in a high-altitude Mach 15 flow around a blunted projectile in a dusty environment. Magnified views of the trajectories of liquid droplets through a Mach 3 oblique shock wave created by a wedge-shaped projectile using (b) a rigid sphere drag model with no droplet breakup allowed and (c) an empirical drag model for high-Mach-number flows that incorporates the effects of droplet deformation along with a model for droplet breakup based on Kelvin-Helmholtz and Rayleigh-Taylor wave stability theory. Probability of impact varies from 100% for the models used in (b) to near-0% for the models used in (c). Figures highlight the sensitivity of particulate impact prediction to underlying physical models for hypersonic flows.

Title: Jet Noise Reduction Studies

Author(s): Y. Khine

Affiliation(s): Naval Research Laboratory, Washington, DC

CTA: CFD

Computer Resources: HPE SGI 8600 [AFRL, OH]; SGI ICE X [AFRL, OH], [ARL, MD]; Cray XC40 [ARL, MD]; Cray XC40/50 [ERDC, MS]

Research Objectives: The goal of this project is to investigate and assess jet noise-reduction concepts for representative military aircraft jet engines in order to address workplace health and safety issues and environmental concerns.

Methodology: Jet noise simulations require a very large computational domain to include both the near- and far-fields for long enough duration of physical time to study the effect of noise propagation. Thus, it requires significant HPC resources to simulate realistic conditions. For this project, the NRL-developed flow solver JENRE^{®1} is used to simulate turbulent flows in nozzles. JENRE[®] is a large eddy simulation (LES) model that uses a nodal finite-element method and is implemented with multiple levels of parallelism. Both structured and unstructured meshes can be used with JENRE[®], and it has been verified to provide an ideal scalability for thousands of processors. Various jet conditions are considered for noise-reduction technology called Micro-Vortex Generators (MVGs). The height of the blade is much smaller than the nozzle-exit diameter, and hence they are called the “micro”. It is expected that applying MVGs to a military aircraft nozzle surface can possibly reduce supersonic jet noise, especially at takeoff. Many parameters play important roles in producing desired effects from using the MVGs and many cases of simulations are needed to understand the effects caused by the presence of MVGs.

Results: This work is in collaboration with University of Cincinnati (UC) and a case of interest is presented in Fig. 1. This case presents simulation of jet noise at far-field for pressure ratio of 2.7 with respect to the ambient pressure and is at the ambient temperature. The red curve labeled LES depicts the simulated results by JENRE[®] and the green curve labeled Mic presents the experimental measurements performed at the laboratory at UC. It is observed that the experimental and simulated results are in excellent agreement. The noise reduction in the upstream direction is by 6dB. Figure 2 presents the instantaneous Mach number distributions in the XY plane inside and outside the nozzle for both the baseline and the nozzle with MVGs for the same jet conditions. It is obvious that the vortex generators have a great impact on the shock cell formation inside and outside the nozzle. The downstream shock cells are significantly weakened, therefore, reducing the jet noise as the flow propagates.

DoD Impact/Significance: Hearing disability caused by the noise generated by supersonic military aircraft has been a serious concern for DoD. These studies offer better insight of the physical phenomena for different jet conditions and allow us to optimize MVGs that can provide significant reduction in noise level. This research also supports ongoing jet noise-reduction studies at other government agencies and academics.

¹ JENRE[®] is a registered trademark of the Department of the Navy.

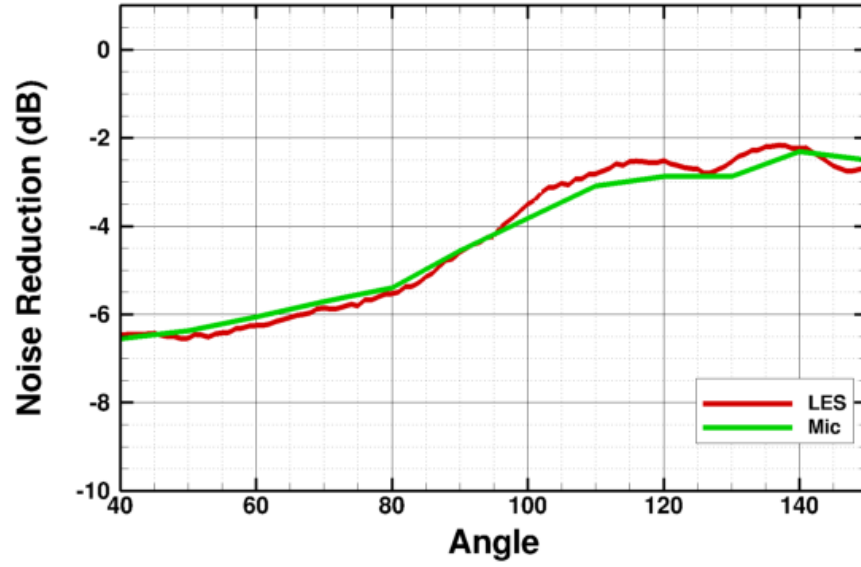


Figure 1. Comparison of the far-field noise reduction between the LES prediction by JENRE[®] and the experimental data measured in laboratory facilities of the University of Cincinnati.

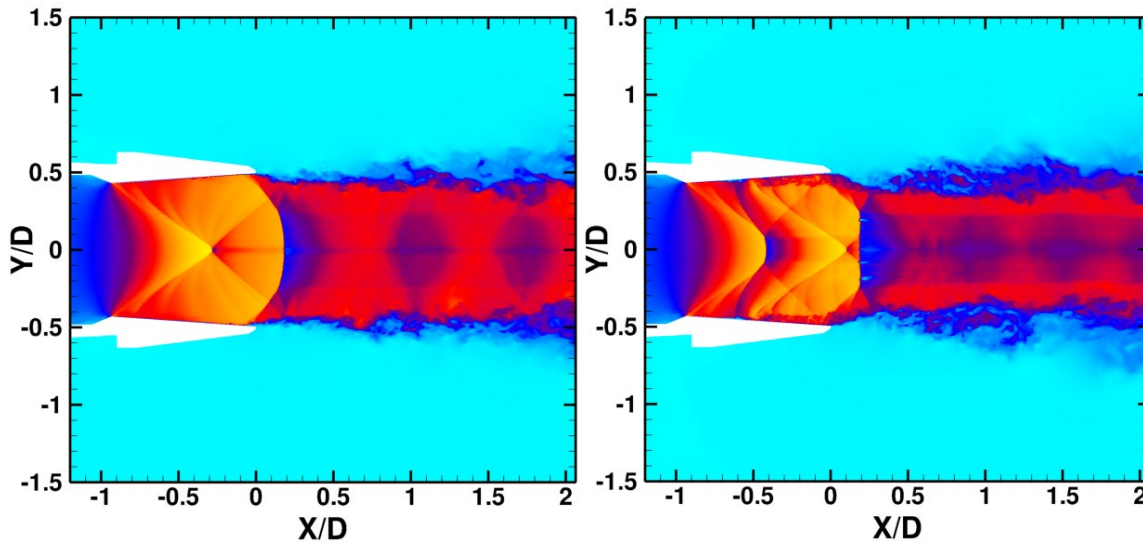


Figure 2. Instantaneous Mach number distributions. (a) Baseline nozzle. (b) The nozzle implemented with micro vortex generators (MVGs).

Title: Simulations of the Ionosphere/Plasmasphere/Thermosphere System

Author(s): J. Krall¹ and J.D. Huba²

Affiliation(s): ¹Naval Research Laboratory, Washington DC; ²Syntek Technologies, Fairfax VA
CTA: CFD

Computer Resources: HPE SGI 8600 [AFRL, OH]; Cray XC40/50 [ERDC, MS]

Research Objectives: Predict the dynamics of the ionosphere/magnetosphere environment as it relates to operational communications and navigation systems used by the warfighter. Develop a first-principles physics-based model of near-Earth space based on the NRL Code SAMI3, including understanding and predicting equatorial spread F disturbances.

Methodology: The research uses the NRL SAMI3 code, a comprehensive 3D simulation model of Earth's ionosphere/plasmasphere system, coupled to a model of the thermosphere (e.g., TIE-GCM, GITM, WACCM-X) and inner magnetosphere (e.g., RCM, CIMI) to self-consistently describe the geospace system. SAMI3 optionally includes heavy metal ions, Fe⁺ and Mg⁺, that form low-altitude ionosphere layers. These simulations use measured solar wind and irradiance data as inputs that drive the system.

Results: We have extended our simulations of metal ion dynamics in the E and F regions, showing that a) tidal wind forces can explain observed metal layers observed at Arecibo and b) these metal ion layers modify the growth of the equatorial spread F (ESF) ionosphere bubbles that often disrupt communications. This work was reported at the 2019 Fall AGU Meeting and was published in *J. Geophys. Res.* [Krall et al., 2020] and *J. Geophys. Res. Lett.* [Huba et al., 2020].

We presented the first results of a global ionosphere/thermosphere simulation study that self-consistently generates large-scale ESF plasma bubbles in the post-sunset ionosphere. The coupled model comprises the ionospheric code SAMI3 and the atmosphere/thermosphere code WACCM-X. Two cases are modeled for different seasons and geophysical conditions: the March case (low solar activity: F10.7 = 70) and the July case (high solar activity: F10.7 = 170). We find that equatorial plasma bubbles formed and penetrated into the topside F layer for the March case but not the July case. For the March case, a series of bubbles formed in the Atlantic sector with irregularity spacing in the range of 400–1200 km, rose to over 800 km, and persisted until after midnight. These results are consistent with recent GOLD observations (see Fig. 1). Calculation of the generalized Rayleigh-Taylor instability growth rate shows that the e-folding time was shorter for the March case than the July case. This research was presented at the 2020 Fall AGU meeting and was published in *Geophysical Research Letters* [Huba and Liu, 2020]. In addition to the above, SAMI3, along with the CIMI inner magnetosphere model, was used to compute effect of ring current heating on the ionosphere during a geomagnetic storm. This heating effect, which had not been modeled previously, produced a thermal oxygen ion outflow with densities in excellent agreement with observations of the so-called "oxygen torus" in the inner magnetosphere. This was reported at the 2020 GEM Summer Workshop and was published in *J. Geophys. Res. Lett.* [Krall et al., 2020].

DoD Impact/Significance: Potential protection of communication satellites and the power grid. Support of ongoing experiments in remote sensing of the space environment. Provide input to ionospheric and thermospheric models.

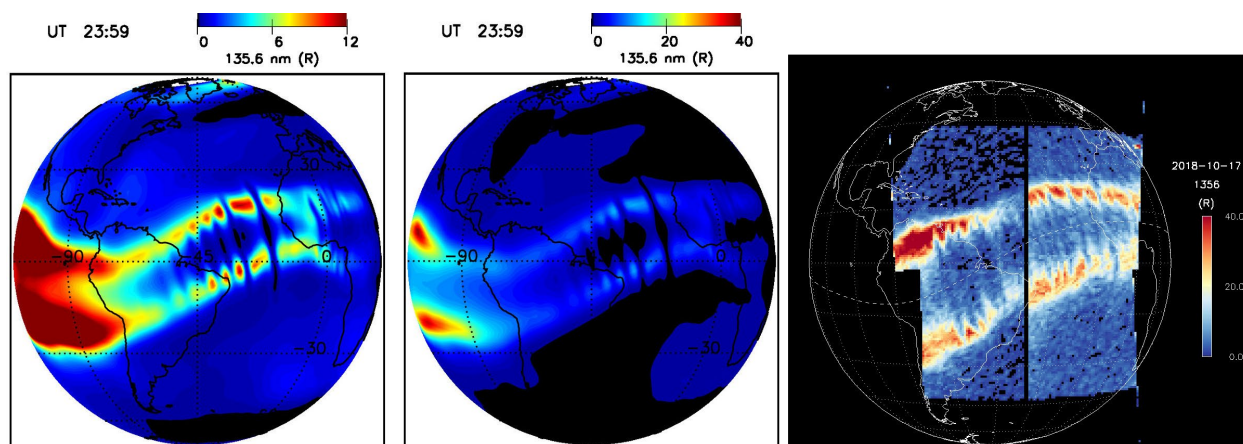


Figure 1. Comparison of 135.6 nm emissions from the simulation for the March case (left and center panels) and GOLD emission data (right panel) observed from geosynchronous orbit. The color scale in the center panel is adjusted to more closely resemble that in the data.

Title: Numerical Investigation of Advanced Military Aircraft Noise Reduction Concepts

Author(s): J. Liu and Y. Khine

Affiliation(s): Naval Research Laboratory, Washington, DC

CTA: CFD

Computer Resources: HPE SGI 8600 [AFRL, OH]; SGI ICE X [AFRL, OH], [ARL, MD]; Cray XC40 [ARL, MD]; Cray XC40/50 [ERDC, MS]

Research Objectives: Use HPC computational resources to predict details of turbulent flow structures and noise generation in supersonic exhaust jets from representative military aircraft jet engine nozzles and use this information to investigate and assess promising jet noise-reduction concepts in support of the ongoing jet noise-reduction programs.

Methodology: The flow solver is JENRE[®]¹ a Navy-based and NRL-developed nodal finite-element code. JENRE[®] can take structured meshes and unstructured meshes with arbitrary cell types and has multiple levels of parallelism: Multi-core CPUs or Multi-core GPUs, and MPI for interprocessor communication. JENRE[®] has achieved exceptional computational performance and scalability. Since using large-eddy simulations (LES) to fully resolve wall-bounded flows at high Reynolds numbers is computationally prohibitive due to the limitations of the available numerical methods and computational resources, the wall-layer model approach is used to simulate the boundary-layer effect of the wall-bounded flows. The far-field noise prediction is based on the Ffowcs Williams & Hawkins (FW-H) Surface Integral method. To simulate the high-temperature effect observed in realistic jet engine exhausts, a temperature-dependent function of the specific heat ratio is developed and implemented in JENRE[®].

Results: LES has become an important tool in developing and optimizing the jet noise-reduction technologies. LES has been used to develop and optimize the noise-reduction technology, Micro-Vortex Generators (MVGs), implemented on a model-scale F404 nozzle, which is a faceted biconic convergent and divergent nozzle made of 12 seals and flaps. Figure 1 shows some MVG implementations in a model scale F404 nozzle. As shown in Fig. 2, the axial location of MVGs greatly affects the shock-cell structure and the noise-reduction performance. Some locations even can increase the noise. The most optimized axial location is found around 30% of the seal length downstream of the nozzle throat. Figures 3(a) and 3(b) show that axial velocity fields in the cross-sectional plane at the nozzle exit for both the baseline nozzle and the nozzle where a single array of MVGs (Fig.1(a)) is implemented. The flow is not attached to the nozzle surface in the flow field (Fig. 3(a)) of the baseline nozzle, but the flow is attached to the nozzle surface in the downwash region between the neighboring pairs when MVGs are implemented (Fig. 3(b)). It is clear that MVGs reduce the boundary-layer separation near the nozzle exit. Figures 3(c) and 3(d) show the turbulence kinetic energy at a plane containing the jet axis. MVGs greatly reduce the turbulent kinetic energy, which is the noise source responsible for the peak noise radiation. Figure 3(e) shows the noise-reduction performance of four MVG configurations. The difference among these four configurations is the angle between the two blades of each MVG pair. This angle is twice of the attack angle of each blade. It is clear that the noise-reduction performance is sensitive to this angle. In addition, a noise reduction of 4 dB in the peak radiation direction (135°) is achieved.

DoD Impact/Significance: There is a growing need to significantly reduce the noise generated by high-performance, supersonic military aircraft. The noise generated during takeoff and landing on aircraft carriers has direct impact on shipboard health and safety issues. It is estimated that the US Veterans Administration pays \$4.2 billion or more for hearing-disability claims each year. The results of our work will provide better understanding of the noise production for both industrial and military aircraft, and will aid the current effort of noise reduction, especially for supersonic aircraft.

¹ JENRE[®] is a registered trademark of the Department of the Navy.

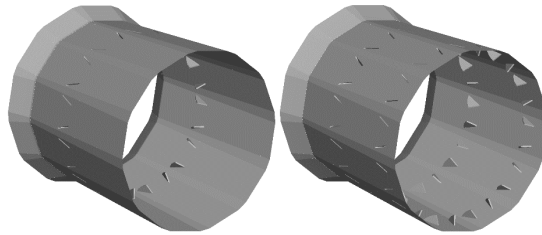


Figure 1. Two MVG implementations in a model-scale F404 nozzle. Patent pending.

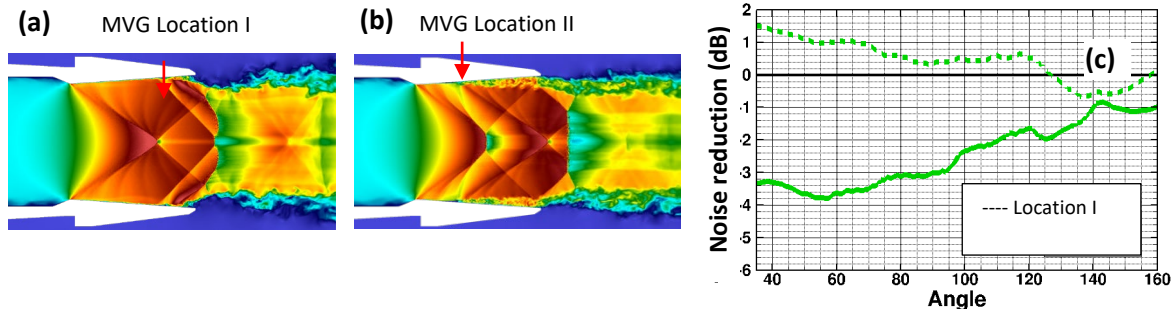


Figure 2. The impact of the MVG axial location on the shock-cell structure and the noise-reduction performance: (a) and (b) shock-cell structures; (c) noise-reduction performance

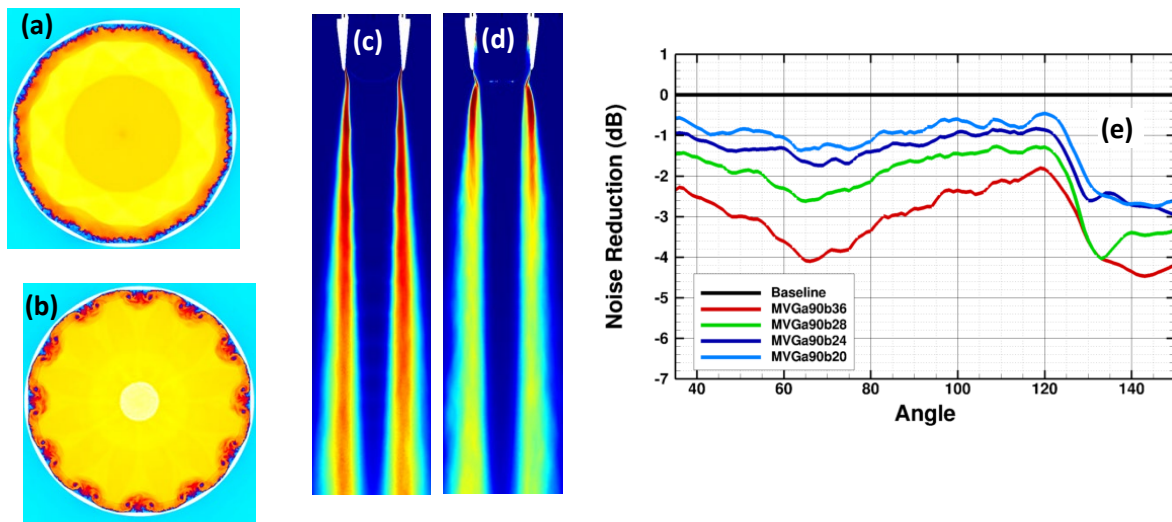


Figure 3. The impact of the MVGs on the flow field and the noise-reduction performance: (a) and (b) the velocity flow field of the baseline nozzle (a) and the nozzle implemented with MVGs (b); (c) and (d) turbulent kinetic energy of the baseline nozzle (c) and the nozzle implemented with MVGs (d); (e) noise-reduction performance of four MVG configurations.

Title: Numerical Simulations of Turbulence Impact on Optical Signal Transmission and Near-Surface Turbulence

Author(s): S. Matt

Affiliation(s): Naval Research Laboratory, Stennis Space Center, MS

CTA: CFD

Computer Resources: SGI ICE X, Cray XC40 [ARL, MD]

Research Objectives: The objective is to continue work on the computational fluid dynamics (CFD) representation of the numerical tanks that are part of the Simulated Turbulence and Turbidity Environment (SiTTE) laboratory, the large Rayleigh-Bénard tank for convective, optically active turbulence, to study optical turbulence impacts and the laminar-to-turbulent-flow tank flowSiTTE for boundary-layer dynamics and drag reduction. A large numerical wind-wave tank is designed to emulate the state-of-the-art SURge-Structure-Atmosphere INteraction (SUSTAIN) facility at the University of Miami, supporting companion laboratory experiments on near-surface turbulence and air-sea interface dynamics. The CFD results provide crucial information to the companion laboratory work: The use of a wave-like boundary condition in OpenFOAM emulates actuated boundary motion, and a volume-of-fluid multiphase model allows to solve for stresses across the air-sea interface in the wind-wave tank model. The numerical work supports development of a new underwater communications system, fiber-sensor technologies, novel methodologies and mechanisms for active boundary-layer control and drag reduction, as well as insight into the dynamics underlying near-surface turbulence and boundary-layer processes to improve air-sea interface flux parameterizations.

Methodology: To reproduce the turbulence dynamics accurately, the representation of the numerical tanks is accomplished using large-eddy simulation (LES) and the physical domain size of the respective tanks. The numerical experiments build on our previous work with OpenFOAM, including custom developments to simulate Langmuir turbulence and boundary actuation. In the air-sea simulations, the model resolves both air and water, as well as the air-sea interface, in great detail, using high spatial and temporal resolution.

Results: Simulations were performed of the impact of actuated membranes on boundary-layer turbulence. Laboratory and numerical experiments show boundary actuation impacts near-boundary velocity and circulations. Simulations of wind-wave dynamics exhibit a multiscale pattern of coherent structures in the near-surface layer, consistent with both shear-driven short-lived features and more persistent Langmuir-type footprints (Fig.1). The model also indicates that phase-dependent dynamics may significantly impact air-sea stresses over waves (Figs. 2, 3).

DoD Impact/Significance: CFD simulations emulating the convective SiTTE tank, the flow SiTTE tank, and the SUSTAIN wind-wave tank, are critical for the success of research on a novel optical communication system based on orbital angular momentum (OAM), novel methodologies for active boundary-layer control and drag reduction, and new fiber-optics sensor development (temperature, flow), as well as parameterization of air-sea interface dynamics.

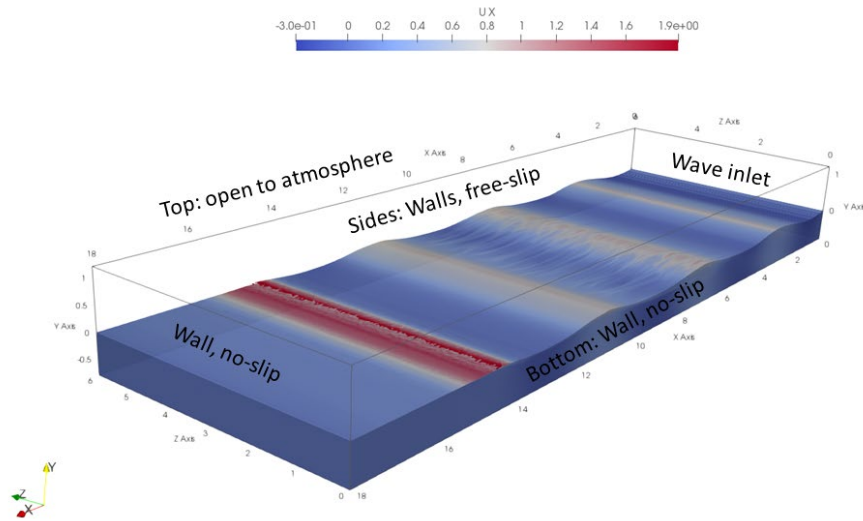


Figure 1. Schematic of setup and boundary conditions for wind-wave tank model. The isovolume of water is shown colored by along-tank velocity U_x , as well as the wave field at model time $t = 15$ s. Colorbar in m/s.

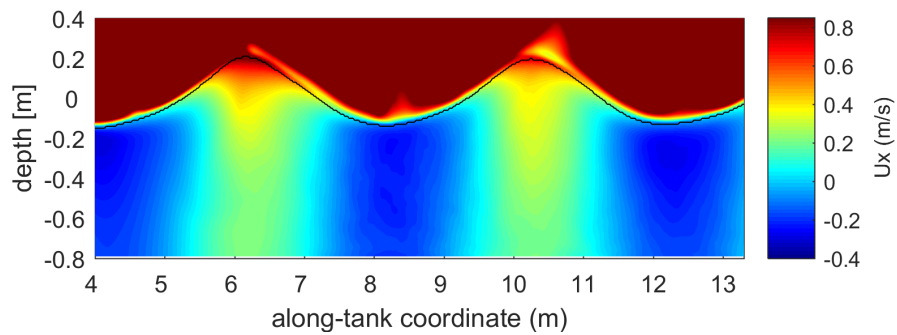


Figure 2. Phase-averaged along-tank velocity. Average is taken over 43 spatial fields exhibiting the same wave phase from times $t = 400$ s to $t = 472.24$ s, saved every 1.72 s (the wave period). Colorscale is chosen to emphasize velocity in the water. The water level is indicated by the black line.

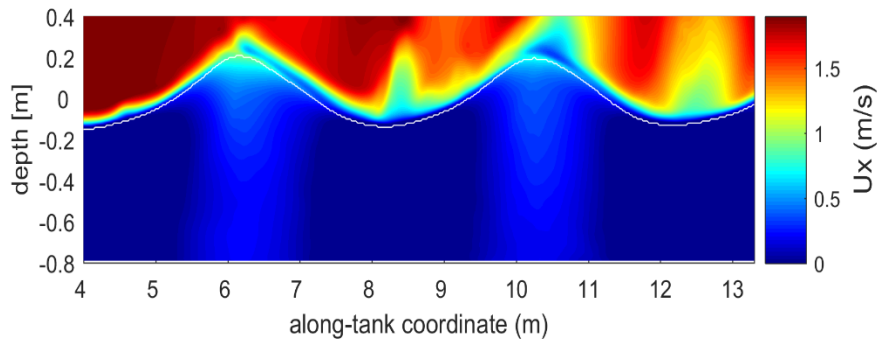


Figure 3. Phase-averaged (averaging as in Fig. 2) along-tank velocity U_x (top) for an along-tank section at the tank centerline $z = 3$ m. The color scale for the contour plot is chosen to illustrate the velocities in the air and across the air-sea interface, which is indicated in white. Note the sheltering effect from the wave crests.

Title: Predicting Fluid-Structure Interaction for Military Applications

Author(s): D.R. Mott, Y. Khine, and A.D. Kercher

Affiliation(s): Naval Research Laboratory, Washington, DC

CTA: CFD

Computer Resources: HPE SGI 8600 [AFRL, OH]; SGI ICE X [ARL, MD]; Cray XC40/50 [ERDC, MS]

Research Objectives: Create the computational capability to predict the interaction of fluids with complex structures that also can be flexible, including large, high-rate deformations due to blast loading. Flows may include advection and diffusion of multiple materials and may include convective and evaporative heat transfer and species transport at ambient atmospheric conditions. Use the new capability to study other problems of defense relevance including helmet design and microfluidic transport applied to additive manufacturing.

Methodology: A discontinuous Galerkin solver for incompressible multispecies flows, developed at NRL's Laboratories for Computational Physics and Fluid Dynamics within the JENRE^{®1} software framework, was used to simulate transport (convection and diffusion) of target species within a flowing gas. Additionally, software available on DoD HPCMP systems was applied when appropriate for solving particular relevant problems.

Results: FY20's highlighted result is from helmet design. Military helmets traditionally are designed to counter ballistic and blunt-impact threats. Concern over blast interaction has increased in recent years, as well as consideration of thermal loading that can undermine warfighter performance and can result in heat-related injury. To this end, efforts are underway to develop multi-threat design approaches for military helmets, including characterizing the effect of helmet design on evaporative cooling due to perspiration. Figure 1 includes a representative calculation for the thermal plume of a standing Marine. The simulation is performed with the software package CFD++. In this simulation, the body is assumed to be 10° C hotter than the environment, and the head is assumed to be perspiring. Buoyancy generates a vertical convective flow that carries hot, moisture-laden fluid away from the head. The net flux of water vapor away from the body can be used to calculate the net cooling generated by perspiration evaporation.

DoD Impact/Significance: Thermal loading in the field not only undermines concentration and performance of cognitive tasks, it also can result in heat-related injury. A design approach that accurately emphasizes the relative importance of a variety of design factors and threats, and that can be weighted differently for different scenarios, can produce optimal configuration options for targeted theaters and operations.

¹ JENRE[®] is a registered trademark of the Department of the Navy.

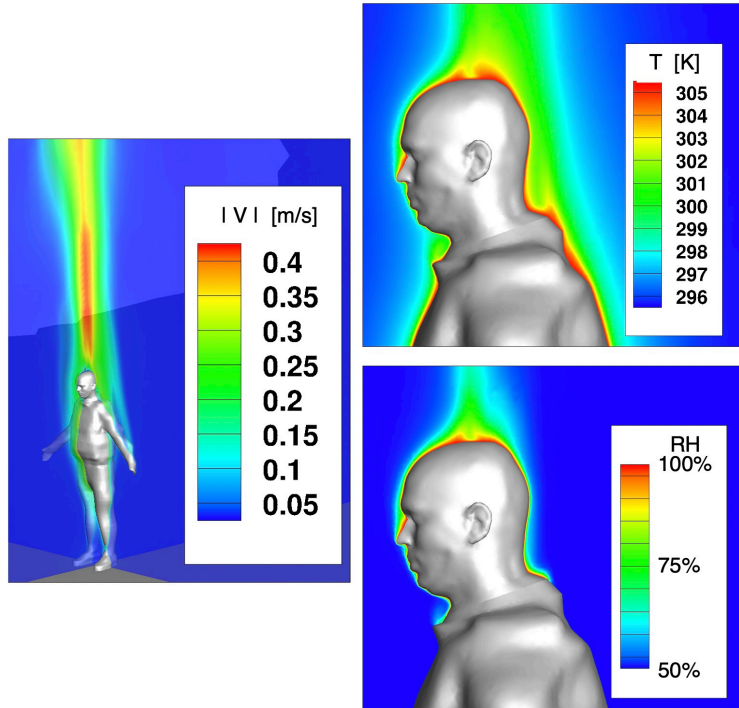


Figure 1. Representative baseline flow simulation for a standing individual with no helmet: instantaneous snapshot of an unsteady flow solution showing the velocity magnitude (left) and the temperature and relative humidity (top right and bottom right, respectively). Simulation assumes that the entire body surface is 10 K above ambient, and that head perspiration maintains a saturated condition (100% relative humidity) in the air adjacent to the head surface. In this simulation with no crosswind, natural convection due to the elevated body temperature generates a plume that carries heated air and water vapor up and away from the head.

Title: Advanced Computational Models that Exploit Emerging Computer Architectures

Author(s): K. Obenschain and A. Moses

Affiliation(s): Naval Research Laboratory, Washington, DC

CTA: CFD

Computer Resources: HPE SGI 8600 [AFRL, OH]; Power9 [ARL, MD]; Cray XC40/50 [ERDC, MS]

Research Objectives: This project aims to expand the use of many-core devices in high-performance computing environments while creating specific needed research capabilities that these devices enable. Specifically, 1) Develop methodologies to enable existing codes to exploit the performance of rapidly evolving many-core devices (MCD) to solve current roadblock problems. 2) Develop approaches to exploit the improved high-bandwidth communication architectures that are becoming available currently. This project also is used to evaluate and advise how emerging architectures impact HPCMP and the wider HPC community.

Methodology: HPCMP's resources are utilized to define a baseline for performance comparisons with exploratory architectures. In turn, the 6.1 project this effort supports looks at different approaches such as algorithm improvements and tactics to allow legacy codes to exploit the additional computing power on leading-edge hardware.

Results: Figure 1 depicts an example of an evaluation performed with a result from the code FDL3DI. CFD simulations and underlying implementations of algorithms were run on Mustang to generate a performance baseline for evaluating emerging architectures. This year, architectures from AMD Rome and NEC Vector engines were evaluated in detail. With some refactoring, the emerging architectures proved to have significant performance advantages for their respective problems.

DoD Impact/Significance: The proposed work and applications proposed above are relevant to expeditionary and irregular warfare (counter-IED, sensors, lethality and survivability), computational environment architecture (open architecture) platform design and survivability (advances platform design, survivability, unmanned vehicles, high-speed platforms), power and energy (energy security, power systems), computational materials science and fluid dynamics.

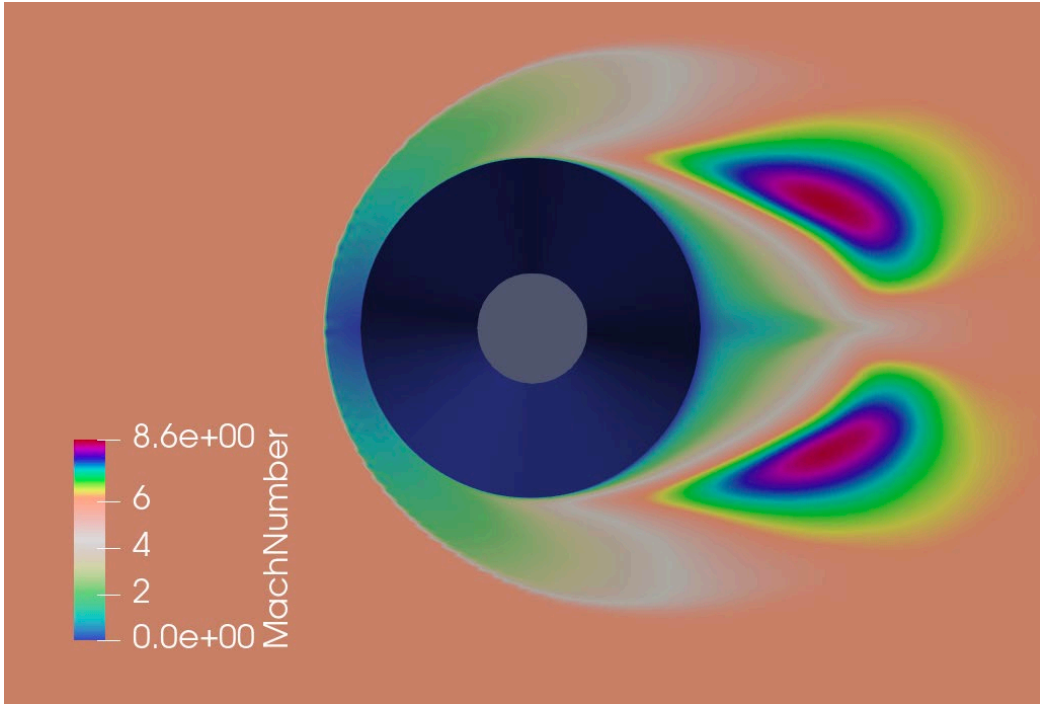


Figure 1. Simulation from FDL3DI

Title: Direct Numerical Simulation of Fluid-Sediment Wave Bottom Boundary Layer

Author(s): A.M. Penko¹, W.S. Kearney², S.P. Bateman¹, J.A. Simeonov¹, J. Calantoni¹, J. Veeramony¹, and W. Lee³

Affiliation(s): ¹Naval Research Laboratory, Stennis Space Center, MS; ²ASEE Postdoctoral Fellow, Naval Research Laboratory, Stennis Space Center, MS; ³NRC Postdoctoral Fellow, Naval Research Laboratory, Stennis Space Center, MS

CTA: CFD

Computer Resources: HPE SGI 8600 [NAVY, MS]; Cray XC40/50, Cray XE6m [ERDC, MS]; Cray XC40 [ARL, MD]

Research Objectives: Predictive models for near-shore bathymetric evolution require an understanding of the physics of fluid-sediment interactions in the wave bottom boundary layer (WBBL). Since such processes are difficult to measure in situ, we performed coupled fluid-sediment numerical simulations to increase our understanding of the sediment and hydrodynamics in the WBBL. Fundamental concepts used in describing the phenomena of sediment transport such as mixture viscosity and diffusivity, hindered settling, bed failure criterion, bedform evolution, and the concept of acceleration-induced transport are addressed with our models. The models produce high-resolution results necessary to gain insight into the small-scale boundary-layer processes and clarify new directions for measurement techniques needed to improve predictive capabilities.

Methodology: Utilization and development of a suite of discrete and continuum WBBL models for simulating sediment transport in the nearshore environment from the microscale (cm to m) to the mesoscale (km) is ongoing. At the microscale (<10 cm), the three-dimensional sediment phase is simulated with a discrete-element method that allows individual grains to be specified uniquely. The fluid-phase model varies in complexity from a simple one-dimensional eddy viscosity to a fully three-dimensional direct numerical simulation. Coupling between the fluid and sediment phases varies from one-way coupling to a system fully coupled at every fluid time step. Between the micro- and mesoscale (1–50 m), a spectral seafloor model simulates seafloor roughness dependent on changing wave conditions. In FY20, we developed a new model to predict the probability of wave-generated ripple geometry and evolution by combining a point process model with a stacked generalized machine learner. At the mesoscale (1–10 km), near-shore hydro- and morphodynamics are simulated with the coupled wave-circulation-morphology model, Delft3D.

Results: The point process model (PPM) and machine learner (ML) were trained using compiled laboratory and field datasets and tested for robustness. The method was compared to observations collected off the Panama City, FL, coast. First, the ripple reset parameter was calculated for the observed time series (Fig. 1A). Then, 100,000 random distributions of ripple length and height were produced by the ML for each observed time step. Lastly, those distributions of ripple lengths and heights are used to run many instances of the PPM, which accounts for the uncertainty in the timing of ripple reset events (Fig. 1B). The coupled system results in a time series of ripple-height and length-probability distributions (Figs. 1C and 1D, respectively).

DoD Impact/Significance: Ultimately, all process-based models for near-shore bathymetric evolution are limited by shortcomings in fundamental knowledge of multiphase boundary layer physics. The microscale simulations provide an unprecedented level of detail for the study of fluid-sediment interactions that is impossible to obtain with available measuring technologies in the field or the laboratory. These results are utilized to improve parameterizations of small-scale processes in larger-scale models. At the mesoscale, our models are highly efficient and well suited for coupling to regional operational hydrodynamic models.

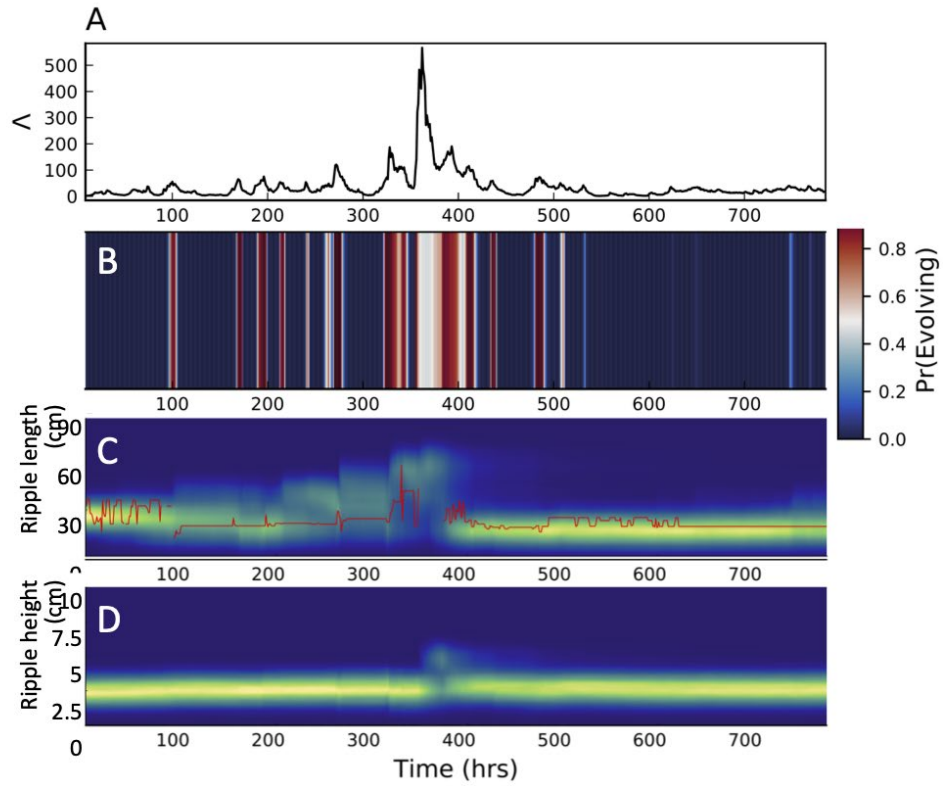


Figure 1. (A) Time series of the ripple reset parameter observed in TREX13 used by the point process model to determine seafloor mobility, (B) the probability that ripples will be generated by the instantaneous wave conditions, and the probability distributions of the (C) ripple lengths and (D) heights in time predicted by the coupled ML and PPM where the warmer colors indicate higher probabilities. The red line in (C) denotes the observed ripple length.

Title: Applications of FEFLO Incompressible Flow Solver

Authors: R. Ramamurti

Affiliations: Naval Research Laboratory, Washington, DC

CTA: CFD

Computer Resources: SGI ICE X [AFRL, OH], [ARL, MD]; Cray XC40 [ARL, MD]

Research Objective: Perform three-dimensional (3D) numerical simulations of flow past complex configurations. The proposed studies will investigate the use of bio-inspired fins for propulsion and to characterize the thrust generated by these propulsive flapping surfaces.

Methodology: A finite element solver, called FEFLO, for 3D incompressible flows based on unstructured grids is used. The flow solver is combined with adaptive remeshing techniques for transient problems with moving grids and also is integrated with the rigid body motion in a self-consistent manner that allows the simulation of fully coupled fluid-rigid body interaction problems of arbitrary geometric complexity in three dimensions. NRL has developed a flapping-fin UUV for effective low-speed operations. Three-dimensional unsteady flow simulations past a flapping caudal fin are performed. Several bio-inspired planforms based on the geometries of the tuna, wrasse and mackerel fins are studied. Limited parametric studies are conducted varying the phasing between the pectoral and caudal fins, the longitudinal offset between them and the incoming freestream velocity.

Results: Based on our previous experience with the bird-wrasse fin and literature on fins based on biological creatures, we had chosen a trapezoidal bio-inspired fin with an aspect ratio of 3 as a pectoral fin. In the current effort, we compiled the morphological data of the caudal fins of various fish of interest from the perspective of building bio-inspired propulsors. These include the lunate fin of the tuna, the caudal fin of the wrasse and two classes of mackerels, shown in Fig. 1. The caudal fin planform based on the mackerel fish provided the best thrust performance for the kinematics tested in this study. Based on the isolated caudal fin studies, the paired pectoral fin and caudal fin studies were conducted using the bio-inspired trapezoidal planform for the pectoral fin and the trapezoidal mackerel planform for the caudal fin. Parametric studies were conducted varying the phasing between the pectoral and caudal fins, the lateral offset and the freestream velocity. At static conditions, the effect of phasing on the mean caudal fin thrust is minimal and the effect on the pectoral fin is to produce a peak thrust at $\pm 90^\circ$. Expanding these parametric studies will lead to the development of reduced models for the thrust production.

DoD Impact/Significance: Simulations have enabled characterization of the thrust-generation mechanisms in flapping-foil propulsion and the interactions of the flow between these propulsors for use in unmanned underwater vehicles. This will provide the next steps toward development of a comprehensive analytical tool for bio-inspired fin and vehicle design.

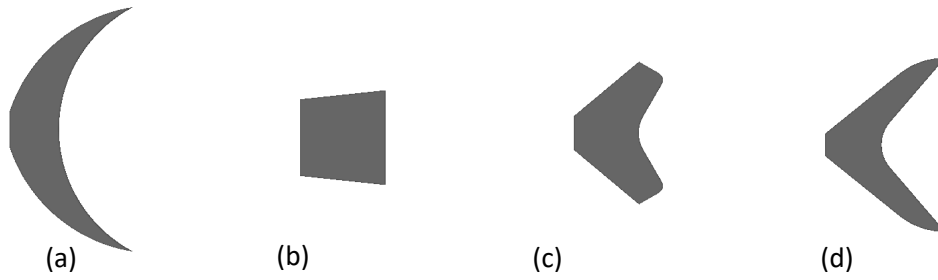


Figure 1. Various bio-inspired caudal fin planforms, (a) a lunate fin, (b) a wrasse, (c) a trapezoidal mackerel fin and (d) a lunate mackerel fin

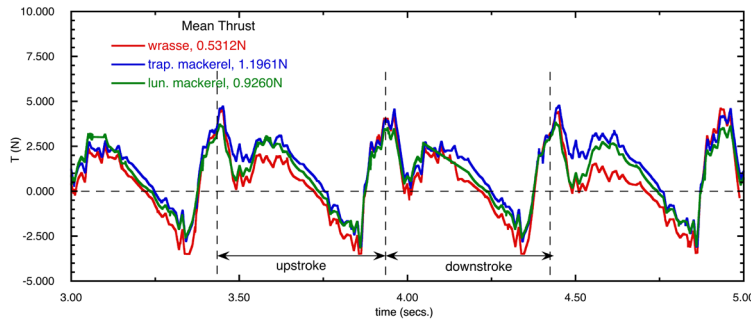


Figure 2. Effect of caudal fin planform on thrust production with fins flapping at 1 Hz

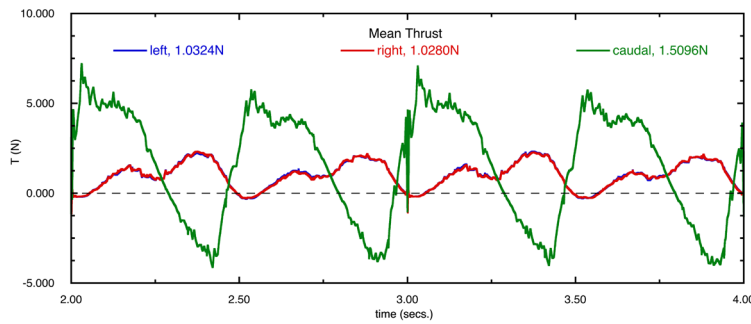


Figure 3. Time history of the thrust production for a pectoral-caudal fin system with the gantry

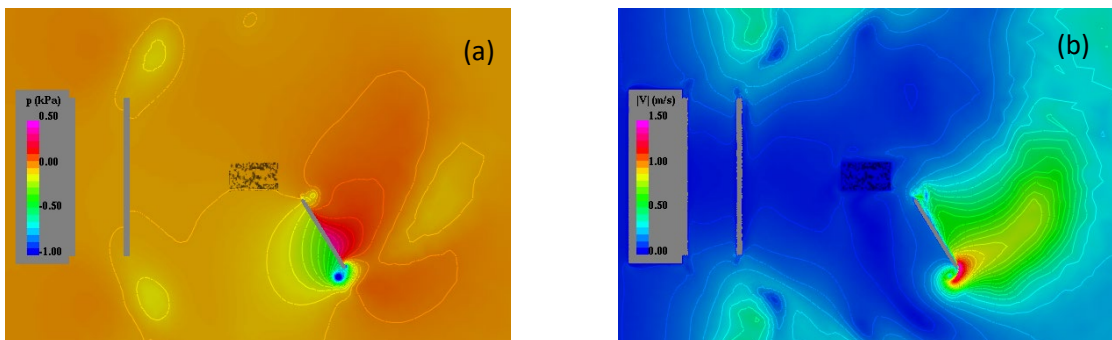


Figure 4. (a) Pressure and (b) velocity distribution on the symmetry plane at maximum thrust production of the caudal fin during the downstroke

Title: Detonations with Multi-Phase Flows for Propulsion
Author(s): D.A. Schwer
Affiliation(s): Naval Research Laboratory, Washington, DC
CTA: CFD

Computer Resources: HPE SGI 8600 [AFRL, OH]

Research Objectives: The main research goal of the present HPC project is to study high- and low-speed multiphase reacting flows for further understanding of advanced engine concepts, with the specific application for detonation engines.

Methodology: We have used two modeling codes for our research into blast and detonation engine simulations. Our main development and simulation code is the JENRE^{®1} code. Due to our extensive experience with using the DET3D codes for detonation propulsion, we will continue to use them as a benchmark for comparison with the JENRE[®] code. JENRE[®] is a new code utilizing unstructured meshes and both continuous- and discontinuous-Galerkin-FEM techniques to solve a wide variety of complex fluid dynamical phenomena. It has been built from the ground up at NRL to make efficient use of CUDA, Thread-Building-Blocks, OpenMP, and MPI through the use of the Thrust library. By utilizing unstructured meshes, the solver can be coupled easily to solid structural models and can provide a pathway for doing fluid-structure-interaction. Both gas-phase and multiphase models from our DET3D codes have been incorporated into the JENRE[®] code.

Results: Because detonation engines are a radical departure from the constant-combustion processes in current engines and power-generation devices, integration of the combustion chamber into those devices requires special care and investigation. Two different centerbodyless rotating detonation combustors (RDC) were investigated and compared to an annular RDC to elucidate some of the physics that occur within these combustors as well as to determine their performance. Centerbodyless RDCs are interesting because removal of the wall has several advantages, assuming similar efficiency and stability can be demonstrated. The hollow RDC had the centerbody removed and replaced with a head-end wall at the injection plane of the RDC. The flow-through RDC had the centerbody removed and the core domain extended upstream of the detonation wave to isolate the inflow of the core. The simulations showed that the resulting flow-field was very similar to the better-studied annular RDCs, but included pressure relief into the central region, which lowered the pressure ahead of the detonation wave for all of our centerbodyless configurations. Placing an exhaust plenum behind the RDC was essential for our computations, particularly for the hollow RDC calculation. Further work focused on extending the domain for a hollow RDC to include a back-pressure constriction and convergent-divergent nozzle, and then comparing the performance of this with current annular RDC designs. Due to the size of the calculations, we used the continuous-Galerkin FEM representation with JENRE[®], and found that the resultant flow-field from the hollow RDC was very similar to comparable annular RDC configurations, and also had similar performance. Further work is being done to quantify the performance of the simulations.

DoD Impact/Significance: The physics involved in rotating detonation engines (RDEs) and other detonation engines is substantially different than for gas-turbine engines, and also is different from more traditional premixed detonation calculations, requiring research into how an RDE can fit into existing frameworks for propulsion and power generation. Our work in computing RDE flow-fields has helped us to better understand the physics and verify our physical models, and our development of JENRE[®] gives us the capability to explore how best to fit RDEs into these existing frameworks. Through this research the potential of significant efficiency gains for detonation engines can be realized in propulsion and power-generation devices.

¹ JENRE[®] is a registered trademark of the Department of the Navy.

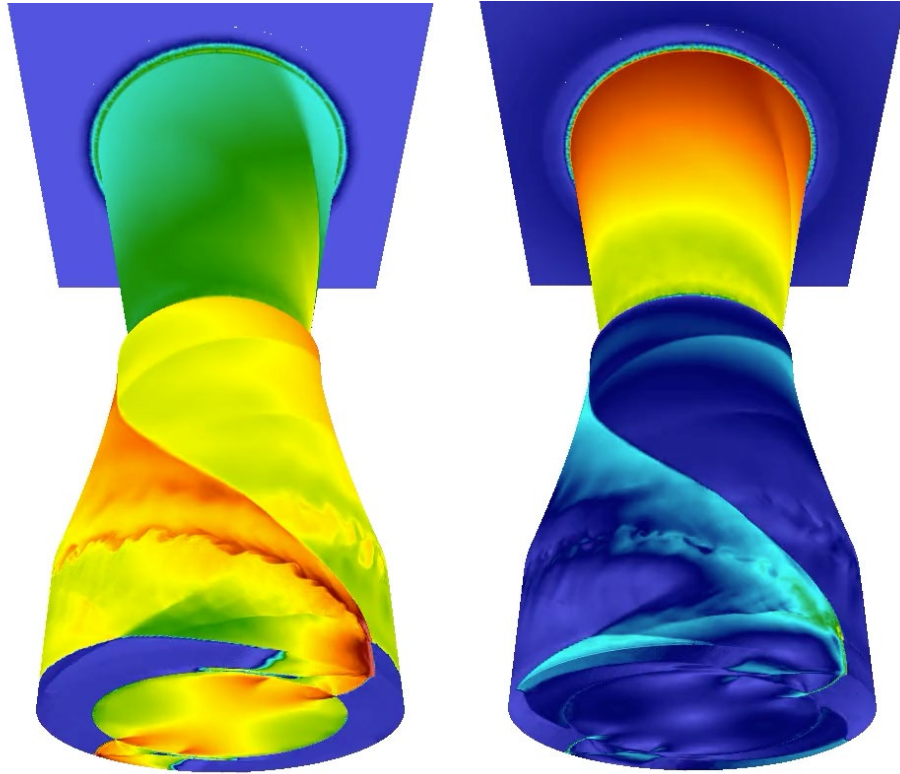


Figure 1. Temperature and Mach number for a hollow RDC with a convergent-divergent nozzle placed on end of combustion chamber, in dual detonation mode operation.

Title: Numerical Simulations of Noise Generated by Non-Circular Advanced Military Aircraft Nozzles

Author(s): K. Viswanath and R. Ramamurti

Affiliation(s): Naval Research Laboratory, Washington, DC

CTA: CFD

Computer Resources: SGI ICE X, Cray XC40 [ARL, MD]; Cray XC40/50 [ERDC, MS]

Research Objectives: Use HPC computational resources to predict details of turbulent flow structures and noise generation in supersonic noncircular asymmetric exhaust jets from representative military aircraft jet engine nozzles. This information will be used to investigate and assess promising jet noise-reduction concepts in support of the ongoing testing program.

Methodology: Simulations are performed using the Jet Noise Reduction (JENRE^{®1}) code developed at the Naval Research Laboratory. JENRE[®] provides unsteady compressible flow solver capabilities that support various numerics, cell-centered finite-volume or nodal finite-element methods, while delivering high throughput on calculations. It was developed with an emphasis on raw performance and the ability to exploit emerging massively parallel, high-performance computing (HPC) architectures. It supports different HPC parallel programming paradigms for message passing such as MPI, OpenMP, CUDA, and hybrid models depending on the HPC cluster architecture. A key bottleneck of HPC throughput is data input-output (IO). JENRE[®] supports parallel IO via MPI/IO or the adaptable IO system (ADIOS) to further complement the multiple levels of parallelism. JENRE[®] uses an edge-based formulation for all flux integration and limiting algorithms. Taylor-Galerkin finite-element method with second-order spatial accuracy for tetrahedral cells is used with the finite-element flux-corrected transport (FEM-FCT) method. The multidimensional FCT flux limiter provides an implicit subgrid stress model, which ensures monotonicity at shocks and sharp gradients with minimal artificial dissipation. JENRE[®] also features a wall model that supports high-speed flows and surface roughness effects while significantly reducing grid resolution requirements.

Results: Simulations of supersonic twin jets at highly overexpanded operating conditions, a nozzle pressure ratio of 2.5, and different wall surface roughness conditions, from nozzle throat to lip, were investigated to understand their asymmetric noise characteristics and to evaluate noise-reduction techniques. A twin-jet rectangular nozzle (equivalent diameter $D = 0.018$ m), with an aspect ratio of 2 and a centerline nozzle separation distance of $2.3 D$, as shown in Fig. 1, was simulated and its noise production and flow features were compared with experimental data from the University of Cincinnati (UC). The simulations predicted the far-field noise and the spatial variation of the noise with excellent agreement compared to UC data for different grid resolutions, shown in Fig. 2. Figure 3 compares the normalized time averaged contours of the streamwise cold jet plume velocity, showing the shock cell structures and the jet core plume breakdown regions, for all cases. Without surface roughness, the plume core length is approximately $6.8 D$, which is close to the experimental result of $7 D$. Introducing surface roughness increased boundary layer thickness and the resulting plume had shorter jet plume core lengths with the shock cells offset closer to the nozzle exit. These changes in the plume were proportional to the surface roughness height used.

DoD Impact/Significance: The results of our work will provide better understanding of the noise production for both industrial and military aircraft, and will aid the current effort of noise reduction, especially for supersonic aircraft, to reduce the impact of the jet noise on shipboard health and safety issues.

¹ JENRE[®] is a registered trademark of the Department of the Navy.

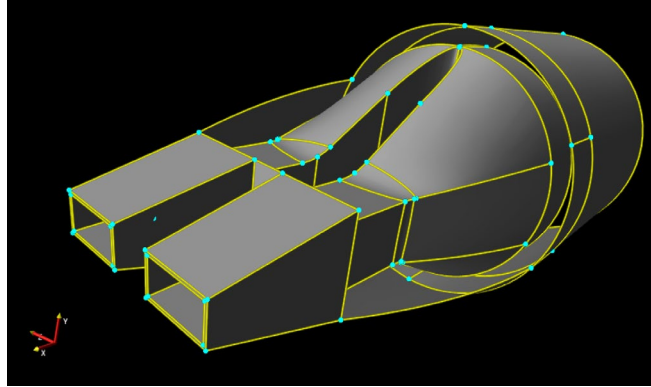


Figure 1. Twin-jet-nozzle geometry, aspect ratio 2 nozzles with separation distance of 2.3 D

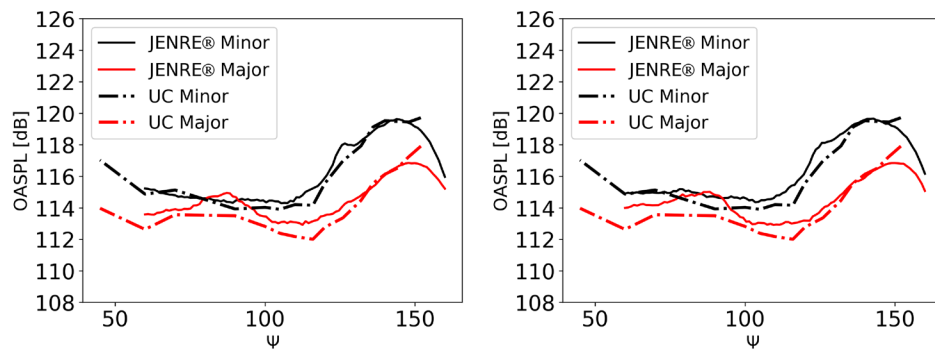


Figure 2. Far-field noise comparison at 60 D for the NPR 2.5 case twin-jet plume with no surface roughness at different grid resolutions. Left shows 30 micron grid. Right shows 45 micron grid.

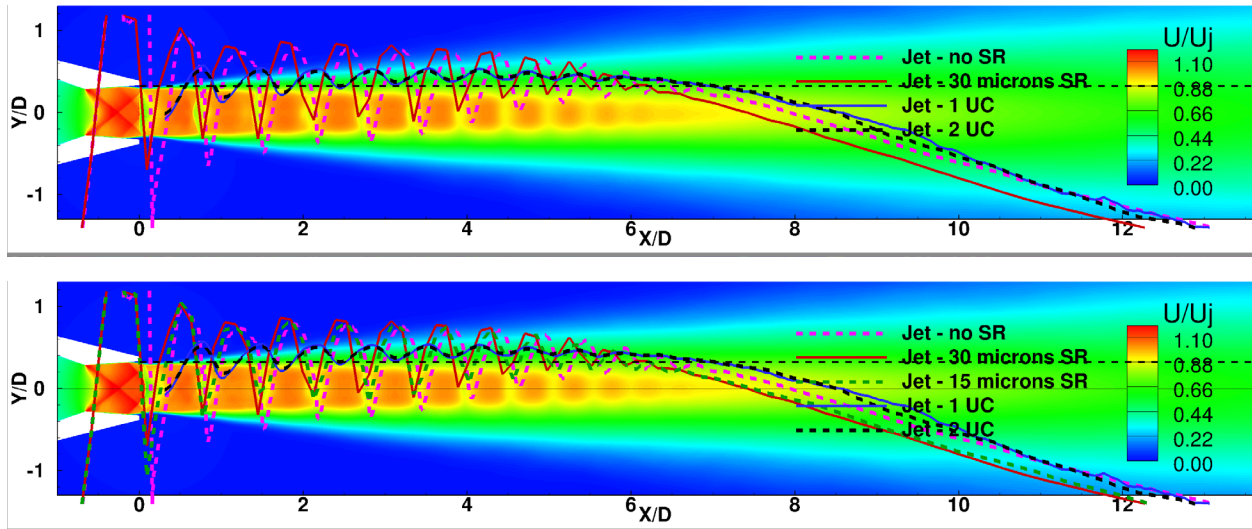


Figure 3. Overlay with centerline jet velocity of the time averaged flow field from JENRE® simulation comparisons for different surface roughness (SR) cases. The nozzle grid resolution is 45 microns at exit. Top shows 30 microns SR. Bottom shows 15 microns SR

Title: High-Temperature and Rarefied Gas Dynamics in Hypersonic Flows
Author(s): E.W. Hyde, G.B. Goodwin, J.R. Maxwell, and R.E. Rogers
Affiliation(s): Naval Research Laboratory, Washington, DC
CTA: CFD

Computer Resources: SGI ICE X [ARL, MD]

Research Objectives: A CFD code, JENRE^{®1}, developed at NRL will be used to model combustion in a Mach 4.5 axisymmetric scramjet. Correlation to pre-existing experimental data obtained from academia provides an opportunity for validation of the code proving its ability to model complex hypersonic flows with reacting flow chemistry.

Methodology: This research has utilized the CFD code JENRE, which employs significant parallel computing to achieve high-fidelity results. A scramjet geometry was created and meshed intelligently so the solver, utilizing high-performance parallel computing, can work to solve the fluid domain. For the present research, a supersonic Mach 4.5 flow through an axisymmetric scramjet was studied to investigate the ability of the code to accurately model the combustion of ethylene in the scramjet cavity. In addition to modeling combustion, the solution was examined thoroughly to ensure the solver correctly predicted viscous effects, shock position, and flame stability.

Results: High-fidelity large eddy simulations (LES) simulations were compared with previously obtained academic results from the University of Illinois. Two-dimensional (2D) simulations were completed with LES and three-dimensional (3D) simulations of 1/16th and 1/8th geometries are underway. The 2D simulation results provided shockwave position, flame location, flame stability, and wall pressure, all of which were compared to experimental results and showed good agreement across the board.

DoD Impact/Significance: This research has contributed to the understanding of supersonic combustion and chemically reacting hypersonic flows. The successful demonstration of this code to model dual-mode scramjet operation accurately builds a solid foundation for this code to simulate future scramjet cases and provides key insights into scramjet design and stability analysis.

¹ JENRE[®] is a registered trademark of the Department of the Navy.

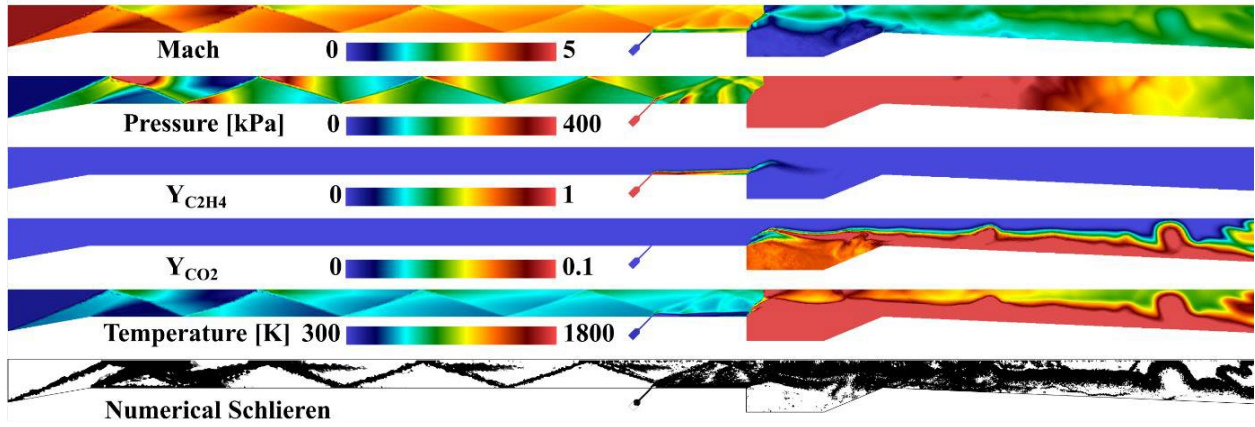


Figure 1. Simulations showing state variables in the scramjet domain during stable combustion

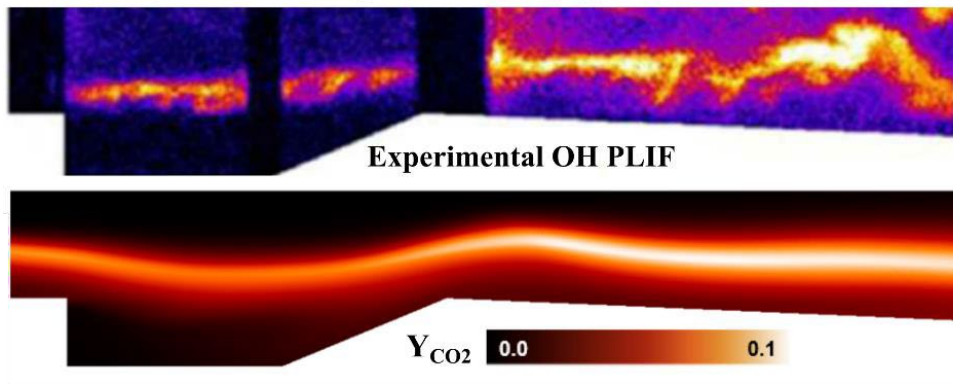


Figure 2. Comparison of simulated CO₂ mass fraction with experimental OH PLIF

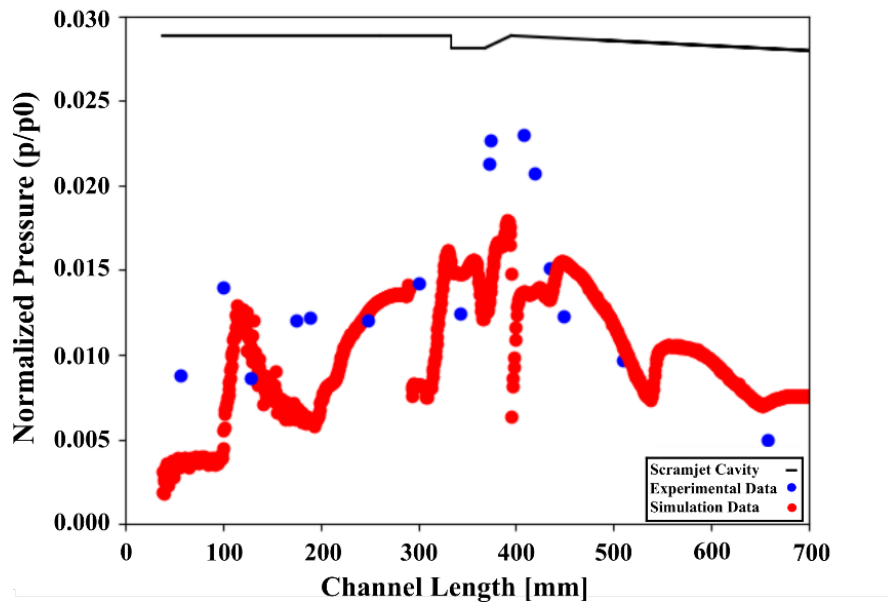


Figure 3. Comparison of simulation and experimentally measured wall pressure

Title: Integrated Radiation Shield Design for 3D Printing
Author(s): M. McDonald, L. Enloe, and M. Georgin
Affiliation(s): Naval Research Laboratory, Washington, DC
CTA: CFD

Computer Resources: SGI ICE X [ARL, MD]

Research Objectives: The objectives of this FY's work were a) to adequately model neutral pressure evolution out of a hollow cathode tube into a vacuum and b) to predict electrical breakdown voltage and location as a function of background pressure and cathode geometry at the exit of a hollow cathode. The expansion of gas into a vacuum spans a transition from continuum to molecular flow regimes, making accurate fluid modeling of the full expansion challenging. However, understanding the neutral pressure evolution is necessary to accurately identify electrical breakdown paths in the resulting flow. Both questions are part of a combined experimentation-and-simulation effort intended to validate models of thermionic cathode heaterless ignition using a tailored electrical breakdown to deposit heat into the thermionic emitter.

Methodology: We use COMSOL Multiphysics software, focusing on the plasma physics module, in conjunction with experimental measurements of an identical test geometry and pressure condition. The main variables to account for in the neutral pressure evolution are the treatment of slip conditions at the cathode walls, which require modification due to poor validity of the no-slip condition in transitional flows with near-unity Knudsen number. Electrical breakdown location amounts to an electrostatic problem, as it precedes plasma formation, so solution of the Laplace equation followed by integration along paths defined by electric field streamlines provides a sufficiently accurate method to reproduce observed experimental electrical breakdown thresholds in matching experiments.

Results: We have demonstrated excellent model capability to identify breakdown locations as a function of gas pressure and cathode geometry in a static background gas created by backfilling of a vacuum chamber, and acceptable reproduction of the neutral pressure profile through the transitional regime exiting a continuum flow tube into the rarefied expansion in a vacuum chamber. Our next step will be to incorporate the flowing gas effects on the neutral pressure profile to permit breakdown prediction in a representative hollow cathode environment. The limiting features of the neutral pressure flow validation appear to be experimental uncertainty in the pressure measurement. Further diagnostic refinement will be required to better characterize the gas plume expansion flow field to validate breakdown path predictive modeling in the flowing gas environment of an operating cathode.

DoD Impact/Significance: Accurate predictive modeling of the breakdown location in a thermionic hollow cathode will enable development of rapid cathode ignition in seconds instead of the current several minutes' preheating for Hall thrusters used on orbit for spacecraft propulsion. Removal of the cathode heater makes the propulsion system more responsive while removing a key point of failure and increasing the power efficiency and thrusting duration in battery-limited operating modes.

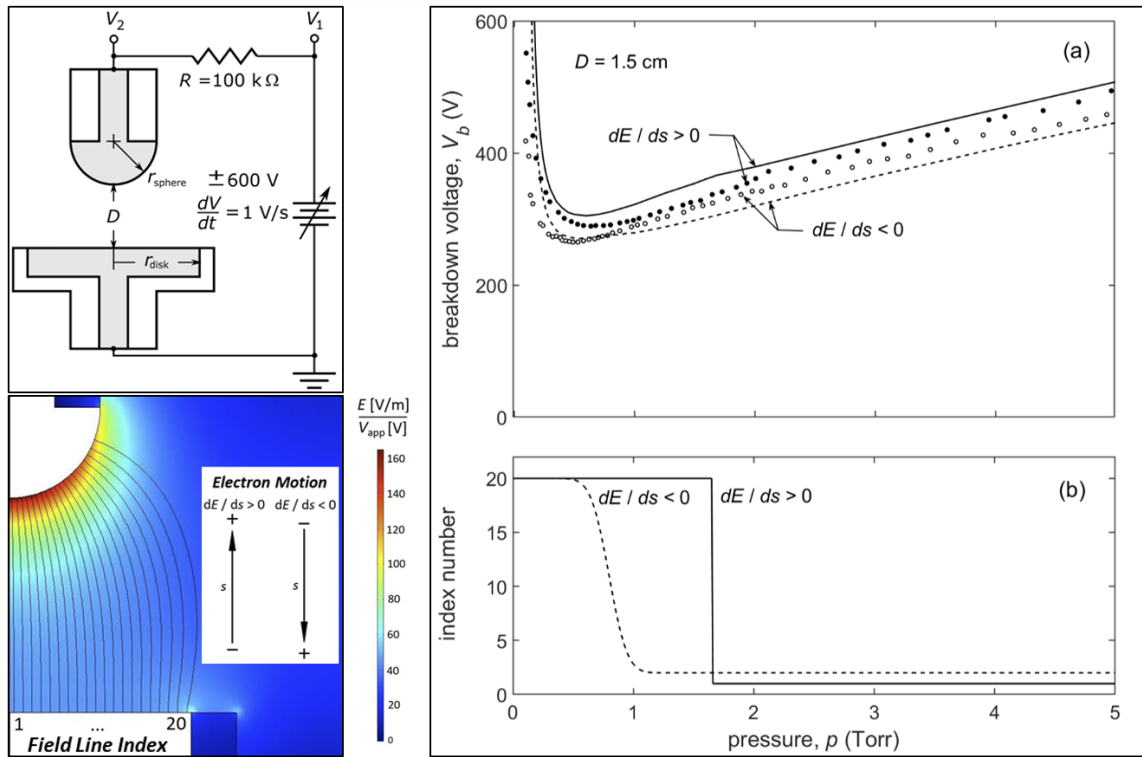


Figure 1. Counterclockwise from top left, a schematic of the breakdown test circuit, a COMSOL model of the experimental geometry, and plots of the experimental breakdown voltage and predicted breakdown field line index. The simulation accurately identifies a sudden shift in breakdown location for one bias polarity, seen as a kink in the experimental curve for $dE/ds > 0$ near 2 Torr.

Title: Multidimensional Chemically Reacting Fluid Dynamics with Application to Flameless Combustors
Author(s): R.F. Johnson
Affiliation(s): Naval Research Laboratory, Washington, DC
CTA: CFD

Computer Resources: HPE SGI 8600 [AFRL, OH]; SGI ICE X, Cray XC40 [ARL, MD]; Cray XC40/50 [ERDC, MS]

Objectives: Use the HPC computational resources to simulate the computationally expensive chemically reacting fluid dynamics in various multidimensional configurations with the goal of better understanding various complex, multiscale, combustion phenomenon.

Methodology: The codes currently in use at The Laboratories for Computational Physics and Fluid Dynamics can predict the flow field accurately in many configurations. These codes employ high-order methods, which are capable of simulating unsteady flows with strong shocks, chemical reactions, and other complex features. This work focuses on developments currently underway that will allow for the simulation of high-speed and low-speed reacting flows using state-of-the-art numerical methods. This year, we produced several important results that demonstrate the superiority of our methods for simulating chemically reacting flows.

Results: This year, we produced a methodology that is able to resolve the mixing of multicomponent chemically reacting flows without the need for legacy stabilization methods. In the past, simulating just the pure mixing of two species, such as hydrogen and oxygen, would result in failure without the use of expensive stabilization methods. The Laboratories for Computational Physics and Fluid Dynamics have developed a novel method for simulating multicomponent flows that utilizes the properties of the discontinuous Galerkin method (DG) and correct thermodynamics to simulate propulsion problems. Figure 1 demonstrates a test case we presented in a paper published by the *Journal of Computational Physics*. With our method, we are able to run this problem with detailed thermodynamics, transport, and chemical kinetics without any issues of stability.

An appealing property of the DG method is resolving structures with high-order accuracy without the need for mesh refinement. Instead, the DG method cell accuracies can be increased arbitrarily to resolve flows within the computational cells. An inherent and long-lasting issue in simulating compressible flows of interest to the Navy is the ability to simulate discontinuities. DG is not removed from these issues. For propulsion, the problem is exacerbated by combining the issue of resolving discontinuities to stably resolve chemically reacting flow that can change dramatically behind these shocked flows, often resulting in detonations (a discontinuity sustained by chemical reactions). Figure 2 shows another test case of our DG method with a detonation. Early results show that at meshes larger than 2nd-order accurate cases that the 3rd-order case is able to sustain the detonation structure. This is a promising aspect that higher-order cells can possibly have a resulting impact on resolving detonations and is still being investigated. Regardless, these test cases give us confidence in the ability to simulate and sustain detonations for Navy applications.

DoD Impact/Significance: Accurately predicting combustion has benefits to Navy engine technologies. The research in producing better numerical techniques for simulating propulsion devices will yield a better understanding and predictive capability for Navy/DoD aircraft.

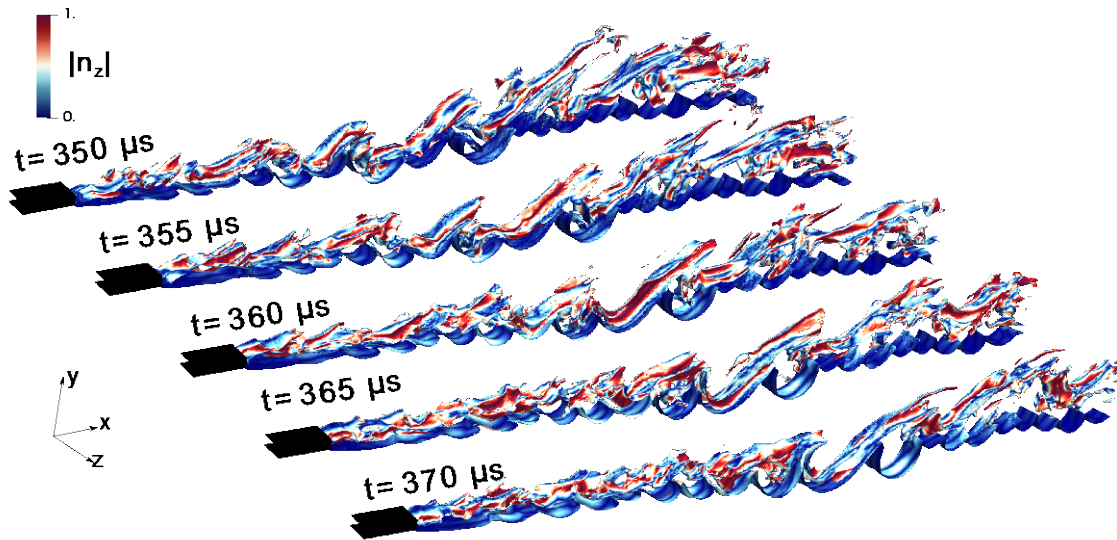


Figure 1. Time-accurate simulations of a hydrogen-air splitter plate. For this test case, hydrogen is injected over the top of a splitter plate where the bottom has air injection. The two streams mix following a splitter plate. The resulting structure is an anchored flame with three-dimensional mixing features. No artificial viscosity, stabilization, or filtering was used to stabilize this configuration.

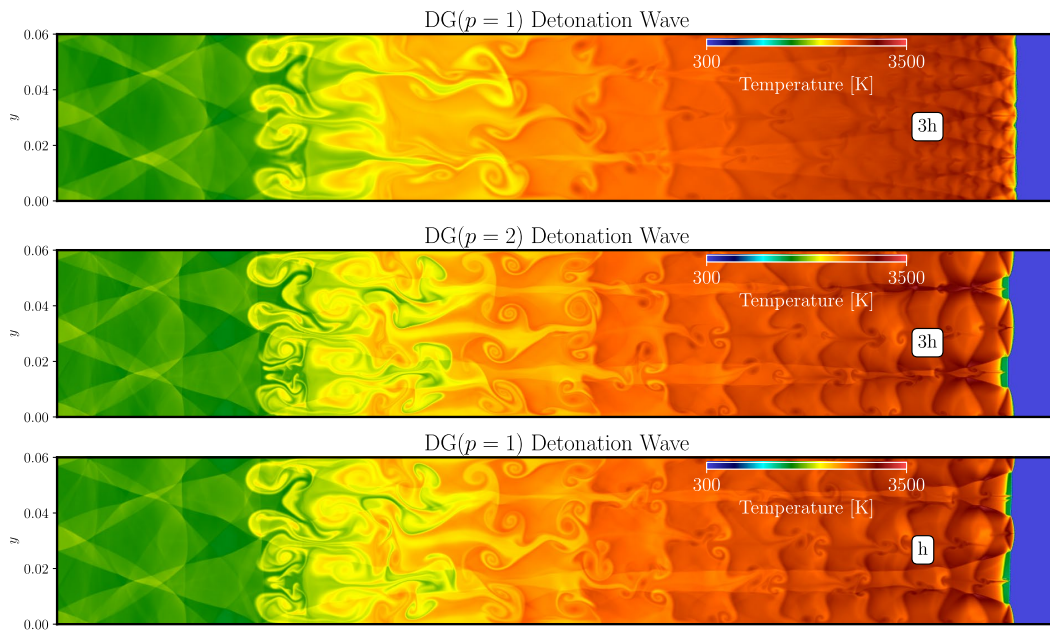


Figure 2. Detonation results for nominally second-order, $DG(p = 1)$ cells and nominally third-order cells, $DG(p = 2)$. The third-order cells resolve the detonation at a larger mesh cell size, $3h$, in comparison to the second-order cells, which require size h . Here $h = 9e-5$ m.

THIS PAGE INTENTIONALLY LEFT BLANK



Computational Biology, Chemistry, and Materials Science

CCM covers computational tools used to predict basic properties of chemicals and materials, including nano- and biomaterials. Properties such as molecular geometries and energies, spectroscopic parameters, intermolecular forces, reaction potential energy surfaces, and mechanical properties are being addressed. Within the DoD, quantum chemistry, molecular dynamics, statistical mechanics, and multiscale methods are used to design new chemical, polymer, nano- and biomolecular systems, for fuel, lubrication, laser protection, explosives, rocket propulsion, catalysis, structural applications, fuel cells, and chemical defense. Solid-state modeling techniques are employed in the development of new high-performance materials for electronics, optical computing, advanced sensors, aircraft engines and structures, semiconductor lasers, advanced rocket engines components, and biomedical applications. Of recent emerging interest in the computational biology, chemistry, and materials science (CCM) CTA are methodologies that cover bioinformatics tools, computational biology, and related areas, such as cellular modeling.

Title: Development of Advanced Pulsed-Power Applications

Author(s): P.E. Adamson

Affiliation(s): Naval Research Laboratory, Washington, DC

CTA: CCM

Computer Resources: SGI ICE X [AFRL, OH]; Cray XC40 [ARL, MD]

Research Objectives: Often in plasma simulations, the molecular electronic states are assumed to be in the ground state of the rotational and vibrational modes. This simplification is reasonable in the dissociated regime that occurs for a beam current density, J_b , in the range $3 \text{ kA/cm}^2 \lesssim J_b \lesssim 50 \text{ kA/cm}^2$. In the weakly ionized molecular regimes that occur for $J_b \ll 3 \text{ kA/cm}^2$, a more detailed consideration of molecular processes, including vibrational kinetics, is required. The purpose of this research is to compute vibrationally resolved inelastic electron scattering cross sections for electron-impact ionization of molecules. Initially, the methods are being applied to the diatomic molecules H_2 , N_2 , and O_2 .

Methodology: A semi-empirical formula is used to compute the electron-impact ionization cross sections. This formula requires the kinetic energy of the participating electron orbital in the target molecule, the threshold energy for the ionization process, and the Franck-Condon factor (FCF) between the target molecule and the relevant cation. Since we are interested in vibrationally resolved state-to-state cross sections, multi-reference configuration interaction (MRCI) potential energy curves are computed for the ground state and all excited states of interest for the target molecules and their cations, resulting in 40 to 50 MRCI calculations per electronic state. This allows us to compute the vibrational-state-averaged target electron kinetic energies from the natural orbitals at each stationary point on the potential energy curve as well as FCFs including anharmonic terms.

Results: Potential energy curves (PECs) and natural orbital kinetic energies for molecules and states of interest were computed using General Atomic and Molecular Electronic Structure System (GAMESS), but the results were not satisfactory (see Figs. 1 and 2 below for example results for PECs). There are several discontinuities in the PECs due to poor convergence and numerical issues that also show up in the kinetic energies and impact the accuracy of FCFs. While GAMESS is certainly capable of the required calculations, in practice, it is difficult to execute our particular workflow given the amount of user intervention required (e.g., reordering starting molecular orbitals, trying various convergence methods). We did make significant progress automating much of the workflow using Bash and Python scripts, but there are still several issues that were not overcome. In FY21, we plan to use Molpro to see if improved results are possible using its advanced MRCI methods and program control features (i.e., compute the entire PEC in a DO loop). Initial studies indicate that it will allow us to use a larger basis set and a finer grid for the internuclear distances. Also, unlike GAMESS, it is possible within Molpro to compute the natural orbital kinetic energies and FCFs directly, greatly improving our overall workflow.

DoD Impact/Significance: The vibrationally resolved ionization cross sections will support increased resolution of reaction networks for plasma chemistry models, directly leading to improved accuracy of plasma simulations in many DoD applications. The primary focus of the current research is to improve accuracy of intense electron beam driven plasma simulations to validate advanced plasma chemistry models for use in particle-in-cell and fluid simulations of system generated electromagnetic pulse.

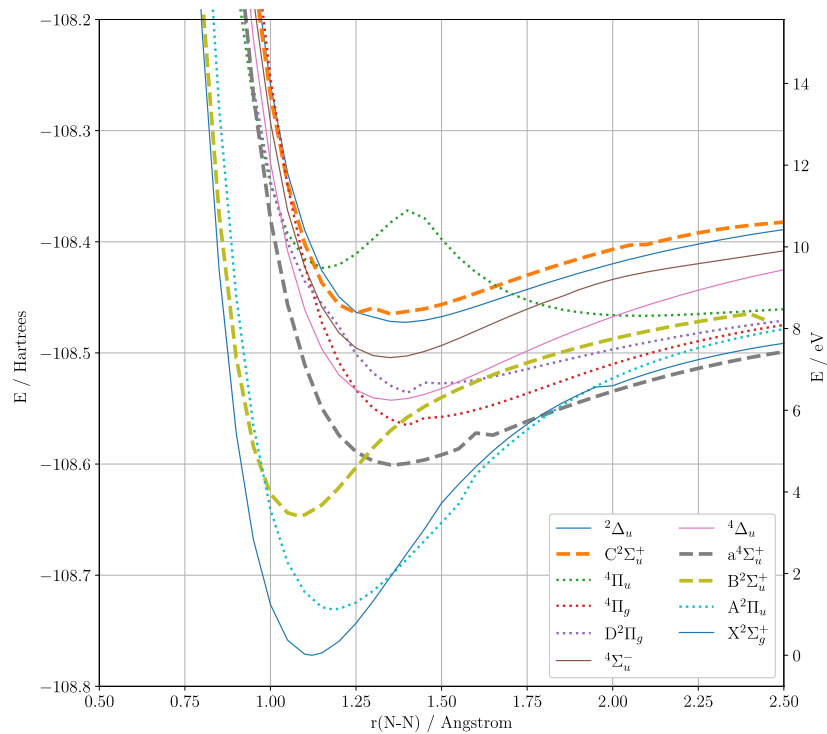
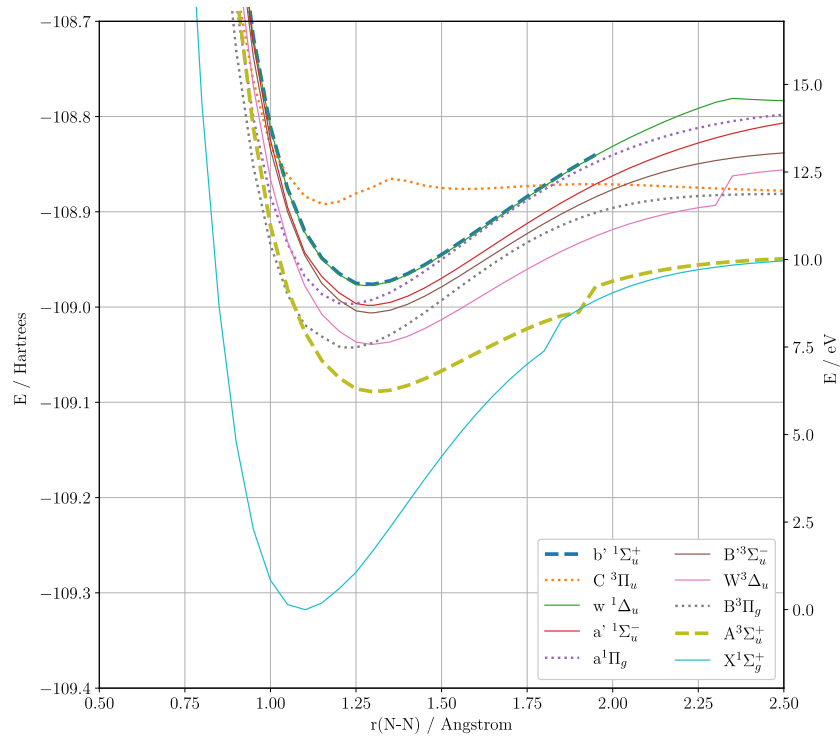


Figure 1. Multi-reference configuration interaction (MRCI) potential energy curves for N_2 (top) and N_2^+ (bottom) computed with GAMESS (aug-cc-pwCVTZ basis set). Note several discontinuities in the PECs. We are exploring the use of Molpro with its advanced MRCI methods and program control features that will allow for better convergence and improved energies due to larger basis sets.

Title: Quantum-Chemical Simulation of Surface-Science Experiments

Author(s): V.M. Bermudez

Affiliation(s): Naval Research Laboratory, Washington, DC

CTA: CCM

Computer Resources: SGI Altix ICE [NRL, DC]; HPE SGI 8600 [AFRL, OH], [NAVY, MS]; SGI ICE X [AFRL, OH]

Research Objectives: The objective of this program is to perform quantum chemical calculations as an aid in interpreting surface-science experiments and in understanding the structure and properties of surfaces.

Methodology: The QUANTUM ESPRESSO (vers. 6.2 and higher) and CRYSTAL (2014) software packages are used for density functional theory (DFT) calculations on periodic structures. The GAUSSIAN-16 program suite is used for DFT calculations on isolated molecules and clusters.

Results: MoS₂ and other two-dimensional transition-metal chalcogenide compounds presently are being developed as materials for chemical sensors, electronic and electro-optic devices and catalysts. This constitutes a wide range of potential applications. There is particular interest in attaining a microscopic understanding of the interaction of small toxic molecules (e.g., NO₂, NH₃, SO₂, etc.) with these substrates. The potential energy surface for NO₂ physisorbed on a MoS₂ monolayer, acting as a chemical sensor, is complex, with several configurations having similar adsorption energies (∇E_{ads}) and charge-transfer characteristics. Hence, this can be considered to be a difficult system to model. A careful exploration of the energy surface is necessary in order to identify any sites at which strong adsorption and/or enhanced charge transfer can occur, which would affect sensor operation. Beyond this, a general computational approach is needed that efficiently can identify the lowest-energy configuration for a molecule weakly adsorbed on MoS₂, since this pertains to many potential sensor applications. In the present study, the computational methods are first tested carefully. Then ab-initio molecular-dynamics simulations are employed for an unbiased sampling of configuration space, which makes use of the approximate correlation between increasing ∇E_{ads} and decreasing NO₂-MoS₂ separation. A simulation temperature of ~225 K, which promotes surface diffusion of NO₂ but not rapid desorption, appears to be nearly ideal. A series of simulations identified several transient configurations with relatively-small separations, and each of these was evaluated and compared with previously reported adsorption models. A well-defined structure with the highest ∇E_{ads} is thus identified and characterized, and further insight into adsorption and surface structure is obtained by computing the charge density at the valence band maximum and the effects of NO₂ on charge density. These results were extended to a preliminary investigation of the intercalation of NO₂ between MoS₂ layers as shown in Fig. 1. This is found to be energetically unfavorable and to destabilize a 2H MoS₂ bilayer at 300 K. However, when relaxed at 0 K, intercalated NO₂ is seen to affect the layer stacking and to increase the charge transfer relative to adsorption on a monolayer.

DoD Impact/Significance: The present work contributes toward the goal of developing reliable chemical sensors for toxic and/or hazardous compounds. In another context, an NO₂ sensor capable of operating under harsh conditions is potentially of great value in the real-time monitoring and control of emissions from internal combustion engines.

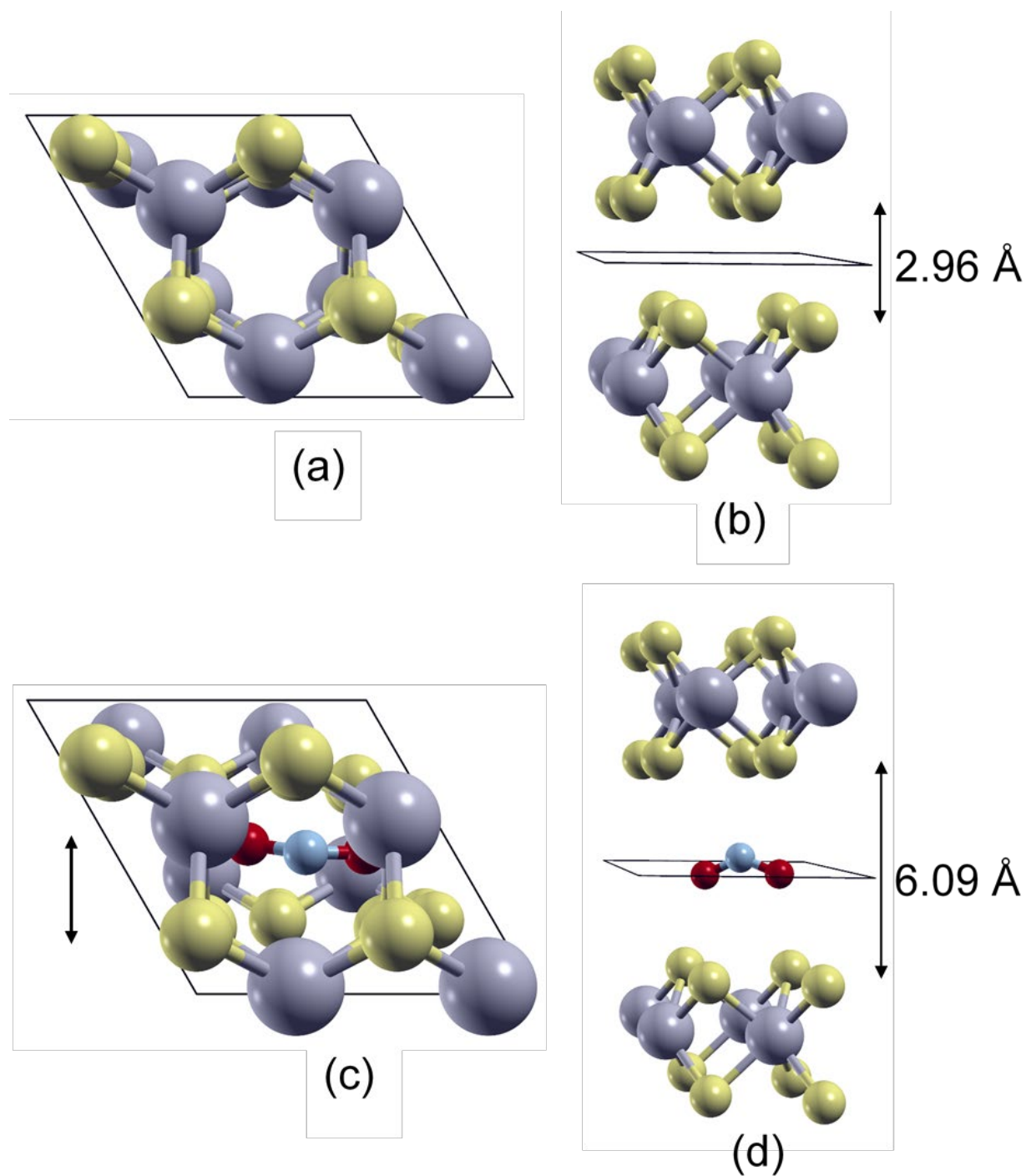


Figure. 1 Model structure (not to scale) for intercalated NO₂. Images (a) and (b) show top-down and side views, respectively, of the relaxed bilayer ((2x2) unit cell) before insertion of NO₂; (c) and (d) show the same structure after relaxation with intercalated NO₂. All figures are shown with perspective projection. The vertical arrows on the right show the interlayer separation. The arrow on the left of (c) shows the direction of the relative lateral displacement of the two layers after relaxation with intercalated NO₂. Gray, yellow, blue and red spheres represent Mo, S, N, and O, respectively.

Title: Multiple Length and Time Scale Simulations of Material Properties

Author(s): N. Bernstein

Affiliation(s): Naval Research Laboratory, Washington, DC

CTA: CCM

Computer Resources: HPE SGI 8600 [AFRL, OH]; SGI ICE X [AFRL, OH], [ARL, MD]; Cray XC40/50 [ERDC, MS]

Research Objectives: To understand and predict mechanical, structural, and energetic material properties.

Methodology: Molecular dynamics (MD) and Monte Carlo (MC) are used for the time evolution and sampling of atomic configurations. Trajectories use energies and forces from density functional theory (DFT) and interatomic potentials. Nested sampling is used for calculating thermodynamic quantities and phase diagrams. The Gaussian approximation potential (GAP) method is used for developing single- and multispecies interatomic potentials. The software implementing these methods included VASP for DFT simulations, LAMMPS for interatomic potential MD, ASE and libAtoms/QUIP for GAP development and interfacing between various programs, and pymatnest for nested sampling.

Results: GAP machine-learning (ML) models were applied to structural transformations of amorphous silicon under high pressures. HPC resources led to a groundbreaking combination of accuracy and length scale essential for describing the heterogeneity, where various structures (high-density and very-high-density amorphous, and high-density hexagonal crystal) coexist. The work's explanation of this previously hidden process has resulted in a high-profile publication (*Nature*, in press). HPC resources also were used to improve the model by using higher-quality reference data generated with RPA, providing a qualitatively better description of bonding than the standard DFT approach.

A major ONR-sponsored project on paramagnetic steels transitioned into production mode, using various HPC facilities. A simple workflow based on scripts that invoke, process, and manipulate DFT simulation inputs and output was used to calculate structural properties such as elastic constants and defect (vacancy, impurity) energies. The HPC resources were essential for these computationally demanding simulations, which require large numbers of atoms in disordered systems, averaging over many random instances of chemical and magnetic order. The work on PdAg phase diagrams with nested sampling and ML interatomic potentials was accepted for publication, and is now in press (*npj Comput. Mater.*).

DoD Impact/Significance: Atomic scale simulations can provide explanation and understanding of processes that occur on length and time scales that are too small for experimental probes. With sufficiently accurate models of interatomic interactions, these can be predictive, and our simulations have shown that this is possible for systems with a challenging variation in bonding type such as amorphous silicon under high pressures. This success will enable further simulations of amorphous materials, which have many applications including phase-change-based non-volatile storage and high-bandwidth switching, and as an inexpensive solar-cell material. The particular application to high-pressure phase transformations also will be applicable to pressure-modified synthesis of other novel materials with improved performance. Steels are an essential structural component of nearly all Navy platforms, but their magnetic signature makes them easier to detect. Nonmagnetic steels can reduce this signature greatly, but their mechanical properties need to be improved. These simulations provide parameters for models by other ONR-sponsored collaborators who use simulated deformation and plasticity that control strength and toughness. This combination will make it possible to design new compositions with improved combinations of magnetic and mechanical properties for structural applications.

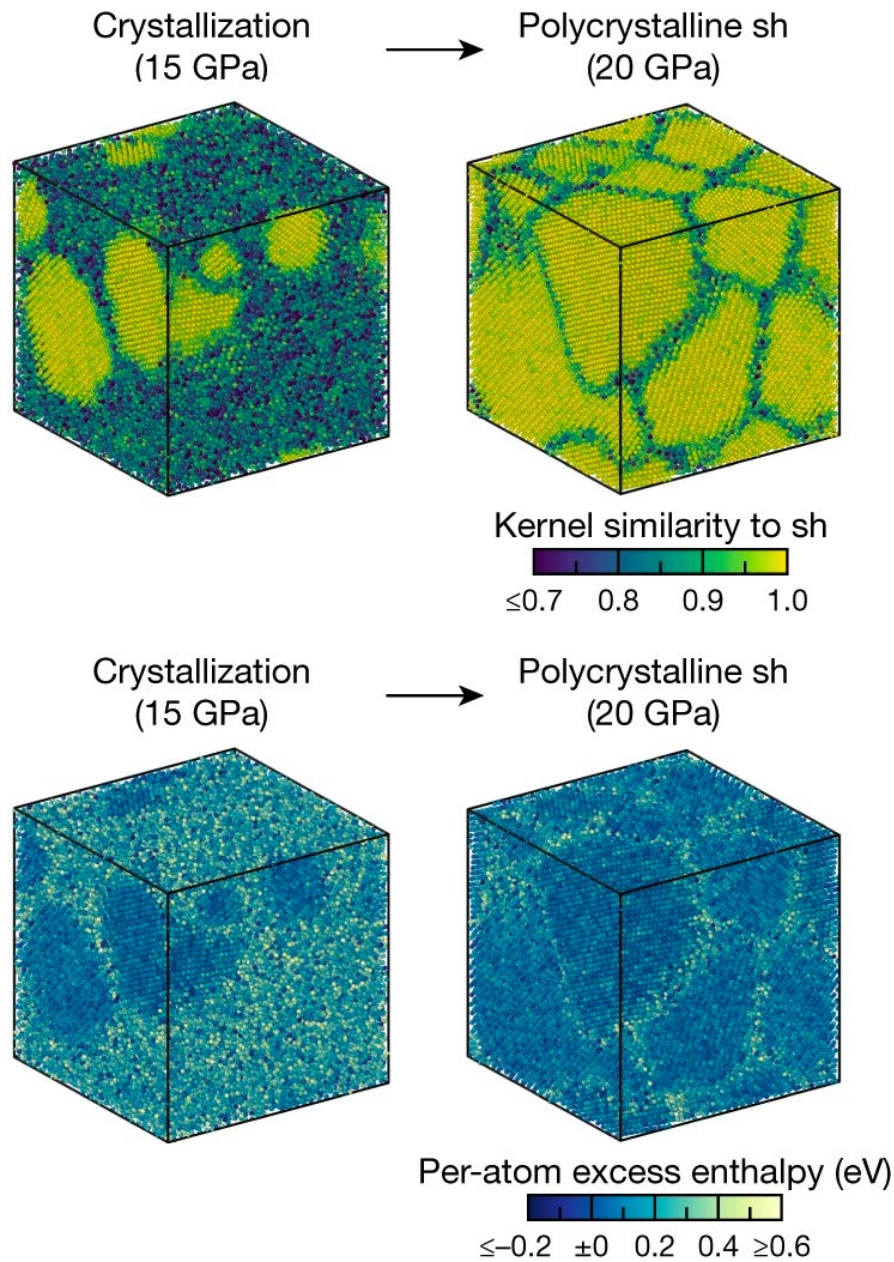


Figure 1. Distribution of local energies and atomic environments in amorphous silicon produced by quenching from the liquid at various rates. Gray dots indicate nominally non-defect (i.e., with four neighbors) atoms, showing a wide range of atomic energies and local structures (the ground state diamond structure is shown by an asterisk). Blue dots indicate undercoordinated (three-neighbor) atoms, all of which show high energy and are all qualitatively different in local structure from the normal-coordination atoms, while green dots indicate overcoordinated (five-neighbor) atoms, which overlap the distribution of local energies and structures present in normal coordination.

Title: Improved Calculation of Solid-Phase Heats of Formation Using Intermolecular Interactions Observed in Crystal Structures

Author(s): I.D. Giles and G.H. Imler

Affiliation(s): Naval Research Laboratory, Washington, DC

CTA: CCM

Computer Resources: Cray XC40 [ARL, MD]

Research Objectives: Prediction of material properties using computational methods is used widely to select the ideal candidate molecule for synthesis. For example, improved thermal stability can be predicted for a selection of candidate molecules so that synthesis is only carried out on the best materials and circumvented for candidates anticipated to have unfavorable properties. This work investigates the prediction of enthalpy of sublimation using geometric parameters observed in crystal structure data. Enthalpy of sublimation is relevant to a wide range of fields of study and is often measured experimentally using instrumentation such as thermogravimetric analysis. Enthalpy of sublimation can be used to calculate the solid-phase heat of formation (HOF). Gas-phase HOF is currently calculated accurately with computation methods but solid-phase HOF remains challenging to compute. This project will use an accurately measured enthalpy of sublimation to convert gas-phase HOF to solid-phase HOF according to Hess's Law.

Methodology: DFT and time-dependent DFT (TDDFT) through the Gaussian package will be used to geometry-optimize a starting structure based on single-crystal X-ray diffraction data (XRD) using a suitable method-and-basis set (B3LYP and 6-311++g to start). Further energy and frequency optimization will ensure a global energy minimum as well as determine the electronic structure and heats of formation, and will help to understand their vibrational spectra. TDDFT methods will be used with solvation models (H₂O and acetone to start) to understand the electronic transitions seen in their electronic spectra in the corresponding solvents. Default tolerances will be employed unless deemed insufficient. Intermolecular interaction distances and angles will be used as the starting point for determination of individual interaction energies. The sum of these interaction energies will be used to calculate the approximate sublimation energy. Edward Byrd and Betsy Rice at ARL have developed scripts that accurately calculate gas-phase HOF using the atom and group-equivalent methods. Access to gas-phase HOF using the atom/group-equivalent methods along with enthalpy of sublimation using the method developed in this project will provide accurate calculation of solid-phase HOF.

Results: Enthalpy of sublimation has been calculated for a series of 50 molecules selected from a large variety of molecular weights, functional groups and fields of study. Currently, this method is limited to neutral C-, H-, Cl-, N-, and O-containing molecules. This data set demonstrated average errors of 14.5 kJ mol⁻¹ which is comparable with methods used in literature. The method is currently functional, is applicable to a wide range of molecules and is not computationally demanding. Further optimization of the method through the study of larger sets of molecules will allow this method to achieve greater accuracy.

DoD Impact/Significance: At the current iteration, this method approaches or matches the accuracy of popular methods used to calculate enthalpy of sublimation. Enthalpy of sublimation can be used to calculate solid-phase HOF. Additional improvements have the potential to surpass methods in use today. Accurate calculation of sublimation energy and solid-phase HOF are relevant to a wide range of fields and are important for the safe storage of a solid-phase material.

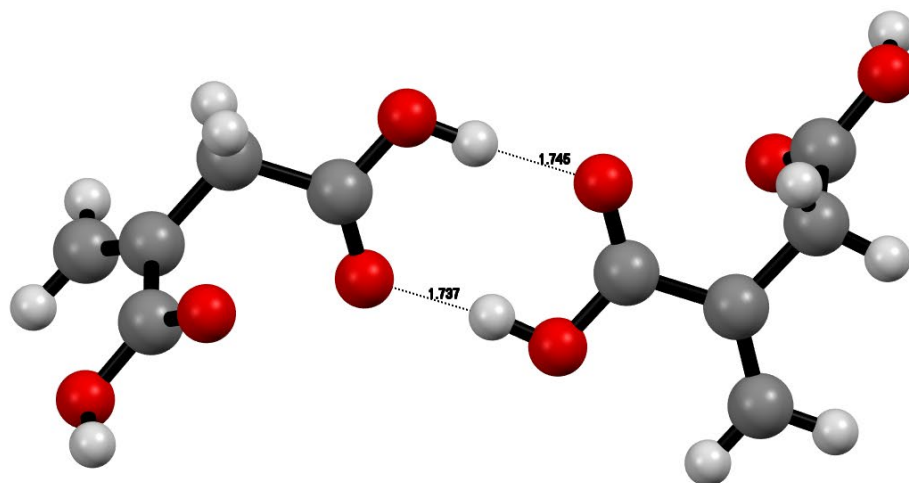


Figure 1. Structure plot demonstrating strong hydrogen bonds in itaconic acid as identified in single-crystal X-ray structure. An equation has been developed that uses hydrogen bond lengths to calculate interaction energies.

Title: Surfaces and Interfaces in Oxides and Semiconductors

Author(s): C.S. Hellberg

Affiliation(s): Naval Research Laboratory, Washington, DC

CTA: CCM

Computer Resources: HPE SGI 8600 [AFRL, OH]; SGI ICE X [AFRL, OH], [ARL, MD]; Cray XC40 [ARL, MD]; Cray XC40/50 [ERDC, MS]

Research Objectives: Determine the atomic and electronic structure of twisted monolayer structures.

Methodology: We performed highly accurate first-principles density functional calculations of very large (containing up to 570 atoms) MoSe₂/WSe₂ computational cells of a monolayer of MoSe₂ on a monolayer of WSe₂ to determine the atomic structure of the domain walls at small twist angles. Smaller twist angles require more atoms in the computational cells. We used the VASP Density Functional Theory (DFT) code at the AFRL, ERDC, and ARL HPC centers.

Results: By varying the size of the domain walls, we show that elastic interactions between domain walls extend approximately 3 nm. Fortunately, we are able to separate the domain walls in the calculations by more than 6 nm, well beyond the interaction range. There is significant strain in the domain walls, both out-of-plane and lateral strain. The electronic band edges vary strongly with strain in dichalcogenides. We find a conduction band state moves into the intrinsic band-gap of the bilayer, binding electrons to the domain wall. In contrast, the valence band moves down — holes are repelled by the domain wall.

DoD Impact/Significance: Twisted dichalcogenide bilayers are candidate materials for hosting strongly correlated carriers, where the interactions between the carriers can be tuned by adjusting the angle of the twist. Our results show that at the band edges, electrons bind to the domain walls, while holes are repelled by the domain walls. Thus, two types of confined carriers will form in the experimental structures: electrons at the domain walls and holes in the “bulk” regions between the domain walls. Due to their tighter confinement, the Coulomb interaction will be stronger between electrons than between holes. However, the kinetic dispersions for both electrons and holes will be flat, so interesting behavior may occur with both types of carriers.

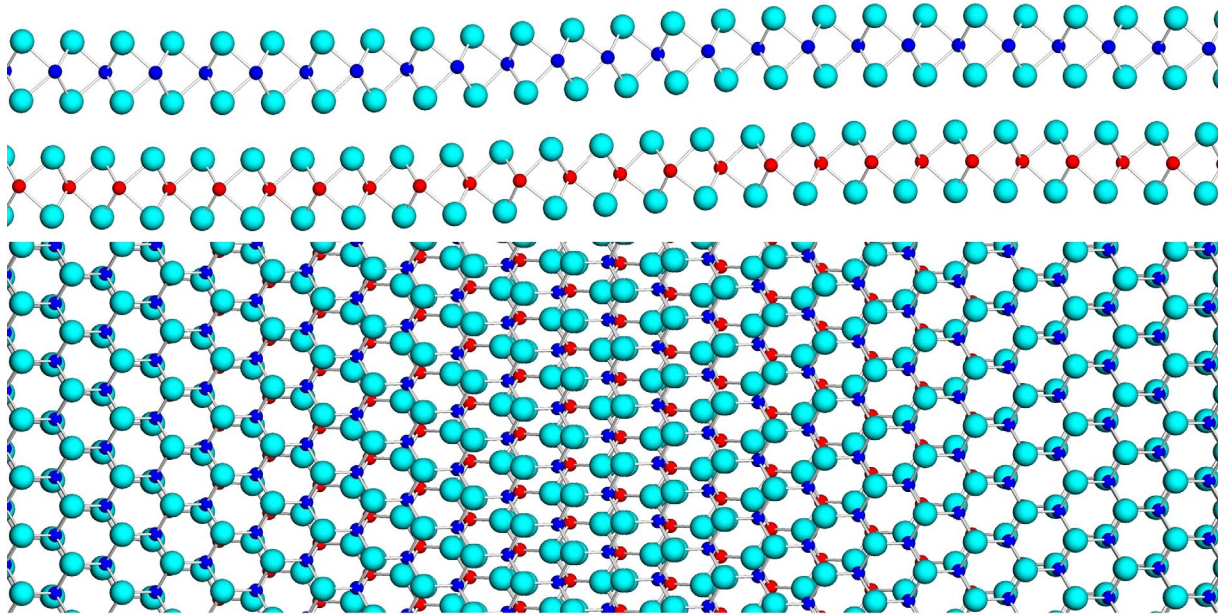


Figure 1. Buckling of MoSe₂/WSe₂ at a domain wall. The domain wall is located in the center of each figure. Mo atoms are dark blue, W atoms are red, and Se atoms are light blue. The significant buckling is apparent in the side view (top panel). In the view from above (bottom panel), the MoSe₂ shifts up by half of a lattice constant moving from left to right across the panel, while the WSe₂ shifts down by the same amount.

Title: Marine Biofilm Metaproteomics
Author(s): W.J. Hervey, J. Schultzhaus, G. Ellis, and G.J. Vora
Affiliation(s): Naval Research Laboratory, Washington, DC
CTA: CCM

Computer Resources: HPE SGI 8600, SGI ICE X [AFRL, OH]; Cray XC40 [ARL, MD]; Cray XC40/50 [ERDC, MS]

Research Objectives: To maintain and adapt a distributed, modular suite of bioinformatics software applications from the public domain. This effort leverages a previous HPC Application Software Initiative (HASI) awarded for multi *-omics* data analytics of complex biological systems. While the majority of bioinformatics applications are, by nature, embarrassingly serial, this project has assembled a workflow to leverage HPC resources efficiently on emerging architectures. Selectively tailoring bioinformatics applications to specific Department of Defense use cases continues to enable *-omics* characterizations of microbiomes, biofilms, and complex marine eukaryotes.

Methodology: Factors limiting analysis and interpretation of large-scale genomic (DNA), transcriptomic (RNA), proteomic (protein), and metabolomic (metabolite) datasets include a code base of largely serial bioinformatics software tools and an increasing data volume. To alleviate computational bottlenecks among these *-omics* data analyses, the applications DISCO, MetaCarvel, and Sipros Ensemble (SE) are used for metagenome assembly, metagenome scaffolding, and metaproteome identification, respectively. DISCO, **D**istributed **C**o-assembly of **O**verlap graphs, assembles genome reads by an overlap-layout-consensus (OLC) approach while using both OpenMPI and distributed memory. DISCO output is passed to the multithreaded MetaCarvel scaffolding application, which joins contiguous DNA segments (or “contigs”) into larger genome scaffolds. MetaCarvel output is representative of multiple genomes present in a microbiome, but is also able to retain genome sequence variants among assembly graphs as SPQR trees. SE leverages hybrid OpenMP/MPI capabilities to search tandem mass spectra for potential matches among millions of proteins arising from *in silico* translations of MetaCarvel metagenome scaffolds. SE significantly reduces the false-discovery identification rate in metaproteome profiles by applying a random forest classifier to multiple scoring functions. For each biological system’s study and HPC use-case, any combination of these 3 distributed bioinformatics tools may be applied for *-omics* analyses and analytics.

Results: This subproject contributed to data analyses among a range of biological systems: soil microbiomes, marine planktonic and biofouling microbiomes, diver microbiomes, and the acorn barnacle, *Amphiblanus amphitrite*. In FY20, HPC allocations on this subproject yielded contributions to three peer-reviewed publications, three oral presentations, and one invitation to participate in an intralab study (1 non-peer-reviewed professional society report).

DoD Impact/Significance: This HPC subproject has broad DoD significance. It is directly applicable to “sense and sense-making” from large data, biotechnology, artificial intelligence, machine learning, biologically inspired materials design, biosensing, synthetic biology, systems biology, alternative energy sources, and platform sustainability.

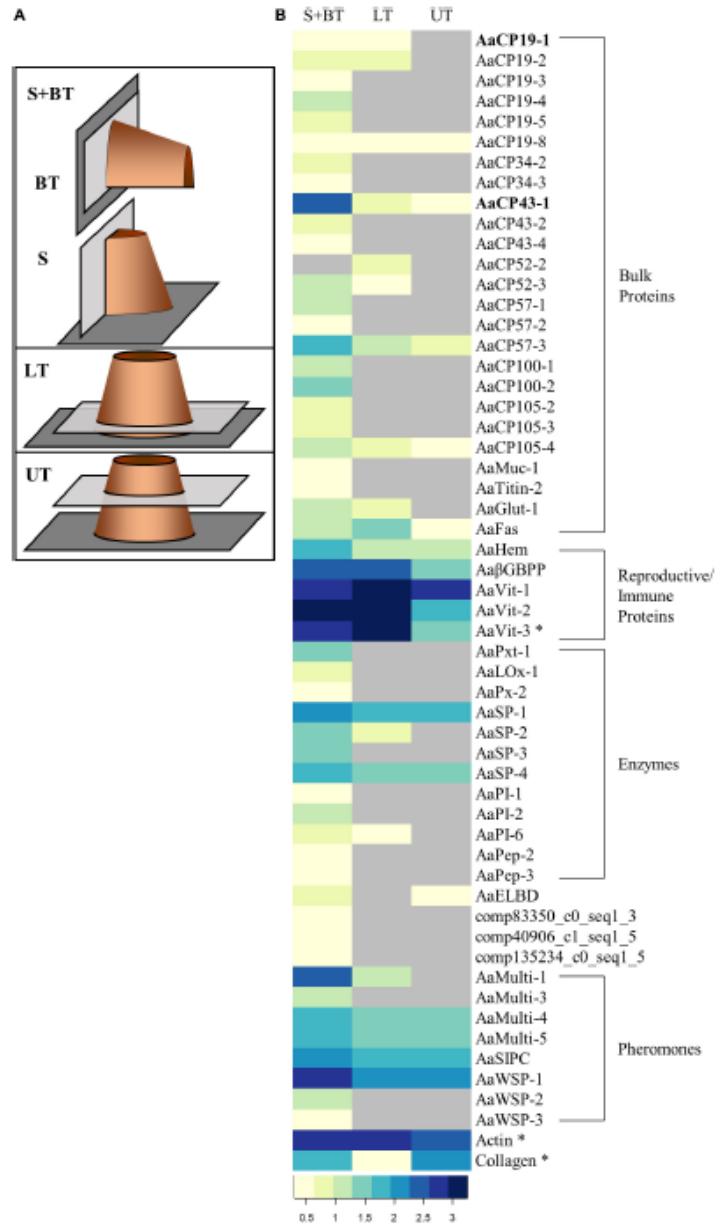


Figure 1. “Proteomic analysis of Acorn Barnacle Tissue Sections. (A) Schematic representations indicating the location (light gray rectangles) of the sections along a barnacle (orange cylinder) settled on a substrate (dark gray rectangle) analyzed for proteomics. Sagittal = S; BT = Basal Transverse; LT = Lower Transverse; UT = Upper Transverse. S and BT sections were combined (S + BT). The locations indicated here match exactly with the sections in Figure 1. (B) Heatmap illustrating total spectrum counts (log10 transformed) for S + BT, LT, and UT FFPE sections. The proteins are grouped by predictive function: bulk proteins that compose adhesive at the interface; proteins that play a role in reproduction and/or immunity; and pheromones. Gray cells indicate no identification. Asterisks indicate proteins that have not been identified in the adhesive previously. AaCP19-1 and AaCP43-1 identifiers are in bold.” (Figure shown above is Figure 5, Schultzhaus JN *et al.*, *Frontiers in Marine Science*. 2020.)

Title: Synthetic Biology for Military Environments

Author(s): W.J. Hervey, J.R. Compton, D.H. Leary, and G.J. Vora

Affiliation(s): Naval Research Laboratory, Washington, DC

CTA: CCM

Computer Resources: HPE SGI 8600 [AFRL, OH], [NAVY, MS]; SGI ICE X [AFRL, OH]; Cray XC40 [ARL, MD]; Cray XC40/50 [ERDC, MS]

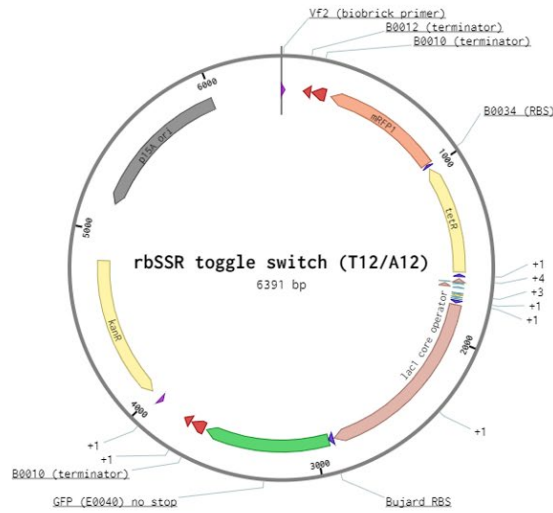
Research Objectives: To deploy genetic circuits, operational envelopes, and designer molecular toolkits in microbes (or synthetic biology host chassis). Conventional host chassis, such as *E. coli*, and recombinant expression systems limit *on-demand* production of military-relevant analytes, molecules, or materials. For military-relevant synthetic biology applications, NRL has demonstrated the potential of two marine microbial species, *Marinobacter atlanticus* and *Vibrio natriegens*. To assess *plug-and-play* compatibility among genetic circuits engineered for use in *E. coli*, we examined expression of an inducible genetic circuit in *Vibrio natriegens* using mass spectrometry-based proteomics. A prerequisite for engineering synthetic biology platforms is systematic, high-throughput assessment of newly imparted, desired functions **and** any collateral effects on the host chassis. Proteome profiling yields this insight in a single measurement. When integrated with disparate genomics (DNA) and transcriptomics (RNA) measurements, proteome profiles provide molecular-level insight necessary for optimizing and streamlining genetically tractable synthetic biology chassis. Among DoD tri-service labs engaged in biotechnology research, this HPCMP subproject serves an essential role for co-investigators to collaboratively analyze ‘-omics’ data and benchmark emerging bioinformatics software applications.

Methodology: An active area of synthetic biology research is engineering desirable, yet controllable, functions into cells. Engineered functions are often modulated by genetic means, ranging from simple antibiotic resistance to encoding elaborate genetic circuits. High-throughput proteome profiling of engineered systems enables simultaneous measurement of genetic circuit performance, as well as potential collateral effects on microbial physiology. After genetic circuit induction, *Vibrio natriegens* proteomes were profiled by liquid chromatography tandem mass spectrometry (LC-MS/MS). Mass spectrometry data were transferred to HPCMP systems, where large memory nodes extracted these highly multidimensional data into disparate formats. To identify expressed proteins, the Sipros Ensemble application (SE) applied a random forest classifier to correlate peptide masses and fragmentation patterns to *in silico* predicted patterns of *V. natriegens*. SE, an HPCMP HASI sponsored application, leverages OpenMPI to distribute computationally intensive tasks. Additional data features, such as precursor ion intensities, mass-to-charge ratios, and analyte retention times were applied to determine gene circuit efficacy and potential collateral effects on microbial physiology. Proteomics results were rendered in two visual snapshots: i) multidimensional representation of spectral intensities, retention times, and mass-to-charge into images, and ii) classification of predicted protein function into Voronoi diagrams.

Results: Preliminary results indicate genetic circuit expression in *V. natriegens* is functional but likely alters core metabolism, which merits further research. In FY20, HPC allocations enabled *V. natriegens* studies and other synthetic biology chassis. Allocations contributed to two peer reviewed publications, an invitation to an intralab study (1 non-peer reviewed publication), and one publication in final preparation.

DoD Impact/Significance: This subproject is a collaborative tri-service resource for synthetic biology and biotechnology. It is directly applicable to “sense and sense-faking” from large data, biotechnology, artificial intelligence, machine learning, biologically inspired materials design, biosensing, synthetic biology, systems biology, and alternative energy sources.

a.



b.

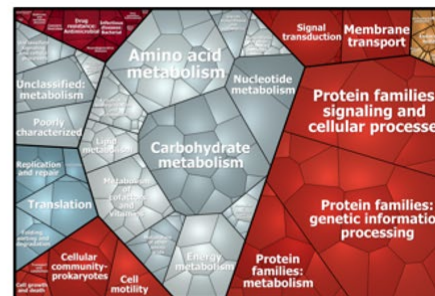
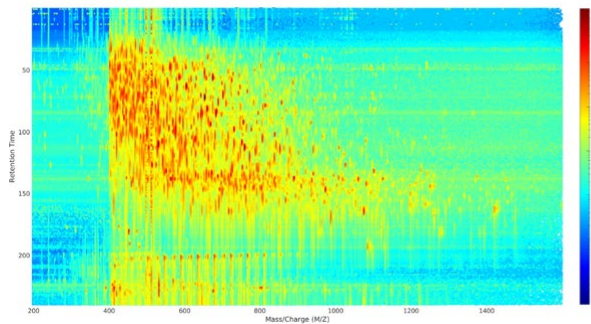


Figure 1. Gene circuit activation and protein expression profiling in *Vibrio natriegens*. a. A gene circuit engineered for expression in *E. coli* (top left; Egbert and Klavins, *PNAS* 2012), was transformed into the host chassis, *V. natriegens* (top right). Activation of the genetic circuit resulted in expression of five proteins encoded in the circuit among the endogenous 4,748 predicted proteins in the *V. natriegens* proteome. b. Proteome profiles of gene circuit expression in the *V. natriegens* host chassis were acquired via liquid chromatography tandem mass spectrometry (LC-MS/MS). HPCMP allocations were used to extract and visualize raw spectral intensity (bottom left), to identify proteins expressed among profiles studied (not shown), and to evaluate potential collateral physiological effects of gene circuit on metabolism (bottom right, Voronoi diagram). As shown, profiling expression of the genetic circuit in *V. natriegens* impacted carbohydrate, nucleotide, and amino acid metabolism. These results are consistent with laboratory growth rates.

Title: Materials for Energy Storage and Generation
Author(s): M. Johannes
Affiliation(s): Naval Research Laboratory, Washington, DC
CTA: CCM

Computer Resources: SGI ICE X [AFRL, OH], [ARL, MD]

Research Objectives: The objectives of this program are to use density functional theory (DFT) and its extensions, including molecular dynamics, to understand the materials properties that drive functionality in materials relevant to energy storage and generation, including new materials for low-power electronics.

Methodology: First-principles pseudopotential methods are employed to calculate the quantities of interest. The majority of the work was done using the Vienna Ab-Initio Software Program (VASP), but a substantial minority was done using the Wien Code, which is a full potential LAPW code. Post-processing is done using personal codes. Both standard (static) $T = 0$ DFT calculations and temperature-dependent molecular dynamics (MD) calculations were used.

Results: In FY20, the project's focus was on analyzing materials for catalysis, especially in terms of charge transport. The effect of defects was found to be extremely important for both photocatalysis in Au-infused TiO_2 and in solid fuel cell electrolyte material $\text{NH}_4[\text{B}(\text{SO}_4)_2]$. One major finding was that without any defects (i.e., in a perfect crystalline material), the Au nanoparticles that drive catalytic behavior at the surface of a TiO_2 substrate do not interact electronically with the substrate. Another major finding was that proton conduction through $\text{NH}_4[\text{B}(\text{SO}_4)_2]$ is not related to transfer of intrinsic protons between NH_4 units, but rather occurs via extrinsic protons that occur due to the acidic environment. Extremely soft SO_4 phonon modes allow O-O distances to shrink sufficiently to transfer protons along a three-dimensional pathway.

A secondary project has been the analysis of strain effects in topological materials. In materials where degeneracies are "accidental" due to band crossings but "protected" due to the symmetry of the bands, cone like Dirac states form. Straining the materials, though, removes the symmetry protection and gaps out the band crossings. The newly gapped materials may be topologically trivial or nontrivial, depending on the relationship of the phase of the wave functions around a particular loop in the Brillouin zone. We have calculated the topological character of Cd_3As_2 as function of strain and found that strain along the (110) direction significantly gaps the material, resulting in strongly nontrivial topological materials with robustly protected, highly conductive surface states.

DoD Impact/Significance: The DON has set a goal of 50% energy consumption from alternative sources in 2020. Catalysis, especially employing materials not containing Pt, Pd, or Rh (all of which are expensive, rare and found outside US mines), is a possible route not only to fulfill the DON goal, but to provide greater energy security by centering the production of energy within US boundaries and using cheap materials.

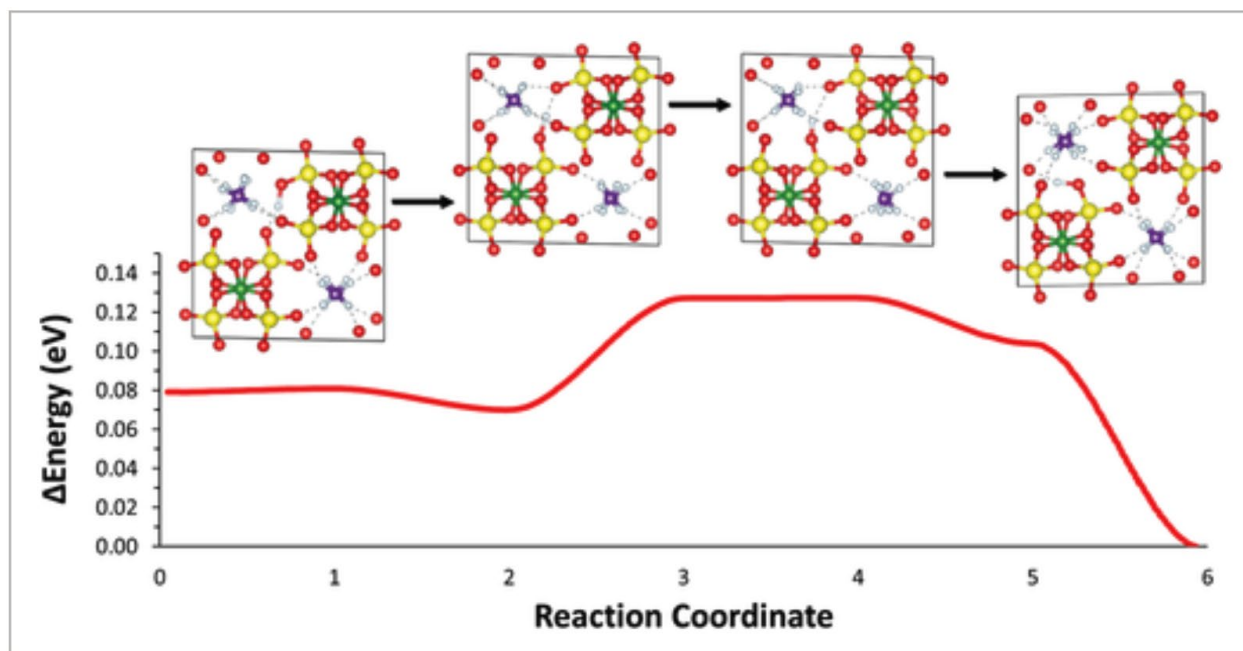


Figure 1. The reaction pathway of a proton through $\text{NH}_4[\text{B}(\text{SO}_4)_2]$. Although the crystal has seemingly one-dimensional channels for diffusions, the SO_4 units are soft and contract around the diffusing p^+ , allowing three-dimensional movement.

Title: Calculation of Fundamental Physical Parameters for Lower Dimensional Materials

Author(s): C.M. Krowne¹ and X. Sha²

Affiliation(s): ¹Naval Research Laboratory, Washington, DC; ²General Dynamics IT Corporation, Falls Church, VA

CTA: CCM

Computer Resources: HPE SGI 8600, SGI ICE X [AFRL, OH]

Research Objectives: The objective is to obtain basic physical parameters of the lower-dimensional materials, such as topological insulators (TIs), thin-film ferroelectric, thin-film ferrimagnetic and ferroic materials, and single- or multilayer graphene, and other lower-dimensional materials in 2D or lower.

Methodology: Concurrent with analytical studies using 2nd quantized Hamiltonians, many-body quantum Green's functions, and renormalization techniques, *ab initio* methods are utilized to obtain fundamental parameters including atomic and molecular structure conformation, electronic band structure, charge distribution, and transport characteristics. Various density functional theory codes including ABINIT, Quantum Espresso, CASTEP and DMOL3 have been used.

Results: We have examined other sister materials to graphene and silicon, which, in graphene's case, may change from a zero-bandgap Dirac material to one with a gap for certain allotropes of graphyne. This is also the case for specific allotropes of borophene, a material related to the monoatomic silicon materials, but shifted by one column in the periodic table of elements. Figure 1 shows the atomic computational structure of the borophene. Figure 2 gives the electronic bandstructure $\epsilon(\mathbf{k})$ vs. \mathbf{k} through symmetry points in the Brillouin zone for the α_1 allotrope of borophene for three different hybrid functionals PEB0, HSE, and B3LYP. Figure 3 provides the self-consistent field (SCF) computational time versus the discretization k-space area N_{grid}^{area} . Since our supercell has relatively large size (~30 angstroms) along the direction perpendicular to the borophene plane, we only need one k point along that direction. The k point sets we tested include five of them with increasing values: 1) 4 x 4 X 1; 2) 6 x 6 X 1; 3) 8 x 8 X 1; 4) 12 x 12 x 1; 5) 16 x 16 X 1. The numerical grid area in k-space is the triple product of these discretization values. Our results will have bearing on using the metal-insulator transition (MIT) for designing materials for new magnetic behavior, superconducting behavior, and other effects in 2D nanoscopic materials and other lower-dimensional materials. See S. Johnson, H. Haucke, C. Krowne, S. Shin, S. Quadri, "Characterization of Ferrimagnetic and Spin Wave Resonance for Frequency Selective Limiting of Iron Garnet Epitaxial Films," Virtual Meeting, Mater. Sc. & Tech., Nov. 3, 2020.

DoD Impact/Significance: Lower-dimensional materials hold promise for moving technology into the realm where conventional devices and materials cannot perform, which is of great importance to the Navy and the DoD. For example, using materials that display MIT, new solid-state microscopic devices could be envisioned that require switching capabilities, avoiding or supplementing those being pursued with phase-change materials, such as vanadium dioxide, which require inconvenient temperature changes. Likewise, transparent conductive materials which display a MIT, could be used in many device contexts, from solar cells to transistors. MIT materials even could be used as shields against incoming interrogating radiation, because they transition under DC electric E fields or even under RF fields, not only under temperature changes. For TIs, this may provide another way to develop 2D types of transport materials with substrates, removing the problem with how to handle single-layer atomic materials like graphene. Similarly, Weyl semimetals could provide contamination free Dirac points for electronic action.

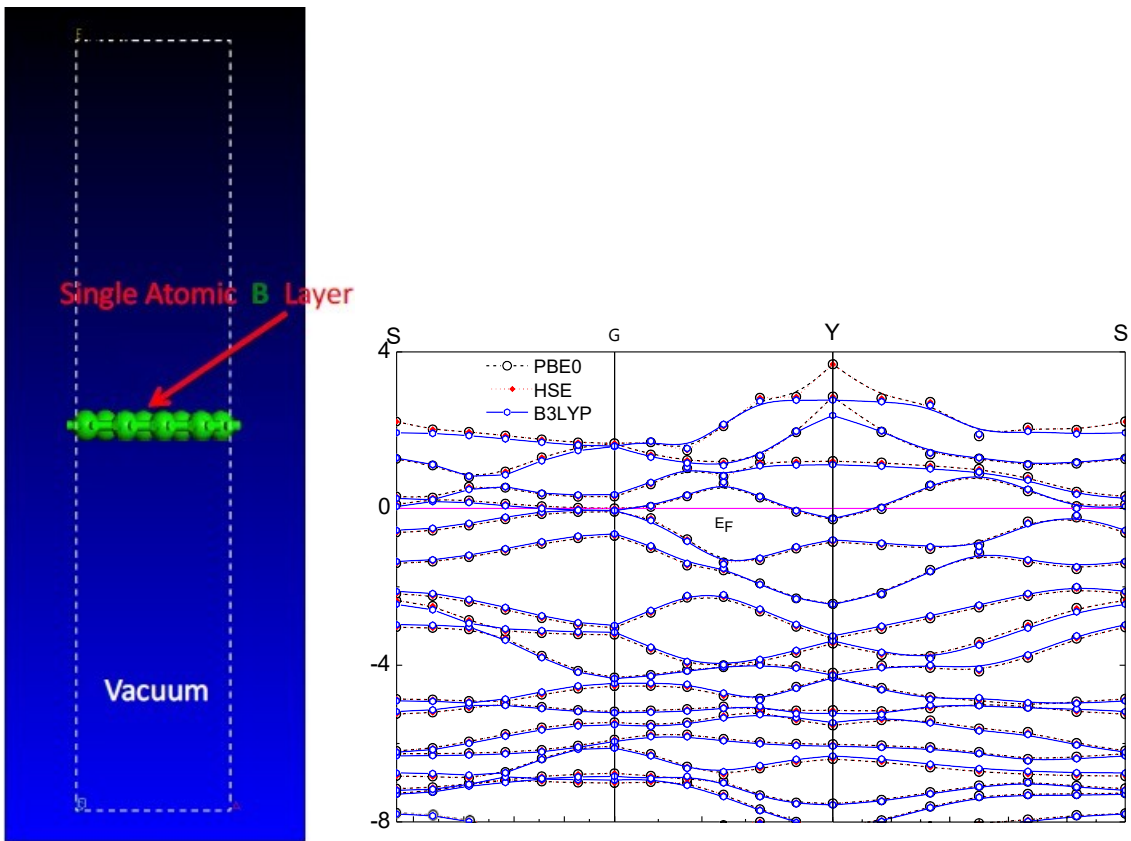


Figure 1. Side view of the 2D atomic layer of borophene computational structure used in DFT calculations. Figure 2. Detailed comparison of the calculated band structures of a_1 borophene nanostructure using PBE0, HSE, and B3LYP hybrid functional DFT calculations.

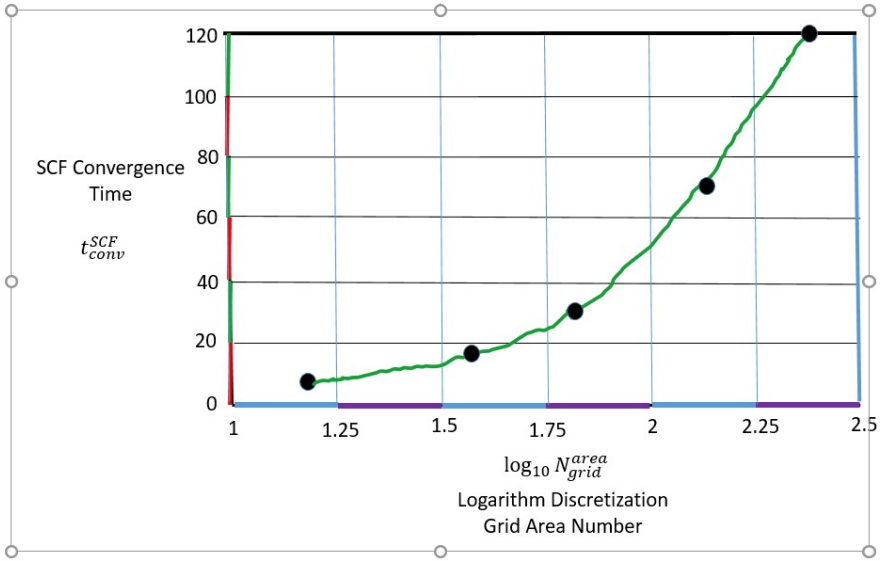


Figure 3. SCF convergence time versus the logarithm of the k-point discretization normalized area grid on the supercomputer Thunder at AFRL DSRC. Notice the green guide line through the points highlights the nonlinear nature of the trend.

Title: Dielectric Functions for Cesium Lead Halide Perovskites

Author(s): A. Shabaev, K. Jensen, and S. Lambrakos

Affiliation(s): Naval Research Laboratory, Washington, DC

CTA: CCM

Computer Resources: HPE SGI 8600, SGI ICE X [AFRL, OH]; SGI ICE X, Cray XC40 [ARL, MD]; Cray XC40/50 [ERDC, MS]

Research Objectives: Calculation of Dielectric Functions for Cesium Lead Halide Perovskites using Density Functional Theory

Methodology: The present study examines physical characteristics of the dielectric response of cesium lead halide perovskites that provide a foundation for formulating quantitative dielectric response functions using quantum theory-based calculations, i.e., density functional theory (DFT) and associated software technology, which provides complementary information to that obtained from spectroscopic measurements. This complementary information is both spectral features and their physical interpretation with respect to crystal structure, and thus prediction of spectral features that complement measurements in the laboratory. The present study adopts the VASP software, where the dielectric function is calculated by solving the Bethe-Salpeter equation and electronic structure calculations within the GW0 method (see [Shabaev, Jensen, & Lambrakos, *SPIE* 11392, 2020] and references therein).

Results: The results of our study are electronic structure and dielectric functions for CsPbCl₃, CsPbBr₃ and CsPbI₃, calculated using computational methods based on DFT. Computational data for dielectric functions of these perovskites are shown in Fig. 1. The computational data shown in Fig. 1 is used to find Drude-Lorentz parameters assuming contributions due to various Lorentzian resonances terms [Shabaev, Jensen, & Lambrakos, *SPIE* 11392, 2020]. The Drude-Lorentz susceptibility model provides a suitable phenomenological parametric representation of experimental values for semiconductor dielectric functions. In insulators and semiconductors, this model can achieve the more detailed representation of band edges in the optical spectrum by including critical points associated with the Van Hove singularities in the joint density of states. The method applied here, although approximate, is rapid and flexible, and provides a reasonably accurate account of critical-point parameters for high photon energies that allows substantial adjustment of Drude-Lorentz parameters.

DoD Impact/Significance: Lead halide perovskites are attractive materials for optical applications, e.g., photovoltaics, light emitters, high energy radiation detection and photocathodes. Low-dimensional structures open new opportunities for engineering the spectrum of the perovskite nanomaterials by changing their size and composition. The emissive spectra of cesium lead halide perovskites CsPbCl₃, CsPbBr₃, and CsPbI₃, can be varied continuously from infrared to ultraviolet by mixing the halide components: iodine, bromide and chlorine. The Drude-Lorentz model of dielectric functions is profitable in the simulation of internal photoemission processes [Jensen et al., *J. Applied Physics* 2020], characterization of photocathode materials, and utilization by beam codes. In the absence of more conclusive experimental studies, dielectric functions of cesium lead halide perovskites can be estimated by approximate fits of the Drude-Lorentz model to computational data obtained using DFT.

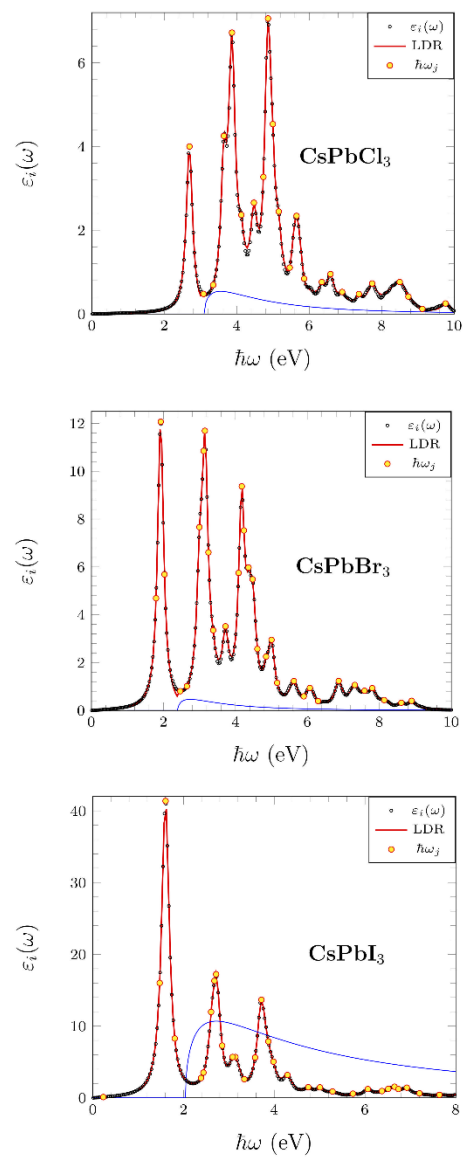


Figure 1. Density-functional calculations of dielectric function $\epsilon_i(\omega)$ (open circles) and the associated Drude-Lorentz (LDR) model (red line and filled circles) CsPbX₃ (X = Cl, Br, I).

Title: Calculation of Materials Properties via Density Functional Theory and Its Extensions

Author(s): J.L. Lyons

Affiliation(s): Naval Research Laboratory, Washington, DC

CTA: CCM

Computer Resources: SGI ICE X [AFRL, OH], [ARL, MD]; Cray XC40 [ARL, MD]

Research Objectives: The prime objective of this project is to understand the electronic structure of wide-band-gap semiconductors (WBGs) such as gallium oxide (Ga_2O_3) and aluminum nitride (AlN) and novel materials such as cesium lead bromide (CsPbBr_3) using techniques including hybrid density functional theory (DFT) which accurately describes the electronic structure and defect properties of WBGs.

Methodology: DFT has long been a proven method for deducing semiconductor electronic structures, but when applied to WBGs, the so-called “band-gap problem” makes difficult the quantitative prediction not only of bulk band structures, but also of defect properties. To overcome these issues, we employ hybrid density functional theory. Hybrid functionals mix in a fraction of screened Hartree-Fock exchange into the exchange-correlation functional, and are capable of quantitative predictive accuracy for band gaps and defect transition levels, even in WBGs. Using hybrid DFT, the charge-state transition levels, formation energies, and optical transitions associated with defects and impurities in WBGs are determined. With the same methods, the electrical and structural properties of semiconductor alloys (such as $\text{Al}_x\text{Ga}_{1-x}\text{O}_3$ and $\text{Sc}_x\text{Al}_{1-x}\text{N}$) also are calculated.

Results: We investigated the electronic structure of $\text{Sc}_x\text{Al}_{1-x}\text{N}$ alloys and performed band alignment calculations between these alloys and gallium nitride (GaN). Alloying ScN into AlN causes an increase in lattice constants, as well as a decrease of the electronic band gap. Surface-slab calculations allowed for the determination of band alignments between $\text{Sc}_x\text{Al}_{1-x}\text{N}$ alloys and GaN. The valence-band offset varied strongly with Sc content, and approached zero near an ScN alloy fraction of 5%. In contrast, the conduction-band offset was large (2.5 eV), but did not vary strongly with alloy content (see Fig.1).

We also examined the structural and electronic properties of κ -phase alloys of Ga_2O_3 and Al_2O_3 . Increasing the Al content of such alloys was found to decrease lattice constants linearly, but gave rise to a nonlinear increase in the band gap and conduction-band offset (with a bowing parameter of 1.41 eV). The valence-band offset in these alloys was nearly zero, as almost entire band-gap variation was reflected in the conduction-band offset. In such alloys, Al atoms strongly preferred to incorporate on octahedral sites, whereas Ga atoms preferred tetrahedral sites. The 50% AlGaO alloy was found to be especially stable. Finally, we also developed a microscopic theoretical model of nitride films grown by atomic layer epitaxy. Surface barriers and island binding energies were calculated from DFT, and these values were used to build a kinetic Monte Carlo (kMC) model of film growth. We found that islands nucleated as small, stable clusters that remain fixed in place as film growth proceeds. These results were well described by a universal scaling model and will serve as a starting point for the more complex modeling of ternary or quaternary alloys.

DoD Impact/Significance: WBGs such as Ga_2O_3 are utilized in power electronics that play a crucial role in many Navy-relevant applications, and afford significant SWAP-C savings when replacing components based on traditional semiconductor materials. Optimizing impurity doping, understanding contaminating species, and characterizing unintentionally incorporated defects are crucial steps for improving such materials.

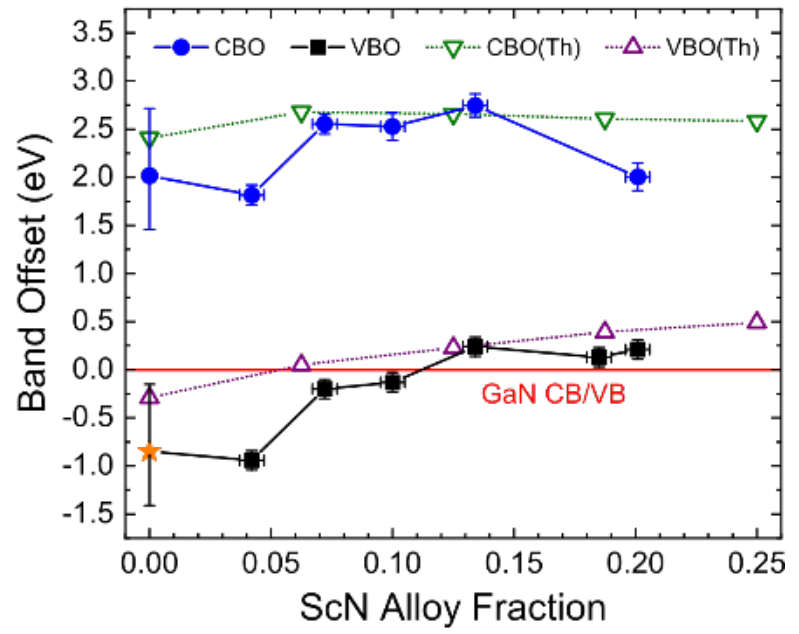
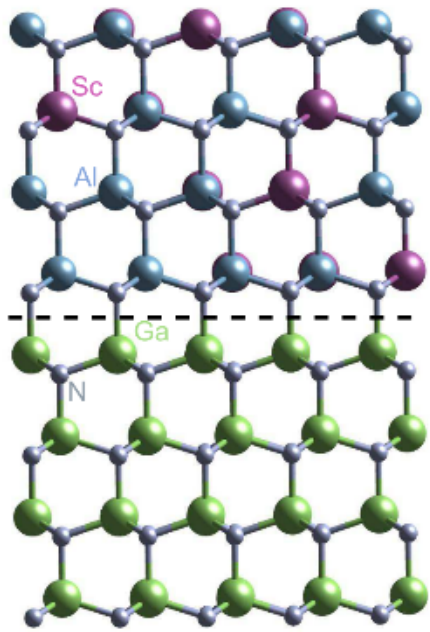


Figure 1.

Title: DFT Studies of Small Molecule Adsorption on Monolayer Transition Metal Dichalcogenide Films

Author(s): F.K. Perkins¹ and C.H. Sharp²

Affiliation(s): ¹Naval Research Laboratory, Washington, DC; ²National Research Council Postdoctoral Research Associate, Naval Research Laboratory, Washington DC

CTA: CCM

Computer Resources: HPE SGI 8600 [AFRL, OH]

Research Objectives: The objective of the proposed research was to perform electronic structure calculations of small-molecule adsorption on monolayer transition metal dichalcogenide (TMD) films to understand how electronic charge donation and interaction strengths between adsorbates and TMDs affect chemical sensor response. The results will aid in developing a model for the response of TMD-based sensor devices, thus suggesting a path toward specificity.

Methodology: The methodology used as part of this research involved the use of the computational chemistry software packages Gaussian and Quantum Espresso.

Gaussian: Gaussian employs localized basis sets to construct molecular orbitals of small molecules. Gaussian was employed to perform structure optimizations of the small-molecule adsorbates as well as to provide calculated vibrational spectra that will serve as a reference for infrared spectroscopy studies performed in the laboratory at NRL. The graphical user interface Gaussview was used to design chemical structures and to set up calculations.

Quantum Espresso: Quantum Espresso utilizes plane wave basis sets and pseudopotentials to analyze periodic structures. Using literature-based crystallographic data, we constructed TMD supercells and used Quantum Espresso to perform structure optimizations of small gas molecules adsorbed at different binding sites to quantify the adsorption energy.

Results: Results from FY20 include single-point (fixed-ion) self-consistent field calculations of MoS₂ and WS₂ in the 2H, 1T, and 1T' phases calculated with Quantum Espresso on AFRL ERDC "Mustang", which will provide the basis for the electronic band calculations and structure optimization in the presence of adsorbate gases.

DoD Impact/Significance: Computational studies of CWA and toxic industrial chemical (TIC) interactions with monolayer TMD films will support laboratory experiments currently underway at NRL, ranging from fundamental ultrahigh vacuum-based investigations to in situ chemical sensor testing. Calculated band diagrams of TMD surfaces before and after exposure to adsorbates will be used to validate ultraviolet photoelectron spectroscopy and low-energy electron diffraction data as well as to help in predicting chemical sensor response. The combination of electronic structure calculations and experimentation will yield high-quality publications. The anticipated results also will benefit a current NRL base 6.2 program investigating such materials as sensors, work unit 6B30 (Opto-Electronic Fingerprinting of Chemical Vapors).

Ammonia Adsorbed on MoS₂

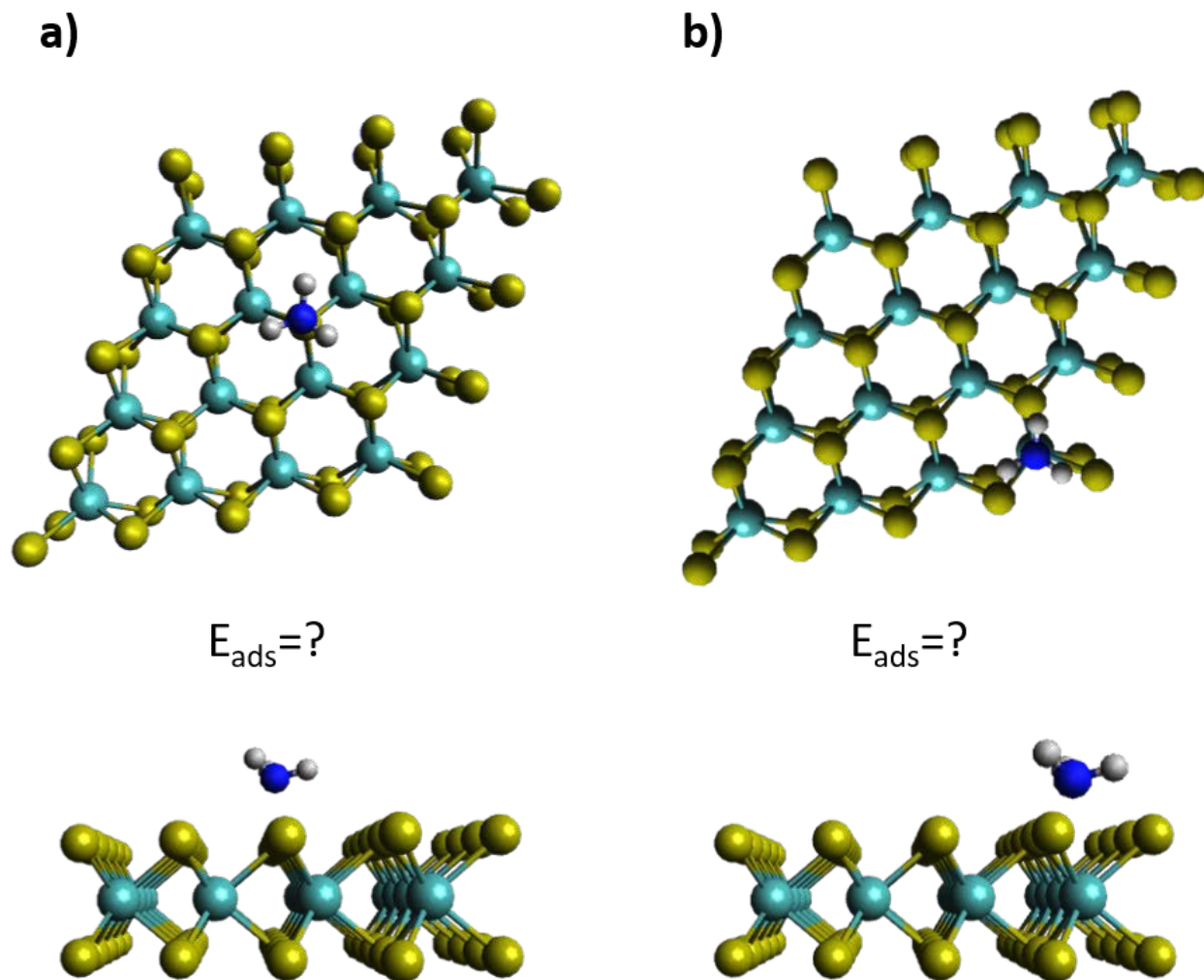


Figure 1. Ammonia adsorbed on 4x4x1 MoS₂ periodic slab over S atom (a) or over Mo atom (b). White, blue, cyan, and yellow colors refer to hydrogen, nitrogen, molybdenum, and sulfur, respectively.

Title: Numerical Studies of Semiconductor Nanostructures

Author(s): T.L. Reinecke¹ and S. Mukhopadhyay²

Affiliation(s): ¹Naval Research Laboratory, Washington DC; ²National Research Council Postdoctoral Program, Washington, DC

CTA: CCM

Computer Resources: HPE SGI 8600, SGI ICE X [AFRL, OH]; Cray XE6m [ERDC, MS]

Research Objectives: To make first-principles calculations of the thermal properties of a range of novel nonmetallic materials in order to predict new, high-thermal-conductivity materials for cooling electronics by heat sinking, and also new materials with low thermal conductivities and with good electronic properties for high-efficiency thermoelectrics for cooling and power generation.

Methodology: Ab initio density functional methods are used to calculate the phonon frequencies and the interactions between phonons in a range of nonmetallic materials and nanostructures. Inelastic Boltzmann equation methods are used to calculate their thermal conductivities. Calculations are made using Quantum Espresso and VASP codes.

Results: New materials with high electrical conductivities and low thermal conductivities are needed for high-efficiency thermoelectrics in cooling and power generation. In recent work, we developed first-principles calculations of electronic and vibrational properties and inelastic Boltzmann techniques to calculate thermal conductivities and used them to identify several classes of new materials that are expected to exhibit particularly high and low thermal conductivities, and we have traced these results to their underlying physical characteristics. In the cases of Tl_3VSe_4 and In_3VSe_4 we find low thermal conductivities $\kappa \approx 0.1 - 0.2$ W/mK, and we associate this behavior with their low-phonon-group velocities due to weakly bonded Tl and In atoms associated with s^2 lone-pair electrons. In general, we find that materials with lone-pair bonding frequently have low thermal conductivities.

We also have shown that Cs_3SbSe_4 (~ 0.1 W/mK) and $CsSbSe_4$ (~ 0.3 W/mK) have low thermal conductivities, but they do not have lone-pair bonding. In this case, we trace the low thermal conductivities to phonon anharmonicity due to their local lattice instabilities. The small ionic radius of Sb^{5+} brings the Se^{2-} closer to one another, leading to Coulomb repulsion and to lower stability.

The above materials have relatively complex crystal structures that give large anharmonicities and low thermal conductivities. However, it is less uncommon to find materials with simple crystal structures that have low thermal conductivities. Using high-throughput computational methods, we have shown that a simple bcc structure material, Cs_3VSe_4 , has a low thermal conductivity of $\kappa \sim 0.1$ W/mK. In this case, quartic terms are needed to describe their lattice anharmonicity, and the lattice structures are found to be stable. With its good electrical properties, this material will have a desirable thermoelectric figure of merit, $ZT \sim 0.9$ at 300 K.

DoD Impact/Significance: New high-thermal-conductivity materials and systems make possible their exploitation in thermal management. New low-thermal-conductivity materials with good electronic properties can provide thermoelectrics for cooling and power generation.

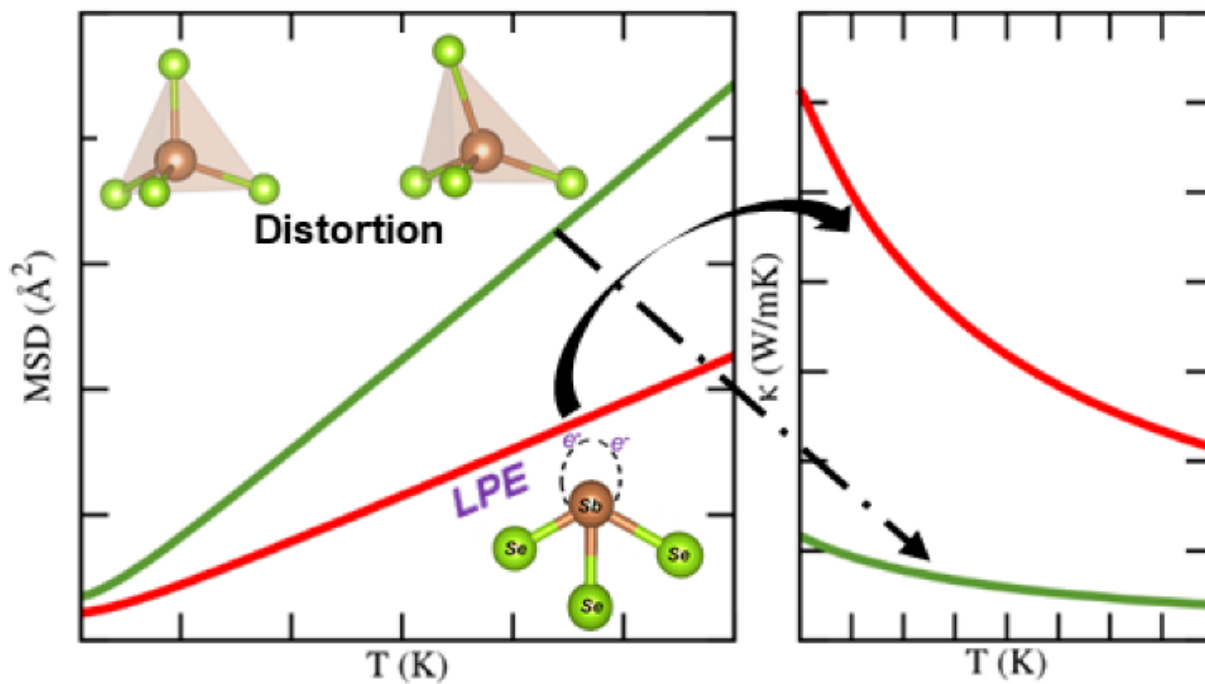


Figure 1. Designing low- κ materials based on lattice instability.

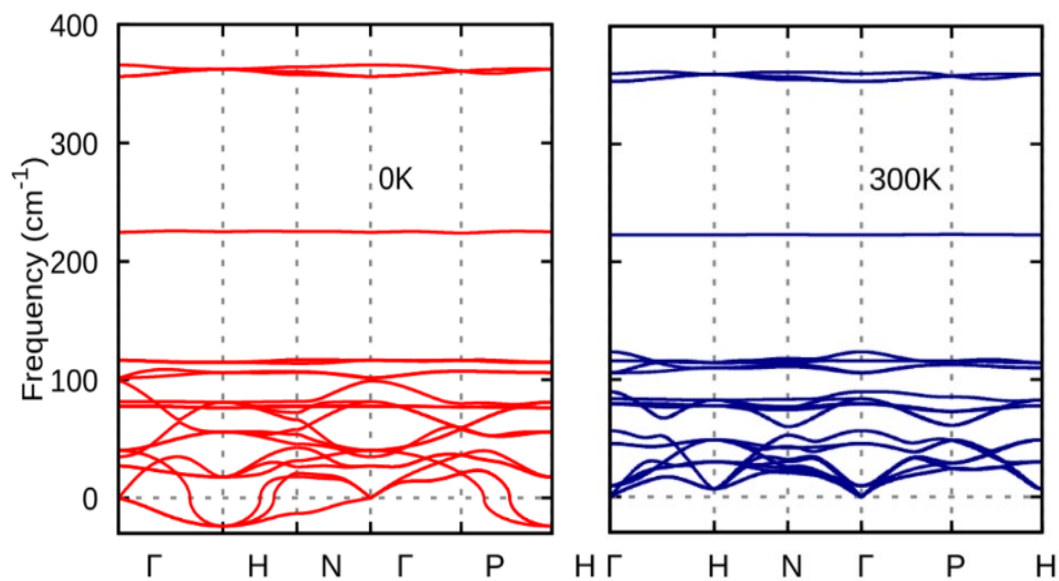


Figure 2. Effect of quartic anharmonicity in Cs_3VSe_4 : Phonon dispersion with force constants calculated at (a) 0 K and (b) at 300 K.

Title: First-principles Simulations of Condensed-phase Decomposition of Energetic Materials

Author(s): I.V. Schweigert

Affiliation(s): Naval Research Laboratory, Washington, DC

CTA: CCM

Computer Resources: HPE SGI 8600 [AFRL, OH], [NAVY, MS]; SGI ICE X [AFRL, OH], [ARL, MD]; Cray XC40 [ARL, MD]

Research Objectives: To predict thermal, mechanical, and chemical properties of explosives subjected to elevated temperatures and pressures.

Methodology: We use crystal structure optimizations and ab initio molecular dynamics (AIMD) simulations to study physical and chemical changes in energetic materials subjected to elevated temperatures and pressures. Structure optimizations use variable-cell optimization algorithms to determine changes in atomic coordinates and lattice constants at elevated pressures. AIMD simulations use constant-pressure, constant-temperature (NPT) integrators combined with multiple replicas to simulate changes in crystal structures at elevated temperatures. Atomic forces needed to perform these simulations are estimated from first principles, using density functional theory (DFT) combined with periodic-cell models of crystalline environments. Python and Perl scripts are being developed to facilitate the execution and analysis of these simulations.

Results: This year, we performed AIMD simulations of the anisotropic coefficients of thermal expansion (CTEs) of the HMX explosive. Periodic cells containing four ($2 \times 1 \times 2$) primitive unit cells of β -HMX (8 molecules) were used to approximate the ideal (defect-free) crystal structure. Atomic coordinates and lattice parameters were first optimized at 0 K using a variable-cell optimization algorithm, starting with the experimental crystal structure. The optimized structure was simulated at temperatures ranging from 100 to 298 K using an ensemble of five NPT trajectories for each temperature value. All trajectories were 12 picoseconds long. After a 6-picosecond equilibration period, instantaneous values of temperature, stress tensor, and lattice parameters were recorded every 50 femtoseconds and were averaged over the remaining 6 picoseconds. The trajectory-average values were averaged over the ensembles of five trajectories to provide the final estimates for the lattice parameters as functions of temperature. In addition to AIMD simulations, we tested two other MD variants: one based on self-consistent charge density-functional tight binding (SCC-DFTB) method and one based on a bond-order interatomic potential (ReaxFF/1g). The ensemble-averaged lattice parameters and tilt angles for β -HMX extracted from the three types of MD simulations are compared to the experimental values in Fig. 1. We note that only DFT-based AIMD simulations predicted lattice parameters that correctly followed the experimentally observed trends for each lattice parameter, including the weak dependence of the a constant on temperature. Overall, the lattice parameters extracted from AIMD simulations were within 0.2 Å of the experimental values and the tilt angles were within 0.6° of the experimental values for all temperatures considered. The lattice parameters extracted from the SCC-DFTB-based MD simulations were in a reasonable agreement with the experimental values, with maximum errors of 0.3 Å and 0.8°. The lattice parameters extracted from the ReaxFF-based MD simulations deviated significantly from the experimental values, with maximum errors of 0.8 Å and 1.8°.

DoD Impact/Significance: Thermomechanical equation of state for β -HMX, including shock Hugoniot relationships, is needed to support physics-based modeling of HMX-based explosives and solid rocket propellants. The simulations completed this year ascertained the accuracy of DFT in application to HMX against available experimental data. Future simulations will focus on the equations of state under elevated temperatures and pressures, for which experimental data is currently unavailable.

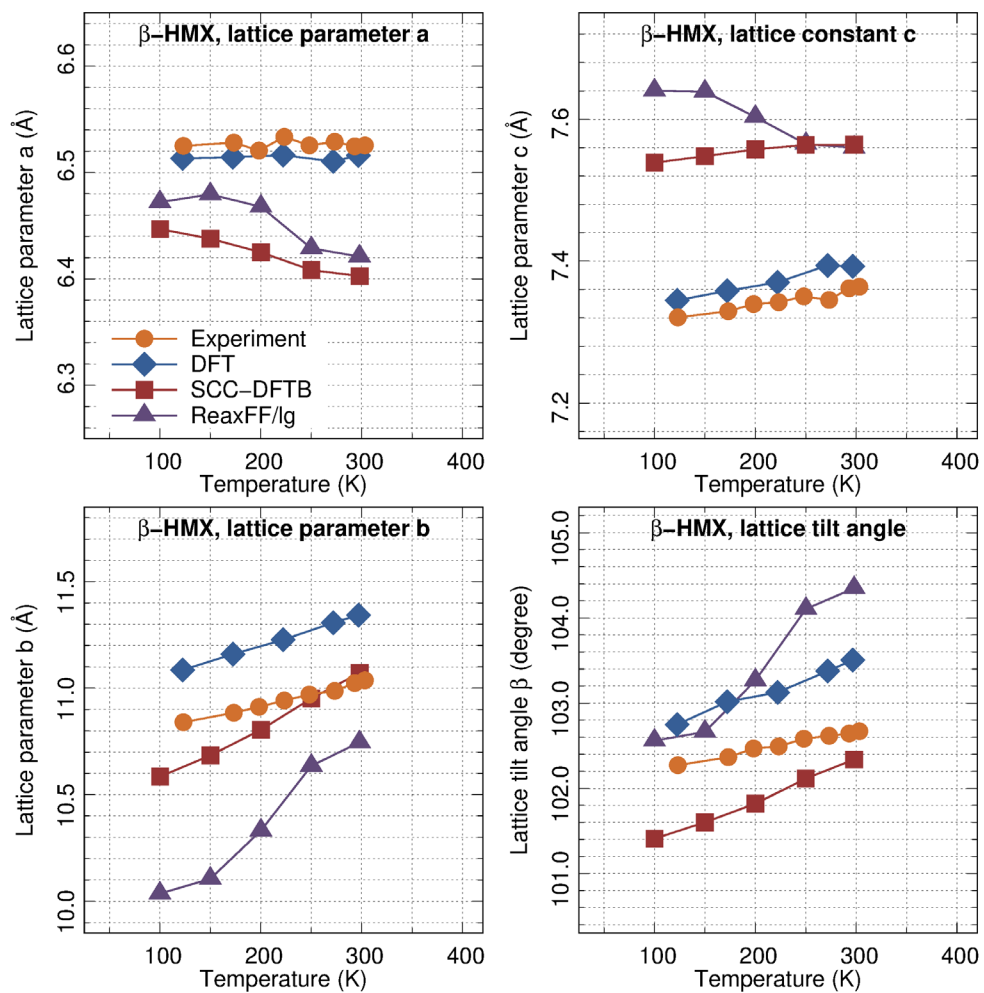


Figure 1. Computed and experimental lattice parameters of β -HMX at various temperatures. Solid lines through the points are provided to guide the eyes.

Title: Point Defects and Interfaces in Two-Dimensional Materials

Author(s): D. Wickramaratne

Affiliation(s): Naval Research Laboratory, Washington, DC

CTA: CCM

Computer Resources: SGI ICE X, Cray XC40 [ARL, MD]

Research Objective: To understand and predict the electronic, structural and optical properties of point defects, dopants and interfaces in bulk and low dimensional semiconductors.

Methodology: We use density functional theory (DFT) and the projector augmented wave (PAW) method as implemented in the Vienna Ab Initio Simulation (VASP) code for our calculations. To accurately describe the band gap of semiconductors, we use screened hybrid functional calculations. Accurate forces and total energy calculations are required to identify the most stable configurations of point defects in their various charge states. We use this information to determine the formation energies, charge-state transition levels and optical transitions of various defects.

Results: We systematically explore the properties of group-IV (C, Si, Ge, and Sn) and transition metal (Hf, Zr, and Ta) dopants substituting on the cation site in $(Al_xGa_{1-x})_2O_3$ (AlGO) alloys using first-principles calculations with a hybrid functional. In Ga_2O_3 , each of these dopants acts as a shallow donor. In Al_2O_3 , they are deep defects characterized by the formation of either DX centers or positive- U ($+0$) levels. Combining our calculations of dopant charge-state transition levels with information of the AlGO alloy band structure, we estimate the critical Al composition at which each dopant transitions from being a shallow donor to a deep donor. We identify Si to be the most efficient dopant to achieve n -type conductivity in high Al-content AlGO alloys, acting as a shallow donor over the entire predicted stability range for AlGO alloys. A paper on these results was published in *Applied Physics Letters* and was selected as an Editor's Pick.

DoD Impact/Significance: There are growing experimental efforts to alloy Ga_2O_3 with Al, which would enable the powering of electronic devices that operate at higher electric fields and UV devices that operate at shorter wavelengths. Such devices are of interest for DoD applications. The successful operation of these devices is predicated in part upon the ability to identify donor dopants that would give rise to n -type conductivity.

This work has helped identify potential donor dopants in wide-band-gap alloys of Al_2O_3 and Ga_2O_3 and the critical alloy composition at which the different donors transition from being shallow to being deep defects, at which point they no longer give rise to n -type conductivity.

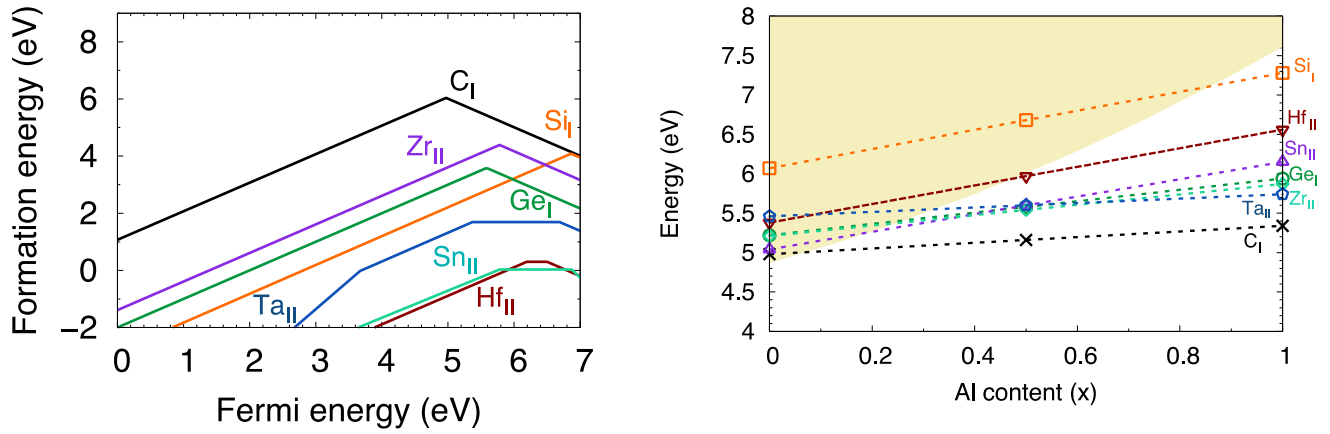


Figure 1. (Left) Formation energy of candidate donors in monoclinic Al₂O₃ under Al-rich conditions on their most favorable sites. Substitution on the tetrahedrally coordinated cation site is marked with subscript (I) and substitution on the octahedrally coordinated cation site is marked with subscript (II). (Right) The (+/-) levels of C_I, Si_I, Sn_{II} and the (+/0) levels of Ge_I, Hf_{II}, Ta_{II}, and Zr_{II} obtained from calculations in Al₂O₃ and AlGaO₃ alloys as a function of Al content. The CBM energy (shaded yellow) across the range of Al content is plotted with respect to the VBM energy of Ga₂O₃.

Title: Atomistic Simulations of Navy-relevant Materials
Author(s): D. Fragiadakis
Affiliation(s): Naval Research Laboratory, Washington, DC
CTA: CCM

Computer Resources: HPE SGI 8600 [AFRL, OH]; SGI ICE X, Cray XC40 [ARL, MD]

Research Objectives: The objective of the work conducted was to determine the phase behavior and mechanics of soda-lime glass under shock compression as well as static conditions of extreme temperatures and pressures such as those encountered during high-velocity impact.

Methodology: Molecular dynamics simulations using a recent simple force field for silica-based glasses were used to model shock compression and static compression/heating of soda-lime glass. The LAMMPS simulation software was used to conduct the simulations on HPCMP resources, with in-house software for data analysis.

Results: In agreement with experiment, simulations show that crystallization of soda-lime glass is much slower than that of silica. Homogeneous crystallization rarely occurs on the simulation time scale (tens of nanoseconds). However significant heterogeneous crystallization is observed. Both crystal “seeds” (stishovite and perovskite) as well as smooth walls were used to trigger heterogeneous crystallization. Three primary crystal forms result: a disordered and defective form of stishovite, a modified form of CaSiO_3 perovskite, and a mixed $\text{CaO}/\text{Na}_2\text{O}$ oxide phase formed in cation-rich regions excluded from the two former crystal structures. Crystallization occurs during static compression above 20 GPa in the 2000 – 3500 K range, as well as under shock compression for shock pressures in the 60 – 80 GPa range, causing a small shift of the Hugoniot towards higher densities. In addition, initial quantum-level calculations were performed on soda-lime glass using Quantum Espresso. These will be extended to model the shock Hugoniot at high pressures, as well as to provide thermodynamic information that can be used by hydrodynamic models

DoD Impact/Significance: The results of this study will enable accurate modeling of high-velocity impact on glass materials; in addition, they provide insight on how high pressure and temperature processing can be used to create glasses with superior mechanical and thermal properties and resistance to high-velocity threats.

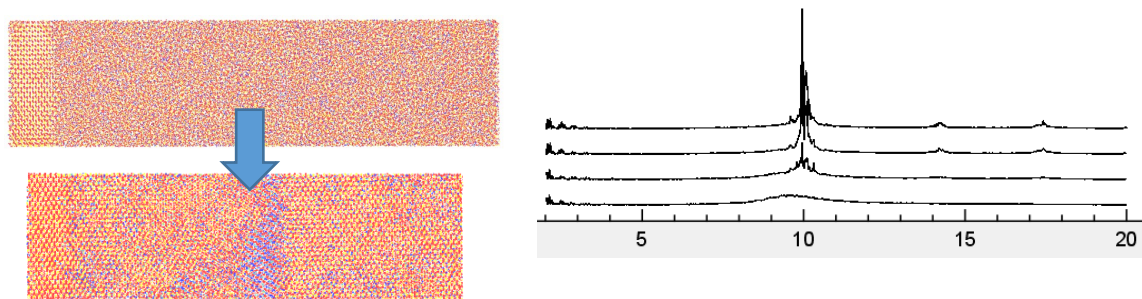


Figure 1. Simulation of soda-lime glass crystallizing during shock compression. Left: snapshots of sample before shock compression (upper) and after completion of crystallization (lower). Right: Simulated X-ray scattering profile at four different times during the crystallization process.

THIS PAGE INTENTIONALLY LEFT BLANK



Computational Electromagnetics and Acoustics

CEA covers two primary computational disciplines. Computational electromagnetics covers the high-resolution multidimensional solutions of Maxwell's equations. DoD applications include calculating radiofrequency (RF) sensor performance, radar scattering of tactical ground, air, and sea vehicles, the electromagnetic signature of buried munitions, high-power microwave performance, as well as the interdisciplinary applications in magnetohydrodynamics and laser systems. The computational acoustics area covers the high-resolution multidimensional solutions of the acoustic wave equations in solids and fluids. DoD applications include the modeling of acoustic fields for surveillance and communication, seismic fields for mine detection, and the acoustic shock waves of explosions for antipersonnel weapons.

Title: Structural-Acoustic Response of Stiffened Elastic Cylindrical Shell

Author(s): S. Dey, M. Villa, E.L. Mestreau, R.M. Aubry, M. Williamschen, W.G. Szymczak, and D. Williams

Affiliations(s): Naval Research Laboratory, Washington, DC

CTA: CEA

Computer Resources: HPE SGI 8600 [AFRL, OH], [NAVY, MS]; SGI ICE X [AFRL, OH]; Cray XC40 [ARL, MD]

Research Objectives: Develop and validate the acoustic response of a parametric model for a stiffened elastic cylindrical shell. Quantify the impact of uncertainty in the material parameters and variations in structural arrangements on the scattering response of the shell.

Methodology: We utilized a high-order *hp*-finite and infinite element-based solver (STARS3D) developed at NRL for solving the coupled elastoacoustics problem. This enables highly accurate solution of the scattering response up to the mid-frequency regime. Use of fully three-dimensional elasticity in modeling the structure requires accurate geometric representation of the stiffened shell. In this effort, we used cubic ($p = 3$) basis functions, which require accurate representation of mesh geometry. Both of these requirements were met by using the DoD HPCMP CREATE (TM) Capstone platform for geometry and mesh generation, also developed by a team based at NRL. We have used a feature-based scripting approach to fully automate the generation of parametric structural geometry and mesh, including statistical variations in the geometric arrangement such as the stiffener spacing.

Results: We computed the scattering response for the nominal structures as well as for geometrically perturbed assemblies in both monostatic and bistatic configurations for frequencies in the range [1kHz, 50kHz]. The computed scattering responses (an example is shown in Fig. 1) were compared and validated against experimental data. Numerical studies demonstrate the impact of uncertainty of material properties on the predicted scattering response as shown in Fig. 2, which depicts the distribution of the scattering response due to statistical variation in the elastic modulus of the target.

DoD Impact/Significance: Parametric models like the one developed in this effort help improve the understanding of structure-acoustic response of complex elastic structure and its sensitivity to various design parameters. This is critical to the development of better undersea warfare technologies.

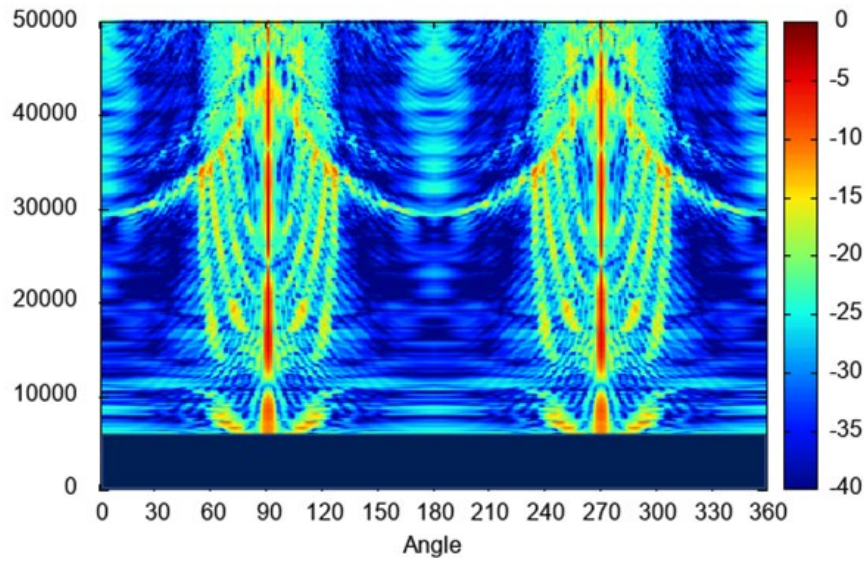


Figure 1. Monostatic response of the Anderson shell.

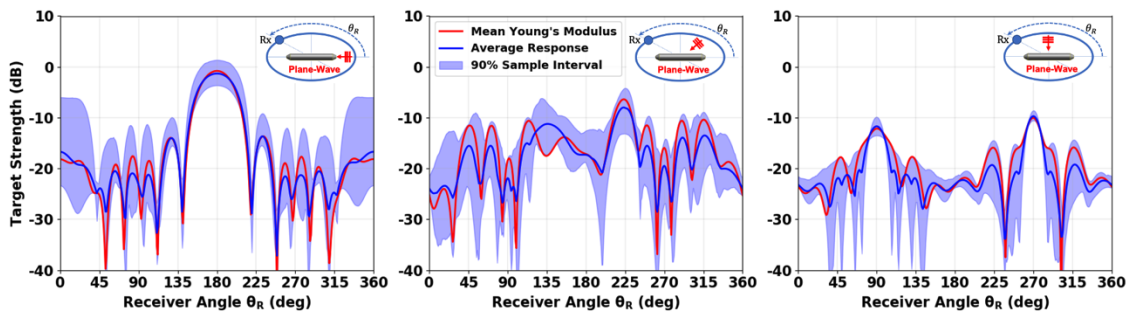


Figure 2. Bistatic response at 0-, 45-, and 90-degree angles of incidence due to statistical variation in elastic modulus.

Title: Acoustic Parameter Variability over an Ocean Reanalysis (AVORA)

Author(s): J.P. Fabre

Affiliation(s): Naval Research Laboratory, Stennis Space Center, MS

CTA: CEA

Computer Resources: HPE SGI 8600 [NAVY, MS]

Research Objectives: Long-time reanalyses of the ocean are becoming available (e.g., NRL 7300) and are potentially extremely useful for understanding the variability of environmental parameters that impact acoustic sensor performance. The objective of this effort is to investigate such potential, to provide recommendations for future Navy products to support operations, and to develop prototype products for test and evaluation.

Methodology: Investigate the NRL 25+ year Ocean Reanalysis to quantify and understand the variability over various time frames. Investigate the sensitivity of acoustic propagation and proxy parameters to the environmental variability. Investigate and assess appropriate averaging windows for a number of environments. Develop prototype products and make recommendations based on the results for products that could be derived from the described reanalysis. Such products will facilitate improved understanding of acoustic parameter variability in areas of propagation and ambient noise. Develop prototype products and test various ways of storing and accessing large data sets. NRL has been working extensively in the areas of big data and machine learning. We will include such technologies as part of our analysis, testing, and recommendations, and will incorporate lessons learned into existing products. If successful, these products could become Navy standard.

Results: Extensive difficulties arose in transitioning from Cray to SGI in the COVID environment. In the summer, a PET proposal was written and accepted and work began in September to convert all the Fortran, C, C++, Makefiles and PBS scripts to the new operating system. Software was modernized to reduce the use of Matlab, which added library dependencies such as GDAL and increased use of Python. Due to declining availability of unclassified hours, we have started to focus on local computing capabilities with lessons learned from our efforts on HPC.

We supported a fleet exercise by providing statistics over a year for some acoustic variables of interest. We used the transfer queue to cut out (from the global reanalysis) Navy areas of fleet interest and to transfer to our local and classified systems for a number of current and future efforts including, but not limited to, pre-mission support, data assimilation, model evaluation, and reconstruction and analysis. This year's technical focus was on identifying fronts and model confidence (with Jacobs et al). The example graphic, Fig. 1, shows maximum (over four directions: N, S, E, W) sound speed L1 curve distance across 10 nmi. This metric indicates significant changes in sound speed curves, and is thus an indicator of fronts, acoustic analysis is ongoing to set thresholds for this metric and others for identifying acoustic fronts.

DoD Impact/Significance: "In Joint Vision 2020, the Department of Defense's strategic plan to ensure battlespace dominance in the 21st century, a key element is information superiority enabled by emerging technologies ..." "An important aspect of information superiority is situational awareness. This implies knowing where you are, where allied and coalition forces are and where enemy forces are. It means understanding the environment, from the sea floor to the top of the atmosphere." [Heart of ForceNet: Sensor Grid, Advanced Command and Control by RADM Steven J. Tomaszewski]. Our efforts directly inform environmental variability as it applies to acoustics.

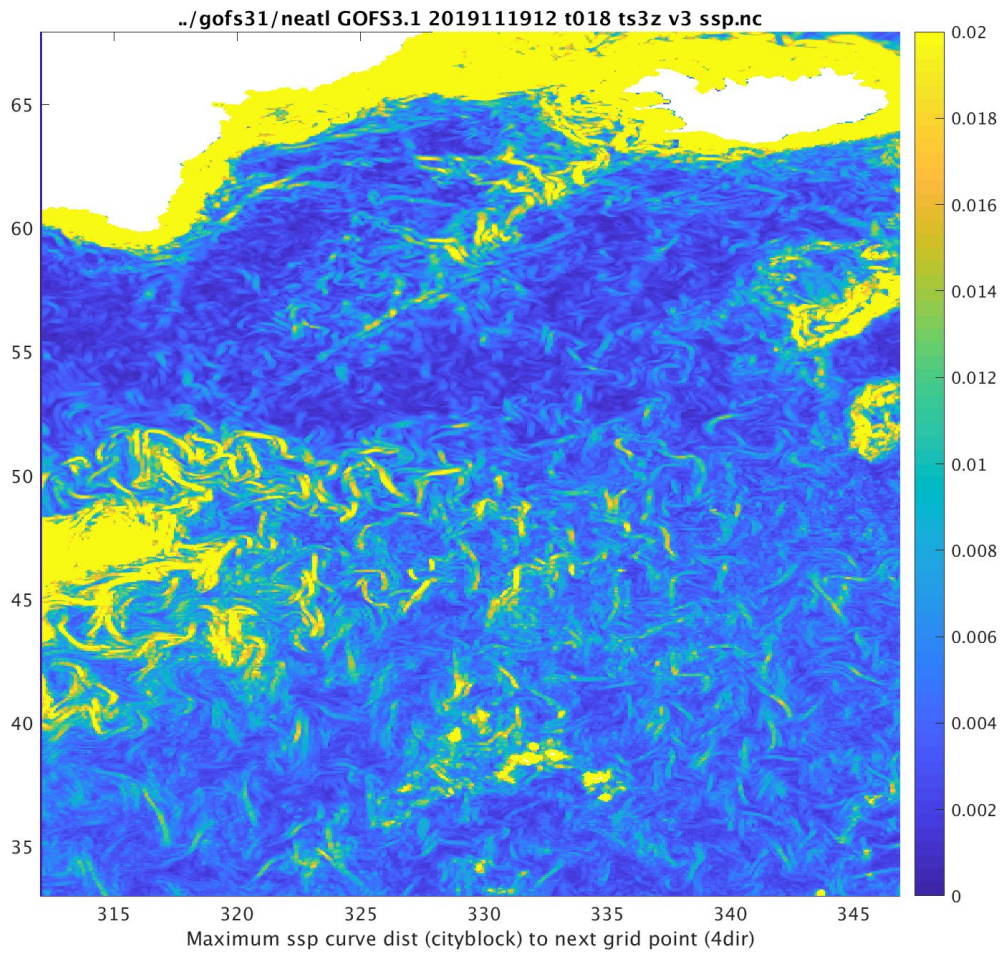


Figure 1. Example maximum (over four cardinal directions) sound speed curve distance (L_1) as an indicator of acoustic frontal locations.

Title: Intense Laser Physics and Advanced Radiation Sources

Author(s): D.F. Gordon¹, J. Penano¹, L. Johnson¹, J. Isaacs¹, D. Kaganovich¹, B. Hafizi¹, and A. Davidson²

Affiliation(s): ¹Naval Research Laboratory, Washington, DC; ²National Research Council Postdoctoral Program, Washington, DC

CTA: CEA

Computer Resources: HPE SGI 8600, SGI ICE X [AFRL, OH]

Research Objectives: The primary objectives of this program are to model the propagation of intense, short-pulse lasers in plasmas and other nonlinear media, and to provide computational support for experiments on the NRL MATRIX laser. Current areas of research include nonlinear laser propagation, plasma-based accelerators, novel sources of short-pulse infrared radiation, and ultrahigh-field physics.

Methodology: HPC resources are utilized using several codes. turboWAVE is an object-oriented framework that contains modules designed to solve a variety of problems. Both fully explicit and ponderomotive guiding center particle-in-cell (PIC) modules are used to model relativistically intense laser pulses propagating in plasmas. Quantum optics modules are used to describe the interaction of the laser pulse with atoms or ions. Fluid modules (SPARC) are used to describe hypersonic flow and shock propagation in gas targets. Optimization for the latest computer architectures requires exploiting three levels of hardware parallelism: vector arithmetic units, shared memory threads, and distributed memory processes. The framework universally supports all of these using a combination of OpenMP directives for vector and loop parallelism, and the Message Passing Interface (MPI) for distributed processes. Some modules support general purpose graphical processing units (GPGPU) via OpenCL.

HELCAP solves a paraxial wave equation with a large number of source terms representing atmospheric turbulence, dispersion, and various nonlinear processes. HELCAP simulates the propagation of short-pulse and high-energy laser pulses, including adaptive optics. It is often useful to run a large statistical ensemble of initial conditions. For this purpose, embarrassingly parallel methodology is effective. Recently, we developed PyCAP, a Python version of HELCAP, which is accelerated using just-in-time compilation, including loop-level parallelism. PyCAP also takes advantage of the parallel FFTW library.

Results: Significant effort was directed toward improvements to turboWAVE and development of PyCAP. We made three-dimensional runs of backward Raman amplification in the long-wavelength infrared, sometimes also called plasma compression. Extremely high-power long-wavelength lasers are still dominated by CO₂ laser technology, which, due to the limited bandwidth, even at high pressure, produces pulse durations of a few picoseconds at the shortest. Plasma compression overcomes this limitation by increasing the bandwidth via a nonlinear mechanism, while at the same time converting a long pump pulse into a shorter and more powerful signal pulse. Simulations have to be carried out in three dimensions because of the possibility of transverse instabilities in the plasma leading to filamentation. Using a combination of fluid and particle-in-cell simulations with turboWAVE, we were able to pinpoint parameter regimes in which the filamentation is minimized.

DoD Impact/Significance: Laser propagation in turbulent atmospheres is relevant for directed energy. High-power pulsed sources of long-wavelength radiation also may be relevant for directed energy. Laser-driven accelerators and radiation sources have potential applications for ultrafast (femtosecond) imaging of chemical and biological systems. High-energy electron beams might be useful as a gamma ray source for detection of special nuclear materials (SNM). High-energy ions also might be useful for SNM detection, or for cancer therapy.

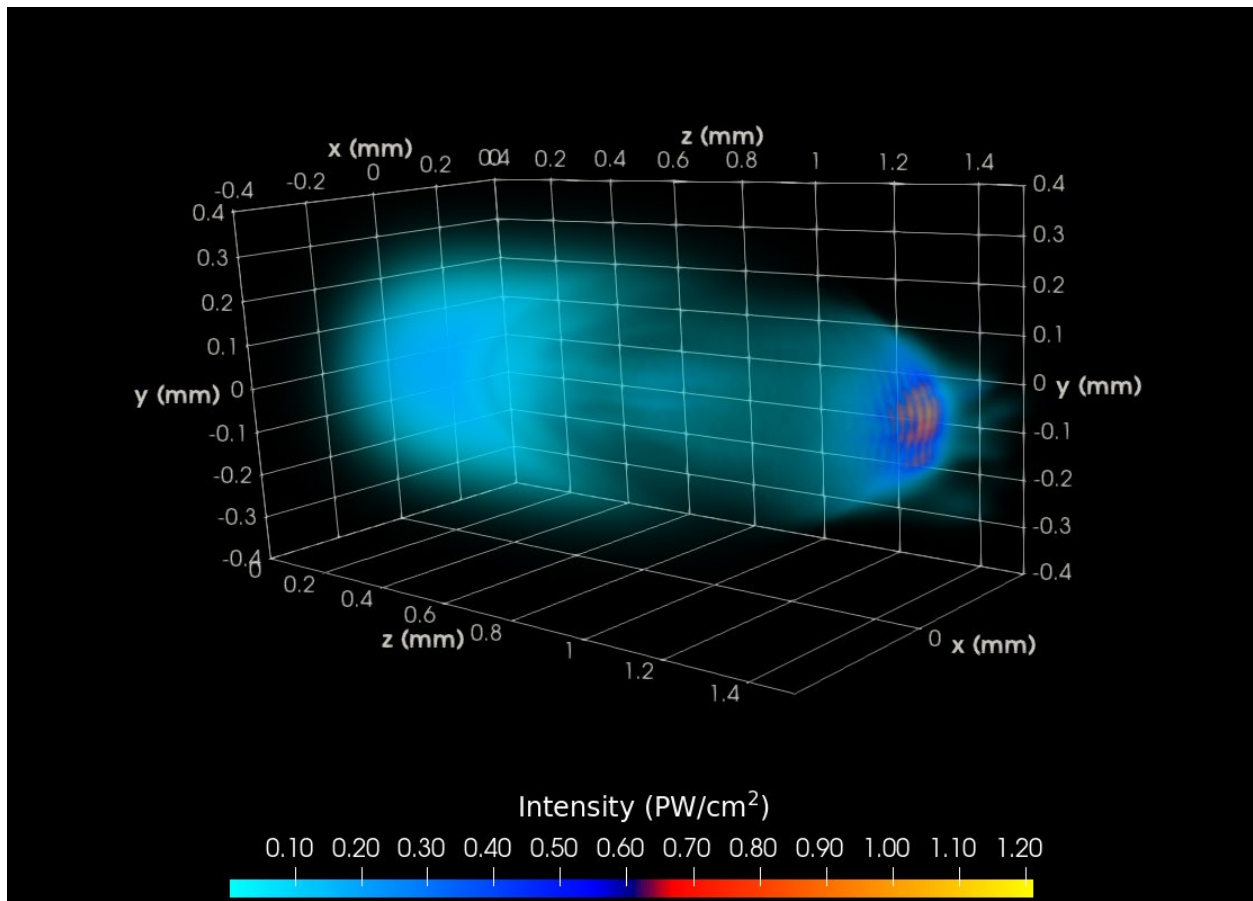


Figure 1. Three-dimensional rendering of the radiation intensity after the backward Raman interaction. The residual pump is on the left, and the compressed signal is on the right. Filamentation, especially along the polarization axis, can be seen in the signal pulse. Visualization is created using Paraview.

Title: Multidimensional Particle-in-Cell Modeling of Ultrashort Pulse Laser with Solid Targets

Author(s): G.M. Petrov

Affiliation(s): Naval Research Laboratory, Washington, DC

CTA: CEA

Computer Resources: HPE SGI 8600, Cray XC40 [NAVY, MS]

Research Objectives: Multidimensional particle-in-cell simulations of the interaction of short-pulse laser with thin foils for better understanding the dynamics of ion acceleration and X-ray generation.

Methodology: Intense lasers interact with matter in a wide range of time scales. For processes occurring on the time scale of picoseconds, multidimensional particle-in-cell models provide proper description. Such models are the primary computational tool for laser-produced plasmas because they provide a self-consistent description of the electromagnetic fields and the response of the material. Nowadays, particle-in-cell models are used extensively for modeling laser-matter interaction on micro- and nano- scales. We use a novel two-dimensional relativistic particle-in-cell code for laser-matter interaction, which was developed in-house at the Plasma Physics Division at NRL and has been parallelized using Message Passing Interface (MPI).

Results: The particle-in-cell code was used extensively to study particle acceleration from thin (sub-micron) foils irradiated by ultrashort (sub-picosecond) relativistic intensity ($>10^{20}$ W/cm²) laser pulses. In this study, the focus was on highly charged ions from mid-Z materials such as Ti and Cu. The code provided valuable insight into the physical processes occurring during the interaction and was employed to analyze experiments and to gain understanding of the target performance. We did a systematic study by varying laser parameters (duration) and target parameters (thickness) in order to optimize targets and to guide experiments, which are very expensive and time consuming. We report the results on simulations of the interaction of short laser pulses with peak intensity of $10^{20} - 10^{21}$ W/cm² incident on ultrathin (10 — 500 nm) titanium foils to investigate the roles of laser pulse duration and ionization mechanisms in the acceleration of titanium ions (Fig. 1). The objective of this study was to find the optimum thickness of the target: if the target is too thin, the laser will go through without coupling its energy; if the target is too thick, the coupling may become inefficient. An optimum thickness exists, which is dependent on pulse duration, as it requires the concurrence of target transparency with the incidence of the peak laser intensity. At the optimum thickness, the target transparency onset occurs at or near the peak of the laser pulse. Thinner targets become transparent too early, and thicker targets favor the TNSA mechanism, which is inefficient. Simulation results for Ti foil irradiated at peak intensity 6×10^{20} W/cm², duration 140 and 650 femtoseconds, wavelength 1 μ m, and spot size 5 μ m are summarized in Fig. 2. Shorter laser pulses require thinner targets (20 nm), while for longer laser pulses, thicker targets (100 nm) are more appropriate. For the longer pulse, highly energetic ions with energy of up to 40 MeV/nucleon (~ 2 GeV) are predicted.

DoD Impact/Significance: This modeling and the results are of significant interest to the Navy and the DoD, as they are directly related to problems such as generation of X-rays and gamma rays, as well as directed particle beams (neutrons, protons, radioactive ion beams), all of which can be used for fundamental research. The research is also of great interest to the scientific community dealing with high-energy-density plasmas, laser nuclear physics, and laser-matter interactions. The simulations have been used to guide experiments related to laser-matter interaction. The payoff of the computational efforts is that long, arduous and expensive experiments have been modeled and guided using virtual experiments on computers, saving time and resources.

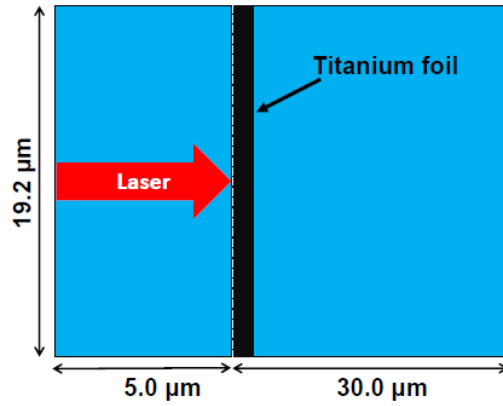


Figure 1. Sketch of the 2D simulation domain. The left boundary of the target is set at $x = 5.0 \mu\text{m}$.

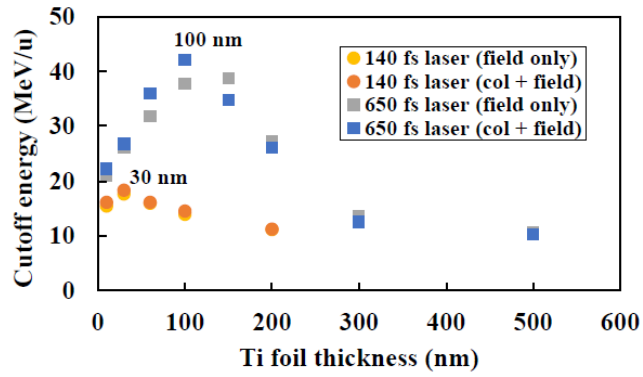


Figure 2. PIC simulations for Ti foils with different thicknesses. Maximum (cut-off) energies per nucleon as a function of target thickness for two laser pulse durations: 140 and 650 fs.

Title: Computer-Aided Design of Vacuum Electronic Devices

Author(s): G. Stantchev¹, S. Cooke¹, J. Petillo², A. Jensen², and S. Ovtchinnikov²

Affiliation(s): ¹Naval Research Laboratory, Washington DC; ²Leidos, Billerica, MA

CTA: CEA

Computer Resources: SGI ICE X [AFRL, OH]; SGI ICE X, Cray XC40 [ARL, MD]

Research Objectives: 1. Enhance the Leidos MICHELLE charged particle beam optics code, the NRL TESLA, NETPUNE and CHRSTINE large-signal codes, and the new Leidos COMPASS design environment to work with the AFRL Galaxy Simulation Builder (GSB) to enable significantly larger simulations, optimizations, and sensitivity studies, to reduce simulation times, and to amplify user productivity in the design and development of vacuum electronic components and systems of interest to the DoD. 2. Employ the new capabilities in the design of new vacuum electronic components with optimized performance characteristics.

Methodology: MICHELLE has been extended to a flexible heterogeneous computing framework that can be deployed on distributed-memory HPC clusters, and that also can use computational accelerators such as multicore CPUs and graphics processing units (GPUs). In addition, we have developed interfaces with existing DoD HPC mesh generation, visualization, simulation environments, and productivity tools, which include the GSB. Including GSB allows us to incorporate design codes in addition to MICHELLE into the pipeline of HPC-based optimizations. The Leidos COMPASS user design environment has been developed to transition the user away from building parametric CAD models and single simulations for early scoping. It will allow for building optimization parameter sets and ultimately building the backbone file set to accommodate HPC runs under GSB. To bridge the software gap we faced, we have the following two broad objectives for the software improvements, specifically targeting the HPCMP objective of exploiting technologies to maintain RDT&E leadership:

- I. **Exploitation of Heterogeneous Computing Architectures:** Leveraging existing and emerging DoD HPC architectures to take advantage of distributed-memory HPC clusters and per-node computational accelerators such as multicore CPUs and GPUs.
- II. **Integration of existing DOD HPC ecosystem:** This includes the DoD CAPSTONE CAD/Mesh generator (CREATE-MG), and DoD HPC tools including AFRLs GSB, and Kitware's ParaView visualization software, available and supported through the DAAC.

Results: The focus of the project during FY20 has been on continuing the integration of the HPC version of MICHELLE and the other NRL physics codes as well as the integration with the productivity tools. Figure 1 shows a GSB optimization of a traveling wave tube. The optimization penalizes zero drive unstable circuits as predicted by NEPTUNE (NRL) and rewards circuits with high gain-bandwidth as predicted by Tesla-Z (NRL). Figure 2 shows how the new COMPASS user environment has been adapted to support a modular approach to building simulation pipelines. A three-module pipeline is shown as an example of how an electron gun, a circuit, and a collector can be run in COMPASS. Figure 3 shows a new capability for simulating TWTs where multiple-piece parts can be simulated individually and merged. It is anticipated that this approach will be used on the HPC for rapid design optimization of TWTs. Figure 4 shows streamlined hybrid meshing capability for user friendly multi-block creation. Figure 5 shows work done towards predicting emission and the Miram curve for cathodes based on material, emission and surface properties and having information about the full-scale electron gun optics. In this project, DoD HPC resources have been used in support of DARPA's INVEST and HAVOC program, researching the latest trends in emission surface physics.

DoD Impact/Significance: This development has impacted three DARPA and four NRL programs in vacuum electronics by providing the ability to perform rapid analysis and optimization of mission-critical vacuum electron devices, previously deemed intractable via state-of-the-art methods.

DoD High Performance Computing (HPC) for Vacuum Electronics

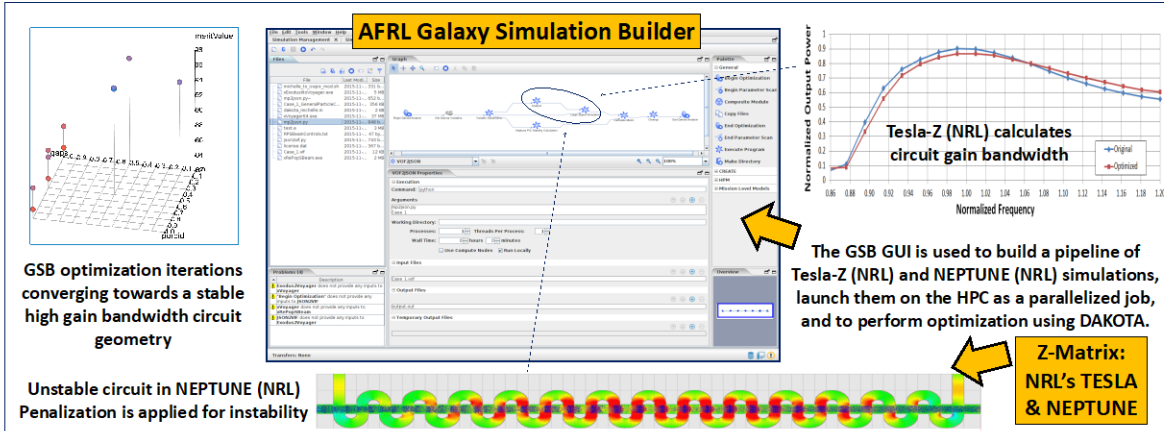


Figure 1

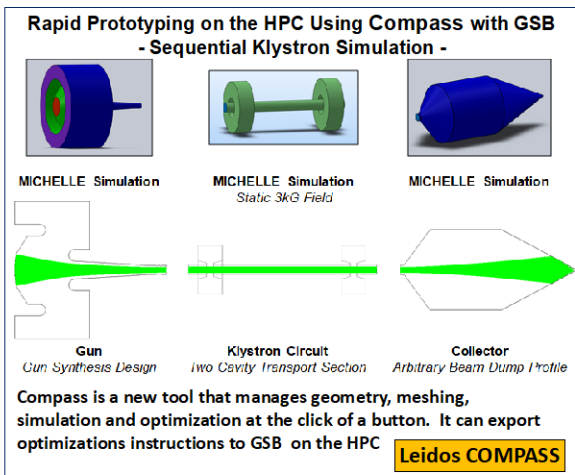


Figure 2

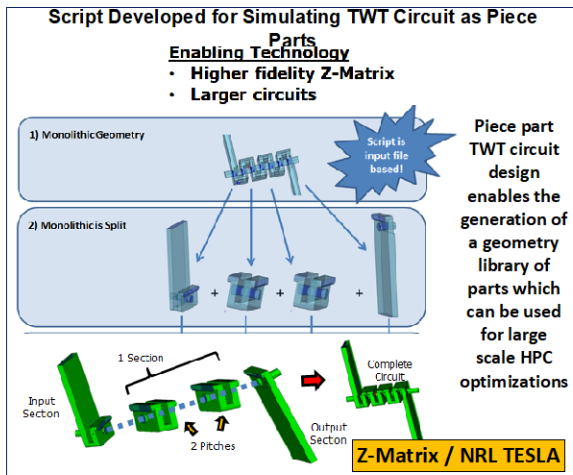


Figure 3

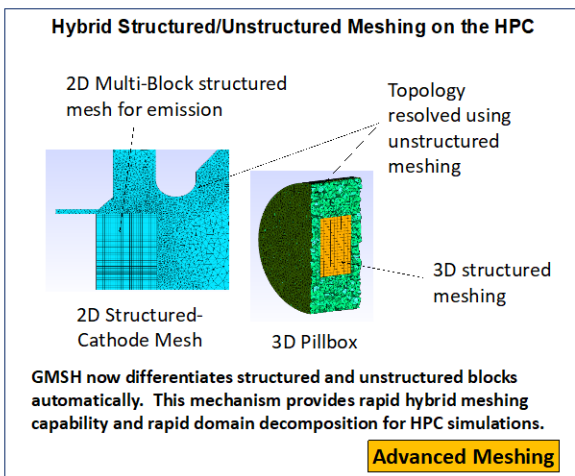


Figure 4

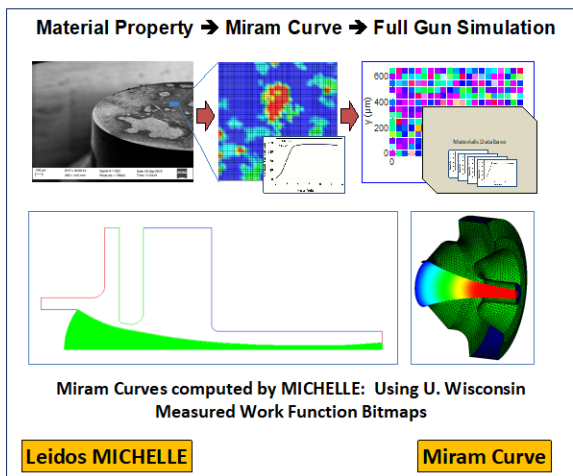


Figure 5

Title: Flowfield and Transport Models for Navy Applications
Author(s): W.G. Szymczak and A.J. Romano
Affiliation(s): Naval Research Laboratory, Washington DC
CTA: CEA

Computer Resources: HPE SGI 8600, SGI ICE X [AFRL, OH]; Cray XC40 [ARL, MD]

Research Objectives: Provide resources for computational fluid dynamics simulations, as well as optimization and inverse problems, supporting a variety of Navy applications. Examples include flow through acoustic sensors, flow and transport over passive filter shelters, and the extraction of anisotropic stiffness coefficients of white matter in brains of both healthy controls and patients with mild to severe traumatic brain injury (TBI).

Methodology: The extraction of stiffness parameters using wave guide elastography (WGE) was performed using a mixed model inversion (MMI) algorithm to treat both the anisotropic and isotropic regions within a human brain. WGE utilizes magnetic resonance elastography (MRE) and diffusion tensor imaging (DTI) (cf. Fig. 1) measurements processed with an orthotropic anisotropic inversion algorithm. Within the anisotropic white matter regions, the orthotropic inversion provides nine independent stiffness coefficients including the three longitudinal terms C_{11} , C_{22} , C_{33} , the three shear coefficients C_{44} , C_{55} , C_{66} , and the three off-diagonal stiffness terms C_{12} , C_{13} , C_{23} . The algorithm was implemented using message passage interface (MPI) directives with work balancing based on the ratios of isotropic to non-isotropic voxels being sent to each processor.

Results: The WGE-MMI code was run using 1152 cores (24 nodes with 48 cores per node) reducing the execution time for a single data set from approximately 24 hours on a single node to a time between 6 and 7 minutes depending on the volume of the brain being processed. In FY20, we computed the full set of nine orthotropic anisotropic stiffness values for data from a study provided by the University of Delaware containing MRE and DTI measurements of hockey players taken pre-, mid-, and postseason. Two different types of MRE head excitation were used, namely left to right, and anterior-posterior, yielding a total of 147 datasets. Traumatic brain injury is often confined to specific regions within the brain. A segmentation of brain regions for each of the datasets recently has been provided, and feature extraction using this localized data and a classification analysis currently is being conducted. Figure 2 shows an example of feature differences extracted from a set of healthy controls and TBI patients using datasets provided by the Mayo Clinic in Rochester, MN. Each of the 21 columns in the figure corresponds to a specific brain region (segment) while the 20 rows correspond to the computed anisotropic stiffness values, as well as other anisotropic metrics. The dark colors inside the circles indicate significant feature differences, thereby providing a subset of the 420 features examined as significant candidates for machine-learning classification.

DoD Impact/Significance: The WGE-MMI provide a unique capability in extracting anisotropic stiffness values of white matter structures. These values, within different segmented brain structures, provide features that are currently being prepared for machine-learning algorithms to distinguish between healthy controls and TBI patients. Thus, it has the potential to be used as a noninvasive test for diagnosing conditions of warfighters exposed to blunt, ballistic, or blast impacts. The additional analysis of the data provided by the hockey player study mentioned above will be used to improve the reliability of TBI detection and classification.

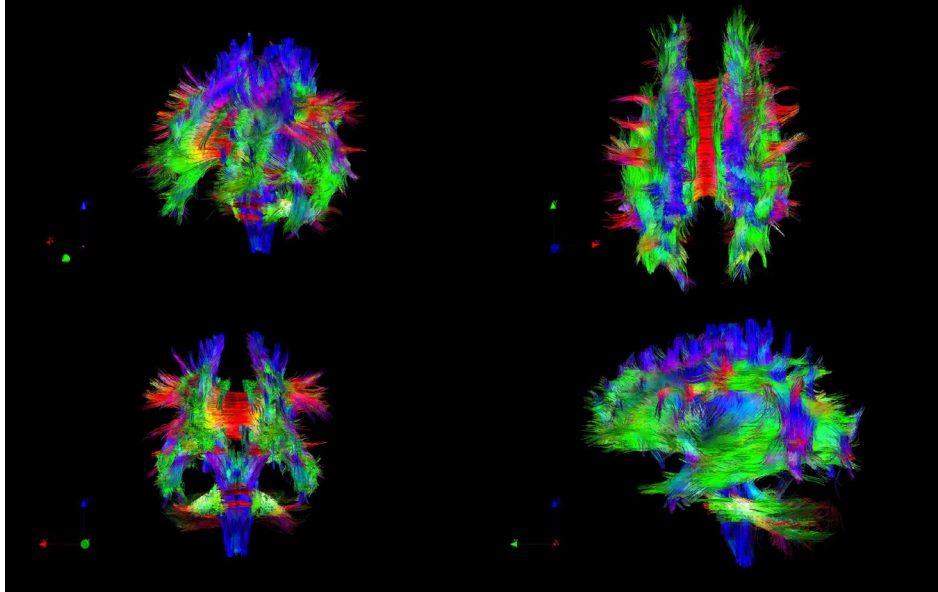


Figure 1. Different views of orientation maps for DTI white matter pathways in a healthy brain.

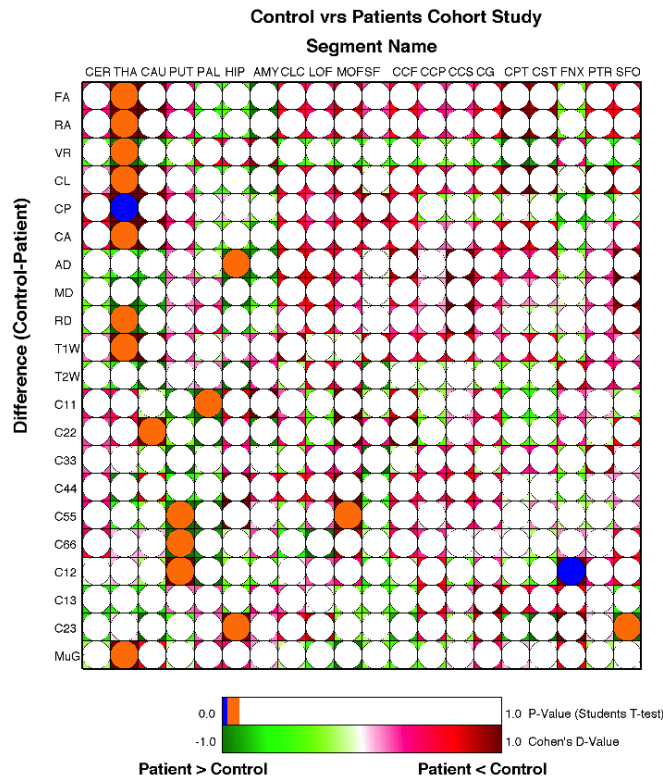


Figure 2. Feature comparison map of a small cohort of healthy controls and TBI patient having the same mean ages from a Mayo Clinic dataset. In the figure, colored circles represent differences with significance $p < 0.01$ in blue and $p < 0.05$ in orange. This study indicates significant differences ($p < 0.05$) in multiple metric measurements for the thalamus (nine metrics), putamen (three metrics) and hippocampus (two metrics) segments.

Title: Low Grazing Angle Radar Backscatter

Author(s): J.V. Toporkov, J.D. Ouellette, and M.A. Sletten

Affiliation(s): Naval Research Laboratory, Washington, DC

CTA: CEA

Computer Resources: Cray XC40 [ARL, MD]; Cray XC40/50 [ERDC, MS]

Research Objectives: Reflections from sea surface are present in many shipborne, coastal and airborne radar systems. They are often regarded as clutter that masks a target return, but also can be a source of information about local ocean conditions. Understanding the properties of sea backscatter, their dependence on environmental parameters, and how they are distinct from those of man-made target echoes is key to improving or even enabling performance of such radar systems and applications. This project investigates detailed characteristics of radar returns from the ocean surface under both monostatic and bistatic observation geometries. The task is accomplished through simulations that involve both direct numerical solution of the scattering problem and, where appropriate, numerical implementations of approximate scattering models.

Methodology: The approach combines a physics-based model for an evolving ocean surface with computationally efficient, exact evaluation of the scattered electromagnetic field. A wind-driven surface is represented by realizations of a Gaussian random process defined by a certain wave spectrum. Interactions between surface harmonics are modeled by subsequent application of the Creamer transformation. The introduced hydrodynamic nonlinearities affect shape and motion of smaller ripples that have great impact on scattering of decimeter- and centimeter-scale electromagnetic waves. The field scattered by a “time-frozen” scene at a particular frequency is found by iteratively solving a boundary integral equation for the induced surface current. The formulation is based on first principles and automatically accounts for many phenomena (multiple scattering, shadowing) known to be problematic for analytical treatment. The calculations can be conducted at a number of frequencies covering certain bands to simulate pulse scattering. The procedure is repeated for every surface profile in the sequence representing temporal evolution. The simulations are limited to the two-dimensional (2D) space but have direct relevance to commonly occurring three-dimensional (3D) geometries (e.g., oncoming or receding long-crested waves).

Results: The simulation efforts supported feasibility studies for passive remote sensing of sea state utilizing illumination from geostationary communication satellites. One numerical experiment re-created the conditions of field measurements conducted at a wave tank facility. The received signals were simulated using the actual dimensions of the antenna horns, the recorded wave spectrum, and other parameters of the actual setup, cf. Fig. 1. The flexibility of the numerical model allowed multiple receivers, as well as exploring the range of scattering angles θ_s going well beyond what was feasible in the real-world experiment. Even with continuous-wave time-harmonic incidence field, a relatively narrow receiving antenna pattern provides for range-resolved sensing (although the size of footprint rapidly expands as θ_s moves towards grazing). Signal fluctuations resulting from water waves passing through the receiver beam potentially can help retrieve the dominant wave period. In particular, one can consider Doppler spectrograms and can look at temporal behavior of centroids of the instantaneous spectra (Fig. 2). There are scattering angles for which the Fourier transform of such centroid variations reveals the peak frequency clearly, cf. Fig. 3. At larger (and perhaps more practical) angles, a single-receiver result in Fig. 4 is not definitive, but incoherent averaging over multiple receivers could help.

DoD Impact/Significance: More comprehensive and detailed characterization of sea clutter will help in design and performance assessment of the Navy radar systems, especially those operating in the LGA regime. Bistatic configurations provide covertness for a passive receiver asset and could yield further performance enhancements due to peculiar scattering characteristics of surface and targets that do not emerge in the conventional monostatic case.

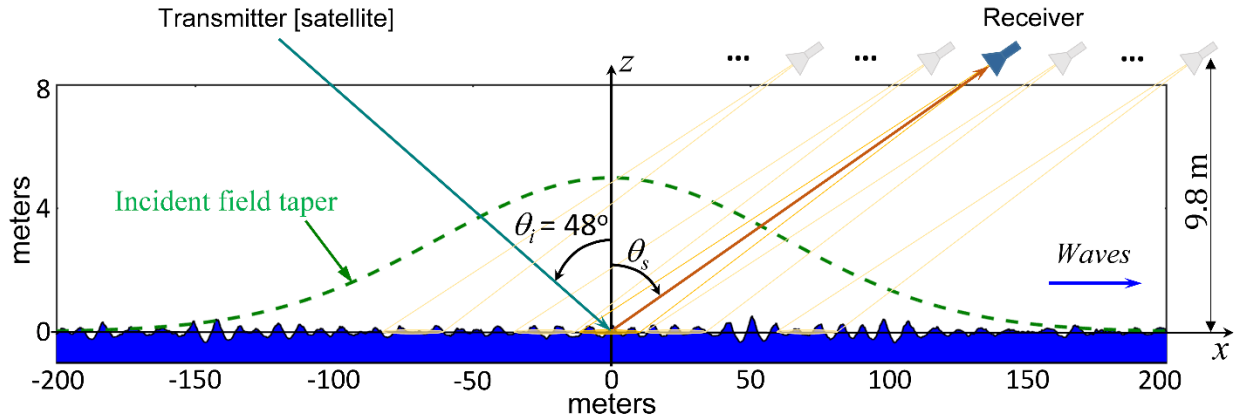


Figure 1. Setup for bistatic scattering simulations from evolving water surface in the wave tank experiment. All calculations are conducted at 2.3 GHz (S band), with a time-harmonic transmitted signal assumed. Multiple receivers (all pointed at the same angle θ_s at different spots along the surface) may be considered to boost measurements ensemble. Per experimental setup, the antenna height is always kept at 9.8 m.

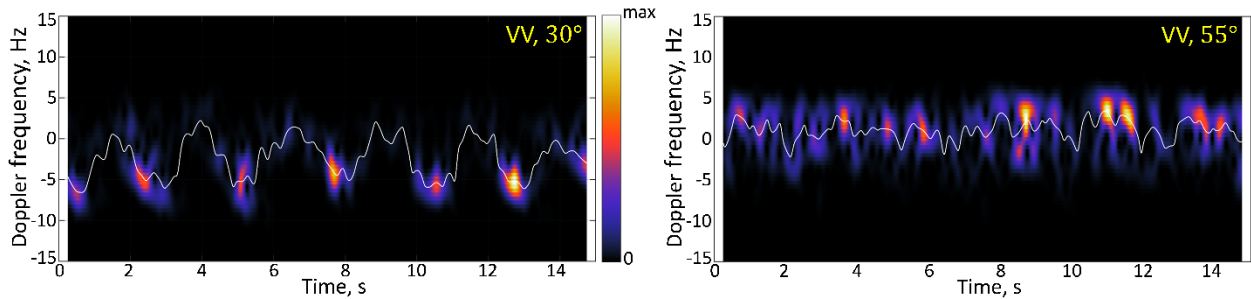


Figure 2. Spectrograms evaluated with a 0.5-s sliding Hann window from the simulated received signals for $\theta_s = 30^\circ$ (left panel) and $\theta_s = 55^\circ$ (right panel). White lines trace the location of spectral centroid at each moment in time. A single receiver is used.

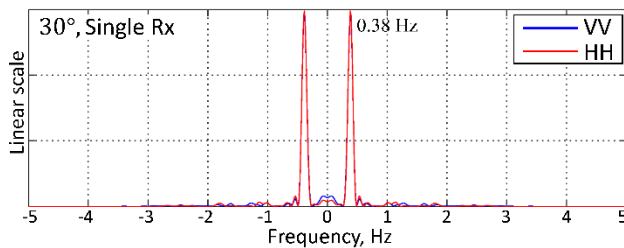


Figure 3. Fourier transform of time-dependent spectrogram centroids such as those shown in Fig. 2, with $\theta_s = 30^\circ$. Results for VV and HH polarizations are very similar and exhibit sharp maxima at ± 0.38 Hz. (The average peak frequency of the simulated waves is 0.42 Hz.)

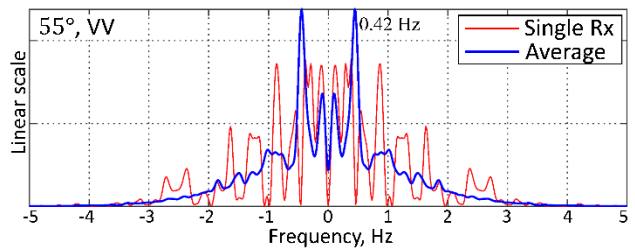


Figure 4. Fourier transform of time-dependent VV spectrogram centroid with $\theta_s = 55^\circ$. While the result from a single receiver is inconclusive, the incoherent average over all 55 distinct locations shows spikes at ± 0.42 Hz, which is the expected peak frequency for the surface waves.

THIS PAGE INTENTIONALLY LEFT BLANK



Climate Weather Ocean Modeling

CWO focuses on the accurate numerical simulation of the Earth's atmosphere and oceans on those space and time scales important for both scientific understanding and DoD operational use. This CTA includes the simulation and forecast of atmospheric variability (e.g., temperature, winds, pressure, relative humidity, cloud cover, precipitation, storms, aerosols and trace chemicals, surface fluxes, etc.) and oceanic variability (e.g., temperature, salinity, currents, tides, waves, ice motion and concentration, sediment transport, optical clarity, etc.). Numerical simulations and real-time forecasts are performed from the very top of the atmosphere to the very bottom of the ocean. CWO also includes the development of numerical algorithms and techniques for the assimilation of in situ and remotely sensed observations into numerical prediction systems. CWO has DoD applications on a daily basis for specific warfare areas, mission planning, and execution (air, ground, sea, and space), as well as for flight and sea safety, search and rescue, optimal aircraft and ship routing, and weapon system design. This CTA provides DoD with: (1) real-time, high-resolution weather and oceanographic forecasts leading to incisive decision making and enhanced operational capability in adverse weather and ocean conditions and (2) realistic simulations of the dynamic oceanic and atmospheric environment to permit effective mission planning, rehearsal and training, and materiel acquisition.

Title: Coupled Ocean-Wave-Air-Ice Prediction System

Author(s): R. Allard¹, T. Campbell¹, E. Douglass¹, D. Hebert¹, T. Jensen¹, T.A. Smith¹, and M. Phelps²

Affiliation(s): ¹Naval Research Laboratory, DC; ²Perspecta, Stennis Space Center, MS

CTA: CWO

Computer Resources: HPE SGI 8600, Cray XC40 [NAVY, MS]

Research Objectives: Perform research studies with the Coupled Ocean Atmosphere Mesoscale Prediction System (COAMPS^{®1}) which is six-way coupled with the Navy Coastal Ocean Model (NCOM), WaveWatch-III (WW3) and SWAN wave models and the COAMPS atmospheric model. Perform modeling studies with the Community Ice Code (CICE v6) which includes a landfast ice parameterization.

Methodology: For accurate simulation and prediction, we have used various configurations of the fully coupled atmosphere-ocean-wave model system COAMPS with very high spatial and temporal resolution. For the Bay of Bengal (BoB) the following model configuration was used: The atmospheric component has 60 vertical levels. The ocean model has a 0.5 m resolution in the upper 10 m, 45 sigma levels and up to 15 z-levels for a total of 60 levels in water deeper than 330 m and includes eight semi-diurnal and diurnal tidal components. The numerics apply third-order upstream differencing schemes, fourth-order pressure gradient and Coriolis terms for increased accuracy. The turbulent closure scheme is the Kantha-Clayson 2.5 that includes Stokes drift from the wave model. For these configurations, we use the spectral wave model (SWAN) with 10 km spatial resolution, 34 frequency bands and 48 directions. Coupling interval for data exchange between each of the two models is 6 min.

Results: The COAMPS model showed that tidally generated semi-diurnal nonlinear internal waves radiate from the Andaman Sea in the central BoB and reach the east coast of Sri Lanka. The results demonstrate that the waves also are present in subsurface temperature records from RAMA moorings, and their propagation speed across the BoB agrees well with satellite remote sensing of MODIS imagery. The internal waves are simulated by a fully coupled ocean-atmosphere prediction system, exchanging surface fluxes between the air and the sea at high frequency and at high resolution. The NCOM includes diurnal and semi-diurnal tides and provides a 2 km resolution representation of the entire BoB. In the ocean model simulations, the semi-diurnal internal waves interact with the mesoscale circulation and surface waves and modify the flow and the stratification. By comparing coupled ocean-wave model runs with tides and without tides, but forced by identical surface fluxes from the atmosphere, it was shown that the inclusion of diurnal and semi-diurnal tides act to cool the core of the thermocline while increasing the temperature above and below it along the pathway of the internal waves, likely due to vertical mixing by the waves. It also was demonstrated that the convergence and divergence from the ocean currents associated with the nonlinear internal waves affect surface-gravity waves by modifying their wavelengths and heights. (Jensen et al., *Deep-Sea Res.*, 2020). CICE6 was configured for landfast ice by evaluating the grounding and tensile strength parameterization for regions in the Arctic. We found reasonable agreement with observations of the maximum extent by performing studies on the GOF3.5 grid.

DoD Impact/Significance: The development of a coupled air-ocean-wave prediction system can have a pronounced effect on Navy forecasting by improving ASW performance, tropical cyclone prediction, search and rescue, and mission planning. The relocatable COAMPS-CICE system will provide high-resolution Arctic forecasting of ice thickness, ice drift and concentration to support navigation. Inclusion of landfast ice in the Navy's global ice prediction systems will yield a more realistic representation of pan-Arctic sea ice.

¹ COAMPS[®] is a registered trademark of the Naval Research Laboratory.

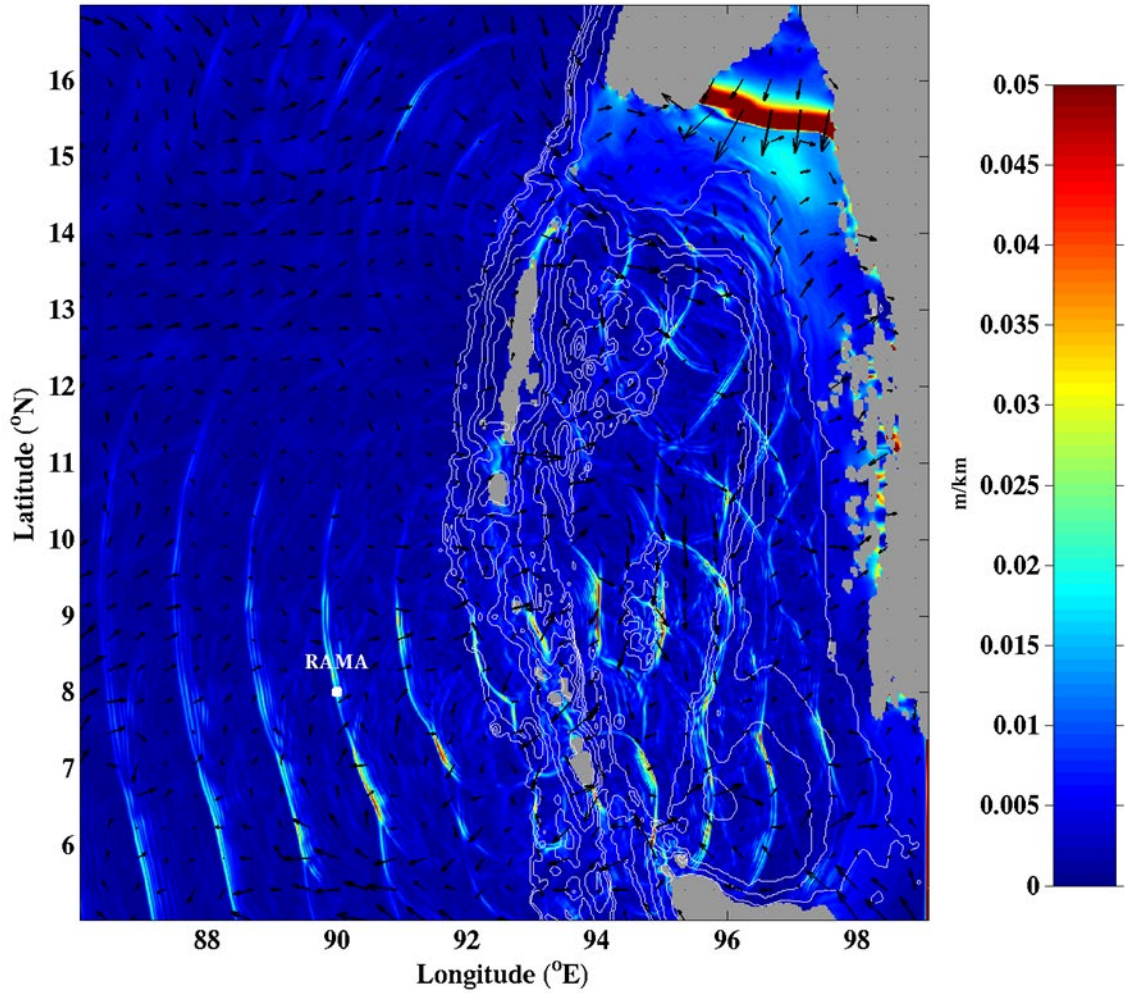


Figure 1. Magnitude of the sea surface height gradient on August 31, 2011, at 00 UTC shows generation of internal waves at three gaps in the Andaman Island Archipelago (color shading). Depth contours are shown in white and instantaneous surface currents are shown by arrows. The location of the Research Moored Array for African-Asian-Australian Monsoon Analysis and Prediction (RAMA) buoy at 90°E, 8°N is shown (From Jensen et al., 2020).

Title: Atmospheric Process Studies

Author(s): N. Barton, T. Whitcomb, J. Ridout, K. Viner, J. McLay, W. Crawford, M. Liu, T. Hogan, and C. Reynolds

Affiliation(s): Naval Research Laboratory, Monterey, CA

CTA: CWO

Computer Resources: HPE SGI 8600, Cray XC40 [NAVY, MS]

Research Objectives: The research objectives of this project are to improve our understanding of the fundamental dynamical and physical processes that operate in the atmosphere and to develop and test a state-of-the-art global atmosphere-prediction system that includes data assimilation and ensembles.

Methodology: Our work focuses on improving the accuracy and efficiency of the Navy Global Environmental Model (NAVGEN). NAVGEN is the Navy's current global atmosphere operational numerical weather prediction model, and is used for basic and applied atmospheric research within this project. NAVGEN is developed in conjunction with its data-assimilation capability, NAVDAS-AR, as initial conditions are very important to the numerical system. In addition, seamless prediction across multiple temporal scales and earth system components is the next frontier of numerical prediction. NAVGEN is being developed and tested when tightly coupled with the HYbrid Coordinate Ocean Model (HYCOM) and the Los Alamos Community sea Ice Code (CICE) using the Earth System Modeling Framework (ESMF) tools under the Earth System Prediction Capability (ESPC) national program. The focus on seamless prediction across temporal scales requires additional research and development on probabilistic prediction and diagnostics using ensembles.

Results: In FY20, two major modeling systems were transitioned to operations. (1) NAVGEN 2.0 became operational at Fleet Numerical Meteorology and Oceanography Center (FNMOC) on April 29, 2020, and (2) the ensemble system of Navy-ESPC v1 became operational on August 31, 2020. NAVGEN 2.0 represents a significant increase in horizontal resolution to about 18 km from about 30 km. With the Navy-ESPC v1 ensemble system transition, it is the first time FNMOC will supply atmosphere forecast to 45 days, the first time a global coupled model runs at FNMOC, and the first time FNMOC runs an ocean ensemble. Development for future operations focuses on ensembles, aerosols, and physics development. The ensemble method Analysis Correction-based Additive Inflation (ACAI, Crawford et al., 2020) has been adapted into NAVGEN and tested in both the stand-alone atmospheric and coupled Navy ESPC systems. Use of ACAI results in decreased biases and is particularly effective at reducing biases in total precipitable water. NAVGEN has been updated to include inline smoke aerosols, and case studies have been performed. When compared to satellite observations, NAVGEN successfully predicts a clean high-elevated smoke plume that very well matches the observation for the height and location on the satellite tracks. A reasonably accurate simulation of smoke transport will ensure the smoke radiative forcing effectively interacts with the atmospheric dynamics. Uncoupled NAVGEN and Navy-ESPC extended range hindcasts were carried out for episodes of the Madden-Julian Oscillation (MJO) that occurred during a field campaign in November 2011. When using updated physics in convection, Navy-ESPC showed significant improvements to the simulated MJO from using the coupled physics, and that the addition of air-sea coupling adds significant further improvements (Fig.1).

DoD Impact/Significance: The continued development of our global forecast system is making significant positive impacts on the skill of our weather forecasts and DoD predictions dependent on weather forecasting (i.e., ocean modeling, wave modeling, ship routing). Developments in coupled modeling and extended range-probabilistic forecasting increase the utility of the forecast and potential number of users. This development serves to provide an improved modeling system for studying the dynamical and physical processes in the atmospheric system.

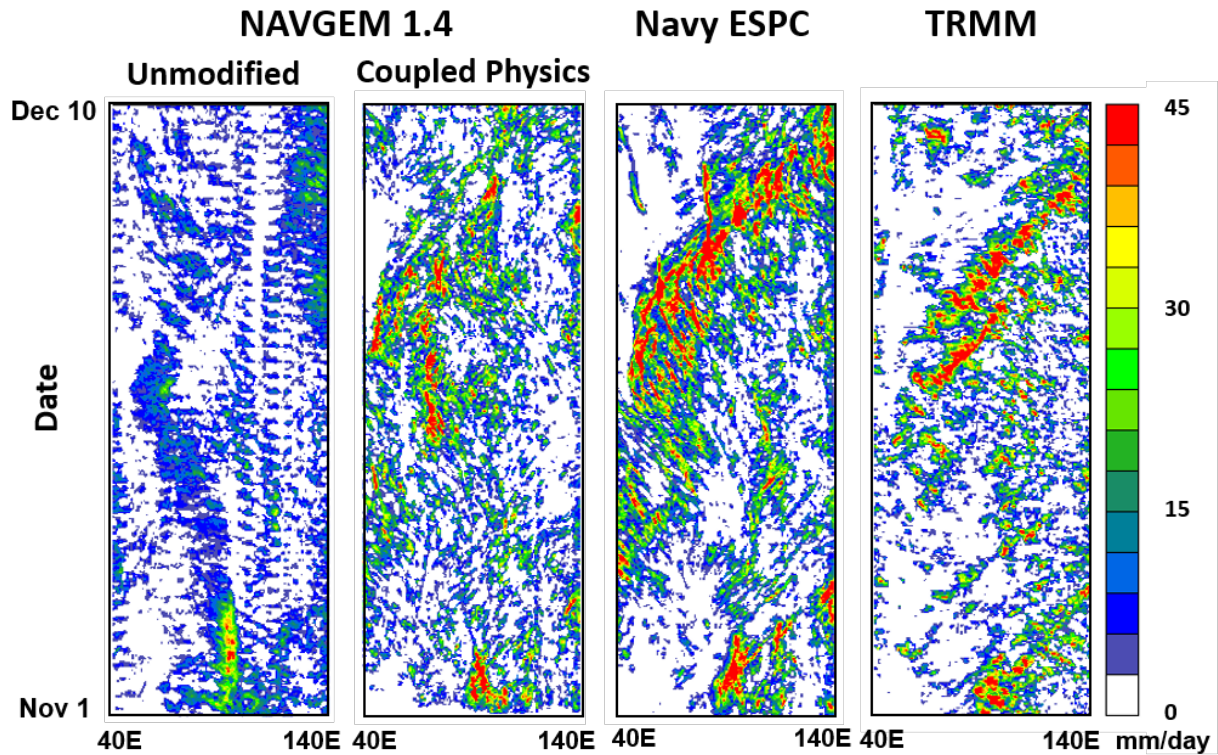


Figure 1. Hovmöller diagram of precipitation from NAVGEM v1.4 with NAVGEM physics, NAVGEM v1.4 with the coupled physics, Navy-ESPC, and The Tropical Rainfall Measuring Mission (TRMM) from 1 November 2011 to 10 December 2011. Precipitation is averaged from 5°S to 5°N and the Hovmöller diagram shows precipitation from 40°E to 140°E. NAVGEM and Navy-ESPC output represent long non-assimilative forecasts starting on 1 November 2011. NAVY-ESPC is configured as a deterministic Navy-ESPC run with 50 vertical levels.

Title: Data Assimilation Studies Project
Authors: W.F. Campbell and B. Ruston
Affiliation: Naval Research Laboratory, Monterey, CA
CTA: CWO

Computer Resources: HPG SGI 8600, Cray XC40 [NAVY, MS]; Cray XC40 [ARL, MD]

Research Objectives: Data Assimilation (DA) corrects model analyses of the atmosphere, ocean or surface using a non-homogenous collection of observations. This project develops, tests, and improves: 1) our 4D-Var assimilation system, which is coupled to the atmospheric global model NAVGEM (Navy Global Environmental Model) and is used by the Navy Earth System Prediction Capability (ESPC); 2) fully ensemble-based data assimilation, now including the ionosphere; 3) hybrid ensemble/4D-Var data assimilation; 4) 4D-Var data assimilation for COAMPS^{®1}; 5) adjoint, tangent linear, and forecast sensitivity to observations; 6) coupled DA (atmosphere, ocean, sea ice, etc., together); and 7) preparation for and test assimilation of new data types, both satellite and conventional. Our goal is to assimilate traditional data (generally in situ, e.g., weather balloons, ship, aircraft, or buoy reports) as well as data from a variety of new sources (often spaceborne) efficiently and effectively, to provide the best atmospheric analysis, and ultimately to improve numerical weather forecast performance.

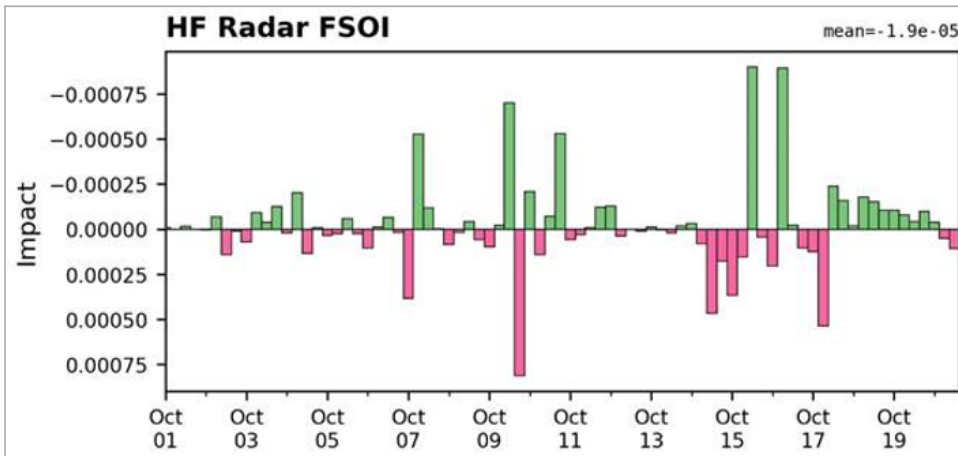
Methodology: A variety of experimental setups are used to develop and test our global and regional models and data-assimilation systems, as well as large datasets of in situ and satellite-based observations for several summer and winter months.

Results: A broad spectrum of research takes place under this project, using the Navy's latest global (NAVGEM 2.0, and Middle Atmospheric NAVGEM (HA-NAVGEM)) and mesoscale (COAMPS) models, along with our global (NAVDAS-AR, hybrid NAVDAS-AR, and coupled hybrid NAVDAS-AR) and mesoscale (COAMPS-AR) data-assimilation systems. Results from FY20 research include: 1) testing an ensemble Kalman filter (EnKF) data-assimilation system to assimilate all-sky IR radiance observations into COAMPS-TC.^{®2} over the Atlantic, Pacific, and Indian oceans that showed robust positive impacts on tropical cyclone track and intensity, 2) development of a weak-constraint 4D-Var formulation for NAVGEM DA, for which it is uniquely well-suited, 3) COAMPS-4D-Var experiments evaluating the impact of high-frequency radar wind retrievals, 4) testing of the world's first ensemble DA system for the ionospheric model SAMI, 5) development of tangent linear and adjoint codes for moist physics parameterizations, 6) continued development of new radiance bias drift mitigation technique for NAVGEM radiance data, 7) developing, testing and delivering to Navy operations at Fleet Numerical Meteorology and Oceanography Center (FNMOC) a first-in-the-world implementation of COSMIC-2 data, and 8) development of the global all-sky microwave satellite data assimilation.

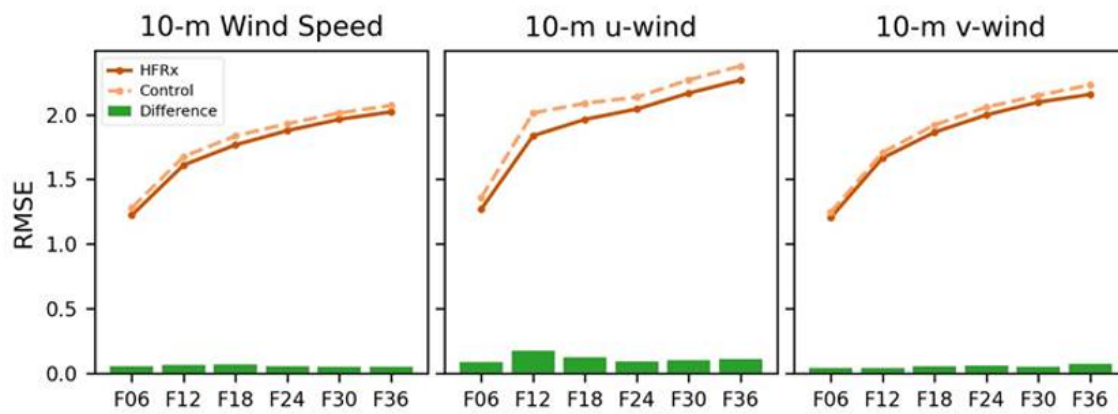
DoD Impact/Significance: HPCMP computing platforms provide a common environment for collaboration and the rapid development of NRL's multiple data-assimilation systems. Large common datasets can be stored and accessed by many researchers, greatly facilitating collaboration between NRL scientists at different locations (Monterey, Stennis, and DC) and scientists in academia, government, and other laboratories. The advancements of NAVDAS-AR, NAVGEM (including hybrid NAVGEM and HA-NAVGEM), and COAMPS-AR systems would not have been possible without the HPCMP systems. The core and future of Navy data-assimilation capabilities are being mostly, and in many cases solely, developed using the resources provided by HPCMP. In summary, the ability to access the HPCMP resources is critical to prepare technology for successful transfer to operations.

¹ COAMPS[®] is a registered trademark of the Naval Research Laboratory.

² COAMPS-TC[®] is a registered trademark of the Naval Research Laboratory.



FSOI of the high-frequency radar wind observations for each run during the study period. HFR was beneficial in over half the runs.



Root-mean-square-error of 10-m wind field was improved when the HFR winds were assimilated (control experiment did not assimilated HFR winds, but the HFRx experiment did).

Title: Coastal Mesoscale Modeling - COAMPS-TC Intensity Prediction

Author(s): J.D. Doyle

Affiliation(s): Naval Research Laboratory, Monterey, CA

CTA: CWO

Computer Resources: HPE SGI 8600 [NAVY, MS]; Cray XC40/50 [ERDC, MS]

Research Objectives: Tropical cyclone (TC) track forecasts have improved in a steady manner during the past several decades, but intensity forecasting has shown much slower increase in skill during the same time period. This is due, in part, to our limited ability to properly model the physical process controlling tropical cyclone structure and intensity, but also is due to the inherent sensitivity that tropical cyclone forecasts exhibit to initial conditions. The objective of this project is to further advance and test COAMPS-TC^{®1}, a state-of-the-science numerical weather prediction (NWP) system designed for the simulation of tropical cyclones in support of Navy and DoD operations, and for civilian applications. The COAMPS-TC system is operational at Fleet Numerical Meteorology and Oceanography Center (FNMOC) and has undergone several substantial upgrades recently. The overall goal is to improve the COAMPS-TC tropical cyclone intensity predictions through improved vortex initialization and representation of physical processes.

Methodology: There are two main types of COAMPS-TC forecasts performed. The first type of application is used to facilitate rapid development and testing of COAMPS-TC. The prototype testing for COAMPS-TC needs to be rigorous and involves running approximately hundreds of individual cases in order to assess the performance of the system in a statistically meaningful manner. Each incremental change in the development process, such as an increase in resolution or improved parameterizations, needs to be tested through this procedure. This rapid prototyping is required to develop and evaluate the new version of COAMPS-TC that will be run operationally at FNMOC. A second type of COAMPS-TC application involves the near-real-time execution of an experimental version of COAMPS-TC, which contains more advanced capabilities than the FNMOC operational version. The testing of the experimental COAMPS-TC system is performed for many tropical cyclones in all basins worldwide.

Results: In the past year, many configurations of COAMPS-TC were tested rigorously over a suite of storms in the Atlantic Ocean and Pacific Ocean basins based on three previous TC seasons. A new version with significant improvements was transitioned to operations at FNMOC in May 2020. These improvements included the use of high horizontal resolution (4 km), along with upgrades to the physical parameterizations and model initialization. Figure 1 shows a series of five-day forecasts of the track and intensity for Hurricane Laura in late August 2020. Hurricane Laura was a destructive Category 4 hurricane that severely impacted the U.S. Gulf Coast. As illustrated in Fig. 1, COAMPS-TC accurately captured Laura's track and landfall location even at longer lead times. COAMPS-TC also correctly and consistently forecasted the observed rapid intensification of Laura, which is one of the greatest challenges for models to capture. COAMPS-TC was the top-performing hurricane forecast intensity model over the Atlantic in 2019 and continues to be one of the top-performing tropical cyclone prediction models worldwide.

DoD Impact/Significance: Tropical cyclones remain the most disruptive and devastating environmental threat that impact U.S. Navy operations. We anticipate that an increase in accuracy of tropical cyclone forecasts will result in significant cost benefit to the Navy through better sortie decisions and avoidance of hazardous winds and seas. Real-time testing and development of the system have led to significant improvements in the predictive skill of COAMPS-TC and more rapid transitions to Navy operations at FNMOC. These improvements will inform future directions of tropical cyclone and mesoscale model development, particularly as computational power increases, allowing for higher resolution capabilities and increased fidelity in the physical process representations.

¹ COAMPS-TC[®] is a registered trademark of the Naval Research Laboratory.

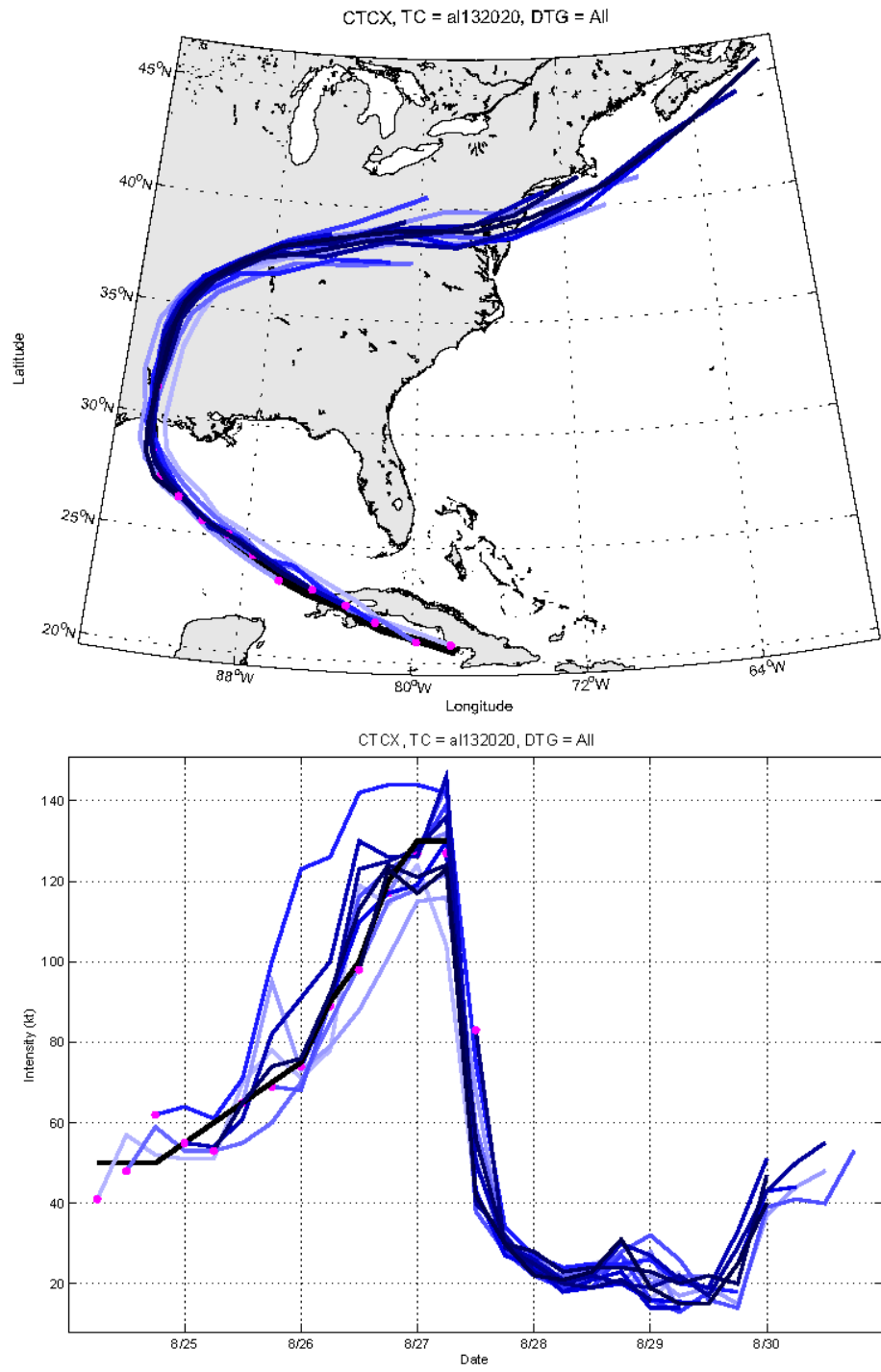


Figure 1. Five-day COAMPS-TC forecast (blue) and observed (black) tracks for Hurricane Laura for August 2020 (top). The magenta dot shows the initial position for each forecast every 6 hrs. Five-day forecast (blue) and observed (black) intensity for Hurricane Laura (bottom). Progressively lighter blue color corresponds to earlier initialization times.

Title: The Effect of Langmuir Turbulence in Upper Ocean Mixing

Author(s): Y. Fan

Affiliation(s): Naval Research Laboratory, Stennis Space Center, MS

CTA: CWO

Computer Resources: Cray XC40 [NAVY, MS]

Research Objectives: The goal of this project is to understand the effect of Langmuir turbulence (LT) in upper-ocean mixing within a broad parameter space and during complex oceanic conditions through extensive ocean, wave, and large eddy simulation (LES) modeling studies. The results from this project will provide a greater understanding of the generation, growth and decay of the LT, how it is affected by the mesoscale and submesoscale structures, and its impact on vertical and horizontal momentum and heat fluxes within the ocean on larger scales.

Methodology: Carefully designed LES experiments are conducted in the Bay of Bengal to study the interaction between LT and internal waves. The nested COAMPS-NCOM-SWAN system is used to provide realistic high-resolution ocean and wave conditions for the NCAR LES model. NCEP/CFSR atmosphere reanalysis, global HYCOM and WAVEWATCH-III are used to provide boundary conditions for the atmosphere, ocean and wave components of the COAMPS^{®1} coupled system. LES simulations are conducted with and without the Stokes drift to quantify the effect of LT. Temperature, salinity, and currents profile measurements at the RAMA buoy located in the Bay of Bengal at (90°E, 8°N) are used to validate the LES model results.

Results: Scale separation analysis is used to modify the momentum equations in the LES model to represent the effect of internal waves in the model domain. It states that the horizontal scales of the large-scale fluxes are much larger than the scales of motions that are contained within the domain of the LES model, such that the horizontal derivatives of the large-scale terms are unaffected by small-scale motions. This assumption allows us to account for the large-scale influence on the small-scale turbulence while still keeping the periodic boundary condition. The advantage for this approach is that there is no need to impose vertical profiles of velocities, temperature and salinity as horizontal boundary conditions, which may cause wave reflections at the lateral boundaries and interfere with small-scale turbulent motions inside the model domain. In this project, modifications are made to the momentum equations to represent strong temperature, salinity, and current gradients due to internal waves. Ocean model simulations using NCOM are used to provide large-scale gradient forcing for the LES. Three LES experiments (without Stokes drift and internal waves, with internal waves but no Stokes drift, and with both Stokes drift and internal waves) are conducted at the RAMA station using the same ocean conditions and meteorological forcing to diagnose the effect of LT, internal waves, and their joint effect on the ML and thermocline dynamics. The LES model results are consistent with NCOM simulations and observations, indicating the new model expansion performs well. From the experiment comparisons, it is found that internal waves can significantly enhance the entrainment of thermocline water into the mixed layer and dramatically shallow the mixed-layer depth. The presence of LT in the water column can reduce the shallowing effect of the internal waves, but evolution of the MLD is dominated mainly by the internal waves. These new findings were used to develop a new LT parameterization that is now implemented in NCOM.

DoD Impact/Significance: This study can help us improve the battlespace environment forecasting accuracy for both ocean and atmosphere (HYCOM, NCOM and COAMPS). Better understanding of the mechanism, growth and dissipation of LT will help us improve the air-sea interaction process in our coupled models (i.e., COAMPS and ESPC), which will lead to more accurate vertical thermal profile simulations in the ocean models and better predication of acoustic and optic properties in the upper ocean.

¹ COAMPS[®] is a registered trademark of the Naval Research Laboratory.

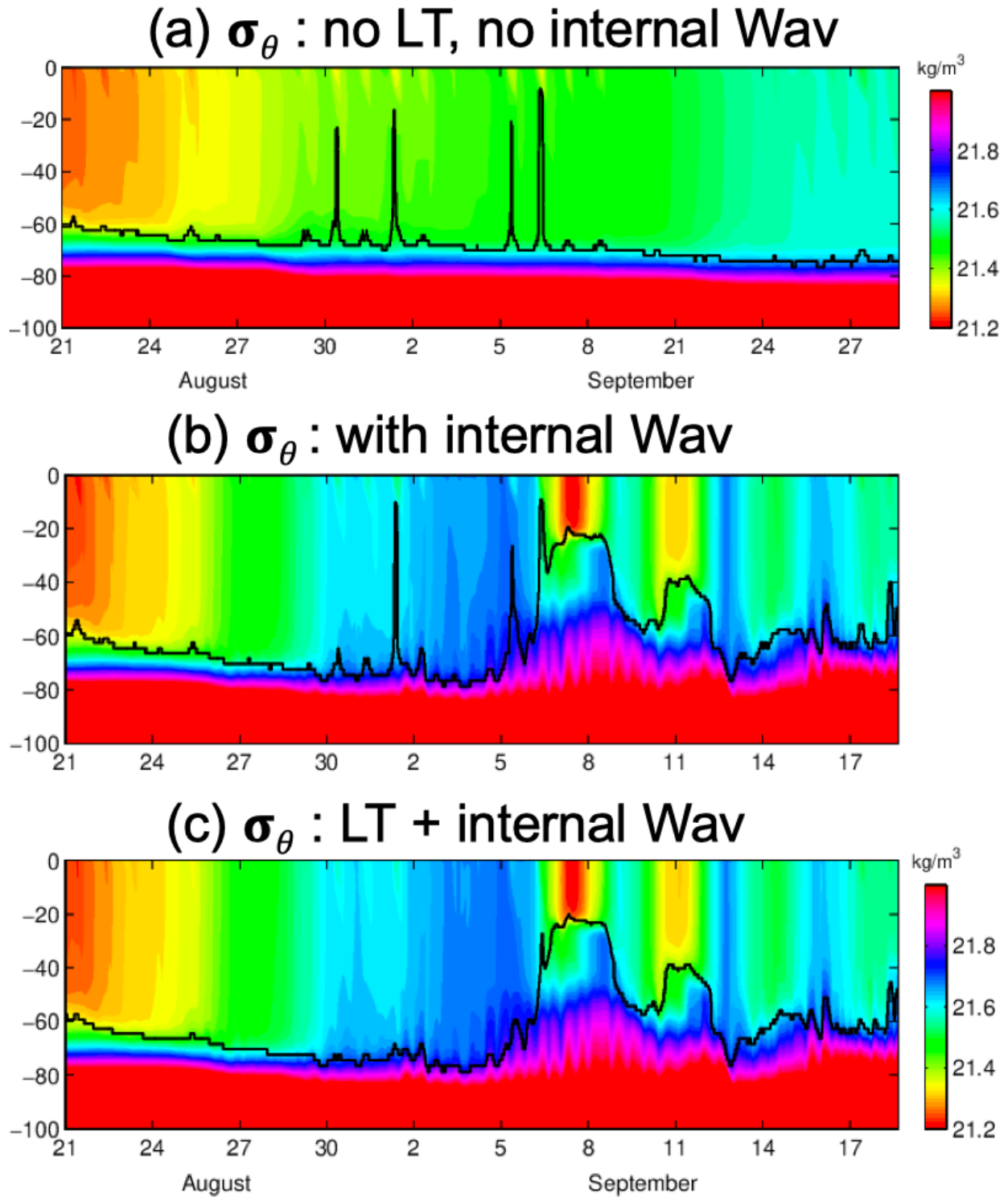


Figure 1. Potential density (σ_θ) in the experiment (a) with no Langmuir turbulence (LT) and no internal waves, (b) with internal waves only, and (c) with both LT and internal waves. The black line is the mixed-layer depth in the experiments defined by the variation of σ_θ is less than 0.1 kg/m^3 from the surface value.

Title: Bio-Optical Modeling and Forecasting

Author(s): J.K. Jolliff, S. Ladner, T.A. Smith, and C. Wood

Affiliation(s): Naval Research Laboratory, Stennis Space Center, MS

CTA: CWO

Computer Resources: HPE SGI 8600, Cray XC40 [NAVY, MS]

Research Objectives: The main research objective for FY20 was to implement an operational data flow of satellite-estimated surface ocean optical properties into operational numerical ocean models in support of the 6.4 “Visible Band Satellite Data to Improve Ocean Model Radiative Transfer” program. Most of the allocated HPC hours were devoted to this task, and so this will be the main focus of this brief report.

Methodology: Numerical ocean models must have a designated numerical representation of the attenuation of solar shortwave radiation into the surface ocean. This attenuation calculation determines the potential ocean heating rate and thermal balance for each time step, and it broadly impacts thermal and density state variables. The default calculation for the present class of operational numerical ocean models is based upon a table of five optical (Jerlov) water types. This is the case for the Navy Coastal Ocean Model (NCOM), the ocean numerical model component of the Coupled Ocean-Atmosphere Mesoscale Prediction System (COAMPS^{®1}). Since these tabular attenuation functions do not recognize real-time optical data from the oceans, they are invariably in error. To remedy this error, we have initiated a program to obtain daily information about the optical state of the surface ocean from the operational constellation of ocean-viewing satellites and to get this information into the operational ocean models via the Navy Coupled Ocean Data Assimilation system (NCODA). NCODA serves as both a data quality control platform and an analytic tool to facilitate the entry of oceanographic data into ocean models. Surface ocean optical data is a new data type for the NCODA system and requires its own quality control and analysis software architecture. The final analysis file then contains a complete spatial analysis field of surface ocean optical properties that can be read by the operational model and used to properly calculate the attenuation of solar shortwave radiation. In many cases, this may significantly impact thermal and other critical ocean and atmospheric variables as well as the simulated exchange of thermal energy. HPC hours were used in the development and testing of these critical tools immediately before transition to operational end users.

Results: NCODA quality control (QC) and two-dimensional variational analysis (VAR) branches were developed and tested to ingest two separate level-3 visible radiometer remote-sensing products: the surface total absorption coefficient (490 nm) and the surface total backscattering coefficient (490 nm). Incomplete two-dimensional surface fields are produced by the Global Optical Processing System (GOPS), which compiles daily data from the ocean-viewing satellite constellation. NCODA VAR optics branch uses these data and a monthly gridded surface optical climatology to render a complete optical field. These completed fields are then available for ocean models to determine the data-based attenuation of solar shortwave radiation, thereby replacing the Jerlov tables. HPC hours were used to develop and test the final configuration for the NCODA QC and VAR optics branches and then to validate the results. An example of the impact these fields have on the COAMPS simulations (Fig. 1) demonstrates the significance these shortwave attenuation calculations can have on the simulated temperature fields.

DoD Impact/Significance: Improvement of operational ocean models when given realistic solar shortwave attenuation data has been previously demonstrated and moving this work to the operational level is of paramount importance. The flow of these data will improve model operations within the ocean and atmospheric domains.

¹ COAMPS[®] is a registered trademark of the Naval Research Laboratory.

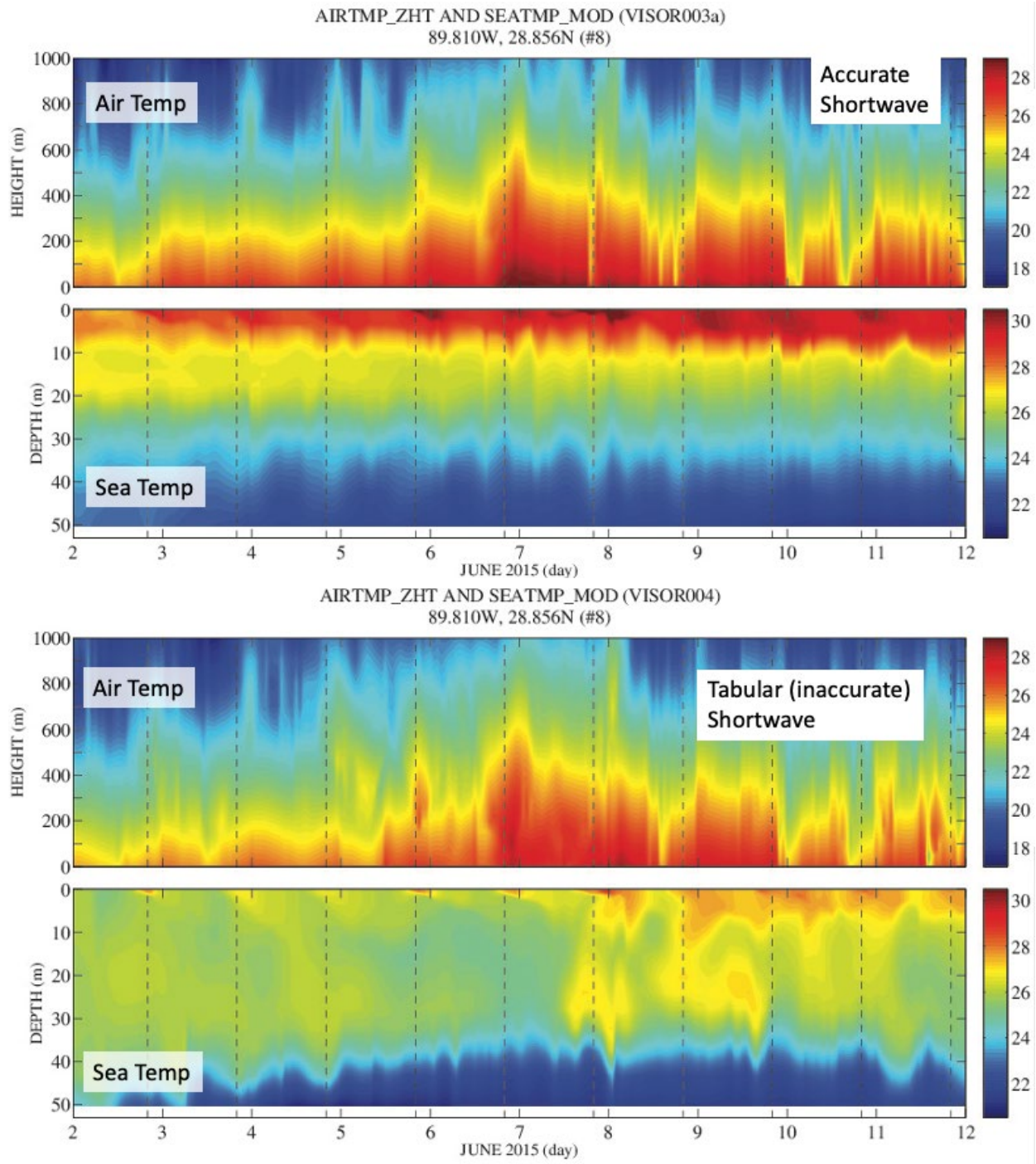


Figure 1. Temporal evolution of COAMPS simulated air and sea temperatures for a coastal location in the northern Gulf of Mexico. When accurate shortwave attenuation fields are used in the model (top panel) more thermal energy is trapped near the air-sea interface. These results contrast markedly with the operational version (bottom panel) that used the default shortwave attenuation values.

Title: Investigation and Implementation of GPU Capability to Next Generation Weather Prediction Code NEPTUNE

Author(s): Y. Khine

Affiliation(s): Naval Research Laboratory, Washington, DC

CTA: CWO

Computer Resources: HPE SGI 8600, SGI ICE X [AFRL, OH]; SGI ICE X, Cray XC40 [ARL, MD]; Cray XC40/50 [ERDC, MS]; HPE SGI 8600 [NAVY, MS]

Research Objectives: The goal of this project is to investigate and implement GPU capability to Navy Environmental Prediction system Utilizing the NUMA core (NEPTUNE) code in order to enhance its performance and to utilize DoD GPU accelerator-based architectures for high-resolution three-dimensional simulations.

Methodology: As a first step, a stand-alone section of NEPTUNE code was studied and profiled on DoD HPC systems to get familiar with the code and to learn the initial bottlenecks in the code. Next, the suitability of GPU implementations OpenMP and OpenACC were investigated on various HPC systems. It was concluded that due to the lack of future support for OpenACC, OpenMP was the better choice for NEPTUNE code. However, we experienced some issues with currently available compilers for OpenMP support, so for the moment, OpenACC implementation was the GPU programming paradigm of choice. Many offloading features between OpenACC and OpenMP have a one-to-one mapping, meaning that current OpenACC refactoring work can guide future refactoring work for OpenMP. Thus, OpenACC implementation was performed for the standalone NEPTUNE code in this project.

Results: Figure 1 presents sample profiling results of a stand-alone section of NEPTUNE code. This information provides us the routines and regions of the codes that need to be targeted in improving the performance. NEPTUNE is coded using object-oriented Fortran to take advantage of object-oriented capabilities. It is observed that while object-oriented programming eases development on traditional CPUs, it required additional programming considerations when working with OpenACC regarding data transfers and consistency on accelerators. Object-oriented programming also uses type-bound procedures, which is the calling of a subroutine or function through an associated object throughout the code. However, OpenACC currently does not support type-bound procedures. Non-type-bound procedures within the code were ported to OpenACC. The implementation was tested, and verified that the results replicate the CPU based solutions. In this project, the groundwork has been laid for the NEPTUNE code to utilize GPUs via OpenACC on DoD DSRCs. The OpenACC implementation effort is currently ongoing in FY 2021. This work is essential to guide future development of NEPTUNE to utilize a more open programming standard for heterogeneous architectures.

DoD Impact/Significance: Since weather modeling requires a large computational domain on the scale of kilometers and a long enough time period, it is important to achieve results in desired time frame. The GPU implementation to NEPTUNE code will allow users to generate realistic simulations within a reasonable turnaround time. Accurate weather forecasting is very important to DoD to achieve successful missions and it is also vital in preventing potential natural disasters.

⌵ **Elapsed Time** [?]: **51.505s** 

- ⌵ **CPU Time** [?]: **80.790s**
 - ⌵ **Effective Time** [?]: **61.599s**
 - ⌵ **Spin Time** [?]: **11.060s** 
 - Imbalance or Serial Spinning [?]: **10.580s** 
 - Lock Contention [?]: 0s
 - Other [?]: 0.480s
 - ⌵ **Overhead Time** [?]: **8.131s** 
- Total Thread Count: 2
- Paused Time [?]: 0s

⌵ **Top Hotspots**

This section lists the most active functions in your application. Optimizing these hotspot functions typically results in improving overall application performance.

Function	Module	CPU Time [?]
cgc_to_elem_core	diffusion_driver.exe	16.350s
compute_laplacian	diffusion_driver.exe	11.229s
__kmpc_barrier	libiomp5.so	10.900s 
gridstash	diffusion_driver.exe	8.470s
__kmpc_atomic_float8_add	libiomp5.so	7.981s 
[Others]		25.859s

**N/A is applied to non-summable metrics.*

Figure 1. Sample profiling results of stand-alone section of NEPTUNE code.

Title: Coastal Mesoscale Modeling

Author(s): W.A. Komaromi and P.A. Reinecke

Affiliation(s): Naval Research Laboratory, Monterey, CA

CTA: CWO

Computer Resources: HPE SGI 8600, Cray XC40 [NAVY, MS]; SGI ICE X [AFRL, OH]; SGI ICE X, Power9 [ARL, MD]; Cray XC40/50 [ERDC, MS]

Research Objectives: Our objective is to develop and validate a fully coupled coastal/littoral prediction system that can be used to provide high-resolution (<5 km) data assimilation (DA) and short-term (0-48h) forecast guidance for tactical-sized areas of the world. This system can also be used for basic and applied research leading to an improvement in our understanding of atmospheric and oceanic processes. Improvements to the mesoscale prediction and DA systems will result from this research.

Methodology: The Coupled Ocean/Atmosphere Mesoscale Prediction System (COAMPS^{®1}) is being developed further for independent and coupled simulations of the atmosphere and ocean for the mesoscale. The atmospheric component of COAMPS is made up of a DA system, an initialization procedure, and a multi-nested, nonhydrostatic numerical model. This model includes parameterizations for moist processes, surface and boundary-layer effects, and radiation processes. The NRL Coastal Ocean Model (NCOM) is currently being used for the simulation of the mesoscale ocean circulation response to the COAMPS forcing in one-way and two-way interactive modes. Ocean coupling is being developed using the Earth System Modeling Framework (ESMF). A new tropical cyclone capability has been developed for COAMPS, referred to as COAMPS-TC^{®2}. Development and testing of the Navy's next-generation prediction system, NEPTUNE (Navy's Environmental Prediction System Using the NUMA Engine) is underway. This system uses a spectral element-based approximation to the atmosphere and can scale to more than 1,000,000 cores.

Results: In FY20, COAMPS was demonstrated to be an accurate DA-and-forecast system capable of predictions and simulations on a variety of horizontal scales of less than 1 km for land-sea effects, topographically driven flows, and tropical cyclones. Numerous studies were performed to explore the impact of the ocean and the sea state on the atmospheric boundary layer. Furthermore, the development of the Navy's next-generation global NWP system, NEPTUNE, continued in FY20 with systematic testing of real-data initial condition forecasts using full physics parameterizations. As shown in Fig. 1, the characteristics of a convective internal boundary layer (CIBL) has been investigated using surface-layer-resolving large-eddy simulation (LES). According to the LES, in the near-shore adjustment zone, the low-level winds and surface friction velocity increase rapidly. An elevated turbulent layer is present immediately below the CIBL top, associated with the vertical wind shear across the CIBL top inversion. Episodic shear instability events occur with a time scale between 10 and 30 min, leading to the formation of elevated maxima in turbulence kinetic energy and momentum fluxes. The turbulence characteristics of the near-shore atmospheric boundary layer will continue to be investigated in FY21.

DoD Impact/Significance: COAMPS continues to play a significant role in providing atmospheric forecasts in support of Navy missions involving the deployment of weapons systems, strike warfare, radar propagation, and search and rescue. Research and development performed at HPC DSRCs have led to significant improvements in the predictive skill of COAMPS that will greatly benefit the operational performance of COAMPS. The HPC DSRCs will be the primary computing resources in FY21 and beyond for the development of the fully coupled COAMPS system, including the emerging tropical cyclone and ensemble capabilities for COAMPS as well as NEPTUNE, the next-generation global and mesoscale modeling system.

¹ COAMPS[®] is a registered trademark of the Naval Research Laboratory.

² COAMPS-TC[®] is a registered trademark of the Naval Research Laboratory.

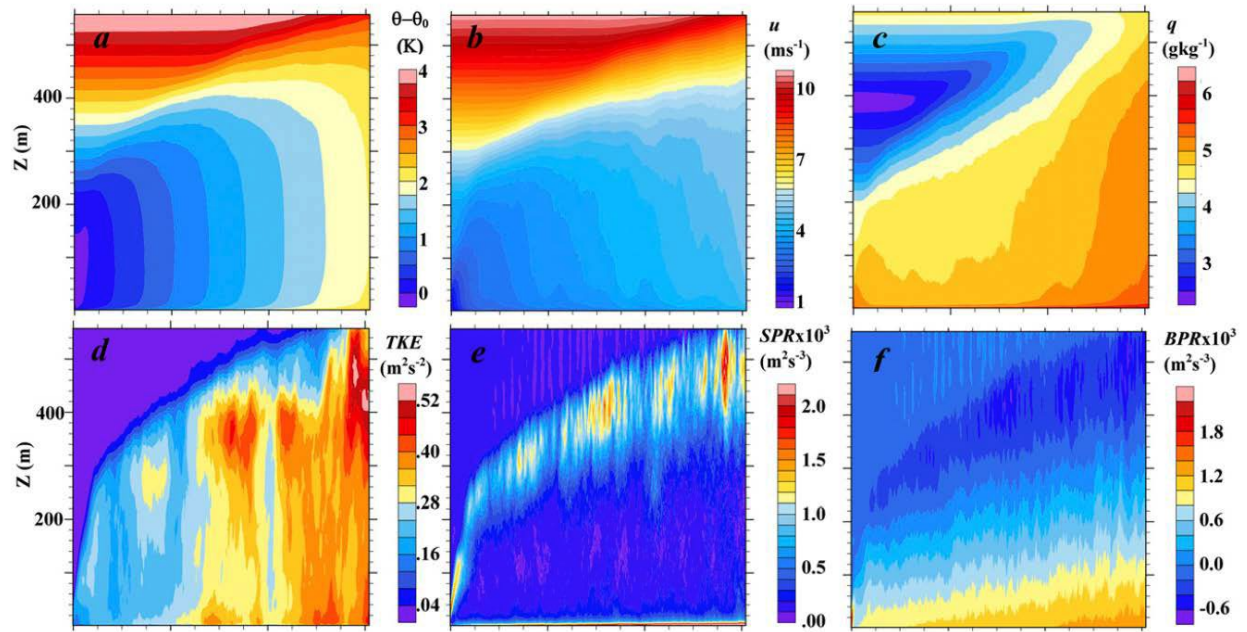


Figure 1. Offshore distance-height cross sections of (a) potential temperature ($\theta - \theta_0$, increment = 0.25 K), (b) u wind (increment = 0.25 m s^{-1}), (c) specific humidity (q , increment = 0.25 g kg^{-1}), (d) turbulence kinetic energy (TKE, increment = 0.1 $\text{m}^2 \text{s}^{-2}$), (e) shear production rate ($\text{SPR} \times 10^3$, increment = 0.1 $\text{m}^2 \text{s}^{-3}$), (f) buoyancy production rate ($\text{BPR} \times 10^3$, increment = 0.2 $\text{m}^2 \text{s}^{-3}$). From Jiang et al. (2020).

Title: Coastal Mesoscale Modeling – COAMPS-TC
Author(s): W.A. Komaromi
Affiliation(s): Naval Research Laboratory, Monterey CA
CTA: CWO

Computer Resources: Cray XC40 [NAVY, MS]

Research Objectives: Tropical cyclones (TCs) are a significant threat to DoD assets around the world. In 2018, Hurricane Michael caused \$6 billion in damage to Tyndall AFB alone. Improved forecast guidance will provide greater lead time to prepare for storms and to protect military assets. The objective of this project is to develop and improve our probabilistic TC track, intensity, and structure forecast guidance system for the DoD and the Navy via the COAMPS-TC^{®1} ensemble prediction system. In FY20, we focused on the following goals: (1) to run an experimental, real-time 21-member ensemble at NRL that is complementary to Fleet Numerical Meteorology and Oceanography Center’s (FNMOCs) operational 11-member ensemble, (2) to update the core model of the experimental COAMPS-TC ensemble from v2018 to v2019 for testing ahead of the FY21 transition, and (3) to upgrade the graphics suite to better meet the needs of the end users, TDO forecast officers.

Methodology: COAMPS-TC is a special variant of the Coupled Ocean/Atmosphere Mesoscale Prediction System (COAMPS^{®2}) developed at NRL to predict TC track, intensity and structure around the globe. While COAMPS-TC produces highly skillful deterministic TC forecasts, weather prediction tends to be probabilistic in nature. Uncertainty in the initial state of the atmosphere due to insufficient observations, errors in our measurements, and approximations in our model equations all contribute to errors in the model forecast which grow with time. For this reason, NRL has developed the COAMPS-TC Ensemble, which is a collection of forecasts made using the same model at the same initial time, but with slightly different assumptions about the initial state of the atmosphere and/or slightly different model physics.

Results: In FY20, an experimental 21-member version of the COAMPS-TC ensemble was run in real time at the NAVO DSRC every 12 hours for the majority of TCs ≥ 25 kt intensity globally. Relative to the version of the ensemble that was run in FY19, the FY20 variant used COAMPS-TC v2019 as its core model, featured tuned initial-condition and boundary-condition perturbations, and an improved graphics suite. As demonstrated in Fig. 1, the ensemble had strong performance for both track and intensity for hurricanes that made landfall in the US in 2020, including Laura, Sally, and Delta. In FY20, the graphics suite was upgraded from Python 2 to 3, and the mapping software was upgraded from basemap to cartopy, a new probabilistic intensity forecast graphic was added, and a new probabilistic “wind swath” graphical product also was added, which depicts the probability of winds exceeding various thresholds at a given location. These upgrades will be transitioned to FNMOC and will be available to TDO forecasters in FY21.

DoD Impact/Significance: Forecasters at the DoD’s Joint Typhoon Warning Center (JTWC), as well as Fleet Weather Centers San Diego and Norfolk rely upon real-time TC forecasts from COAMPS-TC and the COAMPS-TC Ensemble, along with corresponding wind and wave guidance for various decision aids. Improved confidence and increased forecast lead time also increase the lead time for sortie decision making, as well as general fleet routing and awareness. The HPC DSRC provides a unique environment to test and improve the COAMPS-TC probabilistic forecast system prior to transition for operational use at FNMOC. These improvements will inform future decisions regarding the design of probabilistic TC prediction systems.

¹ COAMPS-TC[®] is a registered trademark of the Naval Research Laboratory.

² COAMPS[®] is a registered trademark of the Naval Research Laboratory.

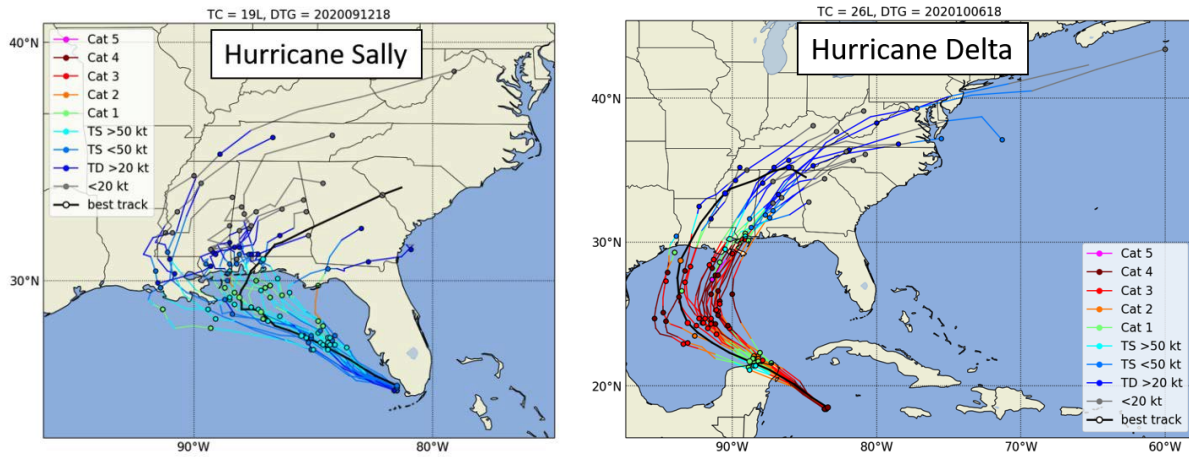


Figure 1. COAMPS-TC ensemble 21-member experimental 120-h track forecasts colored by intensity for Hurricane Sally initialized 1800 UTC 12 September 2020 (left), and Hurricane Delta initialized 1800 UTC 06 October 2020 (right). Forecast and best-track positions are indicated by small circles in 24-h increments. Best-track intensity is indicated by the color-filled circle every 24 h.

Title: Multi-scale Characterization and Prediction of the Global Atmosphere from the Ground to the Edge of Space using Next-Generation Navy Modeling Systems

Author(s): J.P. McCormack¹, S.D. Eckermann¹, C.A. Barton¹, F. Sassi¹, J. Kelly¹, M.A. Herrera¹, K.W. Hoppel¹, D.D. Kuhl¹, D.R. Allen¹, J. Ma², and J.L. Tate²

Affiliation(s): ¹Naval Research Laboratory, Washington DC; ²Computational Physics Inc., Springfield VA
CTA: CWO

Computer Resources: HPE SGI 8600 [AFRL, OH]; SGI ICE X, Cray XC40 [ARL, MD]; Cray XC40/50 [ERDC, MS]; HPE SGI 8600, Cray XC40 [NAVY, MS]

Research Objectives: To develop and test new seamless atmospheric specification and prediction capabilities for altitudes of 0 to 500 km for future Navy Earth System Prediction Capability (ESPC) and Space Environment Prediction with High Resolution (SEPHIR) systems, linking prediction of the ocean, atmosphere, and space over time scales from hours to decades.

Methodology: This project develops and tests key components of state-of-the-art systems required for the improved modeling, prediction and analysis of the extended operational environment for Navy applications, focusing on the atmosphere, the near space and the geospace. Specific systems under development are: (a) a high-altitude version of the Navy Global Environmental Model (NAVGEN-HA), based on an upward extension of the Navy's operational global numerical weather prediction (NWP) system; (b) the next-generation Navy numerical weather prediction model NEPTUNE (Navy Environmental Prediction system Using the NUMA core); (c) the Coupled Ocean-Atmosphere Mesoscale Prediction System (COAMPS^{®1}), the Navy's operational regional NWP system; and (d) the SEPHIR ground-to-space prediction prototype.

Results: Major results include: (a) Successful testing of NAVGEN-HA code for transition to operations at Fleet Numerical Oceanography and Meteorology Center through the Navy ESPC program in FY22; (b) Continued development of a new NEPTUNE modeling capability extending from the surface to 300 km altitude using advanced numerical algorithms that enable the non-hydrostatic dynamical core to operate at high altitudes (e.g., nonlinear and exponential time integrators, a new implementation of viscous diffusion and thermal conduction, new energy equations and prognostic variables valid for vertically varying composition); (c) Development and testing of a new high-altitude data-assimilation capability incorporating wind measurements of the mesosphere and the lower thermosphere (70 – 100 km altitude) from meteor radar observations into the NAVGEN-HA system; (d) New NAVGEN-HA meteorological analysis products with high horizontal resolution to capture upward-propagating small-scale waves generated near the surface by orography and deep convection that impact the mesosphere and the lower thermosphere (see Fig. 1); (e) COAMPS simulations coupled to new Fourier-ray and multilayer gravity wave models and an ionospheric model for end-to-end physics-based prediction of traveling ionospheric disturbances seeded by waves generated in the lower atmosphere; (f) Development and testing of automated gravity wave drag tuning experiments and evaluation of a local ensemble tangent linear model with NAVGEN-HA at operational resolution; (g) Analysis of the impact of Australian wildfire smoke clouds on stratospheric meteorology using near-real-time NAVGEN-HA analyses.

DoD Impact/Significance: This research addresses Navy requirements to develop and test new high-altitude atmospheric specification and prediction capabilities leading to a planned Navy ESPC by 2022. This project performs the R&D needed to install an accurate high-altitude specification and forecast capability in next-generation Navy NWP systems, ultimately providing improved near-space specification and prediction capabilities to the warfighter over both tactical and strategic time frames. The development of a new ground-to-thermosphere prediction capability fully coupled to ionospheric models and data assimilation address key space-environment prediction goals of the Defense Advanced Research Projects Agency's Space Environment Exploitation (DARPA SEE) program.

¹ COAMPS[®] is a registered trademark of the Naval Research Laboratory.

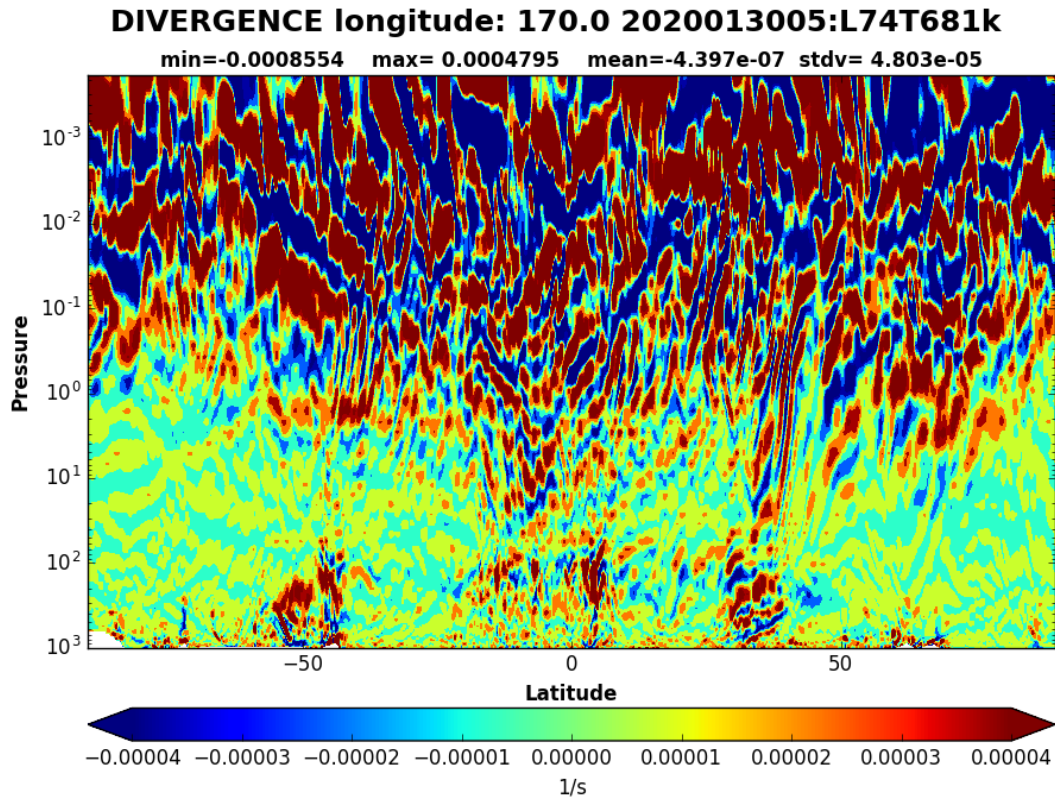


Figure 1. Pressure/latitude cross section of the horizontal wind divergence from the high-altitude version of the Navy Global Environmental Model (NAVGEM-HA) with 74 vertical levels (L74) and high horizontal resolution (triangular spectral truncation at wavenumber 681, or T681). Maximum (red) and minimum (blue) divergence values indicate presence of upward-propagating gravity waves forced by flow over orography (e.g., near 50°S and 35°N latitude) and deep tropical convection (e.g., 15°S-5°N latitude). Vertical domain of plot extends from the surface (pressure = 10^3 hPa) to the lower thermosphere (pressure = 5×10^{-4} hPa, or approximately 100 km altitude).

Title: Eddy-Resolving Global/Basin-Scale Ocean Modeling
Author(s): E.J. Metzger and J.F. Shriver
Affiliation(s): Naval Research Laboratory, Stennis Space Center, MS
CTA: CWO

Computer Resources: HPE SGI 8600, Cray XC40 [NAVY, MS]; Cray XC40/50 [ERDC, MS]

Research Objectives: Modeling component of a coordinated 6.1-6.4 effort on the problem of eddy-resolving global and basin-scale ocean modeling and prediction. This includes increased understanding of ocean dynamics, model development, model validation, transitions to operations, naval applications, oceanic data assimilation, ocean predictability studies, observing system simulation studies, and nested models.

Methodology: The appropriate choice of vertical coordinate is a key factor in ocean model design. Traditional ocean models use a single coordinate type to represent the vertical, but no single approach is optimal for the global ocean. Isopycnal (density tracking) layers are best in the deep stratified ocean, Z-levels (constant depths) provide high vertical resolution in the mixed layer, and terrain-following levels are often the best choice in coastal regions. The HYbrid Coordinate Ocean Model (HYCOM) has a completely general vertical coordinate (isopycnal, terrain-following, and Z-level) via the layered continuity equation that allows for an accurate transition from deep to shallow water. Two-way coupling to the Community Ice Code (CICE) leads to a more realistic cryosphere in the polar latitudes. The Modular Ocean Model, version 6 (MOM6) implements the z^* coordinate, also with a layered continuity equation and vertical Lagrangian remapping, suitable for a global application.

Results: We have three refereed articles, four non-refereed articles published or in press in FY20.

Global modeling: The Global Ocean Forecast System (GOFS) 3.5 ($1/25^\circ$ HYCOM/CICE) software and scripting was transitioned to Fleet Numerical Meteorology and Oceanography Center and is undergoing operational testing. It provides superior ocean and sea ice performance relative to operational GOFS 3.1. One role of the system is to provide boundary conditions for regional ocean models, and the inclusion of astronomical tides generates internal tides to be passed through the boundaries.

Nordic Seas: Twin Nordic Sea simulations, including the Greenland/Iceland/UK gap, have been conducted comparing the solution of moving (MOM6) vs fixed coordinates (Navy Coastal Ocean Model) formulations at high latitudes, where the coordinate representation is most important.

Internal tides: HYCOM M_2 internal tide amplitude and phases show good predictability with an altimeter-based tidal analysis. New HYCOM simulations with data assimilation capture from 43 – 69% of the M_2 stationary internal tide variance in five hot spot regions. Internal tides also significantly impact ocean acoustics, causing large undulations in isopycnal surfaces at depth (Fig. 1).

Sea ice modeling: Testing performed with the landfast sea ice parameterization in CICE version 6 on the GOFS 3.5 grid showed good agreement in the Beaufort, Laptev and East Siberian seas compared to observed landfast ice chart data.

Frontal prediction: HYCOM/CICE have been configured for the North Atlantic with increasing horizontal resolution to establish the effects on frontal prediction.

DoD Impact/Significance: Data-assimilative eddy-resolving models are important components of global ocean and sea ice prediction systems. Ocean forecasts are valuable for tactical planning, optimum track ship routing, search-and-rescue operations, and the location of high-current-shear zones. The sea ice environment has become increasingly important for strategic and economic reasons, given the diminishing trend in sea ice extent and thickness and the potential summertime opening of the Northwest Passage and Siberian sea routes. Fractures, leads and polynya forecasts are also valuable to the naval submarine community.

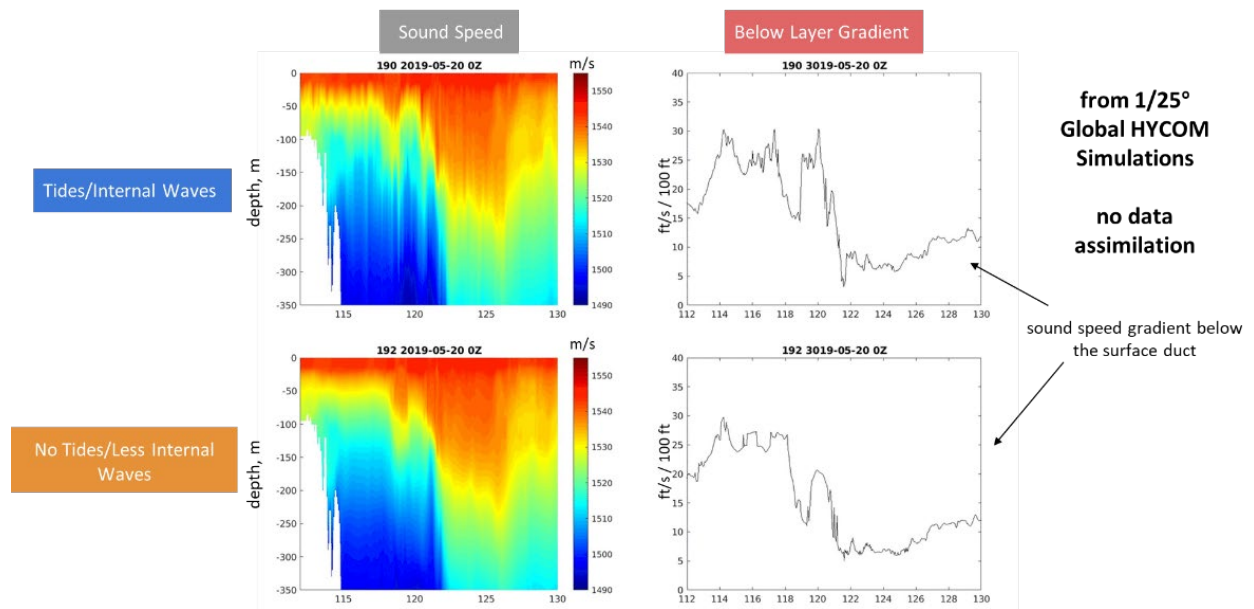


Figure 1. Depth (m) vs longitude of sound speed (m/s, left column) and below-layer gradient (ft/s/100 ft, right column) at 20°N in the western Pacific Ocean in 1/25° global HYCOM that includes astronomical tidal forcing (top row) and without tidal forcing (bottom row). Neither includes data assimilation. Internal tides in the upper panels appear as short-wavelength features that propagate when viewed in an animation.

Title: High Resolution Global Ocean Reanalysis

Author(s): E.J. Metzger

Affiliation(s): Naval Research Laboratory, Stennis Space Center, MS

CTA: CWO

Computer Resources: HPE SGI 8600, Cray XC40 [NAVY, MS]

Research Objectives: Generate a 26-year (1994-2019) Global Ocean Forecast System (GOFS) 3.1-like eddy-resolving, data assimilative reanalysis using all available archived observations. To ensure consistency of results across all years, perform validation and verification error metrics similar to what has been done in past VTRs. Produce annual, monthly and daily climatologies for end users.

Methodology: Integrate the GOFS 3.1 reanalysis forward in time on Navy DSRC supercomputers using HPC Pathfinder hours. Break apart the reanalysis into 3.5-year streams to speed the time to completion and discard the first 6 months due to non-equilibrium issues. Discontinuities may exist between the stream boundaries. Perform “on-the-fly” post-processing to convert from the HYCOM and CICE native grids to the uniform grids currently supplied to Fleet Numerical Meteorology and Oceanography Center (FNMOC) in operational GOFS 3.1. Perform match-ups and error analyses as each model year completes to assess performance. Create annual, monthly and daily climatologies on the uniform grid for end users.

Results: The 26-year GOFS 3.1 reanalysis spanning 1994-2019 was completed using nearly 7.5 million hours of HPC Pathfinder time at Navy DSRC. The total Pathfinder award was 9 million hours and in June 2020, we returned the fraction of hours that would not be needed. The workload was spread out across four supercomputers to speed the integration. We used the allocation on the HPE SGI 8600 computers first because HYCOM is ~35% faster on these machines compared to the Cray XC40s. Error analyses for ocean metrics were completed and these included: temperature and salinity vs. depth bias and RMSE, acoustical proxies (mixed layer depth, sonic layer depth, below layer gradient) bias and RMSE, surface layer trapping of acoustical frequencies and upper ocean velocity speed bias and RMSE and directional vector correlation. Sea ice error analyses included: ice edge error relative to independent observations and sea ice velocity speed bias and RMSE and directional vector correlation. As the number of observations grew as a function of calendar year, the error levels generally decreased, indicating that more observations led to better constraint of the oceanic mesoscale. All validation and verification results were compiled in a validation test report that is 80% complete. All GOFS 3.1 reanalysis output on the native grid, on the post-processed uniform grid and the annual, monthly and daily climatologies exist on the Navy DSRC long-term archive machine. The operational partner (NAVOCEANO) has been given the appropriate permissions to access the output that is limited to DoD and DoD contractors via HPC group permissions.

DoD Impact/Significance: FNMOC and NAVOCEANO have requirements to maintain up-to-date ocean climatologies and databases to provide the fleet with impactful information globally. This ocean reanalysis provides consistently configured, long-term model-based climatologies of prognostic variables (currents, temperature, and salinity) and diagnostic variables (mixed layer depth, acoustic parameters). It has an advantage over observational-based climatologies in that it includes output of the full water column and at three-hourly temporal frequency. Other uses include provision of boundary conditions for regional models run in hindcast mode (i.e., covering previous time periods), initial conditions for global and regional reforecasting, for use as a verifying analysis for reforecasting, and for comparison against other national/international global ocean reanalyses.

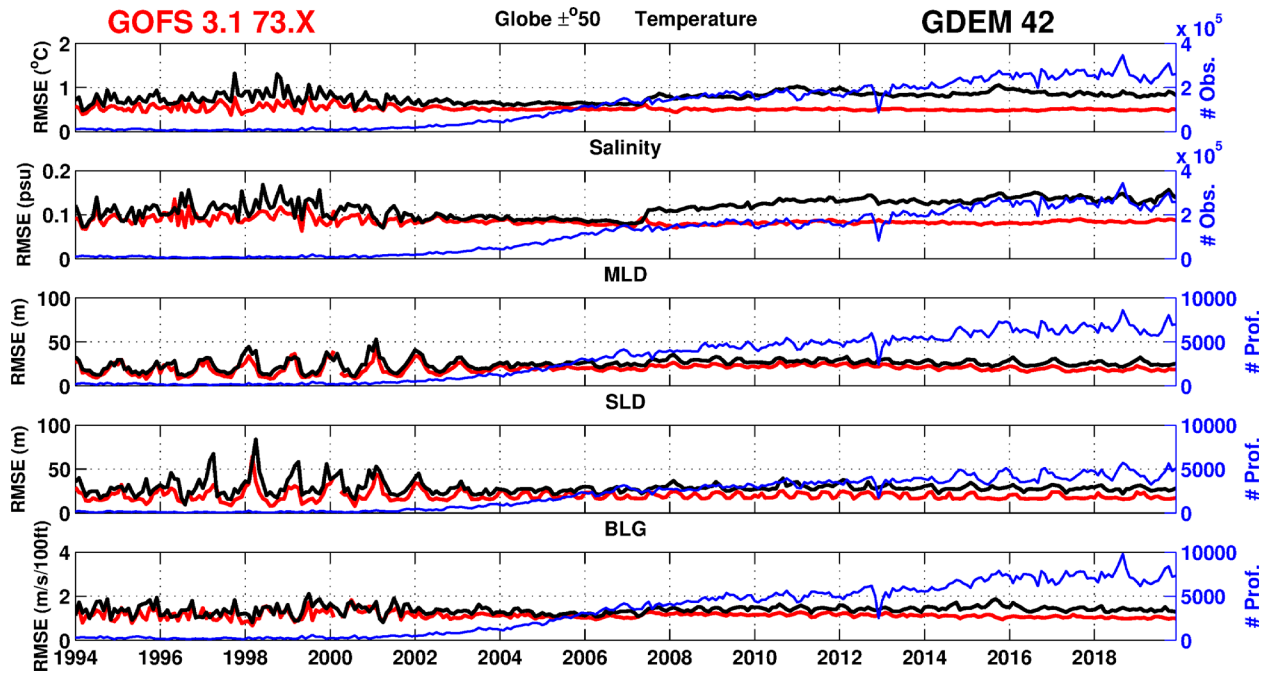


Figure 1. Monthly root mean square error of temperature ($^{\circ}\text{C}$, top panel), salinity (psu, second panel), mixed layer depth (m, third panel), sonic layer depth (m, fourth panel) and below layer gradient (m/s/100 feet, bottom panel) vs. time over the global ocean (50°S - 50°N) from GOFS 3.1 reanalysis 24-hour forecasts (red) and GDEM4 climatology (black) vs. unassimilated observations. The blue line (right y-axis) denotes number of observations or profiles vs. time. As the number of observations increases, the error levels in GOFS 3.1 show a small decrease and more spread between GDEM4.

Title: Rogue Wave Probability Estimator for WAVEWATCH III
Author(s): M. Orzech and J. Dykes
Affiliation(s): Naval Research Laboratory, Stennis Space Center, MS
CTA: CWO

Computer Resources: HPE SGI 8600 [NAVY, MS]

Research Objectives: Overall objective is to develop and transition an integrated utility enabling WAVEWATCH III (WW3) to estimate the relative threat of rogue waves throughout the global ocean. The system operates in a broad range of deep-water wave environments and computes a rogue threat index (RTI), to estimate rogue threat as the product of several scalar metrics representing the contributions of selected environmental causal factors. Computations are based on established theory and extensive analysis of representative sea states. The project was scheduled to move to 6.4 level in FY20, but funding was not approved until May 2020, so work was suspended for the first 7 months of the fiscal year. Objectives for the remaining 5-month period included: (1) completing a 20-year WW3 reanalysis with wave-current interaction enabled and (2) implementing the rogue-threat utility in WW3 and initiating system calibration.

Methodology: For objective (1), the WW3 reanalysis was conducted by J. Dykes during the period 2000 – 2019 inclusive, initiated with a 15-day spin-up from 15 Dec 1999. The simulations used the 3-grid IRI setup, with GOFS 3.1 surface currents and CFSR winds. Wave-current interactions were determined to have a non-negligible effect on reanalysis output (Fig. 1) and were activated in the model for the full 20-year computation. This necessitated a small-but-tolerable increase (~ 9%) in overall computation time. To reduce the required storage space, we extracted and saved only selected WW3 spectra at and near 34 buoy locations that were included in a separate rogue event database (total of 145 spectra per time step). By not storing all spectra, the overall model storage requirement was reduced by approximately 70% (from ~130TB down to ~40TB). For objective (2), model-generated wave spectra, current fields, and wind fields were used with the event database to test system functionality, to examine correlations of RTI values with identified rogue wave events, and to begin calibration of the estimator. In the calibration, we are investigating the effects of adjusting causal factor weights on optimizing the RTI computation; a 5-year section of WW3 data was used for initial testing. The quantitative calibration goal is for the mean RTI for rogue events (“P”) to exceed the mean for non-events (“N”) by the sum of the standard deviations (i.e., $RTI_{\bar{P}} - \sigma_{RTI,P} > RTI_{\bar{N}} + \sigma_{RTI,N}$).

Results: (1) The 20-year WW3 reanalysis was nearly completed by the end of FY20. The products are stored in netCDF files processed to cover 80S to 89.75N at all longitudes. They include most standard bulk parameters (e.g., wave height/period/direction/etc.), gridded wind and surface current data, and complete wave spectra at selected locations. When reviewing the output data, a small number of localized errors and omissions were identified. In early FY21, the entire dataset will be examined to identify and repair any remaining faulty data sections, and a comprehensive quality control effort will be completed. As we have determined that the required input data (ice, currents and wind) are available, the dataset will be expanded to start at 1994. (2) The rogue-threat system has now been fully integrated into WW3. Initial calibration results without any adjustments to causal factor weighting are promising, indicating that mean values of RTI and all individual causal factors are larger for 1530 identified rogue wave events than for a (495,374 value) non-rogue comparison dataset (Fig. 2). The largest difference between rogue event (“P”) and non-rogue (“N”) means for causal factors is +10% for the BFI.

DoD Impact/Significance: Accurate prediction of environmental hazards is important to tactical and strategic operations in the world’s oceans. The results obtained from these simulations will form the core of the configurable WAVEWATCH III rogue threat utility, which will enhance the safety of Navy missions and reduce the potential for damage or loss of Navy assets in rogue wave events.

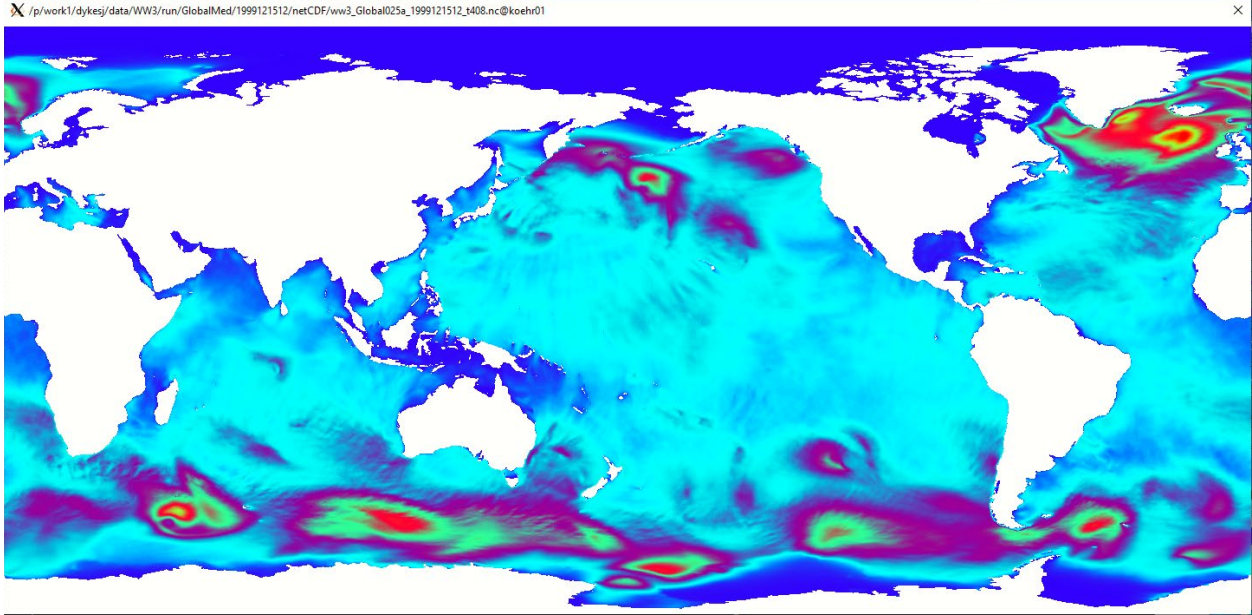


Figure 1. Sample WW3 hindcast of significant wave height for global grid on 15 Dec 1999, with wave-current interactions activated. Colors show wave heights in meters, ranging from near zero (blue) to ~10m (red). Effects of currents on waves are visible as striating oscillations of wave heights, which are not seen in model output without these interactions.

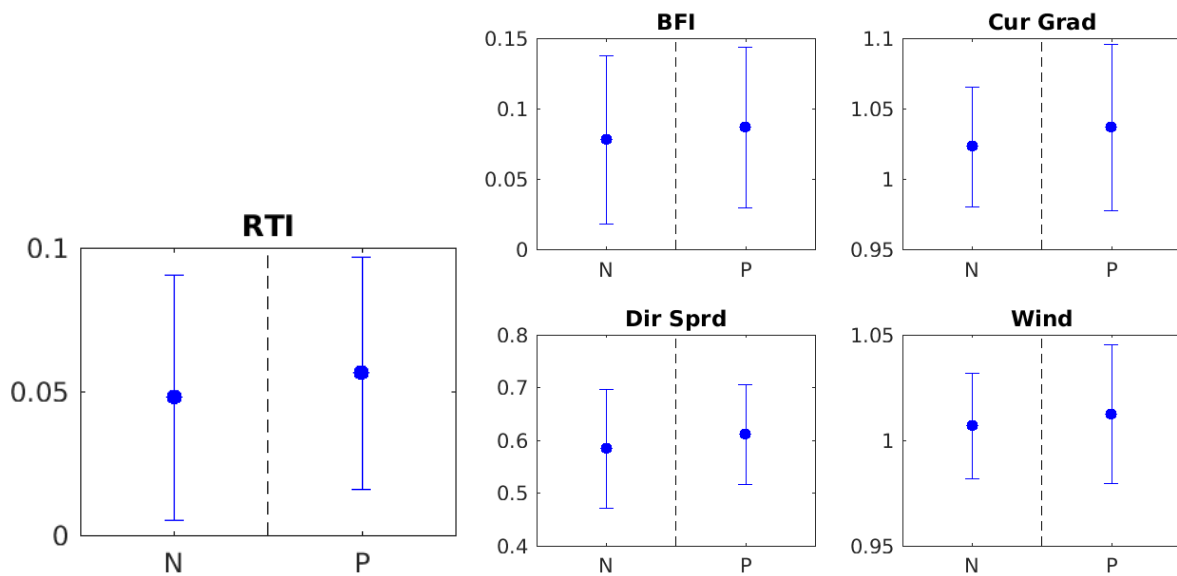


Figure 2. Results of preliminary calibration of rogue threat index (RTI) for 2000 – 2004, comparing rogue event dataset (“P” = positive events) versus much larger non-rogue control dataset (“N” = negative non-rogue cases) for RTI and each causal factor (BFI, current gradients, directional spread, and wind forcing). Here, $RTI = C_{BFI} \cdot C_{cur} \cdot C_{dir} \cdot C_{wind}$, with all causal factor exponential weights set to one. Blue dots show mean value and error bars show standard deviation over the 5-year dataset. (NB: RTI plot shows unnormalized, raw values. Index ultimately will be normalized to run from 0 to 10.)

Title: Probabilistic Prediction to Support Ocean Modeling Projects

Author(s): C.D. Rowley¹, L.F. Smedstad¹, C.N. Barron¹, R.S. Linzell², P.L. Spence², T.L. Townsend¹, M. Yaremchuk¹, J.C. May¹, T.A. Smith¹, J.J. Osborne¹, G.G. Panteleev¹, B.P. Bartels², C.J. DeHaan², B.R. Maloy¹, and Z.W. Lamb³

Affiliation(s): ¹Naval Research Laboratory, Stennis Space Center, MS; ²Perspecta, Stennis Space Center, MS; ³General Dynamics Information Technology, Falls Church, VA

CTA: CWO

Computer Resources: HPE SGI 8600, Cray XC40 [NAVY, MS]; Cray XC40/50 [ERDC, MS]

Research Objectives: Develop ocean and coupled ensemble data assimilation (DA) and probabilistic prediction capabilities using the Coupled Ocean Atmosphere Mesoscale Prediction System (COAMPS^{®1}), the Navy Coastal Ocean Model (NCOM), and the Hybrid Coordinate Ocean Model (HYCOM). Extend ocean data assimilation capabilities and implement new sources of ocean and ocean surface observations.

Methodology: NRL Coupled Ocean Data Assimilation (NCODA) system development was continued in order to support Fleet Numerical Meteorology and Oceanography Center (FNMOC) operational modeling and testing of ice specific improvements to NCODA. Testing of the Global Heterogeneous Observation Systems (GHOST) system was introduced to HYCOM ensemble file cutouts for longer simulations. System improvements allowed for easier visualization of simulated instrument location with respect to interesting features (Fig. 1).

Results: We completed development of NCODA versions pre QC v3.1, NCODA QC v4.2, and NCODA VAR v4.2, and delivered the new codes to FNMOC and to the COAMPS project for validation testing; updated older NCODA VAR versions v3.9 and v4.1 to support current operational forecast systems with new data types; implemented a netCDF output format for the NCODA QC output and tested it with NCODA VAR; developed a quadtree-based observation clustering technique to work in the analysis gridspace to generate superobservations without artifacts on polar cap grids; and developed a multiscale analysis capability in NCODA VAR. To test bias corrections in extended-range deterministic and coupled-ensemble ocean forecasts using surface flux parameter fields from the Ocean Surface Fluxes (NFLUX) project, we developed new Python code to generate time-dependent bias-correction input files for processing during the forecast on the Global Ocean Forecast System (GOFS) tri-pole grid and output them in HYCOM A/B files to assist with completing a 3-month retrospective analysis/forecast cycle to evaluate the NFLUX-modified NAVGEM forcing.

DoD Impact/Significance: Development of extended-range forecasts depends on coupled ensemble forecasting due to the limitations of deterministic predictability and coupled DA to improve initial conditions. High resolutions and large ensembles are needed to ensure forecast reliability and accurate risk assessment in antisubmarine warfare, nuclear-chemical-biological hazard prediction and monitoring, and search and rescue. Operational systems are being embedded with new data types from autonomous systems, and controlling larger amounts of autonomous systems requires more complex algorithms and interface from outside of the DSRC environment which has led to complicated system development.

¹ COAMPS[®] is a registered trademark of the Naval Research Laboratory.

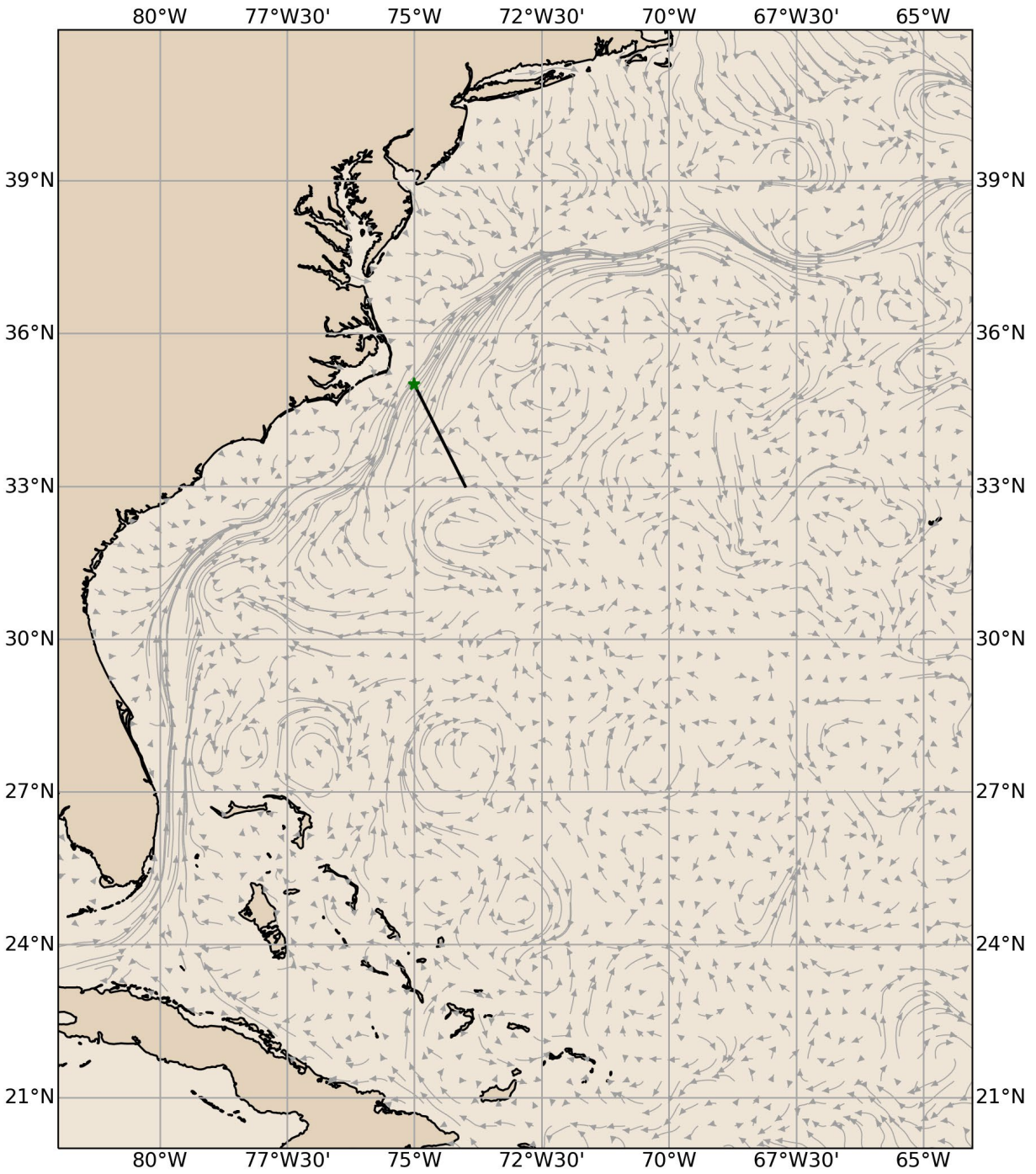


Figure 1. Improved plotting routines allowed for faster visualization of measurements vs features.

Title: Guidance for Heterogeneous Observation Systems (GHOST)

Author(s): L.F. Smedstad¹, C.N. Barron¹, P.L. Spence², and C.D. Rowley¹

Affiliation(s): ¹Naval Research Laboratory, Stennis Space Center, MS; ²Perspecta, Stennis Space Center, MS

CTA: CWO

Computer Resources: Cray XC40/50 [ERDC, MS]

Research Objectives: We intend to extend and verify observation assimilation capabilities of ocean numerical models to ensure accurate use of new types/platforms of ocean and air/ocean surface observations. Researching the optimal balance of available data gives the background needed to improve battlespace environment forecasts.

Methodology: An assimilative regional Navy Coastal Ocean Model of the northern Atlantic Ocean was initiated and run on the Army Engineer Research and Development Center supercomputer Onyx. The simulation had 2 km horizontal resolution with 100 vertical levels ranging from 0.5 meters near the surface to 357 meters at depth. The model was run in hindcast for year 2018 as a prequel to an existing analogous North Atlantic simulation run in real time during 2019. These combined simulations provided continuous model forecasts to sample over a two-year reanalysis period. Testing and analyses were included in the follow-on to the validation test report in support of transition to operations.

Results: High vertical resolution provided improved model forecasts for guidance of observation systems, Fig. 1. During the analysis of the results, we identified shortcomings in the forecast system and applied that to improving our data assimilation and forecasts. When we identified these shortcomings, focus was shifted to resolving issues and the long-term runs were discontinued.

DoD Impact/Significance: Ocean forecasts are critically reliant on regular corrections of initial conditions on a daily basis via use of environmental observations. We must optimize the parameters controlling the influence scales of observations to produce accurate forecasts. This influences the accuracy of battlespace environment forecasts for the operational Navy operations. These include anti-submarine warfare (ASW) operations where sound speed is critical, currents that affect naval special warfare (NSW) and mine warfare (MIW). Search-and-rescue (SAR) operations also are dependent on accurate ocean forecasts. HPC resources support research-and-development efforts on data assimilation and forecasting.

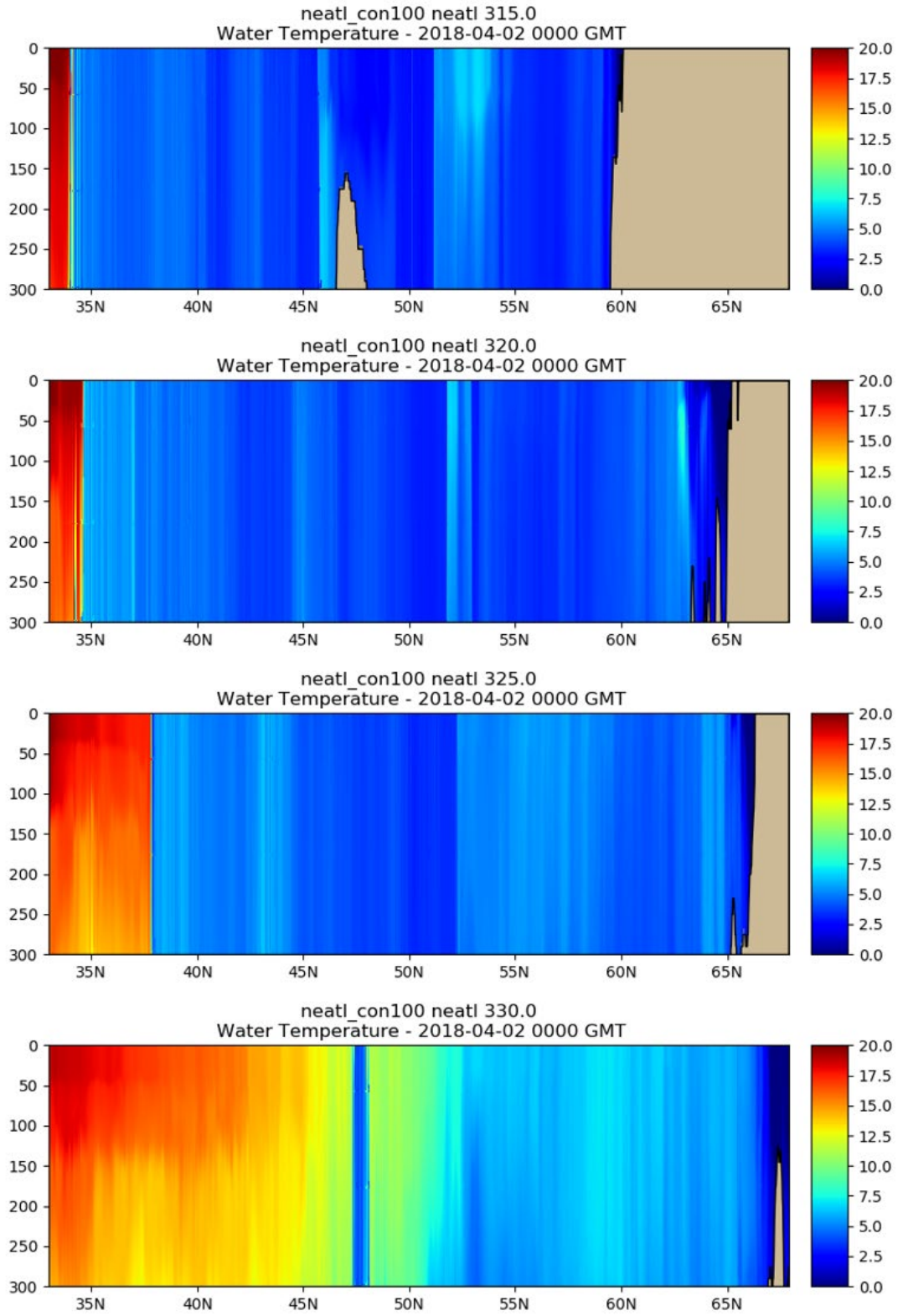


Figure 1. Temperature transects on 02 April 2018 in the upper 300 meters of the ocean.

Title: Dynamics of Coupled Models

Author(s): I. Shulman, B. Penta, S. Cayula, and C.D. Rowley

Affiliation(s): Naval Research Laboratory, Stennis Space Center, MS

CTA: CWO

Computer Resources: HPE SGI 8600, Cray XC40 [NAVY, MS]

Research Objective: Improve our understanding of coupled bio-optical and physical processes in the coastal zone and the variability and predictability of the coastal ocean's optical properties on time scales of 1 – 5 days. Investigate the coupled dynamics of ocean bio-optical, physical and atmospheric models. Provide a foundation for the development of scientifically valid, dynamically coupled atmosphere-ocean models.

Methodology: The approach is based on using nested, coupled physical-bio-optical models of the coastal region together with bio-optical and physical in-situ and remotely sensed observations. Data assimilation techniques for both physical and bio-optical fields are being used to examine project research issues and objectives. Approach is also based on joint studies of the bioluminescence (BL) potential and inherent optical properties (IOPs) over relevant time and space scales. Dynamical, biochemical, physical and BL potential models are combined into a methodology for estimating BL potential and nighttime water leaving radiance (BL_w).

Results: We published a refereed paper “Bioluminescence potential dynamics during Polar Night in Arctic” in the journal *Ocean Dynamics*, Springer. BL potential observations demonstrated significantly higher BL potential emissions in top 50 m in the northern Arctic fjord (Svalbard, Norway) in comparison to offshore stations during the polar night of January 2012. To address questions as to why the values of BL potential in the northern Svalbard fjord are higher than at offshore stations, and what the role of advection, we utilized the ensemble approach when changes in BL potential are modeled with the advection-diffusion-source (ADS) model. Results of our modeling demonstrated that the advection and mixing of BL potential from offshore areas are dominant factors in increases of BL potential in the fjord area in top 50 m in comparison to offshore areas. Figure 1 shows the distributions of adjoint along a section crossing the area of interest. The adjoint tracer distributions show where the model tracer-tagged water masses were in the past (2, 4 and 10 days on Fig. 1) before circulating into the area of interest. It shows that water masses from offshore areas and along the shelf and slope area circulated to the area of interest over 10 days. The interpretation of our results is that during the polar night, the fjord represents an area where bioluminescent organisms from offshore areas aggregate through advection and mixing.

DoD Impact/Significance: Emerging Navy electro-optical (EO) systems under development and special operations missions require an improved understanding of the ocean optical environment. This is critical for operations and weapon deployment, especially in the coastal and littoral zones. Improved basin scale-to-mesoscale forecast skill is critical to both military and civilian use of the oceans, particularly on the continental margins.

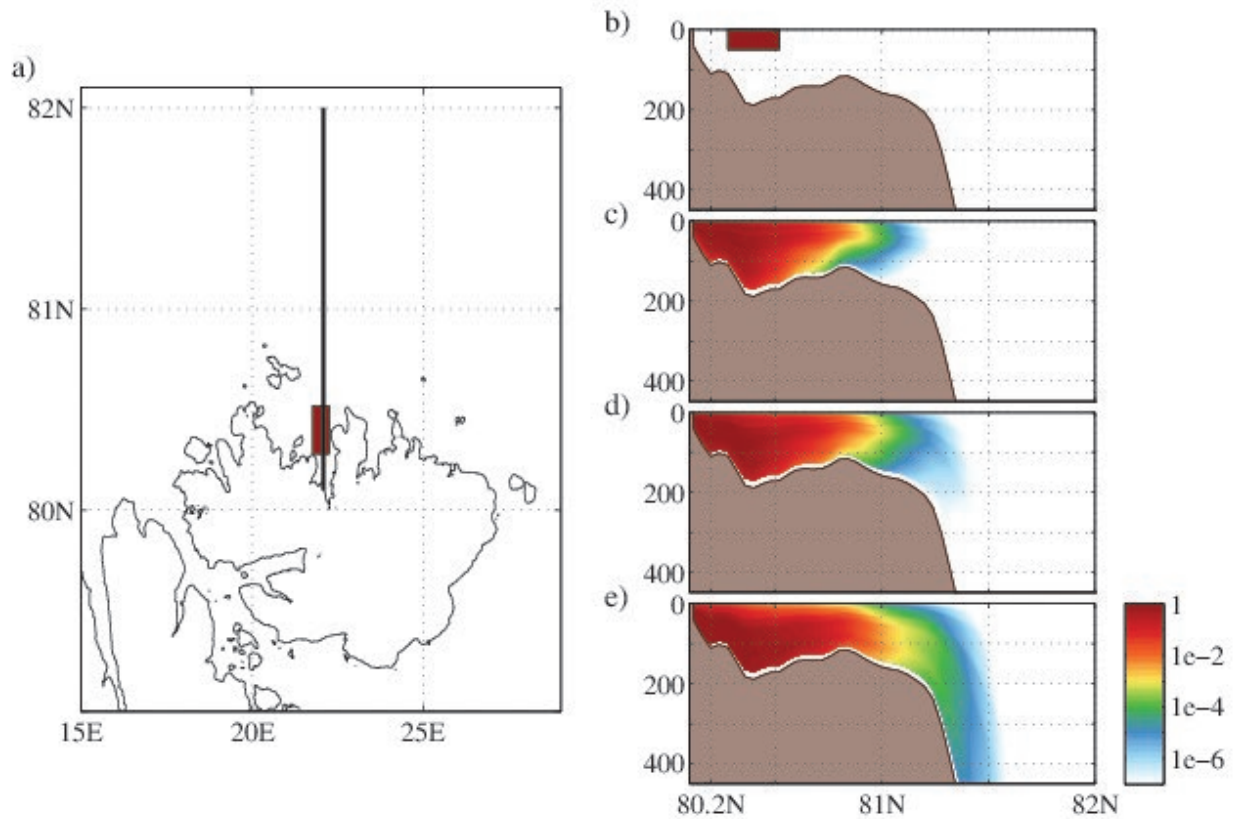


Figure 1. Distributions of the adjoint along the section crossing the area of interest. Image (a) shows the area around Svalbard, red box indicating the area of interest and section crossing the box of interest; (b) the initial distribution of adjoint along the section shown on (a); (c) the distribution of adjoint along the section shown on (a) after 2 days of integration; (d) the same as (c) but after 4 days of integration; (e) the same as (c) but after 10 days of integration.

Title: Variational Data Assimilation

Author(s): S. Smith¹, L.F. Smedstad¹, C.N. Barron¹, B.P. Bartels², M. Carrier¹, J. Crout³, J. D'Addezio¹, C.J. DeHaan², S. deRada¹, R. Helber¹, Z.W. Lamb², R.S. Linzell², B.R. Maloy¹, J.C. May¹, H. Ngodock¹, J.J. Osborne¹, G.G. Panteleev¹, I. Pasmans⁴, M. Phelps², C.D. Rowley¹, T.A. Smith¹, I. Souopgui⁴, P.L. Spence², T.L. Townsend¹, and K. Weber¹

Affiliation(s): ¹Naval Research Laboratory, Stennis Space Center, MS; ² QinetiQ North America, Stennis Space Center, MS; ³American Society for Engineering Education, Stennis Space Center, MS; ⁴ University of New Orleans, Stennis Space Center, MS

CTA: CWO

Computer Resources: HPE SGI 8600, Cray XC40 [NAVY, MS]; Cray XC40/50 [ERDC, MS]

Research Objectives: The scope of this project is to advance the analysis and prediction capability of the Navy's environmental modeling and forecasting systems through the improvement of the Navy Coupled Ocean Data Assimilation (NCODA) software. There were 10 funded NRL projects that focused on either adding or improving capabilities of NCODA in FY20, and the experiments performed under this HPC project went towards satisfying these efforts. A few of these efforts include: 1) further validating the 4DVAR for transition, 2) developing and testing a multiscale capability to better resolve small-scale features, and 3) implementing and testing the capability to assimilate velocity and acoustic observations.

Methodology: This HPC project helped advance the NCODA system in FY20 through the following 10 funded NRL projects: (1) The 6.2 SPREE project tested the 4DVAR assimilation of real acoustic observations with the Range Acoustic Model (RAM). (2) The 6.2 LATTE project tested the coupled ocean-acoustic 4DVAR assimilation system. (3) The 6.2 Smart Glider Teams for Rapid Update of Local Analysis project tested the multiscale 4DVAR for accurately assimilating coordinated teams of gliders. (4) The 6.4 ISOP project performed numerous velocity assimilation tests on the DSRC using both 3DVAR and 4DVAR within COAMPS. (5) The 6.4 Advanced Research Challenge for Velocity assimilation examined the impact of assimilating velocities from various sources including Lagrangian drifter tracks. (6) The 6.4 4DVAR project performed a set of validation experiments in the northern Atlantic Ocean. (7) The NCODA-NEXT project updated and standardized the NCODA software; much of the development and testing of NCODA took place on the DSRC. (8) The 6.4 Ocean Confidence project provided information on ocean forecast uncertainty. This uncertainty algorithm was tested on the DSRC for very-high-resolution, regional simulations. (9) The 6.4 NCODA_Forward project developed and tested a simplified version of NCODA 3DVAR that can be used on a forward-deployed asset, assimilating observations that are collected locally. (10) The Ocean of Things project provided predictions in near-real time using COAMPS with 3DVAR and 4DVAR. These experiments were run on the DSRC for the Californian Coast and the Gulf of Mexico domains.

Results: Numerous 3DVAR and 4DVAR experiments were performed using NCODA under this FY20 HPC project with the overall result of improving the analysis accuracy, prediction skill, portability and robustness of the system. A few of the specific advancements made include: assimilating at very high resolution, coupling assimilation systems, multiscale, and assimilating velocities, acoustics, and SWOT.

DoD Impact/Significance: The assimilation experiments tested under this project went toward improving the Navy's capability of forecasting the ocean environment. Various validation studies for the 4DVAR were performed and showed more accurate analyses and model forecast fields than its predecessor, 3DVAR. Additionally, the work on coupling the assimilation systems for the ocean, atmosphere, and acoustic models made significant progress this fiscal year and these coupled systems ultimately will improve further the forecast skill of all three environments.

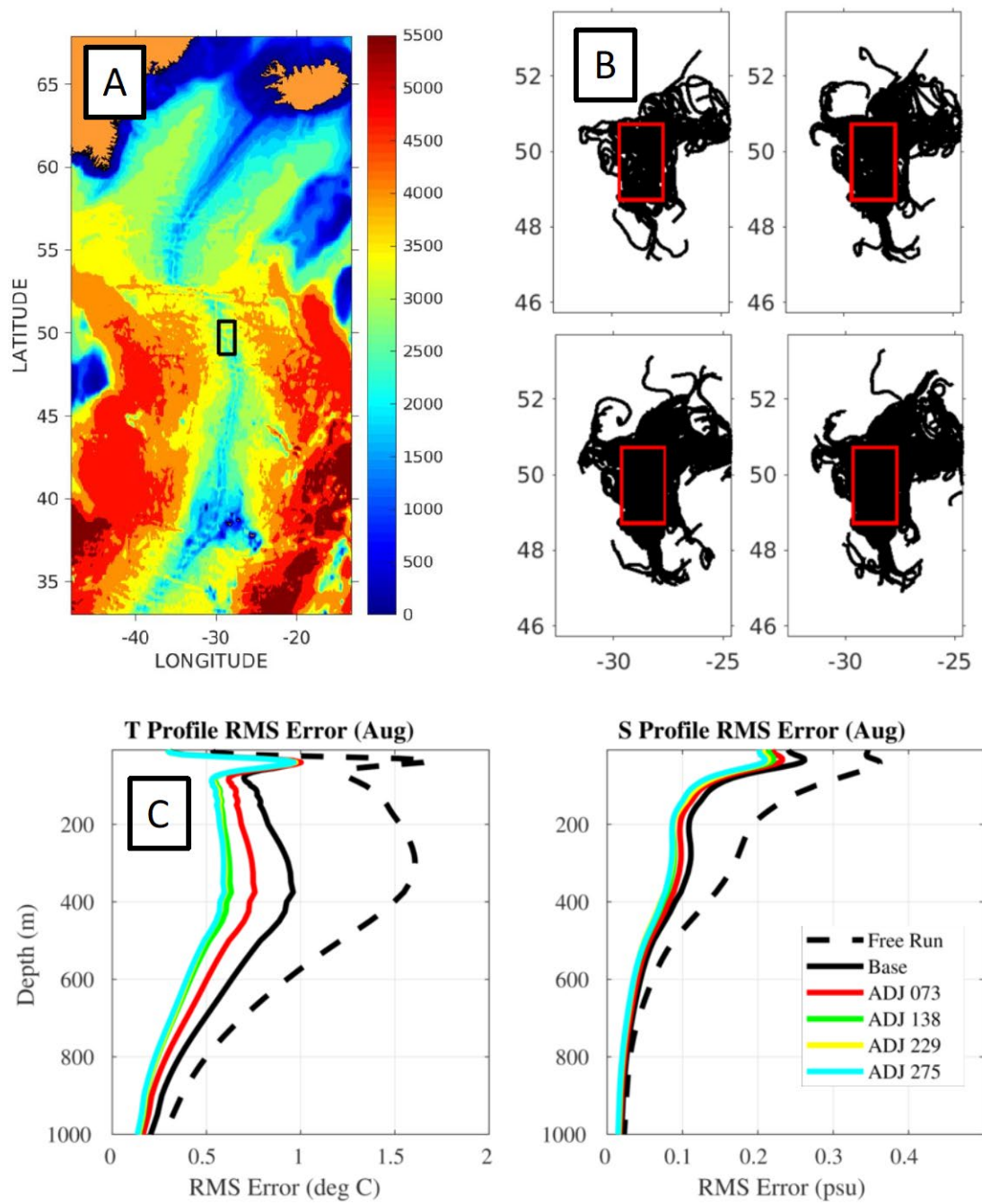


Figure 1. A suite of OSSE experiments were performed in the northern Atlantic Ocean (panel A) to analyze the impact of assimilating simulated float data seeded using an adjoint sensitivity method. Panel (B) shows the simulated float trajectories for four different deployments using 73 (upper left), 138 (upper right), 229 (lower left), and 275 (lower right) floats. The red square in panel B corresponds with the black square in panel A, and this is the region where the analysis in panel C is performed. Panel (C) shows the average temperature (left) and salinity (right) profile RMSE (as compared to the nature run) between the free run (dashed line), the base run (solid, black line), and each of the float deployments (color lines) for August 2019.

THIS PAGE INTENTIONALLY LEFT BLANK



Signal Image Processing

SIP covers the extraction of useful information from sensor outputs in real time. DoD applications include surveillance, reconnaissance, intelligence, communications, avionics, smart munitions, and electronic warfare. Sensor types include sonar, radar, visible and infrared images, and signal intelligence (SIGINT) and navigation assets. Typical signal-processing functions include detecting, tracking, classifying, and recognizing targets in the midst of noise and jamming. Image-processing functions include the generation of high-resolution, low-noise imagery and the compression of imagery for communications and storage. The CTA emphasizes research, evaluation, and test of the latest signal-processing concepts directed toward these embedded systems. Usually, such processors are aboard deployable military systems and hence require hefty packaging and minimum size, weight, and power. System affordability is expected to improve by an order of magnitude through the development of scalable codes running on flexible HPC systems. This will enable the traditional expensive military-unique 'black boxes' required to implement high-speed signal/image processing to be replaced by COTS HPC-based equipment.

Title: Reducing the Burden of Massive Training Data for Deep Learning
Author(s): L.N. Smith, E.A. Gilmour, S.N. Blisard, and K.M. Sullivan
Affiliations(s): Naval Research Laboratory, Washington, DC
CTA: SIP

Computer Resources: Power9 [ARL, MD]

Research Objectives: The successes of deep learning in the past several years rely on three pillars: faster computer hardware, lots of labeled training data, and new algorithms. In this basic research project, we design, develop, and evaluate novel deep-learning algorithms for training deep neural networks that significantly reduce the training time and eliminate the current requirement for massive labeled training datasets in order to allow application of deep networks in situations in which labeled data is scarce or expensive.

Methodology: Our methodology is based primarily on the following scientific process: Based on our understanding, we develop hypotheses, which often requires experimenting with many variations of neural networks and hyperparameters to determine which of those hypotheses are beneficial and when they are beneficial, and to develop a new understanding as to why they work. The majority of the work done was in the most popular deep-learning frameworks — TensorFlow, Torch, and PyTorch. Hence, it is valuable that the HPC staff installs and maintains these frameworks. Typically, our experiments build on previous work, so the first step is to download code from github.com, then to replicate previous results, and then to test our own hypotheses.

Results: In FY20, the majority of the work on this project attempted to combine our primary objective of reducing the amount of labeled data needed to train a neural network with other high-priority goals. In one effort, we demonstrated for the first time ever the potential for boosting one-shot semi-supervised (BOSS) learning to attain test accuracies that are comparable to fully supervised learning. Our method combines novel methods such as class prototype refining and class balancing with the known method of self-training. In another effort, we combined consistency regularization and contrastive representation learning, as shown in Fig. 1. In addition, a novel bootstrapping method speeds up semi-supervised learning and boosts the performance. These efforts break through the barrier of time and effort required to manually label large numbers of training samples.

DoD Impact/Significance: It is widely accepted that large labeled datasets are an essential component of training deep neural networks, either directly for training or indirectly via transfer learning. To the best of our knowledge, we are the first to demonstrate performance comparable to fully supervised learning with semi-supervised learning with only one labeled sample per class. Eliminating the burden of labeling massive amounts of training data creates great potential for new neural network applications that attain high performance, which is especially important when labeling requires expertise.

Our work on boosting one-shot and few-shot semi-supervised learning means new military applications can utilize the powerful tools of machine learning without the burden of labeling. These methods also can be leveraged to solve other challenges, such as making these methods adaptable by allowing continuous learning in changing battlespaces. In addition, the understanding gained by the experiments on the HPC GPU servers builds on all the previous understandings gained from previous experiments, and this understanding is crucial for our future progress in the field.

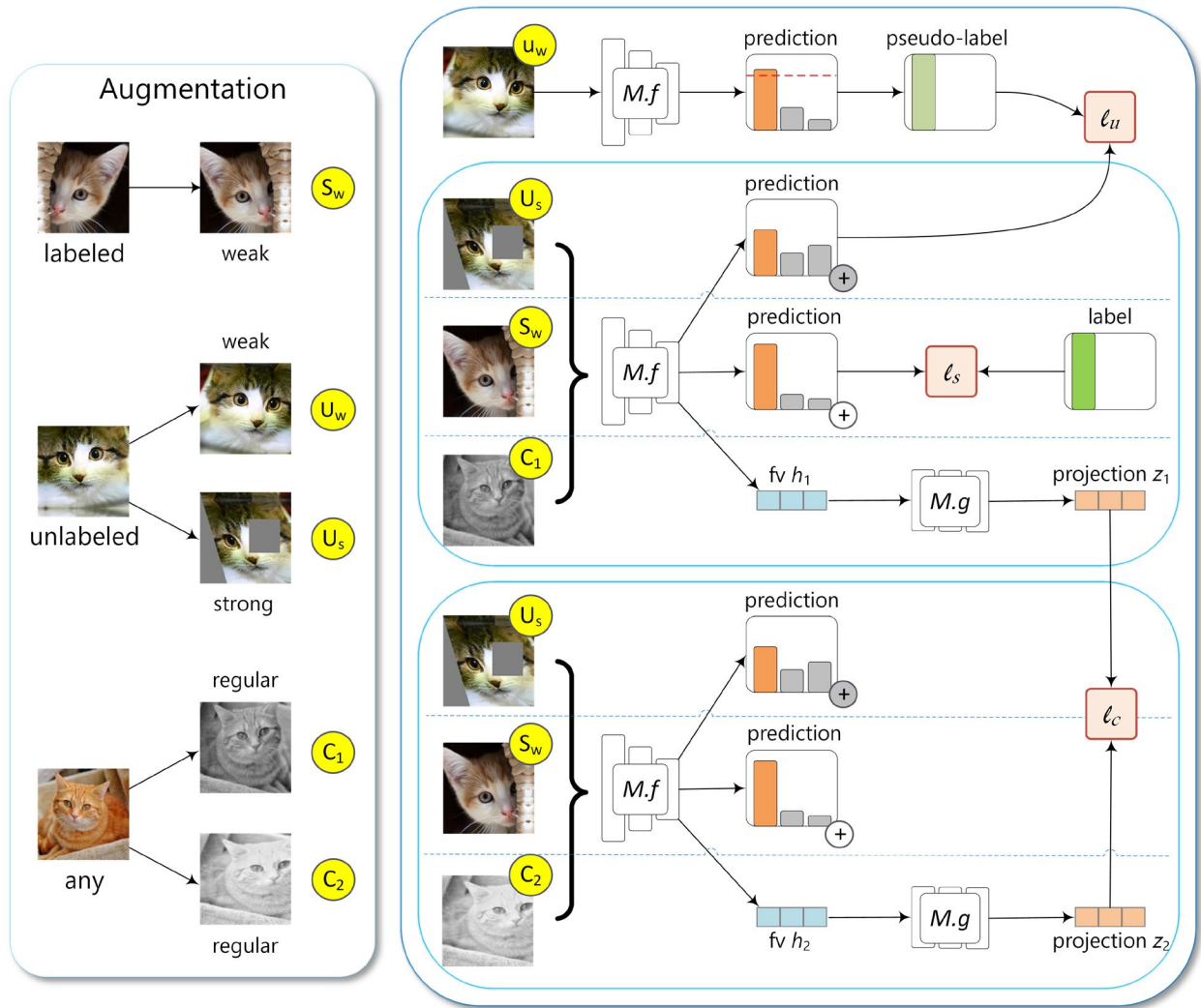


Figure 1. Diagram of the methodology that combines consistency regularization and contrastive representation learning for semi-supervised learning.

THIS PAGE INTENTIONALLY LEFT BLANK



Space and Astrophysical Science

Space and Astrophysical Sciences (SAS) research and development advances understanding, specification and prediction of the Earth's atmospheric and space domains to exploit the extended operational environment for military advantage and to minimize environmental impacts on military operations. The SAS CTA embodies the use of mathematics, computational science, and engineering in the analysis, design, identification, modeling, and simulation of the space and near-space environment, and of all objects therein, whether artificial or natural. The SAS CTA encompasses foundational discovery research to study the atmospheres of the sun and the Earth, including solar activity and its effects on the Earth's atmosphere, ionosphere, and near-Earth space, and the unique physics and properties of celestial sources. SAS employs an extensive array of physical and empirical models and analysis tools to integrate observations and theoretical understanding for ever-improving DoD enterprises within, and exploitation of, the extended operational environment. The CTA melds the strengths of a broad range of physical sciences — atomic and molecular physics, materials science, plasma physics, applied optics, radiation survivability, electronic warfare, directed-energy technology, astronautics and space propulsion, orbital mechanics, space situational awareness, and remote sensing — into a structure that helps the DoD multiply force combat effectiveness.

Title: Electromagnetic Pulses from Hypervelocity Impacts on Spacecraft

Author(s): A. Fletcher

Affiliation(s): Naval Research Laboratory, Washington, DC

CTA: SAS

Computer Resources: SGI ICE X [ARL, MD]

Research Objectives: The objective of this project is to use large-scale simulations to understand electromagnetic pulses (EMPs) and other electrical effects that are associated with hypervelocity impacts (HVIs) on spacecraft and to develop mitigation strategies.

Methodology: The problem can be split into two regimes (impact and EMP) for which we will run separate codes. ALEGRA, a hydrocode from Sandia National Laboratories, is used to simulate the impact and plasma generation. JABBERWOCK, a particle-in-cell code from Naval Research Laboratory, is used to simulate the plasma expansion and generation of the EMP. We run a series of simulations to verify the predictive capability of the simulation pipeline by validating against ground-based Van de Graaff impact experiments. We then run a series of simulations in order to build a model that describes the EMP properties as a function of impact parameters.

Results: This year, we continued exploring cases of hypervelocity impacts using the hydrocode ALEGRA. There were three primary results. First, in addition to examining the plasma plume that expands from the impact site, we also characterized the strong shock wave in the target material. Using simulations, we developed a concept for determining impact parameters by measuring this shock wave using acoustic sensors. The objective is to determine impactor location, mass, and velocity using a set of acoustic sensors in a target. ALEGRA provided the strength and propagation dynamics of these shock waves for normal impacts. In the future, we also will use these ALEGRA simulations to see if we can determine impactor composition from a subset of possible impactors. Second, we extended the velocity regime up to ~ 250 km/s; previously, we only simulated impacts up to 72 km/s. This higher-velocity range allowed us to simulate impacts on the Parker Solar Probe mission. We will compare these simulations to the thousands of measured impacts that mission has seen in the past couple of years. Third, we began an analysis of the dust content in the plasma plume. Experiments suggest dust grains can affect dynamics of the plasma plume. We also see evidence of charged dust altering the magnetic field near the impact site in the ALEGRA simulations.

DoD Impact/Significance: Protection of critical DoD space assets from this threat is necessary to ensure uninterrupted C4ISR capability, which is critical for operational success as envisioned in the Navy's S&T strategic plan for information dominance. Countermeasures against hypervelocity impacts of microprojectiles on DoD space assets depend on the knowledge of the electromagnetic power and frequency spectrum of the impact-associated EMPs.

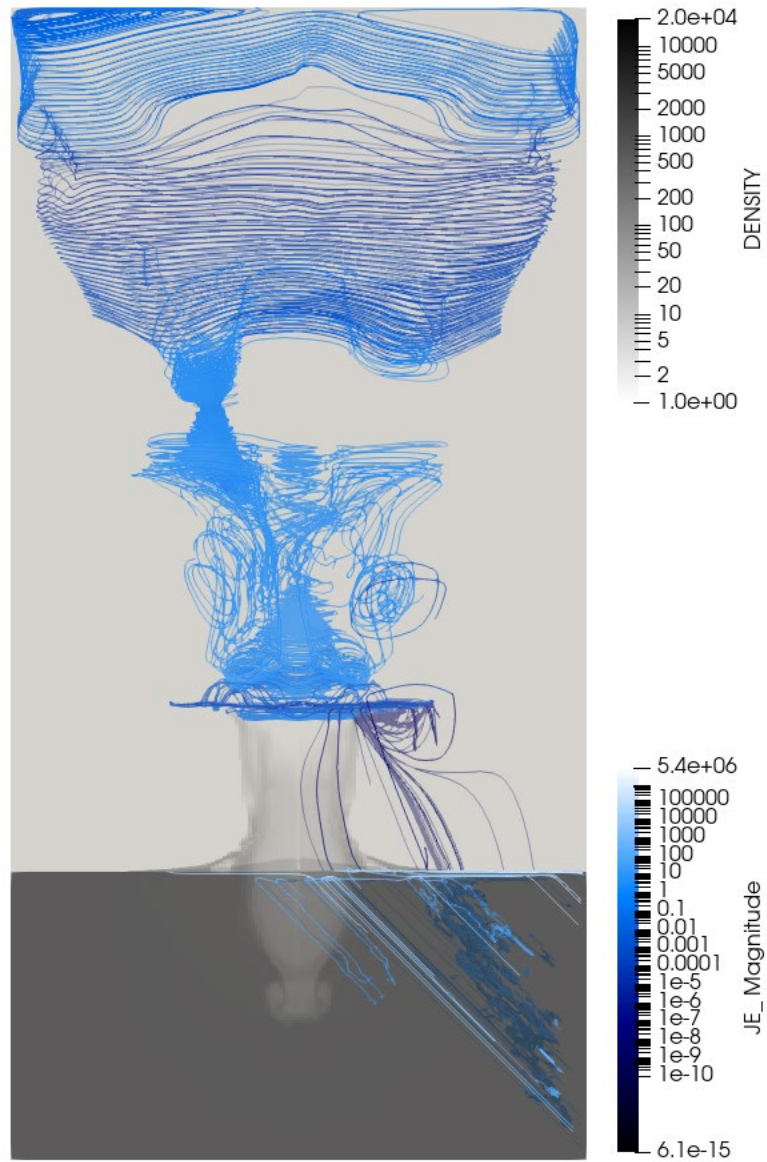


Figure 1. Density and current density in a 3D ALEGRA simulation of a hypervelocity impact. The target is the lower, dark-gray region. A crater is beginning to form, and a plume is expanding upward. The blue lines show the current density. A 3D simulation is necessary to accurately incorporate an ambient magnetic field. The current in this case is running in a circular direction around the plume as it expands.

Title: Global Kinetic Simulations of Space Plasma Waves and Turbulence

Author(s): A. Fletcher

Affiliation(s): Naval Research Laboratory, Washington, DC

CTA: SAS

Computer Resources: SGI ICE X [ARL, MD]

Research Objectives: The objectives of this project are 1) to support an NRL and DARPA sounding rocket experiment program, SMART (space measurement of a rocket-released turbulence, launching in fall 2021), by helping to choose mission parameters and understanding the data from the experiment, and 2) to develop the capability to simulate near-Earth space plasmas on a global scale while including kinetic effects.

Methodology: We will use a combination of two codes. The first is JABBERWOCK, a particle-in-cell (PIC) and direct simulation Monte Carlo (DSMC) code, and the second is WICKED, a wave-in-cell (WIC) code. Both have been developed at NRL and both simulate kinetic plasma phenomena. We will determine the density and optical/radar signature of the barium cloud, the amplitude and spectrum of the electrostatic and electromagnetic waves, and the rate of particle precipitation from the radiation belts. WIC, which could simulate the entire process, will need validation via comparable PIC runs. WIC then will be used to simulate as much of the cascade as possible within one simulation.

Results: Numerous simulation results have been used to help design the SMART experiment, including choosing the altitude, the instruments on the payload, and the optimal launch conditions. We expanded the direct simulation Monte Carlo (DSMC) simulations to include the chemistry of the neutral and ionized barium, including interaction with the background neutral atmosphere and with excited states that emit measurable optical signatures. We characterized the delay in ionization due to metastable states in neutral barium and predicted the density and distribution function measurements from the payload in the SMART experiment. The line emission amplitude was predicted for 15 separate lines and was transmitted through the atmosphere to predict the optical measurements we expect on the ground. Inclusion of neutral collisions allowed us to choose the optimal altitude for rocket apogee. The DSMC+PIC simulations were instrumental in many experimental design decisions for SMART.

Hydrocode simulations of the barium release were performed in order to quantify the amount of barium that would be vaporized and accelerated to above ~ 5 km/s in the experiment. Other modeling efforts could not include the vaporization of barium, which is an uncommon material that is not well characterized in most production codes. We developed a method for vaporization of barium and predicted a total vaporized mass of ~ 1.25 kg of barium gas with a speed greater than 6 km/s. This showed that the design met the experimental requirements, and that sufficient energy would be contained in the barium jet in order to produce plasma waves, including whistlers, in SMART.

DoD Impact/Significance: The SMART experiment and associated simulations will study turbulence in the ionosphere coupling to waves in the magnetosphere. Given the DoD/Navy reliance on spaceborne assets, understanding the space environment is critical to ensure uninterrupted C4ISR capability and maintain information dominance.

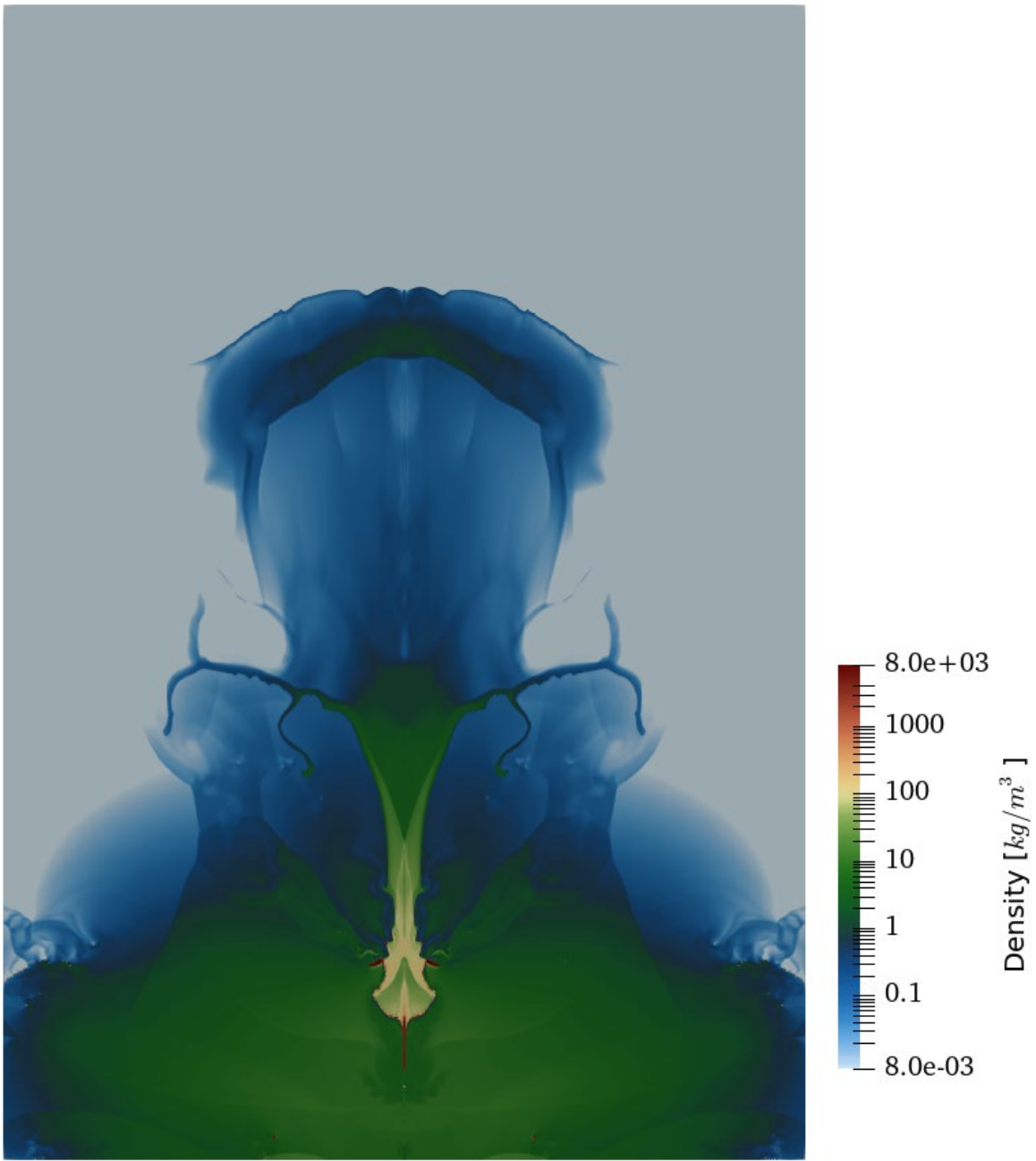


Figure 1. Formation of barium jet (moving upward) tens of microseconds after release the flight configuration. The color is the mass density in a log scale.

Title: Modeling Propagation of Ionospheric Disturbances Initiated by Magnetospheric Substorms

Author(s): J. Haiducek¹ and J. Helmboldt²

Affiliation(s): ¹National Research Council Postdoctoral Fellow, Naval Research Laboratory, Washington, DC; ²Naval Research Laboratory, Washington, DC

CTA: SAS

Computer Resources: HPE SGI 8600 [AFRL, OH], [NAVY, MS]; Cray XC40 [NAVY, MS]

Research Objectives: A traveling ionospheric disturbance (TID) consists of a wavelike density perturbation that moves through the ionosphere. Our primary objective is to improve understanding of TIDs, their spatial structure, and the physical processes that drive them. Our main focus will be on TIDs that are observed by the Very Large Array (VLA) Low-Band Ionosphere and Transient Experiment (VLITE), an observational capability developed jointly by the Naval Research Laboratory and the National Radio Astronomy Observatory. VLITE provides the capability to measure total electron content (TEC) in the ionosphere. Our computational efforts aim to model TIDs observed by VLITE in order to better understand how the area observed by VLITE interacts with the surrounding environment. A secondary objective is to better understand the production of TIDs by magnetospheric substorms, which are explosive releases of energy from the night-side magnetosphere. We aim to better understand these processes by using a combination of VLITE observations and numerical simulations.

Methodology: We are modeling TID propagation using the SAMI3 (SAMI is Another Model of the Ionosphere 3D) simulation code. SAMI3 is an MPI-parallel code. In order to better simulate the ionospheric density perturbations associated with TIDs, we are developing a data assimilation system that uses TEC observations collected by VLITE and GPS receivers to update the SAMI3 simulation state. The data assimilation will be performed using an ensemble Kalman filter to update an ensemble of SAMI3 simulations. We are developing an MPI-parallel implementation of the ensemble Kalman filter to accomplish this. SAMI3 will be used to simulate TID events that are observed by VLITE, with a focus on TIDs that occur following magnetospheric substorms. The SAMI3 output will provide context for the VLITE and GPS observations. By analyzing the output from SAMI3 and the parameters required to reproduce observed TIDs in a computational simulation, we hope to gain insights into the physical processes governing the production and propagation of TIDs.

Results: We have developed a new data assimilation code in Fortran, building on a proof-of-concept implementation in Python. The Python implementation used MPI through the mpi4py module, while the new implementation uses the Fortran MPI interface. At the same time, we implemented new communications patterns, replacing the previous manager-worker pattern with a more efficient scheme that achieves more efficient resource utilization and can accommodate parallel reading and writing of the assimilation input and output. The implementation has a modular interface to accommodate different types of models, observations, and assimilation algorithms. It has been tested by assimilating simulated observations into a 1D advection solver. Work is in progress to integrate this assimilation system with SAMI3 using the Cylc workflow engine to orchestrate assimilation steps. In addition, we published two papers utilizing our substorm identification procedure, which will be used for event selection when the assimilation system is applied to TID scenarios.

DoD Impact/Significance: The density perturbations associated with TIDs can introduce errors in Global Navigation Satellite System (GNSS) positioning solutions, with particular impacts on applications requiring centimeter-level-or-better precision. TID activity also can impact radio communications. The assimilative modeling capabilities developed by this program will lead to predictive capabilities that can be used to provide advance notice of TID-related impacts on navigation and communications.

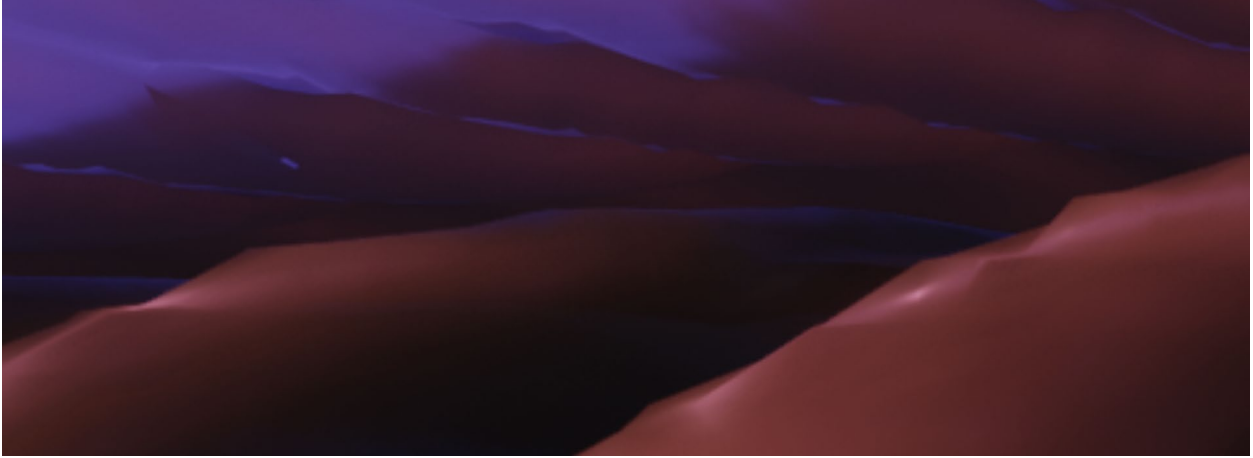


Figure 1. Isosurfaces of electron density in a SAMI3 simulation of a traveling ionospheric disturbance.

Title: Dynamic Phenomena in the Solar Atmosphere
Author(s): K.J. Knizhnik
Affiliation(s): Naval Research Laboratory, Washington, DC
CTA: SAS

Computer Resources: SGI ICE X [AFRL, OH], [ARL, MD]; Cray XC40 [ARL, MD]; Cray XE6m, Cray XC40/50 [ERDC, MS]

Research Objectives: The goal of this HPC program is to investigate the solar drivers of the space weather that disrupts DoD and civilian communications and navigation systems. The program is focused on understanding, and ultimately predicting, the initiation processes of the two key solar drivers: coronal mass ejections (CMEs) and solar flares. The fundamental questions that we are investigating are how the emergence of magnetic fields through the photosphere into the corona drives CMEs and flares, and how the reconnection that releases energy in these events occurs in both coronal and chromospheric conditions.

Methodology: Our work focuses on explorations of the emergence of magnetic fields from the convection zone into the solar corona, with the goal of determining how solar activity is generated. This year, we performed high-resolution three-dimensional (3D) numerical simulations of the buoyant rise and emergence of untwisted toroidal flux ropes through the convection zone and into the corona. Although twist has been assumed to be a key ingredient in the coherent rise and emergence of a cylindrical magnetic flux rope, we investigated whether this was true for toroidal magnetic flux ropes. We compared our 3D simulations with two-dimensional (2D) simulations to compare the behavior of a rising torus to that of a rising cylinder. In parallel, we focused on implementing and testing our new wave-characteristics-based boundary conditions, with the goal of driving the simulated coronal evolution with observed photospheric magnetic and velocity field information. For these studies, we used our magnetohydrodynamics (MHD) code LAREXD for two- and three-dimensional simulations.

Results: We have worked this year to study the rise and emergence of untwisted magnetic flux ropes. We showed, using 2D simulations, that untwisted cylindrical flux ropes get destroyed during their rise by viscous forces. In these simulations, the cross section of an untwisted cylindrical flux rope was allowed to rise in the convection zone. The simulations revealed that this cylindrical flux rope quickly broke up into segments, none of which was able to emerge through the photosphere. We compared this simulation to a fully 3D simulation of a rising untwisted toroidal flux rope. The simulation revealed that the cross section of our 3D untwisted torus remained intact. We hypothesized that this is due to the relatively small segment of the rising flux rope that is experiencing such viscous forces. In addition, we showed that untwisted toroidal flux ropes are able to emerge through the photosphere. We found that the theoretical temporal and spatial scales of the undular instability closely matched those of the instability observed in the simulation, and thus hypothesized that the emergence occurs via the undular instability, which interchanges magnetic field and plasma across a thin layer of the solar atmosphere. The instability manifests itself in the form of salt-and-pepper magnetic features on the photosphere that qualitatively match those observed on the Sun. In our simulation, the instability also resulted in an explosive energy release, and we associated this event with known solar phenomena called Ellerman bombs. This effort addresses important aspects of how the convection zone affects the rise of magnetic fields, and reveals that, contrary to prior assumptions, flux ropes need not be twisted in order to rise coherently and emerge through the photosphere into the corona.

DoD Impact/Significance: These numerical simulations are providing new insight into how magnetic flux emerges at the solar photosphere, and how solar flares and coronal mass ejections are driven by this emergence. Furthering understanding of how solar activity is generated is a critical step toward building space weather prediction models, and toward mitigating dangers of space weather.

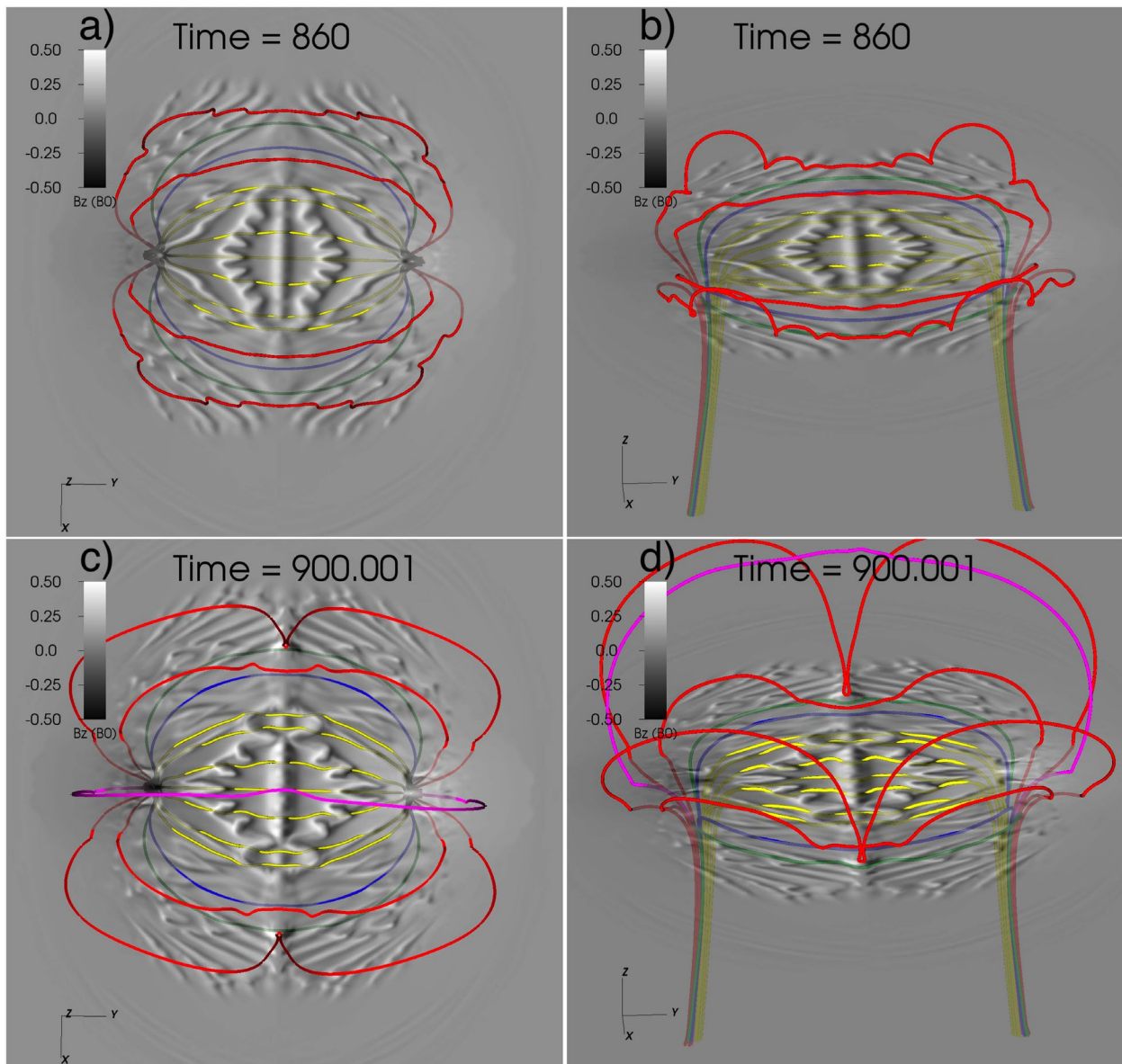


Figure 1. Magnetic field lines overplotted on photospheric magnetograms at various stages of a flux emergence simulation, showing the undulations of the magnetic field into and out of the photosphere. These undulations are manifestations of the undular instability, which plays a key role in the emergence of magnetic flux from the solar interior into the solar atmosphere. Yellow, blue, green, red, and pink field lines are colored by increasing distance from the center of the initial magnetic flux rope. The left panels are viewed from above, and the right panels are from the side.

Title: Development of a Weather Model of the Ionosphere

Author(s): S.E. McDonald¹, F. Sassi¹, C.A. Metzler¹, J.L. Tate², and M.S. Dhadly¹

Affiliation(s): ¹Naval Research Laboratory, Washington, DC; ²Computational Physics, Inc., Springfield, VA

CTA: SAS

Computer Resources: Cray XC40 [NAVY, MS], [ARL, MD]

Research Objectives: The scientific goal of the proposed research is to characterize and simulate the physical processes that are important for improving numerical forecasting of high-frequency (HF) radio wave propagation through the Earth's atmosphere and ionosphere across the range of conditions relevant to DoD operations. To achieve the objectives of this project, we have developed a fully coupled atmosphere-ionosphere model. In FY20, the main objectives were to perform validation studies and to investigate lower atmospheric effects on the ionosphere.

Methodology: We have developed the Navy Highly Integrated Thermosphere and Ionosphere Demonstration System (HITIDES), which couples SAMI3, a state-of-the-art NRL model of the ionosphere, to the Whole Atmosphere Community Climate Model eXtended (WACCM-X). HITIDES uses the Earth System Modeling Framework (ESMF) for interpolation between the atmosphere and ionosphere grids. SAMI3/HITIDES is also being designed to work with any National Unified Operational Prediction Capability (NUOPC) and ESMF-compliant whole-atmosphere model that includes a thermosphere.

Results: We have performed stand-alone WACCM-X and SAMI3/WACCM-X simulations for April 2013 through December 2014. In these runs, the WACCM-X atmosphere was nudged with atmospheric analyses from the Navy Global Environmental Model – High Altitude (NAVEM-HA). These simulations are being used to understand how well the coupled ionosphere-atmosphere model captures the day-to-day variability of the ionosphere. In particular, we have studied the variability of the bottom-side ionosphere that extends from ~ 80 km to the peak of the electron density in the F-region at ~ 350 km; this region is of particular importance for high frequency (HF) communications and geolocation applications that reflect radio waves off the ionosphere. Our simulations have been compared with ionospheric measurements and show that while the model captures the variability near the peak electron density in the F-region, it exhibits very little of the observed day-to-day variability in the region below 200 km in altitude. These results will help us improve the SAMI3 in the lower ionosphere.

In a separate study, we have found that the impacts of middle atmospheric meteorological variability on the ionosphere, as simulated in the SAMI3/WACCM-X runs, can significantly impact HF radio absorption in ionosphere. The decrease in HF radio attenuation occurs after the onset of mesospheric cooling. HF radio absorption after the mesospheric onset, increases in the D-region, but decreases in the E-region of ionosphere, as shown in Fig. 1.

We also have analyzed WACCM-X simulations performed with and without middle atmosphere observations in NAVEM-HA. We have demonstrated that lack of middle atmosphere observations have substantial and statistically significant impacts on the amplitude of solar non-migrating tides and planetary-scale waves emerging in the thermosphere.

DoD Impact/Significance: This effort will lead to a better understanding of the physics, dynamics, and chemistry of the bottom-side ionosphere, with direct implications on future capabilities for nowcasting and forecasting of the environment relevant to DoD/Navy systems.

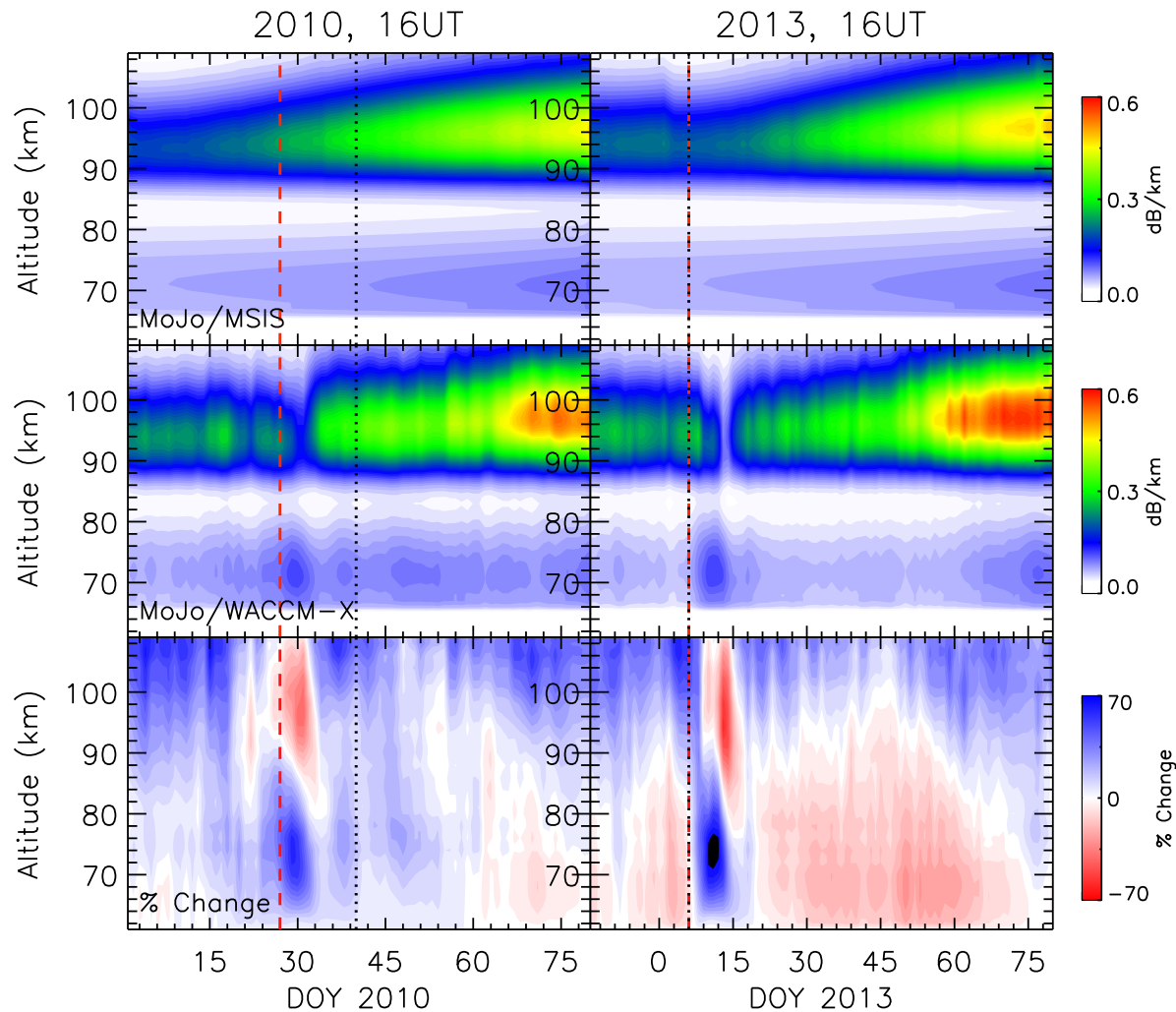


Figure 1. High-frequency (HF) absorption (dB/km) in the ionosphere, as calculated with the NRL MoJo ray tracer and the SAMI3 ionosphere model, is shown as a function of altitude and day of year (DOY) at Sondrestrom. (Top row) HF absorption calculated from SAMI3 simulations using a climatological thermosphere. (Middle row) Same as top row but using SAMI3 driven with a whole-atmosphere model (WACCM-X) nudged with meteorology from NAVGEM-HA. (Bottom row) The percent difference in HF absorption between the simulation with lower atmospheric weather (SAMI3/WACCM-X) and with climatology. The results are shown for both 2010 (left column) and 2013 (right column), at 16 UT. The selected period (16 UT) at Sondrestrom corresponds to the local time of peak HF absorption. The black, vertical, dotted lines mark the onset of a sudden stratospheric warming (SSW), whereas the red, vertical, dashed lines mark the onset of mesospheric cooling (MC). In 2013, MC and SSW occurred simultaneously.

Title: Navy Ionosphere Model for Operations

Author(s): S.E. McDonald¹, C.A. Metzler¹, J.L. Tate², R.K. Schaefer³, P.B. Dandenault³, A.T. Chartier³, G. Romeo³, G.S. Bust³, and R. Calfas⁴

Affiliation(s): ¹Naval Research Laboratory, Washington, DC; ²Computational Physics, Inc., Springfield, VA; ³The Johns Hopkins Applied Physics Laboratory, Laurel, MD; ⁴The University of Texas at Austin Applied Research Laboratories, Austin, TX

CTA: SAS

Computer Resources: HPE SGI 8600, Cray XC40 [NAVY, MS]; Cray XC40 [ARL, MD]

Research Objectives: The objective of this effort is to develop a physics-based ionosphere model coupled to an ionospheric data assimilation system that provides global and regional electron density specifications and short-term forecasts (0 – 24 hours). This capability will form the basis of a future Navy operational ionospheric forecasting system, running at multiple resolutions and fully coupled to operational atmospheric forecast models. In FY20, the main objectives were to complete the development of the regional high-resolution capability, to complete the data preprocessing routines, and to continue testing the full system.

Methodology: The Navy Ionosphere Model for Operations (NIMO) is a physics-based model, SAMI3, and a 3DVAR ionospheric data assimilation system (IDA4D) that can ingest a wide variety of ionospheric datasets. NIMO also includes couplers that use the Earth System Modeling Framework (ESMF) for interpolation of the ionosphere and data assimilation grids. IDA4D previously used an empirical ionosphere, the International Reference Ionosphere (IRI), as its background model. For NIMO, IRI is being replaced with SAMI3, which will enable improved specifications and short-term forecasts. The MPI-enabled Earth System Modeling Framework (ESMF) interpolation routines are used to interpolate between the unstructured IDA4D grid and the geomagnetic field-aligned SAMI3 grid.

Results: In FY20, we continued to improve the data-processing algorithms in NIMO and began running by cycling the full system using an archive of operational ionospheric datasets. NIMO is capable of ingesting a wide variety of ionospheric measurements that are linearly or nonlinearly related to electron density; these include line-of-sight measurements of total electron content (TEC) from ground-based Global Positioning System (GPS) receivers and space-based radio occultations from COSMIC-1 (and soon COSMIC-2), electron densities from ionosonde soundings and in situ satellite instruments, and ultraviolet (UV) radiances from space-based sensors. The data-processing algorithms have been decoupled from IDA4D and rewritten in Python, and they now run independently from the data assimilation and forecast system. HPC resources are being used to perform integration testing of global low-resolution NIMO in preparation for transition to operations at Fleet Numerical Meteorology and Oceanography Center (FNMOC). We also are developing a regional high-resolution capability that will be capable of reconstructing ionospheric features on the order of 100 km. In this case, SAMI3 is run with an embedded high-resolution region within the global grid and the data assimilation grid is specified over a continent-size rectangular region. Figure 1 shows initial results from a simulation over North America on 19 January 2014. In this case, we used a dense network of non-real-time GPS TEC receivers (locations marked with yellow dots), several ionosondes (green triangles), and radio occultation data from COSMIC-1 (red, dashed tracks).

DoD Impact/Significance: The development of an operational ionospheric forecast model will aid in the numerical forecasting of high-frequency (HF) radio wave propagation through the Earth's atmosphere and ionosphere across the range of conditions relevant to DoD/Navy operations.

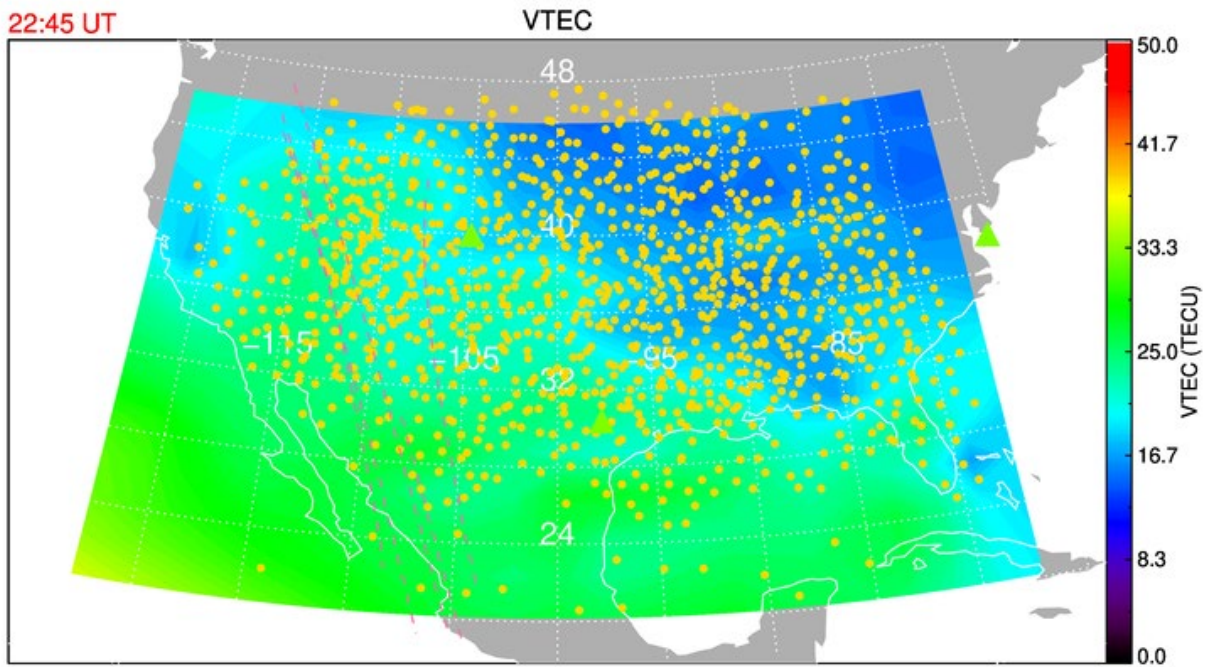


Figure 1. Regional NIMO simulation over North America showing total electron content (TEC) on 19 January 2014 at 22:45 UT. For this test case, a dense network of non-real-time GPS TEC receivers was used in the assimilation (locations are marked with yellow dots), several ionosondes (green triangles), and radio occultation data from COSMIC-1 (red, dashed tracks).

Title: Radio and Gamma-ray Searches for Millisecond Pulsars and Radio Transients*

Author(s): P.S. Ray¹ and J. Deneva²

Affiliation(s): ¹Naval Research Laboratory, Washington, DC; ²George Mason University, Fairfax, VA
CTA: SAS

Computer Resources: SGI Altix ICE [NRL, DC]

Research Objectives: The purpose of this project is to search for millisecond pulsars in gamma ray data from NASA's *Fermi* Large Area Telescope as well as pulsars and radio transients in ground-based data from the Robert C. Byrd Green Bank Telescope in West Virginia and the Arecibo telescope in Puerto Rico. These searches require high-performance computing resources because of the massive parameter spaces that must be searched.

Methodology: We use custom codes to search for pulsations in our radio and gamma-ray data sets. These correct for frequency-dependent delays caused by interstellar dispersion and variable Doppler shifts caused by orbital acceleration in a binary system, then search over a broad range of candidate frequencies using very large Fourier transforms and harmonic summing. We split up the trials over a set of nodes on the cluster.

Results: Before the *polar* NRL cluster went down in Feb. 2020, we searched data from the 327 MHz Arecibo drift pulsar survey (AO327) during FY20. This survey began in 2010 with the goal to cover the part of the sky accessible to the Arecibo telescope. It is the largest conducted with the Arecibo telescope, both in terms of sky coverage and observing-time allocation. Our code for automatically selecting radio transient candidates based on their likelihood of originating from an astrophysical source discovered 7 new objects: 5 pulsars and 2 rotating radio transients.

We also searched 29 hours of Green Bank Telescope data at 5 GHz from a search for pulsations in 10 steep-spectrum radio sources in the Galactic Center. A population of millisecond pulsars in the Galactic Center is one of two competing explanations for the excess of gamma ray emission detected in that region by the *Fermi* spacecraft. Although there are no new pulsar discoveries so far from this project, a pulsation search is a necessary step towards determining the type of compact radio sources in the Galactic Center whose spectra are similar to those of known pulsars.

DoD Impact/Significance: The main goal of AO327 is to find millisecond pulsars that are very stable rotators and therefore useful for detecting gravitational waves with a pulsar timing array (PTA). Among the ~ 2800 known pulsars, only 35 fit this criterion and any addition to this set is a significant contribution to the nanohertz gravitational wave-detection effort as it improves the sensitivity of the PTA. The PTA approach to gravitational wave detection is complementary to LIGO and sensitive to a different range of gravitational wave frequencies. To date, AO327 has contributed four such discoveries to the PTA. Another major goal of the survey is to catalog the local pulsar population at 327 MHz, which would contribute to improved models of the pulsar population and evolution in the galaxy as a whole. Our searches are part of a worldwide campaign to understand the nature of the large population of unidentified gamma ray sources being uncovered by *Fermi*. The large population of millisecond pulsars in short-period interacting binaries (the black widows and redbacks) has been a surprise. This work is an important contribution to the science return of the major NASA mission and will help us understand the physics and astrophysics of neutron stars, one of the most extreme environments anywhere in the universe.

* This work was supported by NASA.

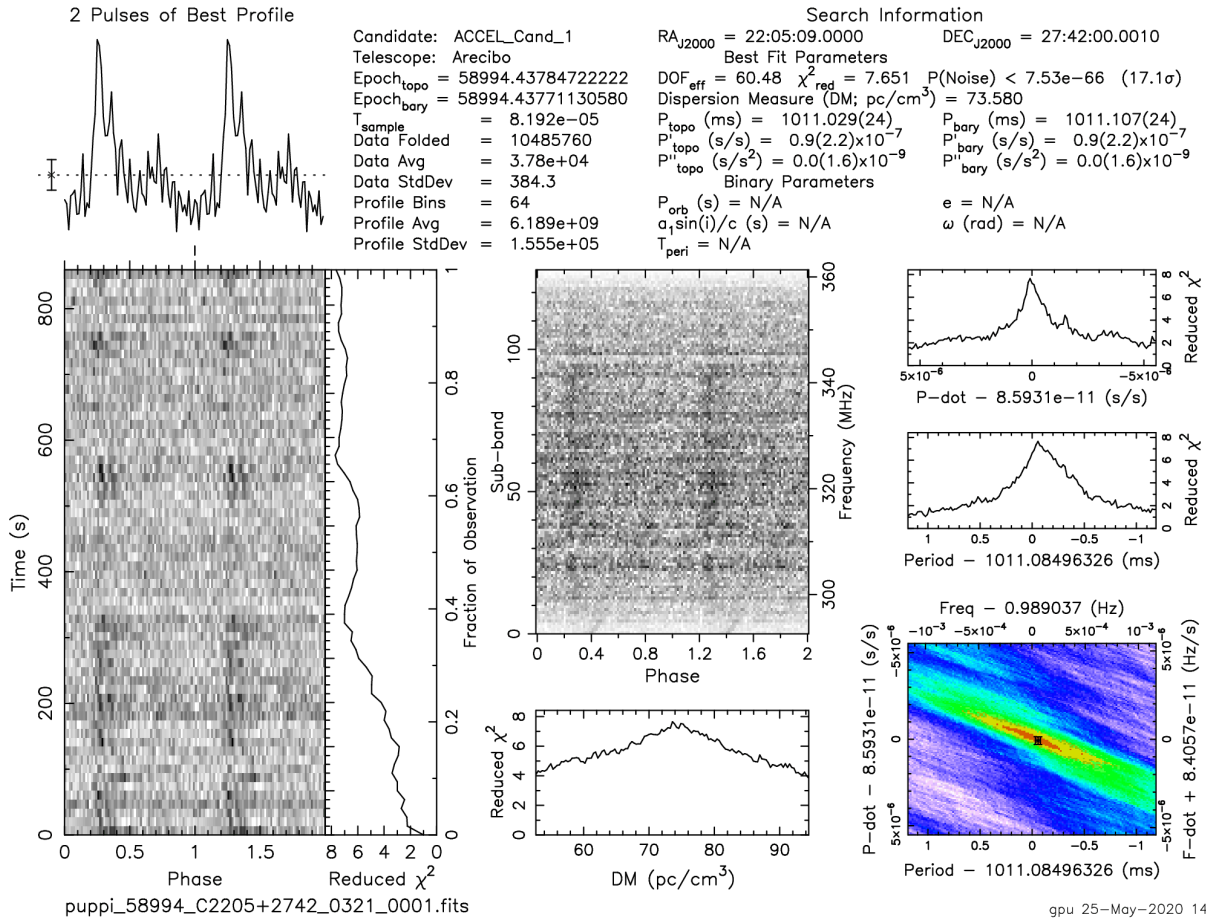


Figure 1. The pulsar J2205+27 was discovered in FY20 by the AO327 survey. This confirmation observation shows that its emission sporadically disappears (“nulls”) and then resumes, which places it in the class of nulling pulsars. These pulsars are harder to detect by conventional periodicity searches; and J2205+27 was identified by our code for automatic classification of individual pulses based on their likelihood of being from an astrophysical source.

Title: Thermosphere & Ionosphere Numerical Models and Ensemble Methods

Author(s): D.P. Drob, M. Jones, and M.S. Dhadly

Affiliation(s): Naval Research Laboratory, Washington, DC

CTA: SAS

Computer Resources: SGI ICE X, HPE SGI 8600 [AFRL, OH], Cray XE6m, Cray XC40/50 [ERDC, MS], HPE SGI 8600, Cray XC40 [NAVY, MS]

Research Objectives: This effort seeks to specify the thermosphere and ionosphere's weather (i.e., space weather) for high-frequency (HF) radio wave applications. This involves an accounting of the composition, winds, and temperatures of the near-Earth space environment as perturbed from below by tides, waves, and subgrid-scale fluctuations; as well as from above by extreme ultraviolet energy and solar wind-driven magnetic field fluctuations. The time evolution of the coupled thermosphere and ionosphere multispecies transport equations, including the self-consistent global electric fields from the ionospheric E- and F-region dynamos currents, are solved via standard coupled multiscale system, numerical model integration methods.

Methodology: This effort modifies, extends, and validates existing space physics research community and NRL first-principles thermosphere and ionosphere models with new physics and ensemble methods to extend data assimilation and forecast capabilities. The focus on ensemble data assimilation and forecast methods is to improve understanding of the plasma transport of long-lived metal ion species such as Mg^+ through the Earth's ionosphere. A plethora of available ground- and space-based ionosphere and thermosphere research data sets provide information for model validation, tuning, and operational data-assimilation experiments. The two main numerical models utilized are the National Center for Atmospheric Research (NCAR) TIME-GCM (Thermosphere-Ionosphere-Mesosphere-Electrodynamics General Circulation Model) and the NRL SAMI3 (Sami is Another Model of the Ionosphere) model.

Results: The SAMI-EnKF (Ensemble Kalman Filter) ionospheric data assimilation and forecast demonstration system advanced considerably this year. The system is capable of producing global 72-hour ionosphere forecasts of up to 64 independent concurrent ensemble members in ~ 1 hr of wall clock time. The system's output time resolution is ~ 15 minutes to capture the fast motion of the solar terminator, with a resolution of $1.25^\circ \times 3^\circ$ in latitude and longitude from 80 km altitude to above ~ 8 Re to also encompass the plasmasphere. The average of the system's 64 independent forecasts provides a most-probable forecast with the standard deviation providing the forecast's uncertainty. Figure 1 shows the ensemble mean peak electron density in the ionosphere vertical column (left) with examples of the ensembles perturbations about that mean (right). Each ensemble member has slightly different model parameter values and variations in the forecast initial conditions, based on those values' estimated uncertainties. Figure 2 shows how the TIME-GCM can be combined with existing lower and middle atmospheric reanalysis products such as the NASA Goddard Modern Era Retrospective Reanalysis version 2 (MERRA2), via a numerical forecast model synchronization and coupling methodology that has been formulated and validated in prior NRL HPC projects. The coupled, potentially concurrent multi-model simulations (TIME-GCM and MERRA2) demonstrate significant improvement over the out-of-the-box TIME-GCM in capturing important effects of space weather, specifically the longitude variability, resulting from waves entering from below and ultimately forcing the ionosphere and even the exosphere.

DoD Impact/Significance: The coupled physics-based thermosphere-ionosphere model validation studies performed here address the DoD/Navy long-term need for environmental prediction of space weather effects for tactical planning purposes, as well as the maximization of DoD HF and space systems performance through adaptation to the variable environment (ref: SECNAVINST 2400.2A).

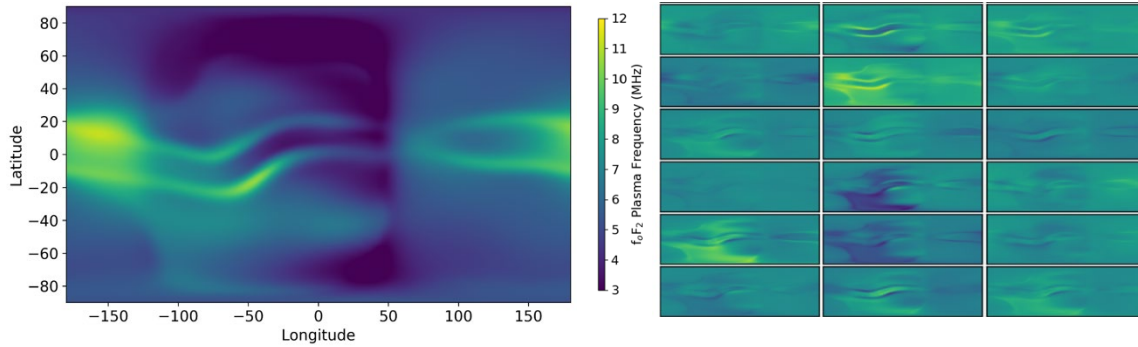


Figure 1. (Left) An example SAMI-EnkF forecast model output for the maximum ionosphere plasma frequency (f_oF_2) for March 23, 2010, at 03:00 UT from a 64-member ensemble. (Right) Example difference fields for 18 of the ensemble members from the average field shown to the left. The color scale of the perturbation fields ranges from -2 to 2 MHz.

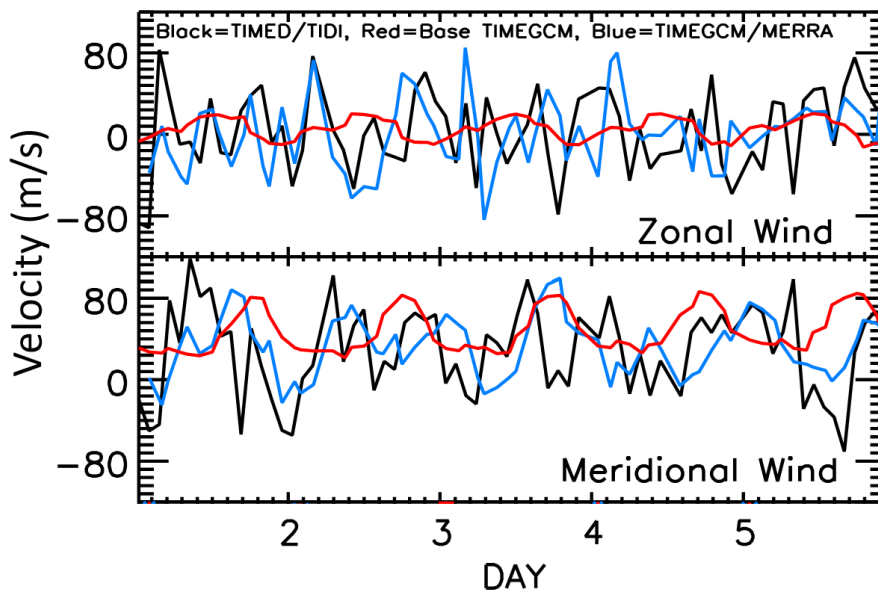


Figure 2. Comparison between NASA Thermosphere-Ionosphere-Mesosphere Energetic and Dynamic (TIMED) mission Fabry-Perot Interferometer (TIDI) wind measurements (black) at 95 km altitude in m/s (left axis) at a fixed local solar time (0 – 2 hr LST) between latitude (10 – 15° N) for five days in January 2010; the corresponding default baseline TIME-GCM simulation/prediction (red), and the improved NRL TIMEGCM/MERRA2 simulation (blue). The y-axis represents wind velocity components in m/s for the zonal (east-west) and meridional (north-south) directions.

THIS PAGE INTENTIONALLY LEFT BLANK

OTH

Other

Work that is not easily categorized as one of the other computational technology areas.

Title: Simulation of High-Energy Radiation Environments
Author(s): J. Finke and A. Hutcheson
Affiliation(s): Naval Research Laboratory, Washington, DC
CTA: OTH

Computer Resources: SGI Altix ICE [NRL, DC]; Cray XC40/50 [ERDC, MS]

Research Objectives: (1) Apply three-dimensional (3D) Monte Carlo methods to simulate the transport of high-energy particles for use in space applications and for modeling detection systems, radiation environments, and the operational concepts relevant to the detection of special nuclear materials and other radiological/nuclear materials in maritime and urban scenarios of interest to DoD and other civilian agencies. (2) To create an improved model of the extragalactic background light (EBL) useful for the study of extragalactic sources by a number of instruments, including the Fermi Gamma-ray Telescope and the future Cherenkov Telescope Array.

Methodology: (1) We use three industry-standard ionizing radiation transport codes: two 3D Monte Carlo packages, Geant4 (CERN) and MCNP (Los Alamos National Lab), and one discrete ordinates package, Denovo (Oak Ridge National Lab). We use an NRL-developed front-end package called SoftWare for Optimization of Radiation Detectors (SWORD) to quickly prototype geometries and radiation environments for running our simulations. (2) We use a model of the EBL created by Co-PI Finke and fit it with a Markov Chain Monte Carlo (MCMC) to a wide variety of data from the literature to determine model parameters, and strongly constrain a number of quantities of astrophysical significance and of use to observations of extragalactic gamma ray sources.

Results: (1) The radiation transport work did not use any HPC resources in FY20. (2) Co-PI Finke's research has led to the measurement and constraints on a number of interesting quantities of astrophysical interest. This includes the mean metallicity and mass-density evolution of the universe across cosmic time, and the cosmic star formation rate (SFR). The latter is demonstrated in Fig. 1, where our 68% constraint from an MCMC fit with our EBL model is shown, with a number of other models from the literature. Of particular interest here is the constraint at $z > 10$, which puts an upper limit on the formation of the first generation of stars in the universe, produced in the first 800 million years of the universe.

DoD Impact/Significance: (1) Our 3D Monte Carlo radiation modeling allows us to provide timely answers to the questions posed by DHS/CWMD, DTRA, NASA, DoD and other government sponsors about radiation environments and detectors. The science addressed by ionizing radiation simulations such as the studies described above is often impractical or not cost effective to study in any manner other than simulation. (2) The EBL absorbs gamma rays from extragalactic objects, and thus understanding the EBL is crucial to studying these types of high-energy sources. Understanding how high-energy particles are accelerated and produce ionizing radiation in these sources helps researchers understand the high-energy-radiation environment that can affect DoD space assets.

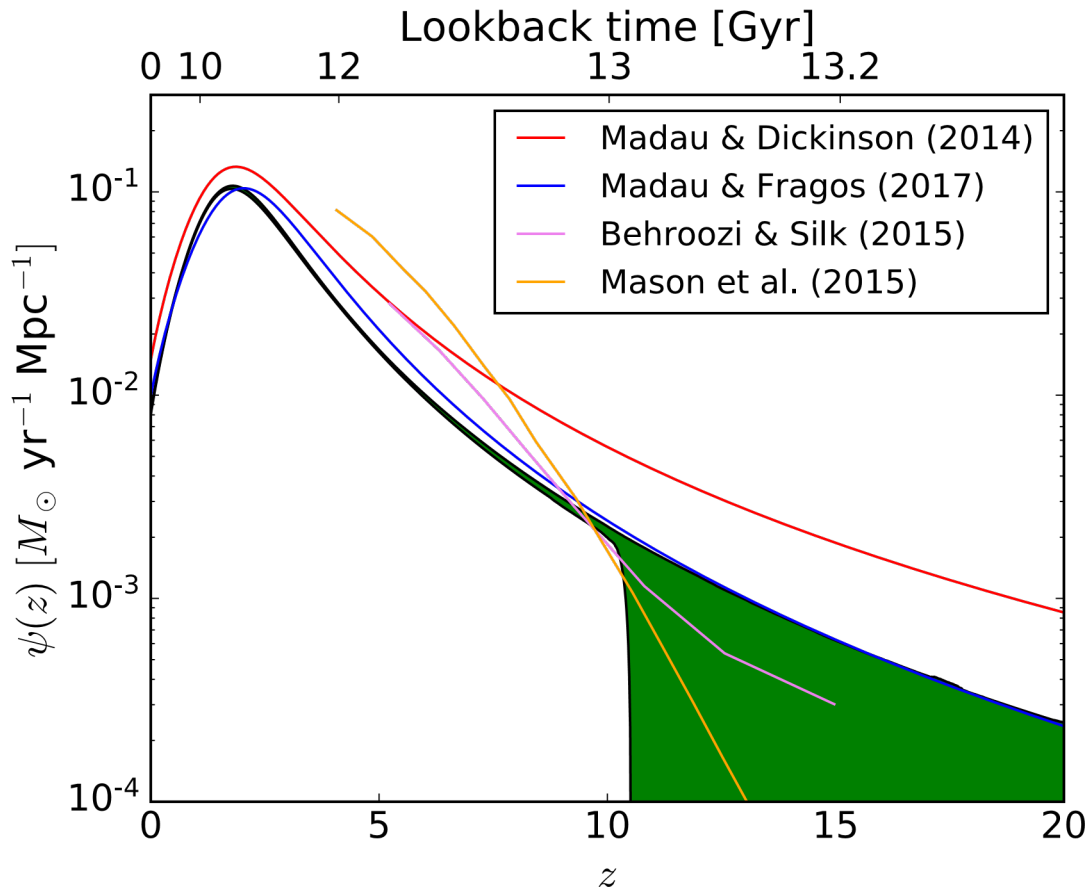


Figure 1. The Star formation rate (SFR) as a function of redshift, or equivalently, lookback time. Several models and other determinations are shown from authors listed in the legend. The green shade regions represent the 68% confidence intervals from MCMC fits to the gamma ray and luminosity density data. At $z > 10$, representing the first 800 million years of the universe, we have put an upper limit on the formation rate of the first generation of stars in the universe.

THIS PAGE INTENTIONALLY LEFT BLANK

Author Index

Adamson, P.E. -----	52	Eckermann, S.D.-----	120
Allard, R. -----	102	Ellis, G. -----	62
Allen, D.R. -----	120	Enloe, L. -----	46
Ananth, R. -----	12		
Antillon, E. -----	2	Fabre, J.P. -----	88
Arcari, A. -----	8	Fan, Y. -----	110
Aubry, R.M. -----	86	Finke, J.-----	160
		Fletcher, A.-----	142, 144
Bachman, C.L. -----	18	Fragiadakis, D.-----	82
Bartels, B.P. -----	128, 134		
Barron, C.N.-----	128, 130, 134	Gamezo, V.N.-----	16
Barton, C.A. -----	120	Georgin, M. -----	46
Barton, N.-----	104	Giles, I.D. -----	58
Bateman, S.P. -----	36	Gilmour, E.A. -----	138
Bates, J.W. -----	14	Goodwin, G.B.-----	18, 44
Bermudez, V.M. -----	54	Gordon, D.F. -----	90
Bernstein, N. -----	2, 56		
Blisard, S.N. -----	138	Hafizi, B. -----	90
Brewick, P. -----	8	Haiducek, J. -----	146
Bust, G.S. -----	152	Hebert, D. -----	102
		Helber, R.-----	134
Calantoni, J. -----	36	Hellberg, C.S.-----	60
Calfas, R. -----	152	Helmboldt, J.-----	146
Campbell, T. -----	102	Herrera, M.A. -----	120
Campbell, W.F. -----	106	Hervey, W.J. -----	62, 64
Carrier, M.-----	134	Hess, A.-----	22
Cayula, S. -----	132	Hogan, T. -----	104
Chartier, A.T. -----	152	Holman, T.D. -----	20
Compton, J.R. -----	64	Hoppel, K.W. -----	120
Cooke, S. -----	94	Huba, J.D. -----	26
Crawford, W.-----	104	Hutcheson, A.-----	160
Crout, J.-----	134	Hyde, E.W. -----	44
D'Addezio, J. -----	134	Imler, G.H. -----	58
Dandenault, P.B.-----	152	Isaacs, J. -----	90
Davidson, A. -----	90		
DeHaan, C.J. -----	128, 134	Jensen, A.-----	94
Deneva, J.-----	154	Jensen, K.-----	70
deRada, S. -----	134	Jensen, T. -----	102
Dey, S. -----	86	Johannes, M. -----	2, 66
Dhadly, M.S. -----	150, 156	Johnson, L. -----	90
Douglass, E. -----	102	Johnson, R.F. -----	22, 48
Doyle, J.D. -----	108	Joliff, J.K. -----	112
Drob, D.P. -----	156	Jones, M. -----	156
Dykes, J. -----	126		

Author Index

Kaganovich, D. ----- 90	Panteleev, G.G. -----128, 134
Kearney, W.S.----- 36	Pasmans, I. ----- 134
Kelly, J. ----- 120	Penano, J. ----- 90
Kercher, A.D. ----- 32	Penko, A.M. ----- 36
Kessler, D.A. ----- 22	Penta, B. ----- 132
Khine, Y. ----- 24, 28, 32, 114	Perkins, F.K. ----- 74
Knizhnik, K.J. ----- 148	Petillo, J. ----- 94
Komaromi, W.A. ----- 116, 118	Petrov, G.M. ----- 92
Krall, J. ----- 26	Phelps, M. -----102, 134
Krowne, C.M. ----- 68	Poludnenko, A.Y. ----- 16
Kuhl, D.D. ----- 120	
	Ramamurti, R. ----- 38, 42
Ladner, S. ----- 112	Ray, P.S. ----- 154
Lamb, Z.W. ----- 128, 134	Reinecke, P.A. ----- 116
Lambrakos, S. ----- 70	Reinecke, T.L. ----- 76
Leary, D.H. ----- 64	Reynolds, C. ----- 104
Lee, W. ----- 36	Ridout, J. ----- 104
Linzell, R.S. ----- 128, 134	Rogers, R.E. ----- 44
Liu, J. ----- 28	Romano, A.J. ----- 96
Liu, M. ----- 104	Romeo, G. ----- 152
Lyons, J.L. ----- 72	Rowley, C.D. -----128, 130, 132, 134
	Ruston, B. ----- 106
Ma, J. ----- 120	Ryou, H. ----- 8
Maloy, B.R. ----- 128, 134	
Matt, S. ----- 30	Sassi, F. -----120, 150
May, J.C. ----- 128, 134	Saunders, R.N. ----- 4, 6, 8
Maxwell, J.R. ----- 44	Schaefer, R.K. ----- 152
McCormack, J.P. ----- 120	Schmitt, A.J. ----- 14
McDonald, M. ----- 46	Schweigert, I.V. ----- 78
McDonald, S.E. ----- 150, 152	Schultzhaus, J. ----- 62
McLay, J. ----- 104	Schwer, D.A. ----- 40
Mestreau, E.L. ----- 86	Sha, X. ----- 68
Metzger, E.J. ----- 122, 124	Shabaev, A. ----- 70
Metzler, C.A. ----- 150, 152	Sharp, C.H. ----- 74
Michopoulos, J.G. ----- 8	Shriver, J.F. ----- 122
Moses, A. ----- 34	Shulman, I. ----- 132
Mott, D.R. ----- 32	Simeonov, J.A. ----- 36
Mukhopadhyay, S. ----- 76	Sletten, M.A. ----- 98
	Smedstad, L.F. -----128, 130, 134
Ngodock, H. ----- 134	Smith, L.N. ----- 138
	Smith, S. ----- 134
Obenschain, K. ----- 14, 34	Smith, T.A. -----102, 112, 128, 134
Orzech, M. ----- 126	Souopgui, I. ----- 134
Osborne, J.J. ----- 128, 134	Spence, P.L. -----128, 130, 134
Ouellette, J.D. ----- 98	Stantchev, G. ----- 94
Ovtchinnikov, S. ----- 94	Sullivan, K.M. ----- 138

Author Index

Szymczak, W.G. -----	86, 96
Tan, X.G. -----	4
Tate, J.L. -----	120, 150, 152
Teferra, K. -----	6
Toporkov, J.V. -----	98
Townsend, T.L. -----	128, 134
Veeramony, J. -----	36
Villa, M. -----	86
Viner, K. -----	104
Viswanath, K. -----	42
Vora, G.J. -----	62, 64
Weber, K. -----	134
Whitcomb, T. -----	104
Wickramaratne, D. -----	80
Williams, D. -----	86
Williamschen, M. -----	86
Wimmer, S.A. -----	8
Wood, C. -----	112
Yaremchuk, M. -----	128
Zhuang, X. -----	12

Division/Branch Index

Systems Directorate (Code 5000)

Information Technology Division (Code 5500)

Navy Center for Applied Research In Artificial Intelligence (Code 5510)	138
Center for Computational Science (Code 5590).....	68

Materials Science and Component Technology Directorate (Code 6000)

Laboratory for Computational Physics and Fluid Dynamics (Code 6040)	14, 16, 22, 24, 28, 32, 34, 38, 40, 42, 48, 114
--	---

Chemistry Division (Code 6100)

Materials, Chemistry and Dynamics (Code 6120).....	82
Center for Corrosion Science and Engineering (Code 6130)	8
Navy Technology Center for Safety and Survivability (Code 6180)	12, 78

Materials Science and Technology Division (Code 6300)

Materials Science and Technology Division (Code 6300)	68
Multifunctional Materials (Code 6350)	4, 6, 8
Materials and Sensors (Code 6360)	70
Center for Computational Materials Science (Code 6390).....	2, 8, 56, 60, 66, 70, 72, 80

Plasma Physics Division (Code 6700)

Plasma Physics Division (Code 6700).....	90
Laser Plasma (Code 6730)	14
Charge Particle Physics (Code 6750)	26, 46, 142, 144
Pulsed Power Physics (Code 6770)	52
Beam Physics (Code 6790).....	90, 92

Electronics Science and Technology Division (Code 6800)

Microwave Technology (Code 6850).....	94
Electronic Materials (Code 6870).....	54, 74, 76

Center for Biomolecular Science and Engineering (Code 6900)

Laboratory for Biosensors and Biomaterials (Code 6910)	58, 62, 64
Laboratory for Biomaterials and Systems (Code 6920)	62, 64
Laboratory for Molecular Interfaces (Code 6930).....	58, 62

Ocean and Atmospheric Science and Technology Directorate (Code 7000)

Acoustics Division (Code 7100)

Physical Acoustics (Code 7130) 86, 96
Acoustics Simulation, Measurements and Tactics (Code 7180) 88

Remote Sensing Division (Code 7200)

Radio/Infrared/Optical Sensors (Code 7210)..... 146
Remote Sensing Physics (Code 7220) 98, 120
Image Science and Applications (Code 7260)..... 98

Oceanography Division (Code 7300)

Information Technology Office (Code 7309)..... 128, 134
Ocean Dynamics and Prediction (Code 7320)..... 36, 102, 110, 112, 122, 124, 126, 128, 130,
..... 132, 134
Ocean Sciences (Code 7330) 30, 112, 132, 134
Center for Geospatial Sciences (Code 7340)..... 134
Seafloor Sciences (Code 7350)..... 36

Marine Meteorology Division (Code 7500)

Mesoscale Meteorology (Code 7503)..... 108
Probabilistic Prediction (Code 7504)..... 104
Atmospheric Dynamics and Prediction (Code 7530) 104, 106, 116, 118

Space Science Division (Code 7600)

Geospace Science and Technology (Code 7630)..... 120, 150, 152, 156
High-Energy Space Environment (Code 7650) 154, 160
Solar and Heliospheric Physics (Code 7680)..... 148

Naval Center for Space Technology Directorate (Code 8000)

Spacecraft Engineering Division (Code 8200)

Space Mechanical Systems Development (Code 8220) 18, 20, 44
Dynamics and Control Systems (Code 8230)..... 46

Site Index

DSRCs

AFRL 2, 4, 6, 8, 12, 14, 16, 22, 24, 26, 28, 32, 34, 38, 40, 48, 52, 54, 56, 60, 62, 64, 66, 68, 70, 72, 74, 76, 78, 82, 86, 90, 94, 96, 114, 116, 120, 146, 148, 156

ARL 4, 14, 16, 18, 20, 22, 24, 28, 30, 32, 34, 36, 38, 42, 44, 46, 48, 52, 56, 58, 60, 62, 64, 66, 70, 72, 78, 80, 82, 86, 94, 96, 98, 106, 114, 116, 120, 138, 142, 144, 148, 150, 152

ERDC 2, 4, 6, 14, 16, 22, 24, 26, 28, 32, 34, 36, 42, 48, 56, 60, 62, 64, 70, 76, 98, 108, 114, 116, 120, 122, 128, 130, 134, 148, 156, 160

NAVY 4, 6, 8, 22, 36, 54, 64, 78, 86, 88, 92, 102, 104, 106, 108, 110, 112, 114, 116, 118, 120, 122, 124, 126, 128, 132, 134, 146, 150, 152, 156

ARCs

NRL 54, 154, 160